AFFDL-TR-66-147

# MEASUREMENT AND ANALYSES OF THE J57-P21 NOISE FIELD

*P. H. HERMES*
*D. L. SMITH*

## FOREWORD

This research effort was performed by the Aero-Acoustics Branch, Vehicle Dynamics Division, Air Force Flight Dynamics Laboratory, Wright-Patterson AFB, Ohio.

The work described is a continuing part of the Research and Technology Division, Air Force Systems Command's, exploratory development program to predict the noise environment of flight vehicles. The work was directed under Project 1471, "Aero-Acoustic Problems" and Task 147102, "Prediction and Control of Noise," with Mr. D. L. Smith as Project Engineer and Mr. P. H. Hermes as Task Engineer. This report covers work conducted from November 1964 to August 1966. The manuscript was released by the authors in August 1966 for publication as a Technical Report.

Contributing personnel included members of the Field Measurements Group of the Aerospace Dynamics Branch who recorded the measurements and members of the Instrumentation Group of the Aero-Acoustics Branch who reduced the data. Appreciation is extended to the Aero Propulsion Laboratory for the use of the turbojet engine and the support provided by their personnel in conducting this program.

This technical report has been reviewed and is approved.

Walter J. Mykytow

WALTER J. MYKYTOW
Asst. for Research and Technology
Vehicle Dynamics Division

## ABSTRACT

A noise survey of a J57-P21 turbojet engine was conducted to provide a basis for the development of a refined empirical noise prediction technique. The measurements were obtained at 65 locations for five engine power settings. The one-third octave and overall sound pressure levels (SPL's) for each location and engine power setting are presented. SPL contours are presented for overall and selected one-third octave bandwidths. Ground reflection effects on the one-third octave band SPL's are evaluated. Comparisons are made with other existing data. Differences of up to 15 decibels (db) are found when comparing the one-third octave band levels. Velocity exponents (n), based on the Lighthill parameter, are presented for each location and compared with existing data. Poor agreement is found among the measurement programs. The effect of ground reflection on the n values is investigated and an n field is presented in which interference effects are eliminated. The effect of varying noise directional properties with jet velocity on the n values is evaluated. An n field, corrected for both ground reflection and varying noise directional properties, is presented. The corrected n values range from 5.0 to 6.0 for 80 percent of the measurement locations between 30 and 90 degrees from the jet axis when jet density effects are neglected. The median value of 5.5 increases to 6.5 with the effects of jet density included. This essentially constant n field clearly indicates the heavy dependence of the n values on noise directional changes with jet velocity. The corrected n field equation is considered the basis of a noise prediction method which appears to be accurate for jet flows with exit Mach numbers ranging from 0.5 to 2.0.

TABLE OF CONTENTS

# ILLUSTRATIONS

ILLUSTRATIONS (Cont'd)

ILLUSTRATIONS (Cont'd)

ILLUSTRATIONS (Cont'd)

# TABLES

## ABBREVIATIONS AND SYMBOLS

| | |
|---|---|
| c | Speed of sound (fps) |
| cps | Cycles per second |
| D | Jet engine exit diameter (ft) |
| $f_c$ | One-third octave band center frequency (cps) |
| h | Source and receiver heights above the ground plane (ft) |
| K | Convection factor |
| n | A number |
| P | Pressure (dynes/cm$^2$) |
| r | Distance between source and receiver (ft) |
| rms | Root-mean square |
| SPL | Sound pressure level in db re 0.0002 microbar (dynes/cm$^2$) |
| TAP | Total acoustic power |
| V | Jet engine exit velocity (fps) |
| X | Axial distance from jet engine exhaust center point (ft) |
| Y | Radial distance from jet engine exhaust center point (ft) |
| $\theta$ | Angle from jet axis |
| $\rho$ | Density |

OVERBAR

| | |
|---|---|
| - | Time average |

SUBSCRIPTS

| | |
|---|---|
| FF | Free-field |
| j | Jet engine parameter |
| m | Measured |
| SA | Space average |
| 0 | Ambient conditions |
| 1,2 | Specific operating conditions |

# SECTION I

# INTRODUCTION

This effort was motivated by the lack of agreement among noise measurements and between the measurements and the estimates based on existing noise prediction techniques.

The present sound pressure measurements, when compared with those in References 1, 2, and 3, illustrate the differences in various measured data. Disagreements of up to 7.5 db in overall sound pressure levels (SPL's) and up to 15 db in one-third octave band SPL's are encountered.

References 4 and 5 compared measured noise levels to estimates from the noise prediction technique contained in Reference 6. Contours of overall SPL were obtained from this prediction technique by correcting reference contours of an engine operating with an exit velocity (V) of 1850 feet per second (fps). The major portion of this correction results from a $V^8$ relationship. The prediction technique was applied to cases where the exit velocity was both higher and lower than the reference exit velocity. For those cases where the velocity was higher, the predicted SPL's were higher than the measured values and where the velocities were lower the predicted SPL's were lower than the measured values. Differences were found to be as much as 10 db.

The above trend with exit velocity is indicative of too high a velocity exponent (n). The Reference 3 investigation into the value of the velocity exponent supports this indication and establishes that a variable velocity exponent field exists with values ranging from 5 to 8. The present measurement program was undertaken to obtain additional information on the velocity exponent field and to further determine reasons for the discrepancies found in measurements and predictions.

This program consisted of noise measurements at 65 locations with a J57-P21 turbojet engine operating at five different power settings. These measurements were made in support of Contract AF 33(615)-1481 "Sonic Fatigue in Combined Environment" and also in support of a continuing effort to refine jet noise prediction methods.

A description of the test site and of the procedures used in obtaining the measurements are presented in Section II.

Overall and selected one-third octave band data are presented and compared to the data of References 1, 2, and 3 in Section III.

The method for correcting the one-third octave spectra for ground reflection effects is presented in Section IV.

Section V presents the method used to determine the velocity exponent (n) from measured data. Comparisons between the n field from the present program to the n field of References 1 and 3 are presented. Refinements are then introduced to correct the velocity exponent for ground reflection and directional effects of the noise.

The conclusions are presented in Section VI.

Two appendixes are included for supplemental information. Appendix I provides the environmental and engine data for those who wish to use the basic information for additional investigations. One-third octave spectra are presented in Appendix II for the 65 measurement points with the overall SPL.

# SECTION II

# DESCRIPTION OF TEST

The measurement program was conducted on a J57-P21 turbojet engine at Wright-Patterson AFB, Ohio. The engine was operated at five power settings over a flat concrete area with the closest obstruction being a building over 1000 feet from the jet exit. Measurements were taken with 65 microphones oriented vertically and in the horizontal plane of the engine center line 78 inches above the concrete. The coordinates, measured from the jet exit, of the microphone locations in this plane are shown in Figure 1. Each microphone location was assigned the spot number indicated in the figure. The coordinates given in the figure are nondimensional where the axial and radial distances, X and Y, are nondimensionalized by the value of the jet exit diameter, D. The exit diameter was 2.33 feet for afterburner operation and 1.85 feet for the lower power settings. The microphone locations for the non-afterburner and afterburner operating conditions were selected on the basis of equal nondimensional locations. The nondimensional values for each microphone location or spot number are tabulated in Table I.

The acoustic measurements were made using the Air Force Flight Dynamics Mobile Dynamics Data Acquisition and Analysis Facility described in Reference 7. All measurements were made using Altec-condenser microphones which were calibrated before and after each test using comparison techniques described in Reference 8. No corrections were deemed necessary.

The measurements were recorded on tape in groups of 12 locations with each group defined as a setup. A typical setup is shown in Figure 2. The spot numbers associated with each setup are given in Table II along with the associated microphone calibration levels.

The 12 microphones associated with each setup were positioned by placing a stand with a microphone attached at the required height over a spot number marked on the concrete. This was done first for coordinates associated with the non-afterburner engine operating conditions. Thirty seconds of acoustic data were then recorded while the engine was in stable operation at 100, 96, 70, and 50 percent of military thrust. The stands were then moved to the same spot numbers with coordinates associated with afterburner operation. Thirty seconds of acoustic data were then taken with the engine in afterburner operation. The microphone at nondimensional spot number 9 was used in each setup for monitoring purposes.

The above procedures were followed for the first six setups. Setups 7 through 11 include only measurements for engine operating conditions of 100 and 96 percent of military thrust and afterburner conditions since it was necessary to repeat these measurements as a result of signal clipping when the first measurements were recorded.

In addition to the acoustic data taken during each setup, engine parameters (thrust, turbine exhaust total pressure, exhaust gas temperature, high pressure rotor speed, and low pressure rotor speed) and atmospheric conditions (pressure, temperature, and wind velocity) were recorded. In Appendix I, these data are tabulated along with the calculated exit velocities for each setup. The values of exit velocity were calculated using information in the J57-P21 engine specification (Reference 9) and measured values of thrust, fuel flow, and atmospheric conditions.

Upon completion of the measurements, the data were reduced at the RTD Sonic Fatique Facility. Data samples of 10 seconds' duration were analyzed for the standard one-third octave and overall bandwidths, and true root-mean square (rms) levels were plotted by an automatic indicator.

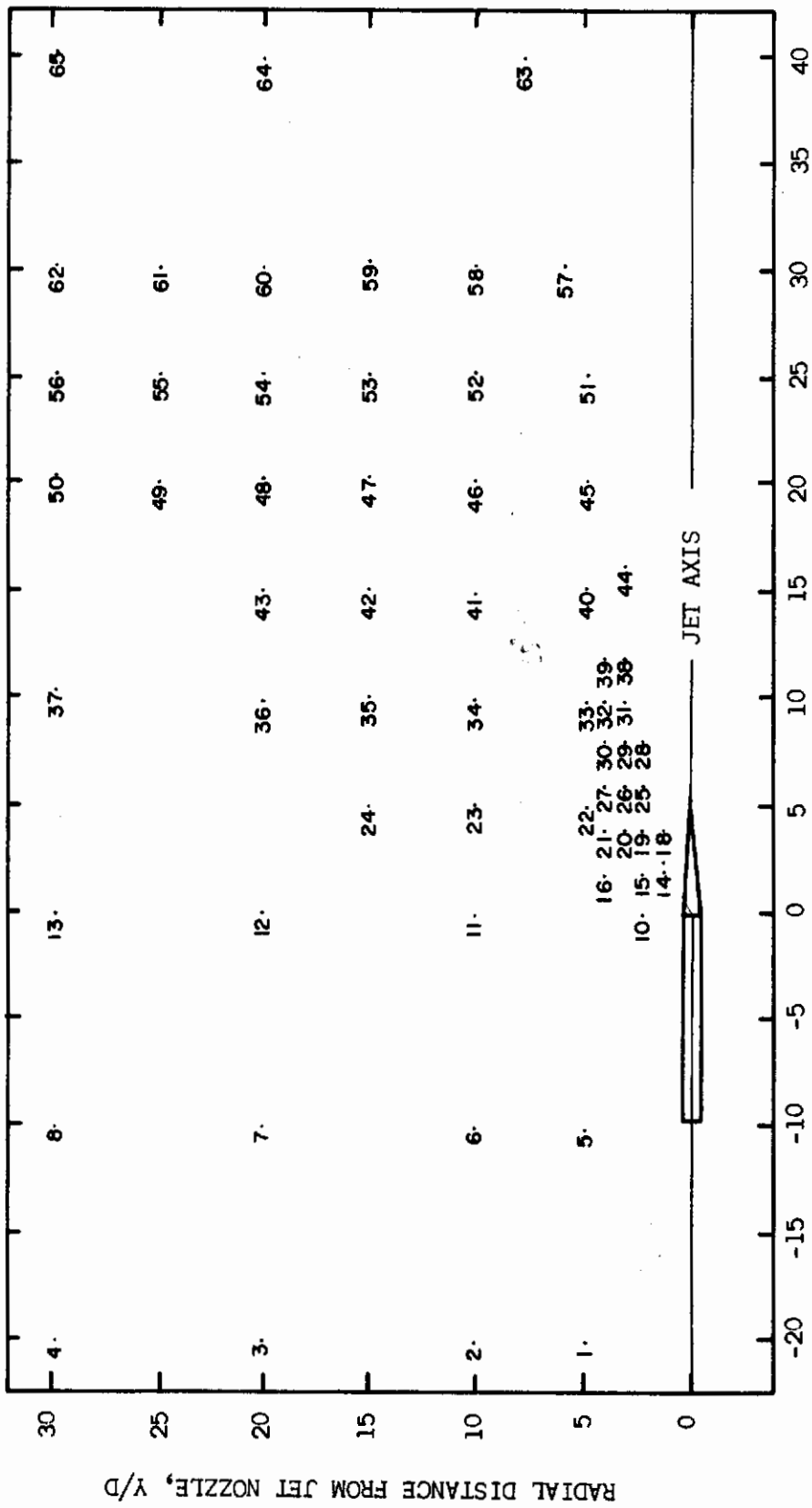


**Figure 1. Microphone Location and Spot Number Identification**

TABLE I

NONDIMENSIONAL MICROPHONE LOCATION VERSUS SPOT NUMBER

| SPOT | MIKE LOCATION | | SPOT | MIKE LOCATION | | SPOT | MIKE LOCATION | |
|---|---|---|---|---|---|---|---|---|
| | X/D | Y/D | | X/D | Y/D | | X/D | Y/D |
| 1 | -20 | 5 | 23 | 5 | 10 | 45 | 20 | 4.02 |
| 2 | -20 | 10 | 24 | 5 | 15 | 46 | 20 | 10 |
| 3 | -20 | 20 | 25 | 6 | 1.56 | 47 | 20 | 15 |
| 4 | -20 | 30 | 26 | 6 | 3 | 48 | 20 | 20 |
| 5 | -10 | 5 | 27 | 6 | 4 | 49 | 20 | 25 |
| 6 | -10 | 10 | 28 | 8 | 1.91 | 50 | 20 | 30 |
| 7 | -10 | 20 | 29 | 8 | 3 | 51 | 25 | 4.9 |
| 8 | -10 | 30 | 30 | 8 | 4 | 52 | 25 | 10 |
| 9 | 0 | -2 | 31 | 10 | 3 | 53 | 25 | 15 |
| 10 | 0 | 2 | 32 | 10 | 4 | 54 | 25 | 20 |
| 11 | 0 | 10 | 33 | 10 | 5 | 55 | 25 | 25 |
| 12 | 0 | 20 | 34 | 10 | 10 | 56 | 25 | 30 |
| 13 | 0 | 30 | 35 | 10 | 15 | 57 | 30 | 5.78 |
| 14 | 2 | 0.85 | 36 | 10 | 20 | 58 | 30 | 10 |
| 15 | 2 | 2 | 37 | 10 | 30 | 59 | 30 | 15 |
| 16 | 2 | 4 | 38 | 12 | 2.61 | 60 | 30 | 20 |
| 17 | 3 | 1.03 | 39 | 12 | 4 | 61 | 30 | 25 |
| 18 | 4 | 1.20 | 40 | 15 | 5 | 62 | 30 | 30 |
| 19 | 4 | 2 | 41 | 15 | 10 | 63 | 40 | 7.54 |
| 20 | 4 | 3 | 42 | 15 | 15 | 64 | 40 | 20 |
| 21 | 4 | 4 | 43 | 15 | 20 | 65 | 40 | 30 |
| 22 | 5 | 5 | 44 | 16 | 3.32 | | | |

Figure 2. Typical Setup of Twelve Microphone Locations

TABLE II

SPOT NUMBER AND CALIBRATION LEVEL VERSUS SETUP

| Setup #1 | | Setup #2 | | Setup #3 | | Setup #4 | |
|---|---|---|---|---|---|---|---|
| Spot | Cal | Spot | Cal | Spot | Cal | Spot | Cal |
| 9 | 145 | 9 | 145 | 9 | 145 | 9 | 145 |
| 14 | 170 | 17 | 165 | 27 | 150 | 57 | 150 |
| 20 | 155 | 15 | 155 | 43 | 140 | 58 | 145 |
| 18 | 170 | 19 | 160 | 45 | 145 | 61 | 145 |
| 30 | 155 | 22 | 147 | 49 | 135 | 56 | 135 |
| 33 | 155 | 29 | 158 | 54 | 140 | 62 | 140 |
| 25 | 165 | 16 | 145 | 46 | 145 | 59 | 145 |
| 28 | 165 | 21 | 150 | 47 | 145 | 60 | 145 |
| 31 | 160 | 26 | 155 | 48 | 145 | 55 | 145 |
| 38 | 160 | 32 | 155 | 53 | 145 | 64 | 145 |
| 44 | 155 | 39 | 155 | 52 | 145 | 63 | 145 |
| 51 | 145 | 42 | 145 | 50 | 135 | 65 | 135 |
| Setup #5 | | Setup #6 | | Setup #7 | | Setup #8 | |
| Spot | Cal | Spot | Cal | Spot | Cal | Spot | Cal |
| 9 | 145 | 9 | 145 | 9 | 155 | 50 | 155 |
| 40 | 150 | - | --- | 14 | 180 | 32 | 180 |
| 41 | 145 | 2 | 130 | 33 | 165 | 15 | 165 |
| 24 | 145 | 5 | 145 | 45 | 155 | 42 | 155 |
| 13 | 135 | 1 | 130 | 16 | 155 | 52 | 155 |
| 36 | 140 | 3 | 135 | 21 | 160 | 47 | 160 |
| 11 | 145 | 10 | 145 | 40 | 160 | 43 | 160 |
| 12 | 145 | 7 | 145 | 22 | 160 | 49 | 160 |
| 23 | 145 | 6 | 145 | 26 | 165 | 46 | 165 |
| 35 | 145 | - | --- | -- | --- | -- | --- |
| 34 | 145 | 8 | 130 | 53 | 155 | 54 | 155 |
| 37 | 135 | 4 | 130 | 39 | 165 | 48 | 165 |
| Setup #9 | | Setup #10 | | Setup #11 | | | |
| Spot | Cal | Spot | Cal | Spot | Cal | | |
| 9 | 155 | 27 | 160 | 34 | 160 | | |
| 17 | 180 | 29 | 180 | 19 | 175 | | |
| 59 | 165 | | | 35 | 155 | | |
| 62 | 155 | | | 36 | 150 | | |
| 65 | 155 | | | 41 | 160 | | |
| 11 | 160 | | | 51 | 160 | | |
| 12 | 160 | | | 55 | 155 | | |
| 24 | 160 | | | 56 | 155 | | |
| 61 | 165 | | | 60 | 155 | | |
| -- | --- | | | | | | |
| 37 | 155 | | | | | | |
| 58 | 165 | | | | | | |

# SECTION III

# OVERALL AND ONE-THIRD OCTAVE BAND SOUND PRESSURE LEVELS

## 1. PRESENTATION OF DATA

The overall and one-third octave SPL's for the 65 microphone locations and the five engine power settings are presented in Appendix II. These data are plotted in the format directly obtained from the analyzer. The spectra have not been corrected for line losses which resulted from using 500 ft of cable in obtaining these data. The corrections for these losses are given in Figure 3.

Contours of overall SPL obtained from these data are presented in Figure 4 for engine power settings of afterburner, 100, 70 and 50 percent military. The microphone locations, represented by dots, are presented in nondimensional coordinates. The origin of the coordinate system is located at the engine exhaust. The engine inlet is located at approximately X/D = -10. The SPL contours were faired in manually around the measured levels and locations. The SPL contour lobes follow the expected pattern of shifting outward from the jet axis with increasing jet velocity.

Contours of one-third octave band SPL are presented in Figure 5. These contours are for the 100 percent military engine power setting and include third octave bandwidths with center frequencies from 100 to 2500 cps. These were obtained in the same manner as was used for the overall contours. The SPL contour lobes follow the expected pattern of shifting away from the jet axis with increasing frequency.

## 2. COMPARISON OF DATA

Noise measurement programs were conducted previous to the present investigation and are presented in References 1, 2, and 3. Comparisons with these data are presented to point out the similarities and differences where they occur.

The factors affecting the noise measurements of each program are given in Table III. These factors include the basic engine parameters, the geometric and ground plane conditions, the orientation and type of microphone, and the type of noise level indicating device.

Contours of overall SPL obtained from the other programs are compared to the present measurements in Figure 6. Near the jet axis Reference 3 noise levels are lower than the present data, however, better agreement is obtained as the angle from the jet axis increases. It was expected that the Reference 3 data would be lower due to the lower exit velocity. The data from References 1 and 2 agree reasonably well throughout the noise field.

In addition to the overall SPL comparisons, one-third octave spectra are compared at five locations in the noise field. These locations are shown in Figure 7. These selected locations did not in every case correspond to the actual measurement position for the various investigations compared. Table IV summarizes how the SPL's were obtained from each measurement program. The resulting error from using these approximate locations is considered negligible. Two values of overall SPL from Reference 2 are presented for each location. One value corresponds to overall SPL contours, and the other is the summation of SPL's obtained from one-third octave band contours. Only selected one-third octave band SPL's from Reference 3 are available for comparison. Comparisons of one-third octave spectra are limited to 100 to 2000 cps.

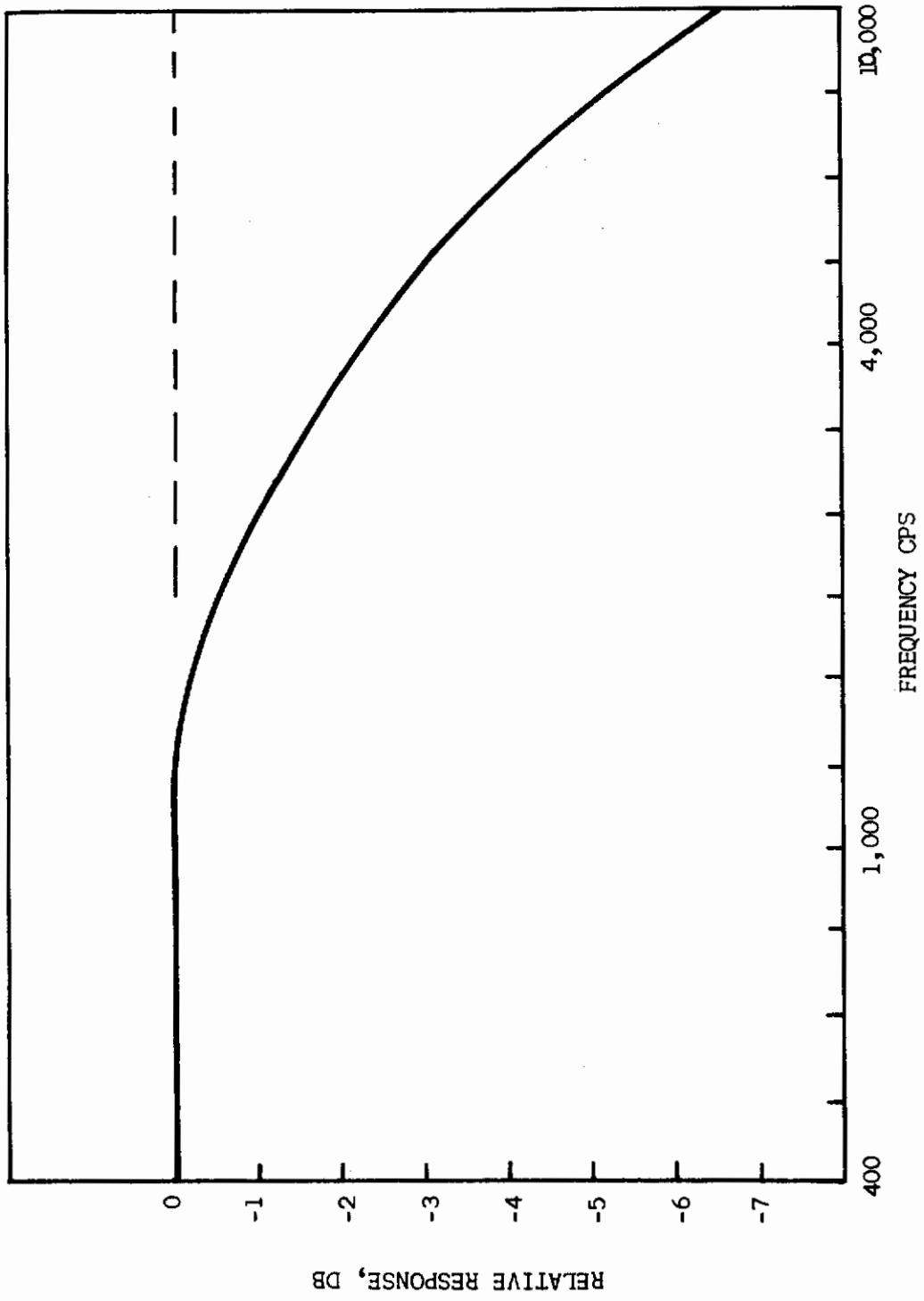


Figure 3. Frequency Response Correction for 500 Ft Cable

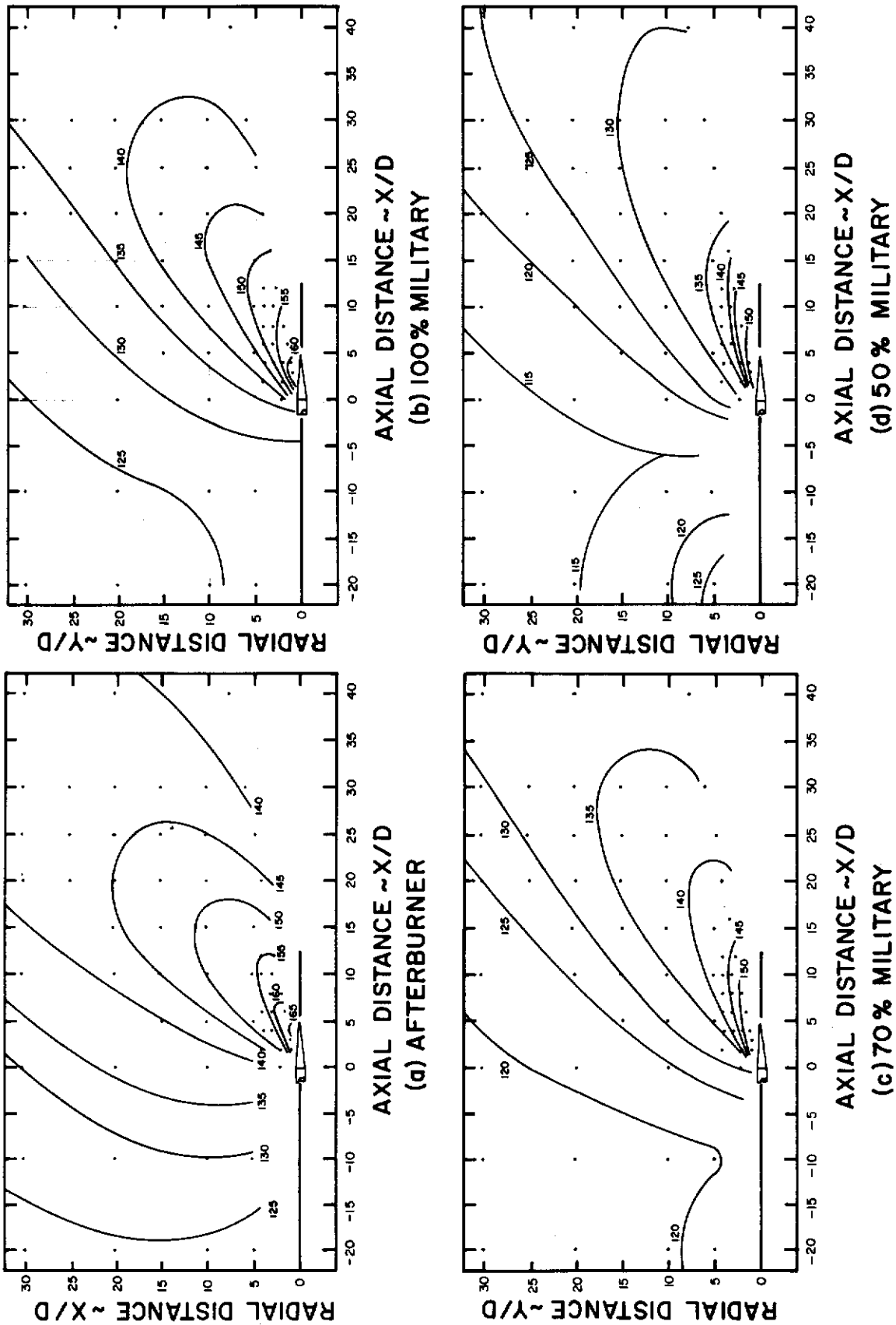


Figure 4. Overall Sound Fields for Different Engine Settings

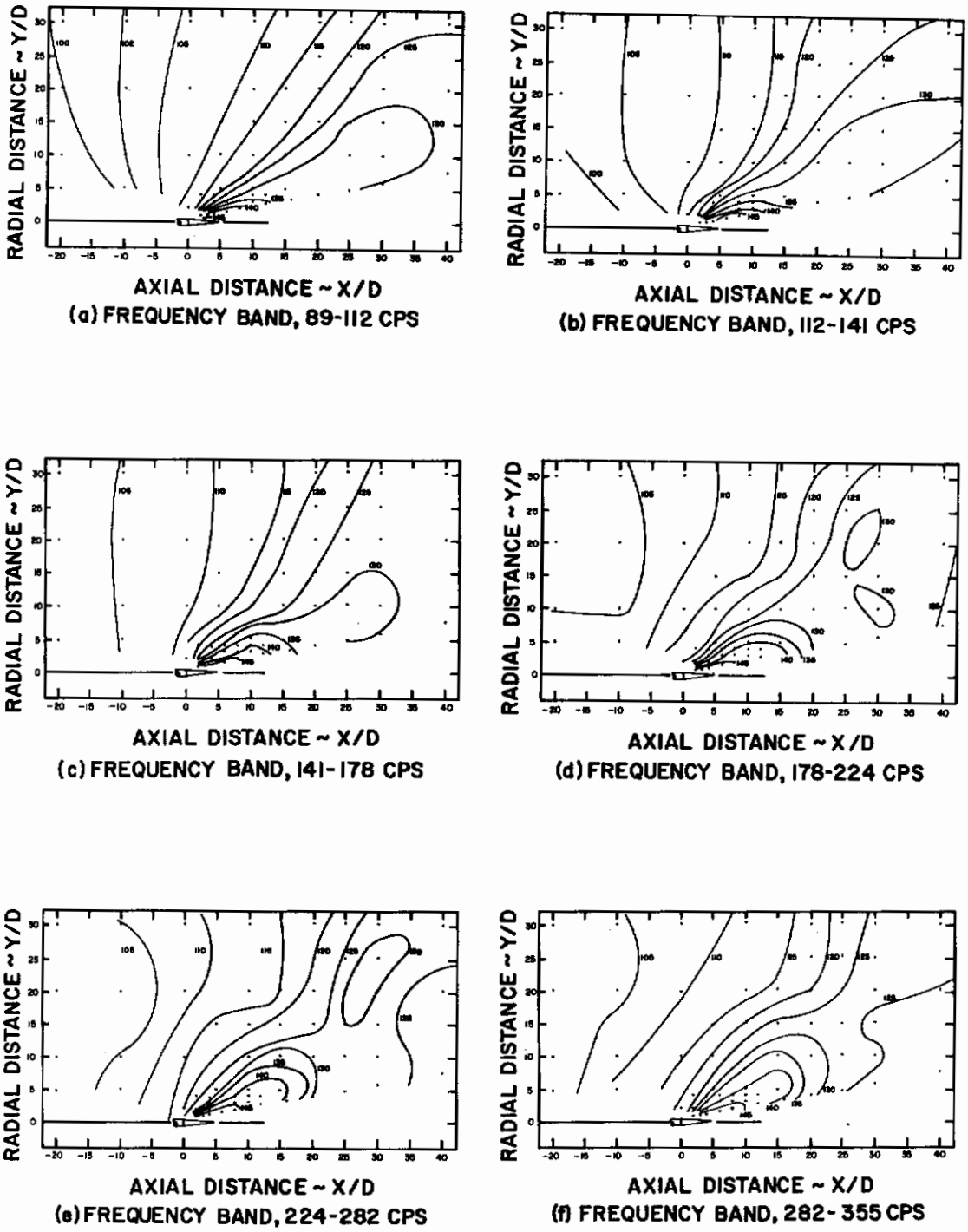


Figure 5. One-Third Octave Band Sound Fields for 100% Military Engine Setting

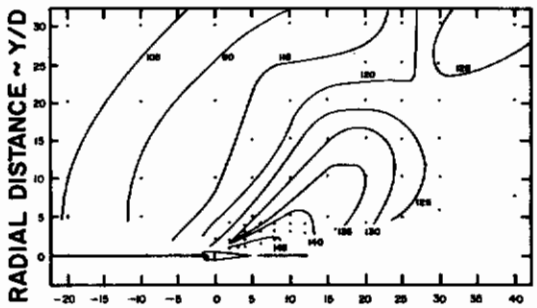


(g) FREQUENCY BAND, 355-447 CPS

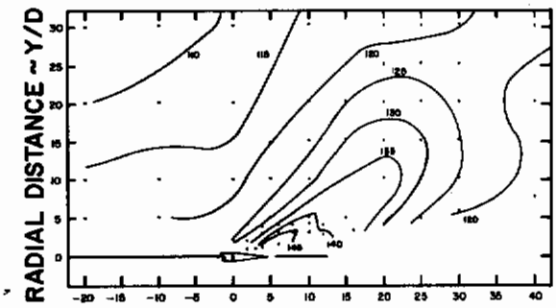


(h) FREQUENCY BAND, 447-562 CPS

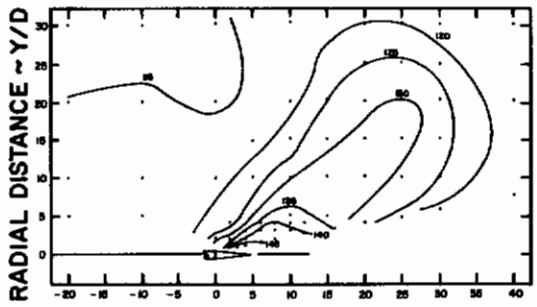


(i) FREQUENCY BAND, 562-708 CPS

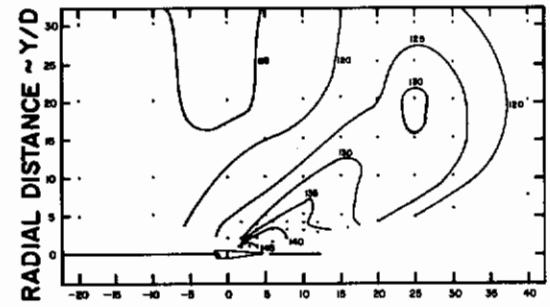


(j) FREQUENCY BAND, 708-891 CPS

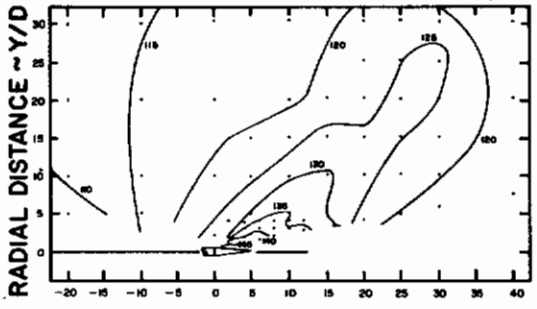


(k) FREQUENCY BAND, 891-1120 CPS

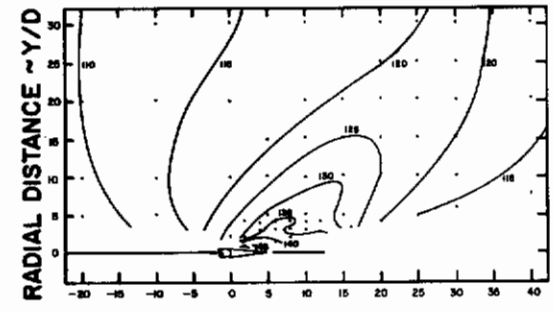


(l) FREQUENCY BAND, 1120-1410 CPS

Figure 5. (Continued)

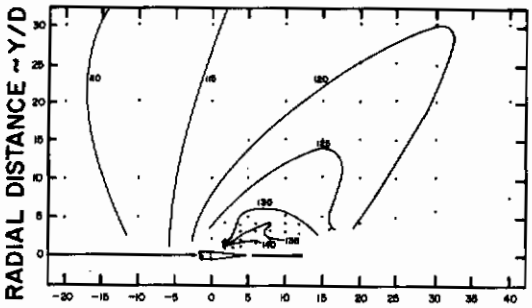


(m) FREQUENCY BAND, 1410-1780 CPS

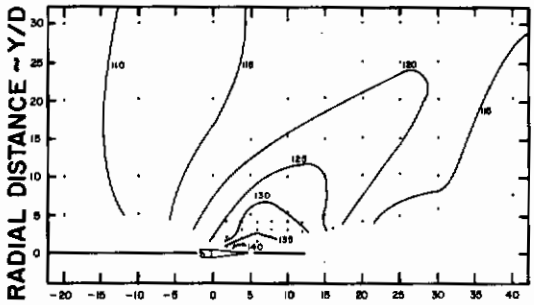


(n) FREQUENCY BAND, 1780-2240 CPS

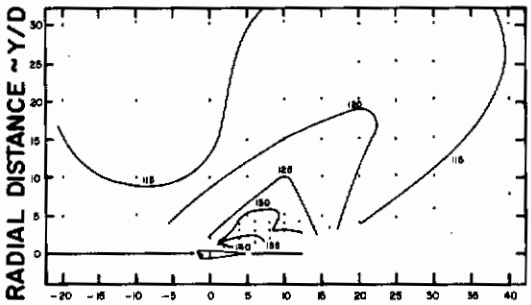


(o) FREQUENCY BAND, 2240-2820 CPS

Figure 5. (Concluded)

TABLE III

COMPARISON OF FACTORS AFFECTING NOISE MEASUREMENTS

| | DIAMETER (Ft.) | NOMINAL VELOCITY (Ft./Sec.) | EXIT HEIGHT (Ft.) | GROUND PLANE CONDITION | MICROPHONE | MICROPHONE AXIS (REFERENCE TO GROUND) | LEVEL INDICATING DEVICE |
|---|---|---|---|---|---|---|---|
| AFFDL | 1.85 | 1920 | 6.5 | CONCRETE | CONDENSER | PERPENDICULAR | TRUE RMS |
| Reference 2 | 1.85 | 1850 | 6.0 | GRASS | CONDENSER | PARALLEL (PERPENDICULAR TO JET AXIS) | QUASI-PEAK |
| Reference 1 | 1.73 | 1985 | 7.5 | GRASS | CRYSTAL | PARALLEL (POINTED TOWARD JET EXHAUST CENTER-POINT) | HALF-WAVE PEAK |
| Reference 3 | 1.75 | 1800 | 6.0 | CONCRETE | CONDENSER | PARALLEL | ---------- |

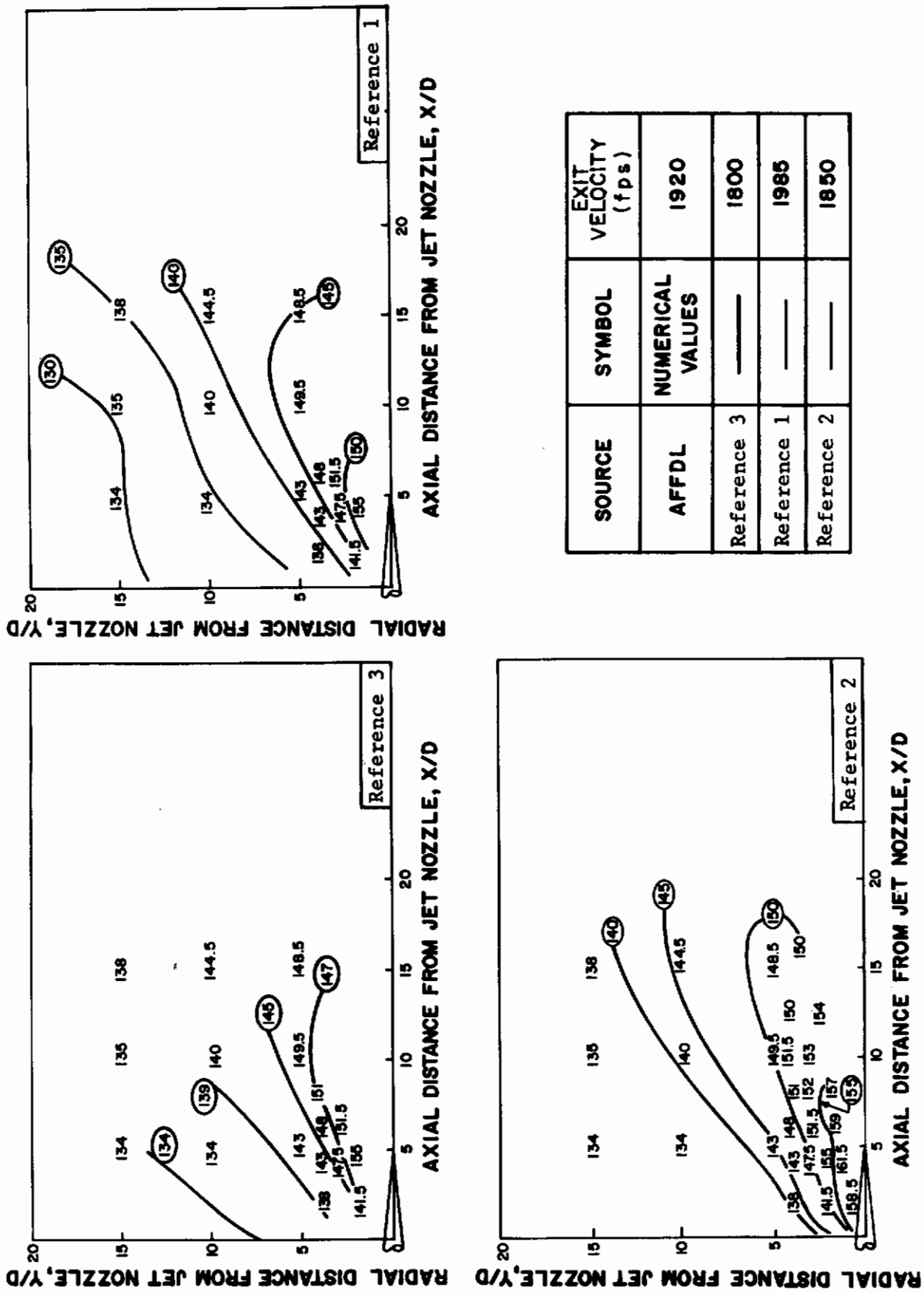


Figure 6. Comparison of Overall SPL Measurements

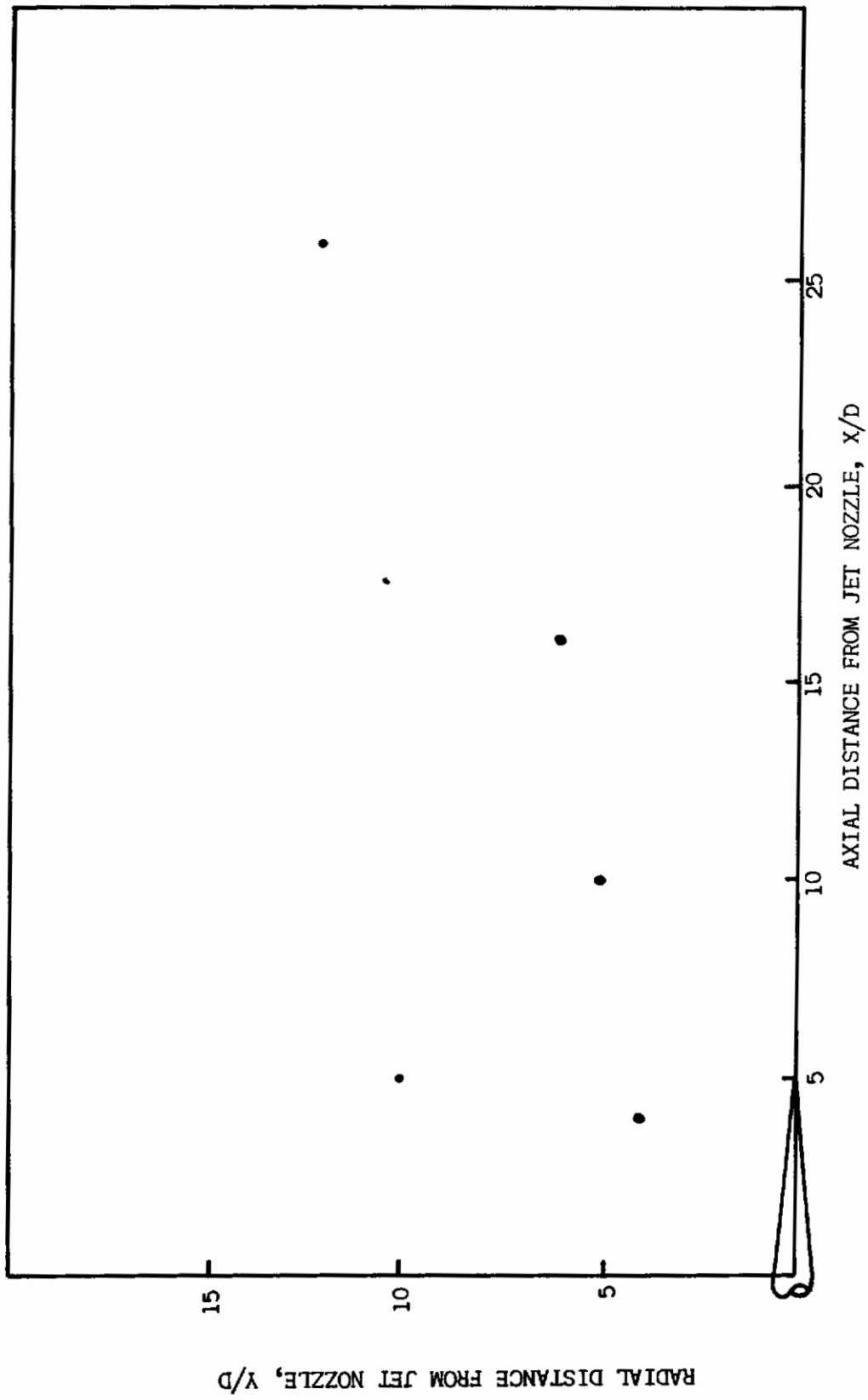


Figure 7. Locations for 1/3 Octave Spectra Comparisons

TABLE IV

MEASUREMENT LOCATIONS USED FOR 1/3 OCTAVE BAND SPL COMPARISONS

| (X/D,Y/D) | AFFDL | Reference 2 | Reference 3 | Reference 1 |
|---|---|---|---|---|
| (4,4) | Measurement at Location ↓ | Estimated from SPL Contours ↓ | Estimated from SPL Contours ↓ | Measurement at Location |
| (10,5) | | | | Measurement at (10.5,5) |
| (16,6) | Measurement at (15,5) | | No Data ↓ | Measurement at Location ↓ |
| (26,12) | Estimated from SPL Contours | | | |
| (5,10) | Measurement at Location | | Estimated from SPL Contours | Measurement at (5,10.7) |

Figure 8 shows the one-third octave spectra at the (X/D, Y/D) location of (4,4). All spectra have the same shape with the exception of the spikes which are present in Reference 2. These spikes occurred at all locations and were not considered when making comparisons. Differences of up to 7 db are encountered when comparing discrete one-third octave SPL's. The overall SPL's agreed well with the exception of the overall from Reference 2 which was slightly higher.

Figure 9 shows the one-third octave spectra at the (X/D, Y/D) location of (10,5). With the exception of Reference 3 data, there is good agreement of the spectra at this location. The overall SPL's agree well and differences in the one-third octave band SPL are up to 6 db.

Figure 10 shows the one-third octave spectra at the (X/D, Y/D) location of (16,6). Good agreement exists between the spectra and overall SPL's of AFFDL and Reference 2. Spectra from Reference 1show major differences as does the overall level. The overall SPL differences are considered to be 5.5 db while one-third octave band levels differ by as much as 9 db.

Figure 11 shows the one-third octave spectra at the (X/D, Y/D) location of (26, 12). At this location the overall levels agree very well. Fair agreement exists between the shape of the AFFDL and Reference 2 spectra. The peaks and valleys present in the Reference 1 spectra occur at different frequencies than those of AFFDL and Reference 2. Differences of up to 15 db occur in specific one-third octave band comparisons.

Figure 12 shows the one-third octave spectra at the (X/D, Y/D) location of (5,10). Fairly good agreement is shown with the exception of Reference 2 data. The differences in SPL's are up to 5.5 db for the overall and up to 8 db for the octave bands.

In summary, the SPL comparisons follow an expected trend with better agreement existing among the overall levels than among the one-third octave band levels. The major differences in the one-third octave band levels are caused by interference effects resulting from the presence of a ground plane. These effects are further discussed in section IV.

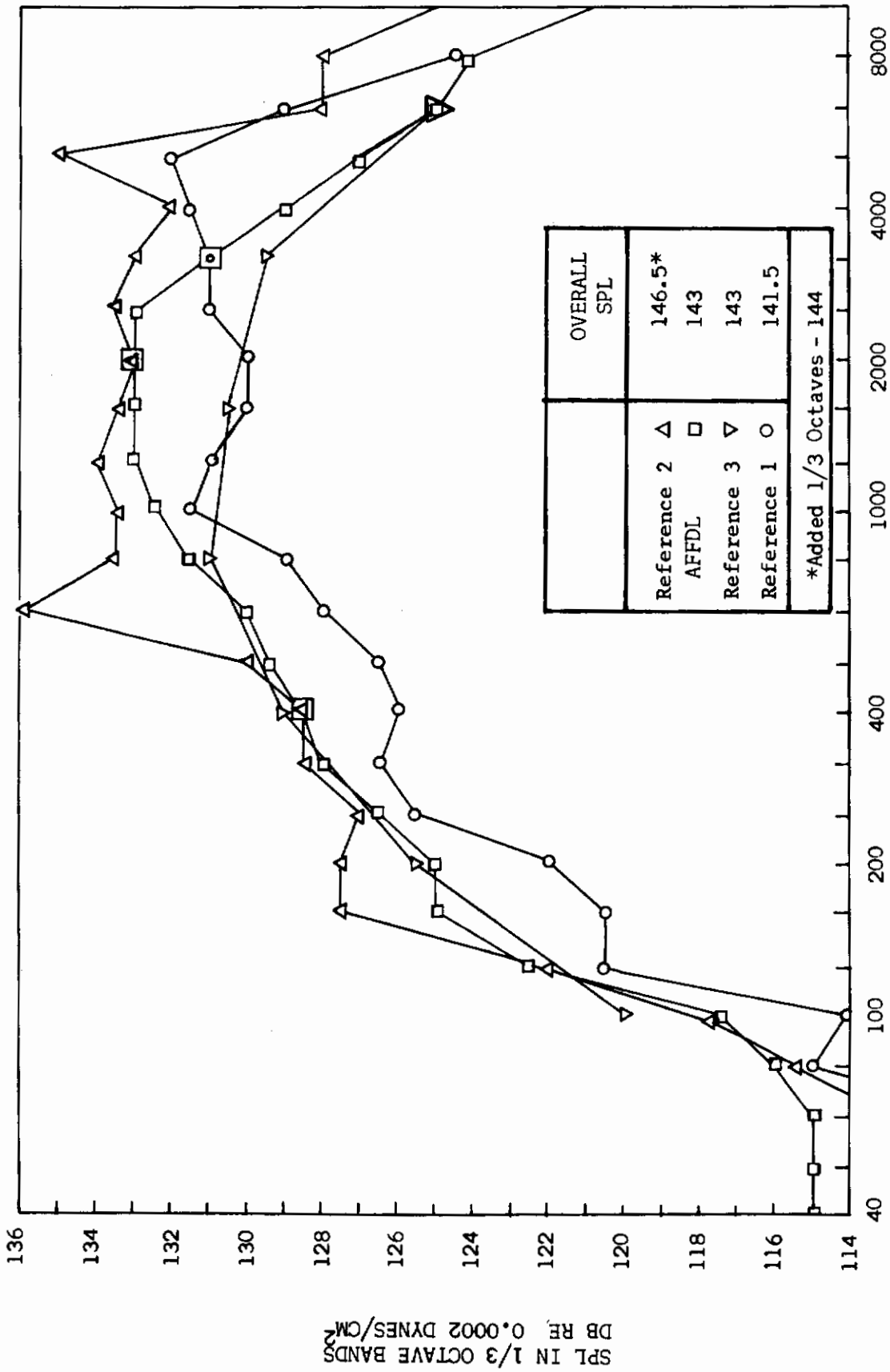


Figure 8. Comparison of 1/3 Octave Spectra at (X/D, Y/D) of (4,4)

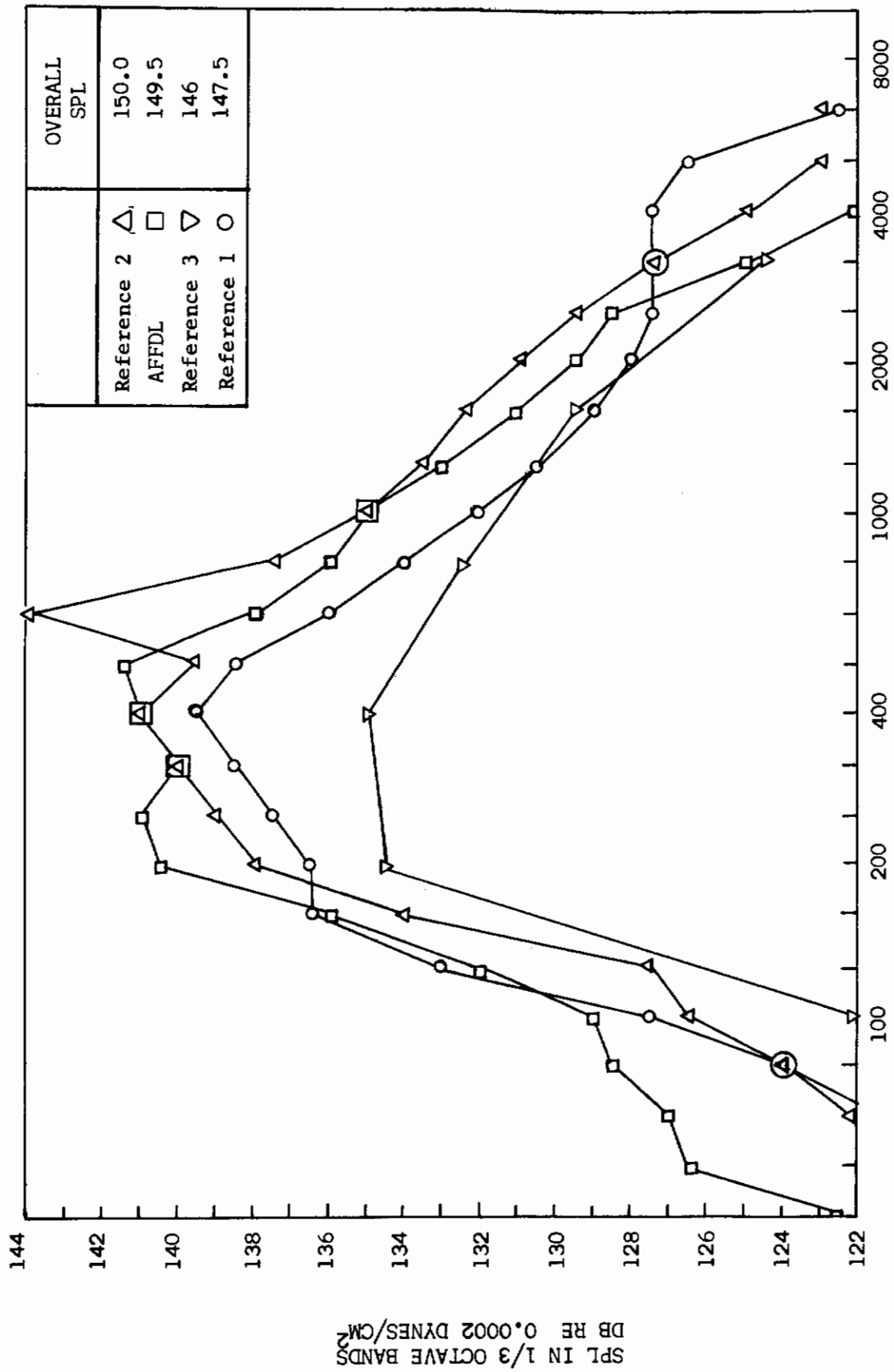


Figure 9. Comparison of 1/3 Octave Spectra at (X/D, Y/D) of (10,5)

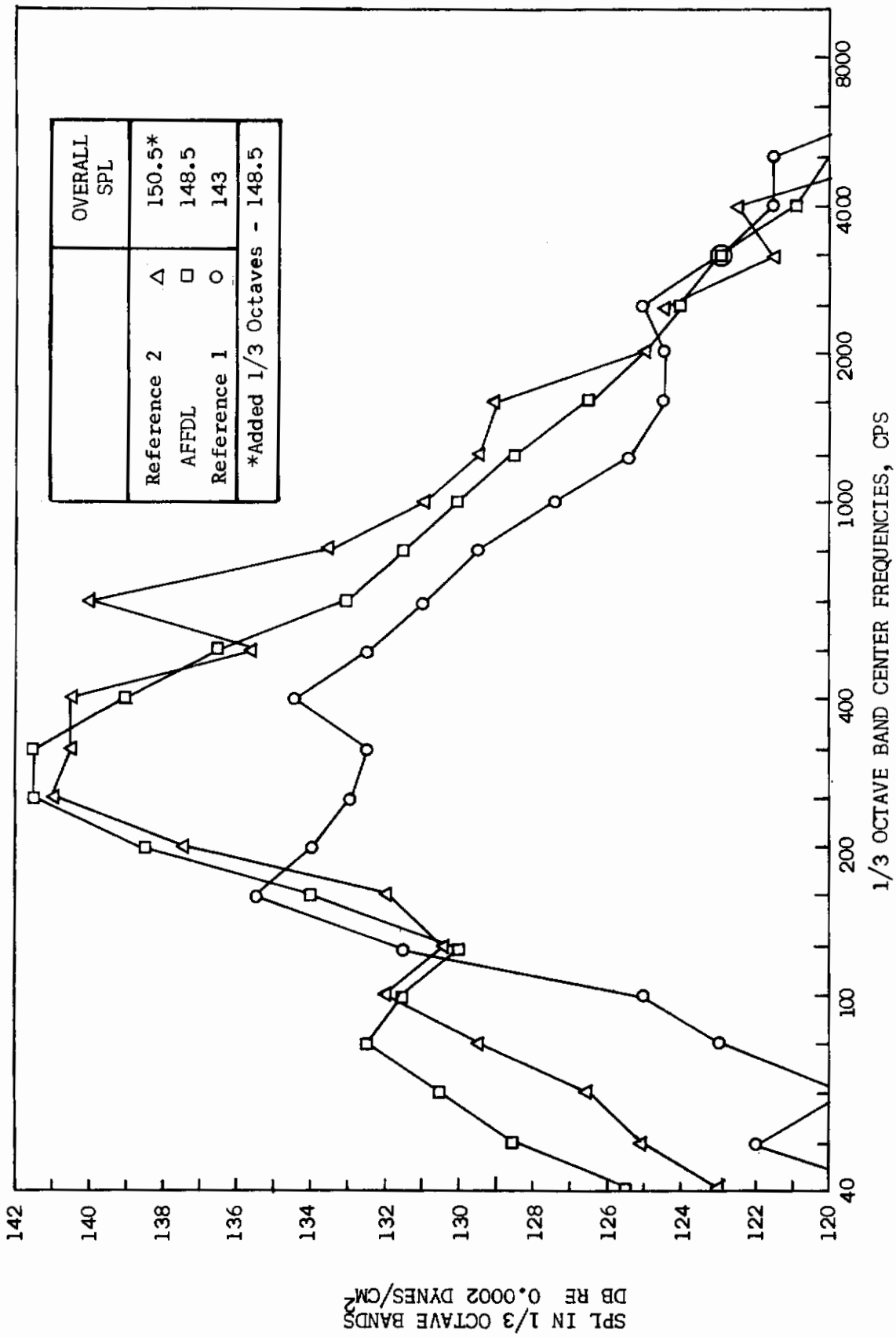


Figure 10. Comparison of 1/3 Octave Spectra at (X/D, Y/D) of (16,6)

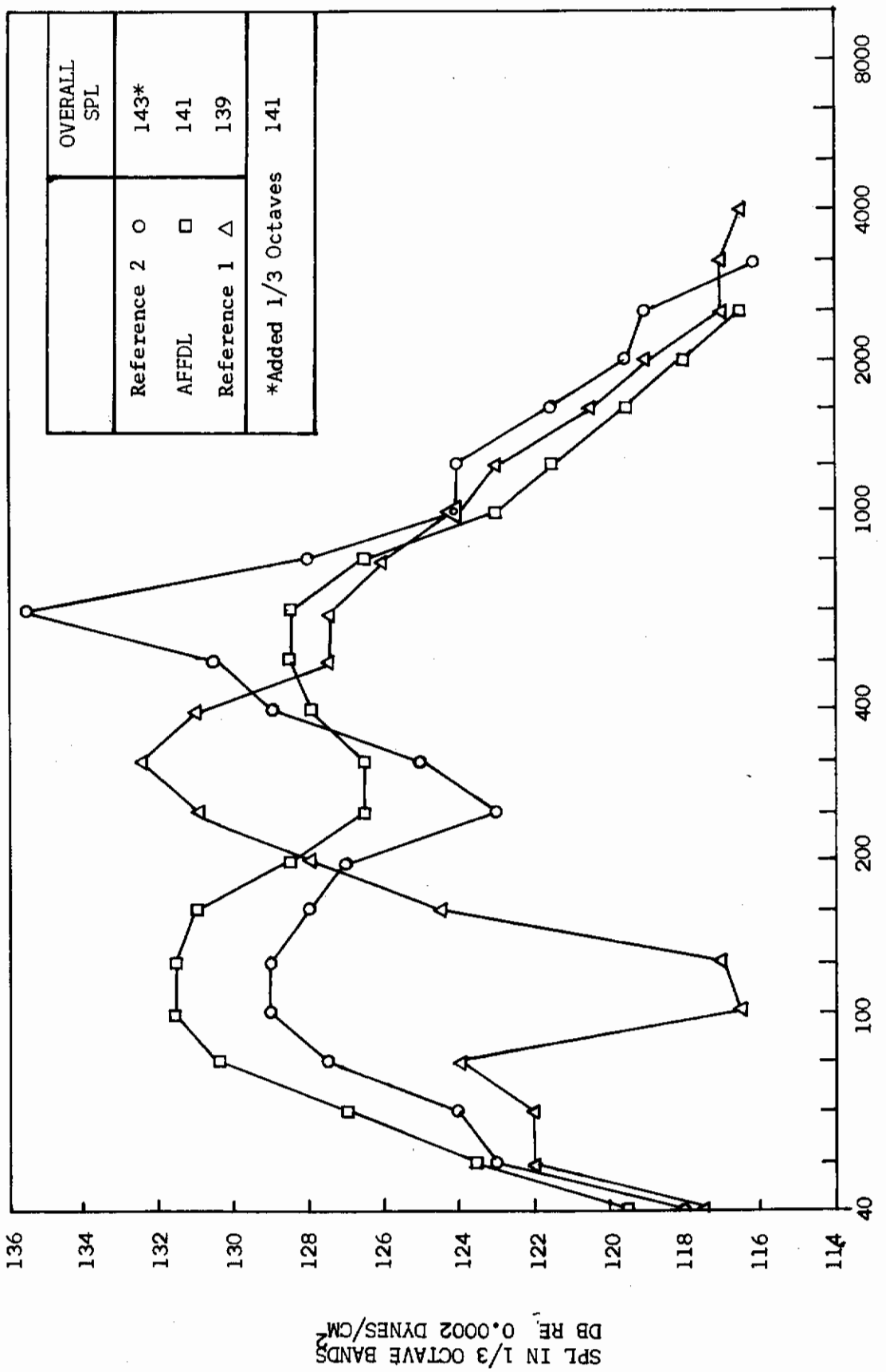


Figure 11. Comparison of 1/3 Octave Spectra at (X/D, Y/D) of(26,12)

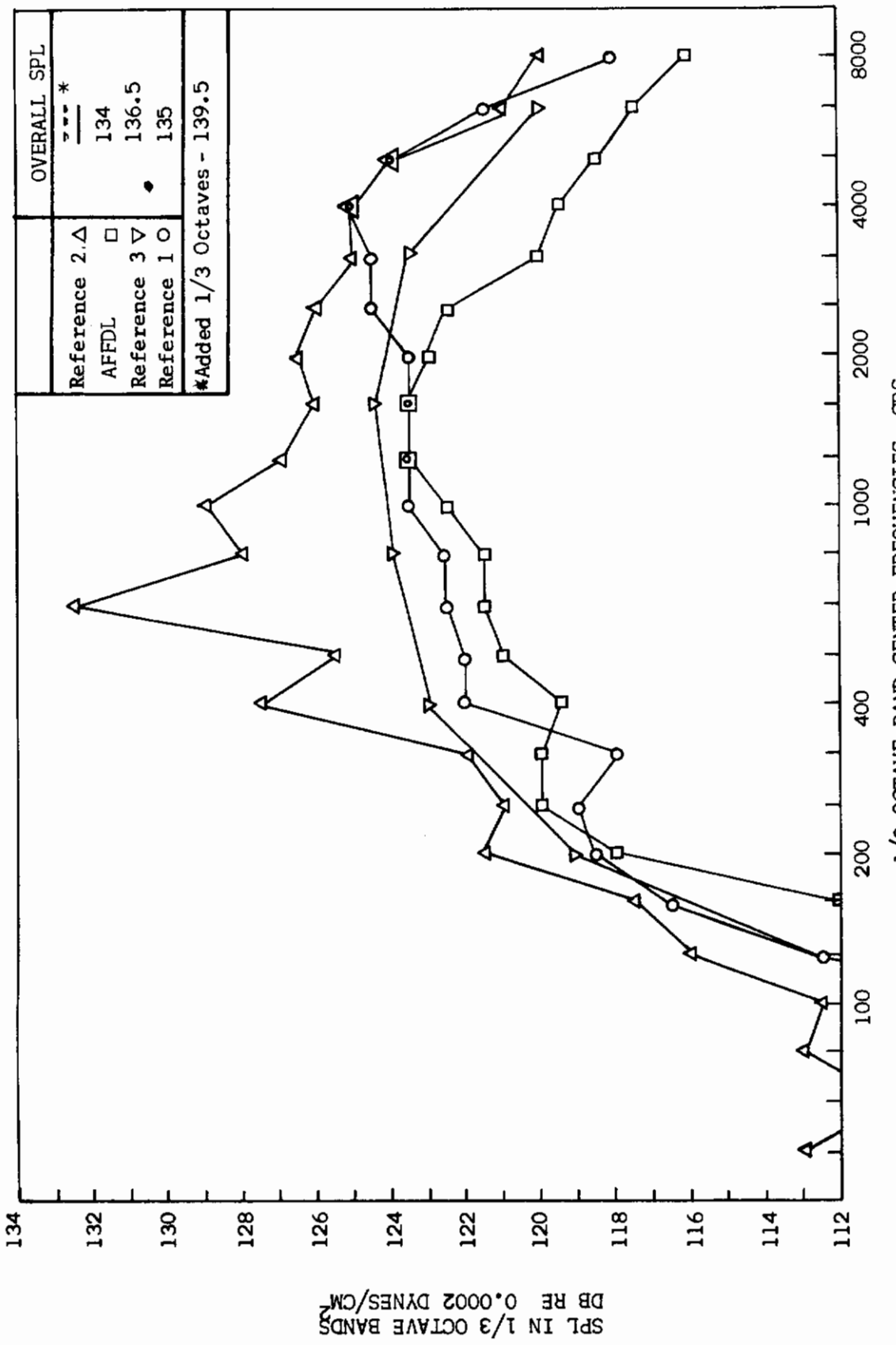


Figure 12. Comparison of 1/3 Octave Spectra at (X/D, Y/D) of (5,10)

# SECTION IV

# GROUND REFLECTION EFFECTS ON MEASURED DATA

## 1. INTRODUCTION

The measurement programs discussed in the previous section were all conducted with a turbojet engine exhausting parallel to and above a ground plane. The presence of the ground plane results in a modification of the noise field that would have existed under free-field conditions. The microphone not only senses the noise signal received directly from the source, but also senses the noise signal received from the source via the ground reflection path. The microphone output represents a summation of the signals received from these two different paths. The summed level is either higher or lower than a free-space level according to the phase relation between the two received signals, i.e., the resulting interference can either reinforce or attenuate the direct path noise signal. In evaluating the effects of ground reflection, the approach of Howes (Reference 10) was used.

This approach consists of selecting the equivalent noise source location for each one-third octave band and plotting the SPL as a function of log distance from the source location along a radial line from the noise source. A decay slope is then drawn tangent to the peaks of this plot. The measured levels are then corrected to this decay slope. These corrected levels represent the condition of perfect reinforcement. The corrected one-third octave SPL's are then summed to obtain the corrected overall SPL. The overall and one-third octave free-field SPL's are obtained by assuming a difference of 3 db between the corrected and the free-field levels.

An example of the above procedure is presented in the next subsection for one specific location.

## 2. EMPIRICAL APPROACH

Spot 54 was selected for evaluation of interference effects as a result of its spectral peaks and valleys. The preceding procedure was followed for both the 100 percent and the 50 percent engine settings. The noise source locations were assumed at the position of the maximum SPL measured along the 10-degree boundary. Figures 13 thru 16 present the $f_c$ = 400 and 800 cps decay slopes for the 100 percent and 50 percent engine settings. These one-third bandwidths represent the maximum interference effects at Spot 54.

The measurement locations of this program were not specifically selected for studying interference effects. As a result, data were not available at exactly the desired locations to determine the decay slopes given in these figures. However, the points used were within one nozzle diameter of all desired locations. In Figure 13 it was assumed that the reinforcement peaks follow the "Inverse Square Law." This assumption was required as a result of insufficient data beyond Spot 54 to define the decay slope.

Figures 13 thru 16 illustrate how corrections were obtained to adjust the measured levels to the conditions of perfect reinforcement. For example, from Figure 13, a value of +9.5 db was added to the measured level. Similar decay slopes and corrections were obtained at this location for one-third octave bands with center frequencies between 80 and 1600 cps. These corrections are shown in Figures 17 and 18 for the 100 percent and 50 percent engine settings. The corrected spectra have the shape of the free-field spectra but have maximum reinforcement levels. The free-field spectra are obtained by subtracting 3 db from the corrected spectra since perfect reflection was initially assumed.

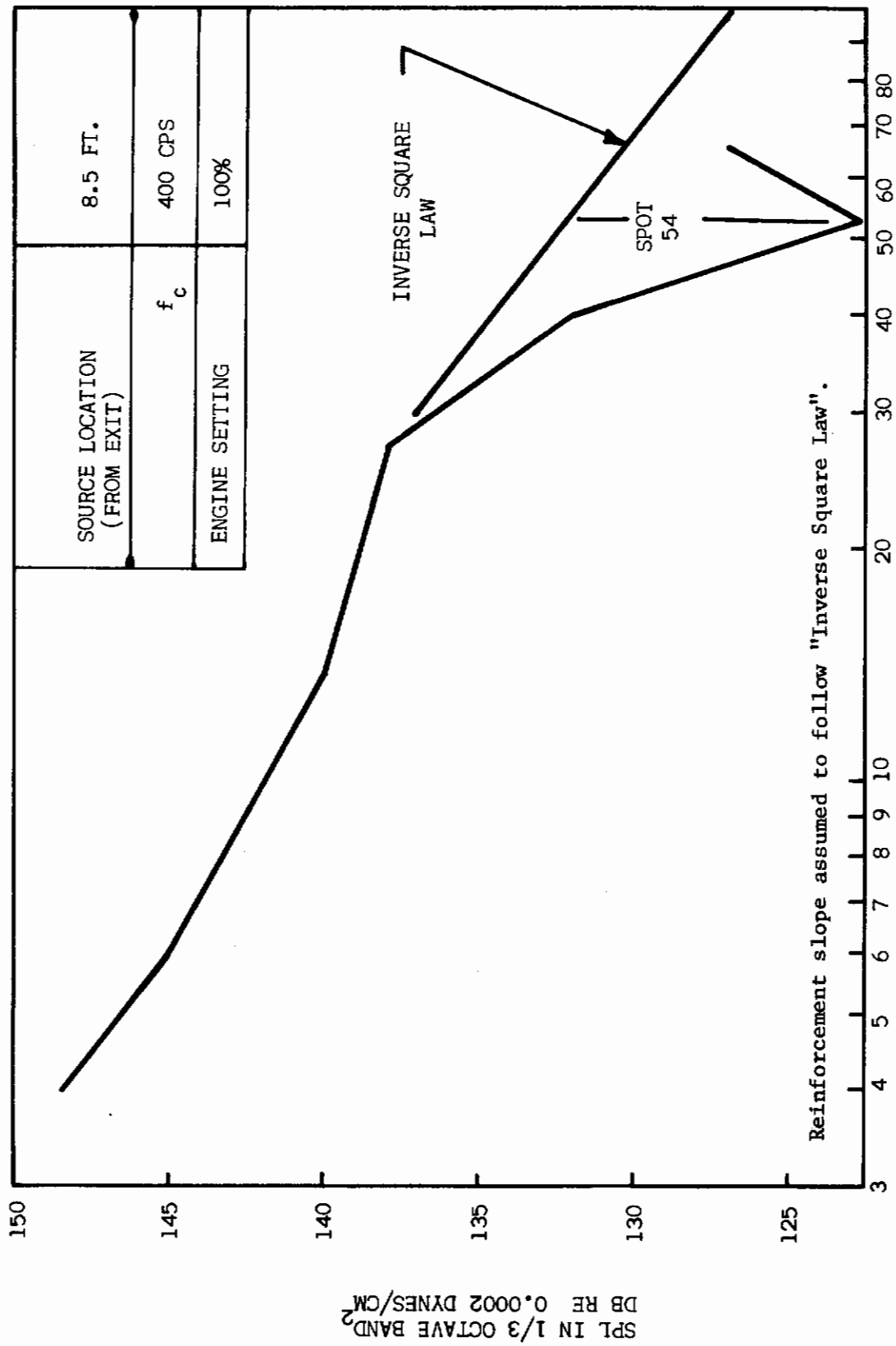


Figure 13. One-Third Octave Band SPL Decay Slope Thru Spot 54

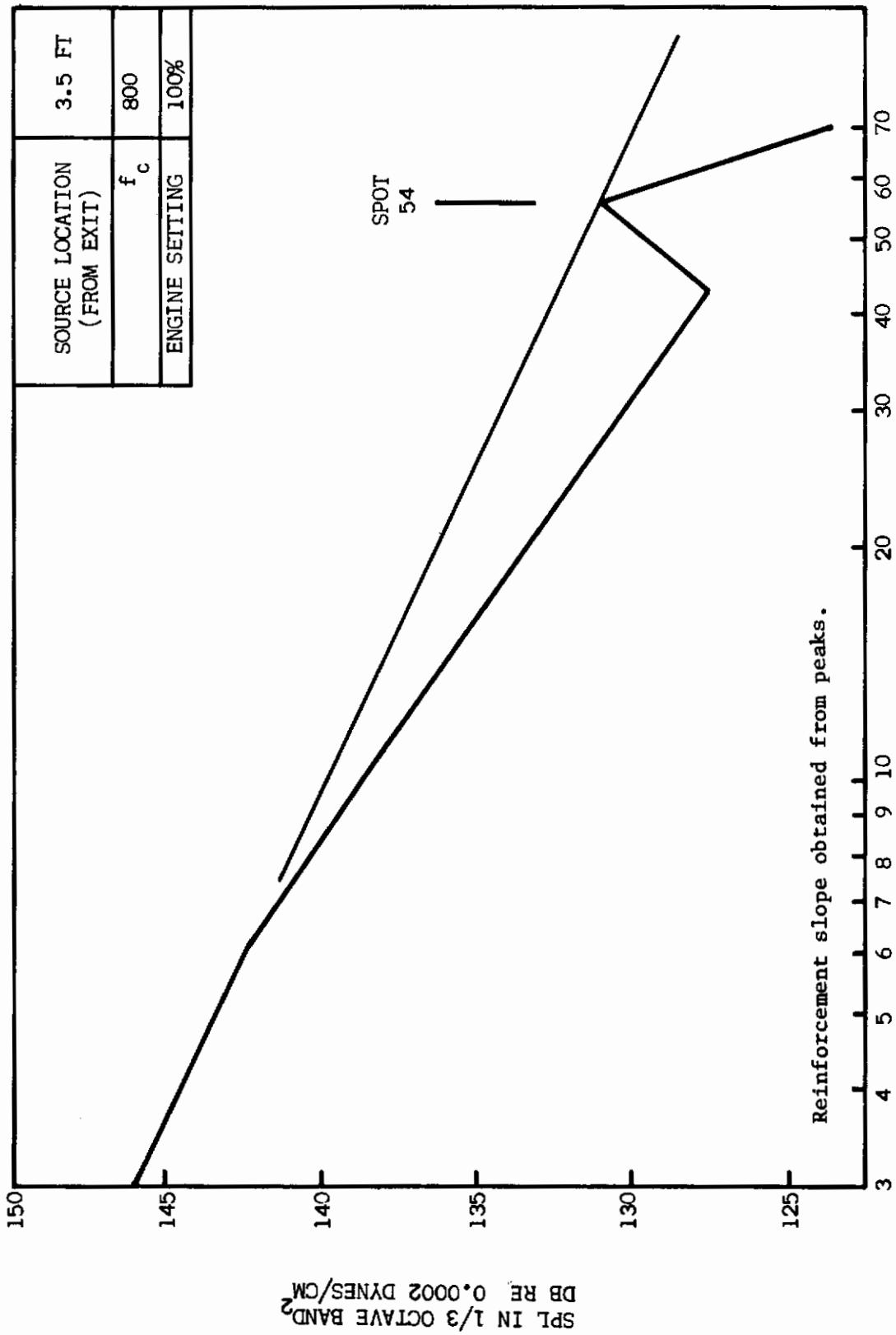


Figure 14. One-Third Octave Band SPL Decay Slope Thru Spot 54

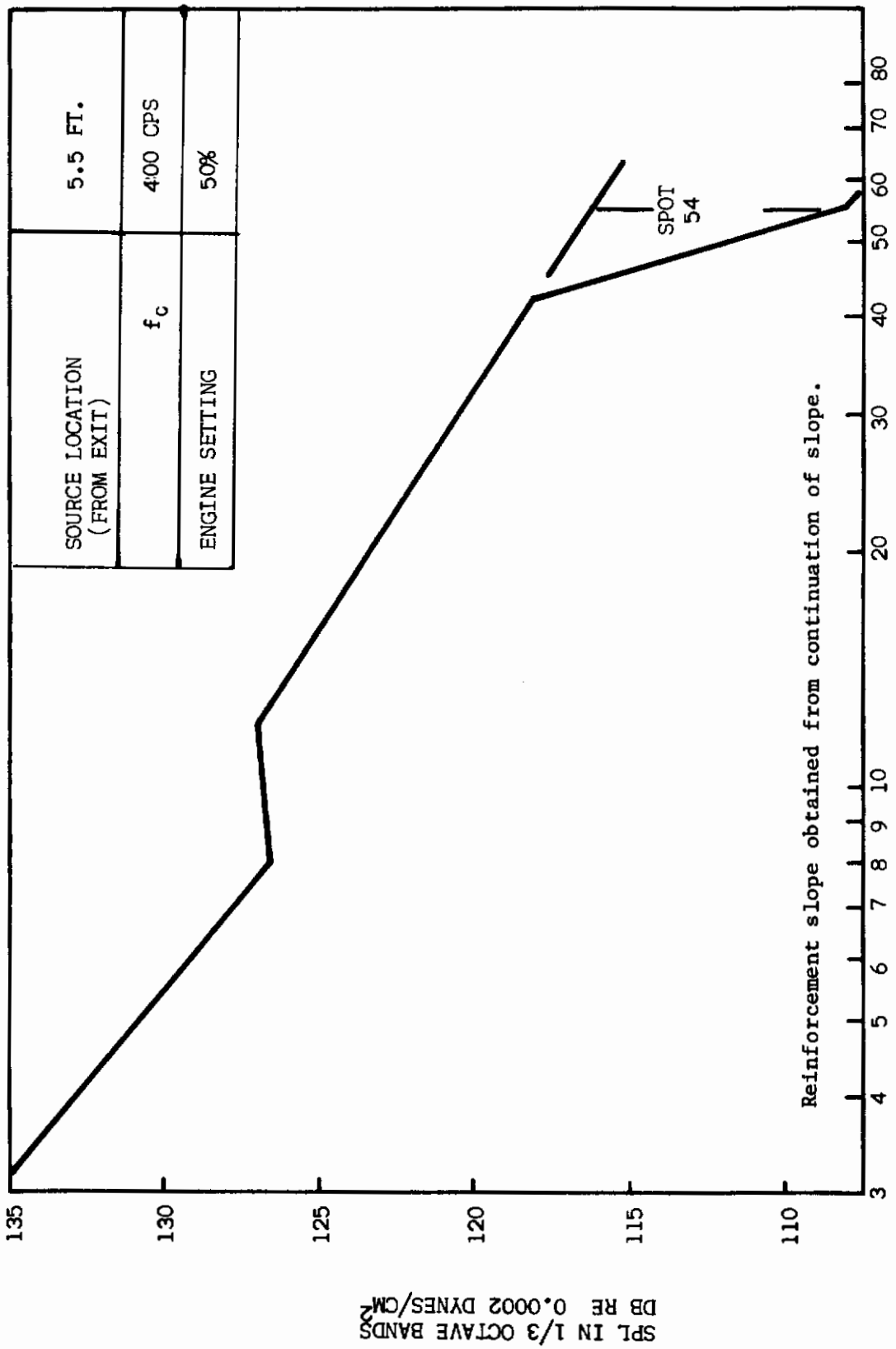


Figure 15. One-Third Octave Band SPL Decay Slope Thru Spot 54

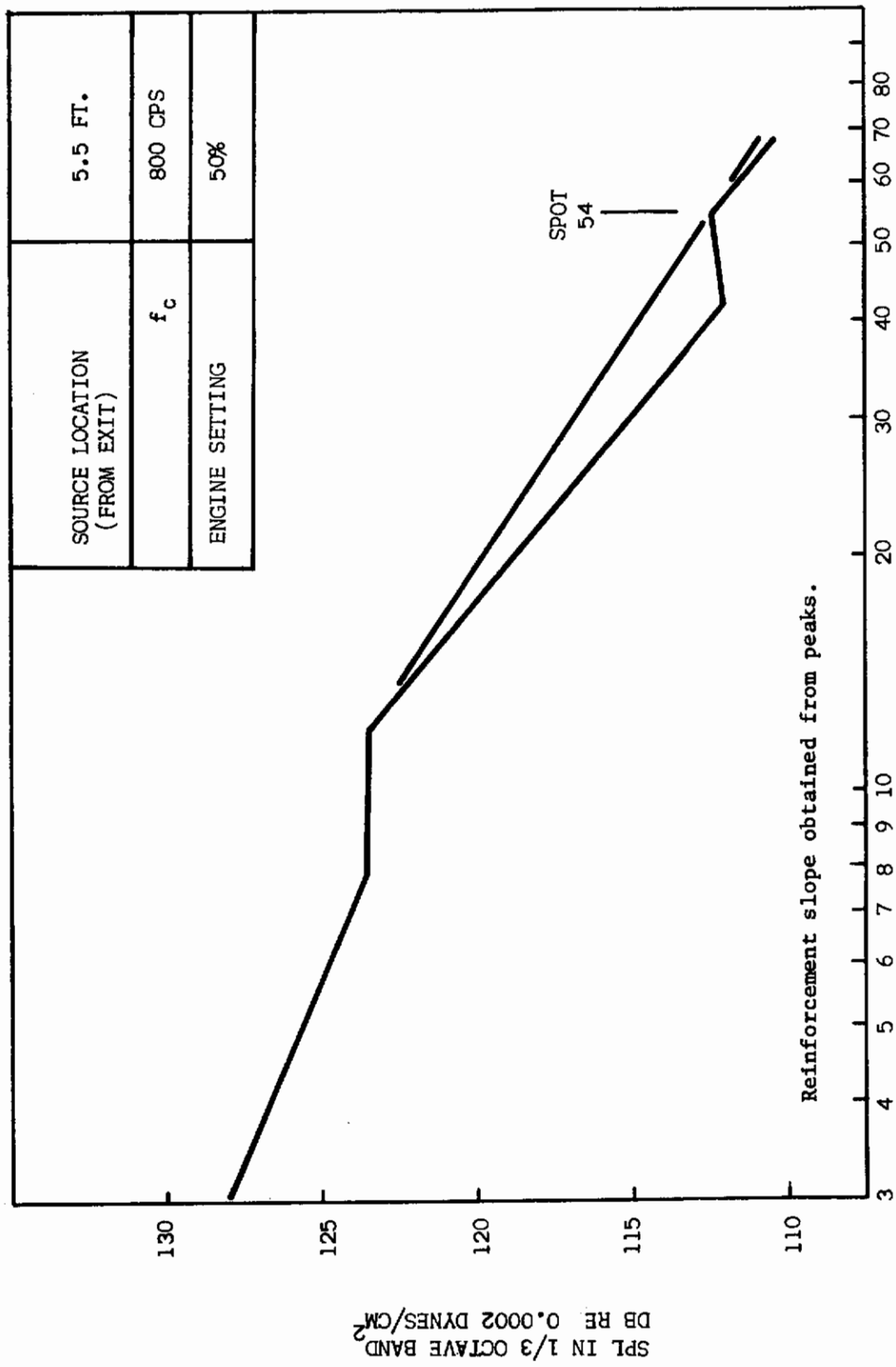


Figure 16. One-Third Octave Band SPL Decay Slope Thru Spot 54

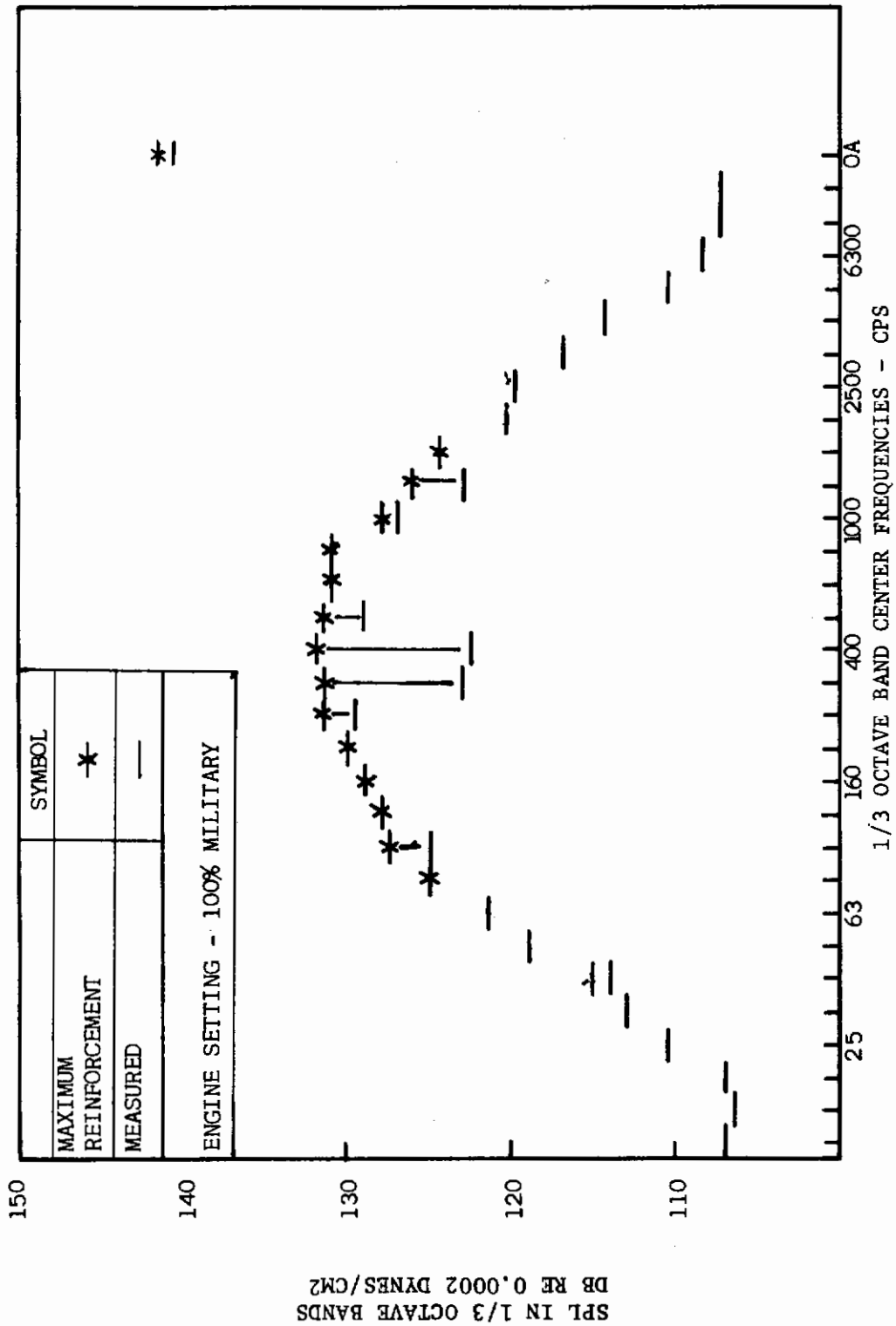


Figure 17. Spot 54 One-Third Octave Spectrum Corrected to Maximum Reinforcement Levels

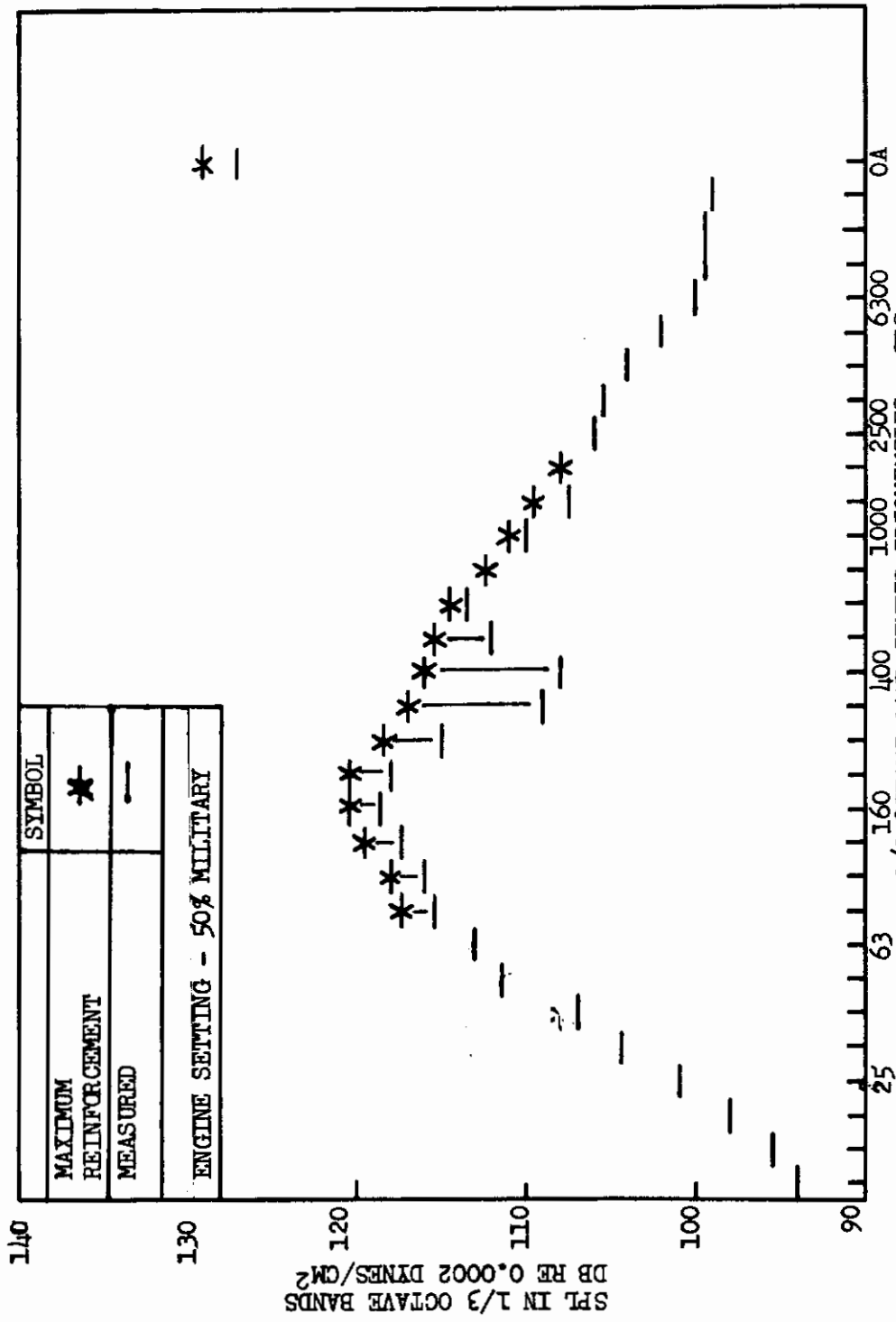


Figure 18. Spot 54 One-Third Octave Spectrum Corrected to Maximum Reinforcement Levels

These smoothly varying corrected spectra indicate that the above approach does indeed account for the interference effects resulting from the ground plane.

The approach may also be applied to measurements where sufficient data are available to determine the necessary decay slopes. When sufficient data are not available, a theoretical approach to account for interference effects may be used as a first approximation. Such an approach is presented in the next subsection.

3. THEORETICAL APPROACH

This approach provides a relation between the measured and free-field spectra. The necessary information to obtain this relation is presented by Howes in Reference 10. As applied to the present measurements, this approach takes the following form.

The one-third octave band noise source locations are assumed to be at the position of the highest SPL along the jet boundary. These locations may be estimated from the following equation presented in Reference 2,

$$f_c \; D/V = (1.25\, X/D)^{-1.22} \tag{1}$$

where, $f_c D/V$ is Strouhal number, X/D is the nondimensional axial distance. The one-third octave source locations from the present measurements agreed very well with Equation 1.

For an arbitrary receiver location, it is possible to determine the frequencies for which the maximum interference effects occur. These frequencies may be determined for one-third octave bands from the following relation:

$$f_c = \frac{nc}{\sqrt{r^2 + 4h^2} - r} \tag{2}$$

where r is the distance between source and receiver,
h is the source and the receiver heights above the ground plane,
$f_c$ is the one-third octave band center frequency,
c is the ambient speed of sound,
n is a series of values where maximum signal reinforcements occur when n = 1,2 and maximum signal attenuations occur when $n = \frac{1}{2}, \frac{3}{2}, \frac{5}{2}$.

Since r is dependent on $f_c$, an iterative approach is required to obtain a solution.

Figure 19 presents the locations for the conditions of maximum reinforcement as applied to the present measurement locations designated by spot numbers. These locations were obtained by using the one-third octave band noise source locations from Equation 1 as the centers of the circles and source-to-receiver distances from Equation 2 as the radii where n = 1. Very good agreement was found between Figure 19 and the measured spectral peaks of the data in Appendix II.

The relation between the free-field and measured mean square sound pressures is given by,

$$\frac{\overline{P_m^2}}{\overline{P_{FF}^2}} = 1 + \frac{r^2}{r^2+4h^2} + 2\sqrt{\frac{r^2}{r^2+4h^2}}\left[\frac{\sin\left[.728\, f_c\left(\frac{\sqrt{r^2+4h^2}-r}{c}\right)\right]\cos\left[6.32\, f_c\left(\frac{\sqrt{r^2+4h^2}-r}{c}\right)\right]}{.728\, f_c\left(\frac{\sqrt{r^2+4h^2}-r}{c}\right)}\right] \tag{3}$$

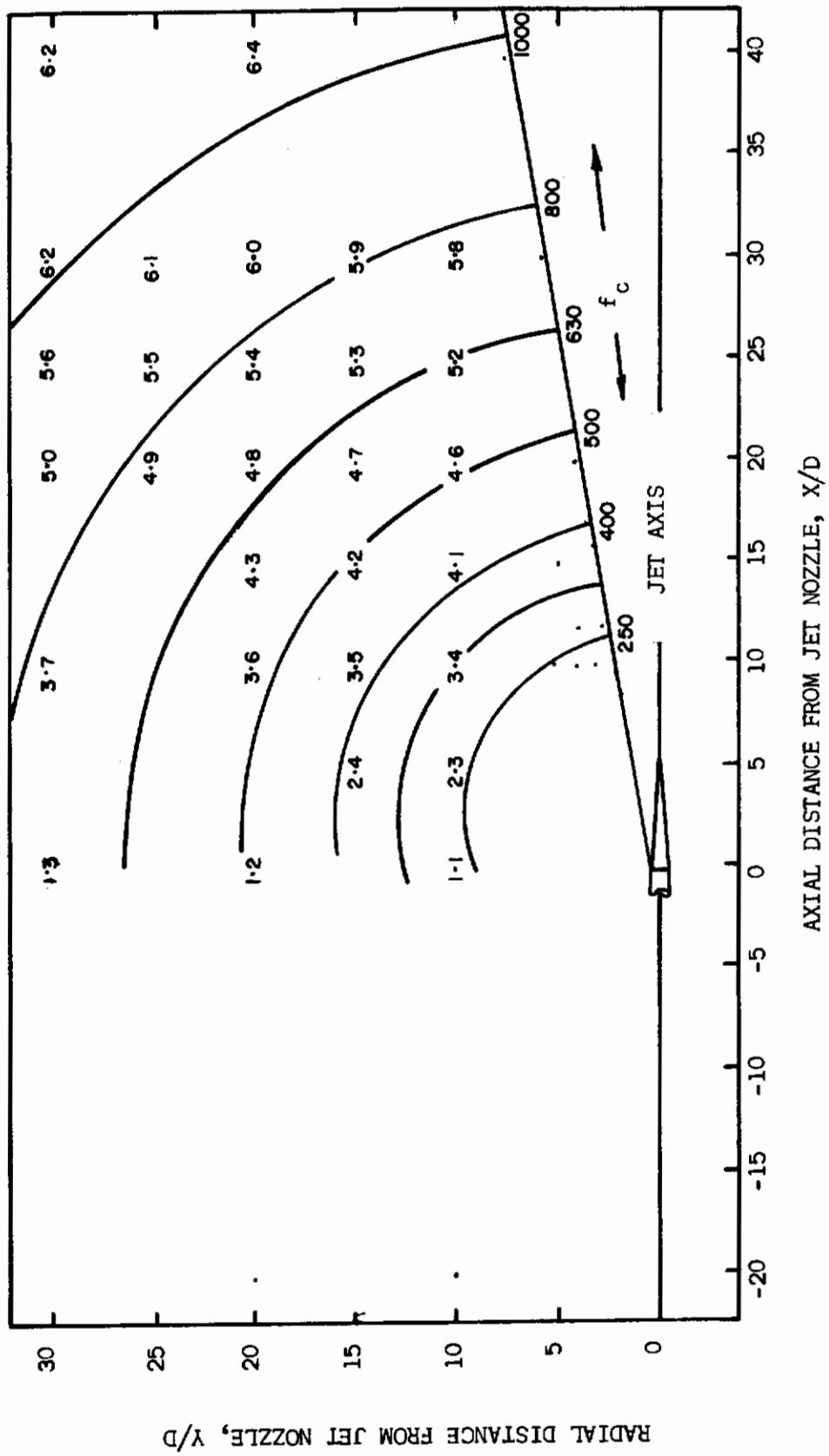


Figure 19. Locations of Maximum Reinforcement for 100% Military Engine Setting

where $\overline{P_m^2}$ is the mean square sound pressure measured in the sound field above a perfectly reflecting ground plane and $\overline{P_{FF}^2}$ is the mean square sound pressure that would exist if the ground plane were not present. This equation is a modified form of an equation given in Reference 10.

The correction in decibels from free-field to measured is given by:

$$\Delta SPL = SPL_m - SPL_{FF} = 10 \log \frac{\overline{P_m^2}}{\overline{P_{FF}^2}} \quad (4)$$

In the third term of Equation 3, the value of sin X/X approaches one as X approaches zero and zero as X becomes large. When the sin X/X approaches one, the third term varies as the cosine function. Equating the argument of the cosine to $2\pi n$ results in Equation 2.

With the above considerations, the frequency spectrum may be divided into three distinct frequency regions for any given r. The first region contains those frequencies associated with n values from 0 to $\frac{1}{4}$. In this region, the $\Delta$SPL is a slowly varying value from 6 to 3 db. The second region contains those frequencies associated with n values from $\frac{1}{4}$ to $\frac{5}{2}$. In this region, the $\Delta$SPL is a rapidly changing value form +6 to $-\infty$ (-15 db for practical considerations). The third region is the $f_c$ range associated with n values greater than $\frac{5}{2}$. In this range, the $\Delta$SPL is essentially a constant 3 db.

As applied to the present measurements, corrections were obtained only for those center frequencies in the second range. A constant 3 db difference was used in the first and third frequency range.

Figure 20 presents the results obtained using Equation 3 to compute the interference spectrum from Spot 54 from an assumed free-field spectrum. This free-field spectrum is obtained by subtracting 3 db from the maximum reinforcement spectrum levels of Figure 17. Good agreement is found between the computed and measured interference spectra of Spot 54 with a maximum error of 3.5 db occurring at $f_c$ = 400 cps.

Although good agreement is found at this location, it should not be assumed that this approach will work equally well for all locations.

In summary it can be seen from both the empirical and the theoretical evaluation that ground reflection is an important factor in sound field distribution. Comparison among measurement programs or between measured and estimated spectra will have little meaning until methods can be developed which will account for the different factors affecting the noise field. An approach towards this is given in Section V.

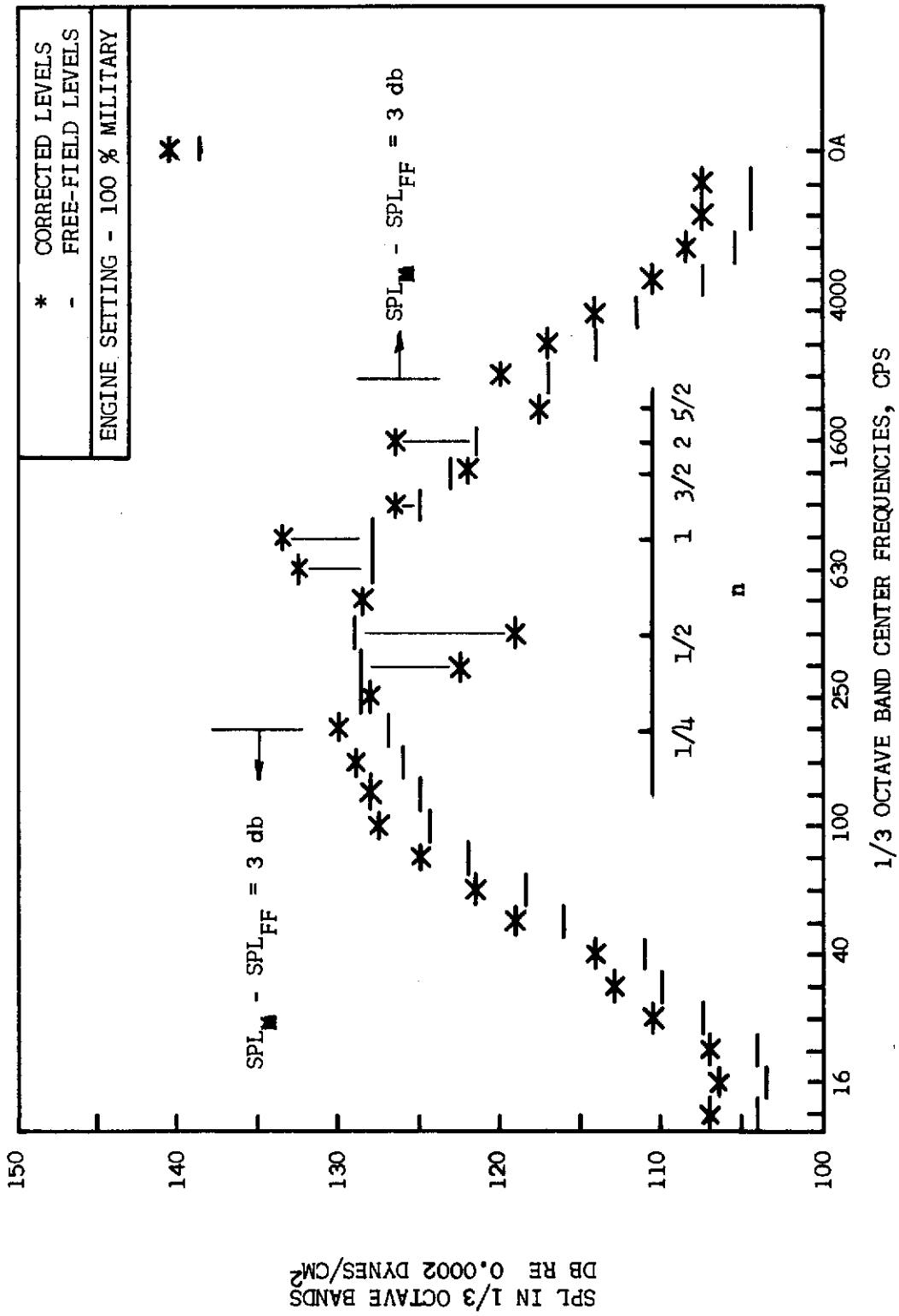


Figure 20. Theoretical Corrections to Empirical Free-Field Spectrum of Spot 54

# SECTION V

# VELOCITY EXPONENT

## 1. INTRODUCTION

The J57-P21 survey included measurements at each of the 65 locations with the engine operating at 50, 70, 96 and 100 percent of military power. From these measurements a velocity index was determined at each point from:

$$\overline{P^2} \alpha V_j^n \tag{5}$$

where P is the rms sound pressure and $V_j$ is the jet velocity.

This expression is derived from a relation for the total acoustic power (TAP) developed by Lighthill (Reference 11):

$$TAP \alpha \frac{\rho_j^2 D_j^2 V^8}{\rho_0 c_0^5} \tag{6}$$

where $\rho_j$ and $\rho_0$ are the jet and ambient densities, $D_j$ is the exit diameter, and $c_0$ is the ambient speed of sound.

For the non-afterburner engine power settings considered here the exit diameter was constant and the variations in $\rho_0$ and $c_0$ were negligible. This results in the total acoustic power being proportional to the square of the jet density and the eighth power of the jet velocity.

Although this relation applies to the entire sound field, it was also assumed at each point that:

$$\overline{P^2} \alpha \rho_j^2 V^n \tag{7}$$

Assuming first that the density has little effect on the value of n, Equation 7 reduces to Equation 5. The procedures used to determine n were to plot on semilog paper the overall SPL for each operating condition relative to the SPL for the 50 percent condition versus the corresponding jet velocity. A best fit straight line was then drawn through the data points. Two points on this straight line were then used to compute n from:

$$n = \frac{SPL_1 - SPL_2}{10\left[\log V_1 - \log V_2\right]} \tag{8}$$

This equation follows from the proportion in Equation 5 and the following definition:

$$SPL = \log \frac{\overline{P^2}}{\overline{P_{ref}^2}} \tag{9}$$

where the subscript 1 and 2 refer to specific conditions.

Had the effect of $\rho_j$ been included the equation for n would be:

$$n = \frac{SPL_1 - SPL_2}{10 \log \frac{V_1}{V_2}} + \frac{20 \log \rho_j 2/\rho_j 1}{10 \log \frac{V_1}{V_2}} \quad (10)$$

which differs from Equation 8 by the second term. Although no detailed calculations were made, it was determined for the condition of this test that the inclusion of the variation in $\rho_j$ would increase the value of n by approximately one. A similar effect of jet density was determined by Middleton in Reference 1.

Figure 21 presents the values of the velocity indexes at the measurement locations and the contours of the n field. The discrete values of n were calculated from Equation 8 using two points on a best fit line through all the data points for each location.

Although these values are given to the nearest tenth, their accuracies fall within ±0.5. Because of this range of accuracy, the contours are presented primarily to show trends in the n field rather than actual values.

Comparisons of the n contours of the present investigation to the n contours of Reference 1 and Reference 3 are presented in Figure 22. Calculated n values from Reference 3 were based on the assumption that sound pressure rather than the square of the sound pressure is proportional to $V^n$. The resulting calculated n value would be one-half the value obtained in Equation 8. Thus a correction factor of two was applied to the Reference 3 n values for the purpose of comparison. Calculated n values from Reference 1 include a correction for the effects of jet density as given in Equation 10. This correction is not included in the comparison since no similar correction was made to the data of the present investigation. In addition, the Reference 1 n values were presented as a function of angle from the jet axis for constant radii. The method of approximating contours between the 30 and 50 feet radii is questionable, but necessary for comparison. Agreement of the n contours seems to be more a matter of coincidence rather than a general rule.

Velocity indexes were also obtained for bandwidths of sound pressure using the same procedure used for the overall sound pressure indexes. These indexes are presented in Figures 23 thru 26 and cover the 90-180, 180-360, 360-720, and 720-1440 cps bandwidths, respectively. The SPL's of these bandwidths are the summation of the included three one-third octave band levels. These bandwidths most closely approximate the octave bandwidths commonly used in jet engine noise measurements.

## 2. GROUND REFLECTION EFFECTS

An investigation into the effects of ground reflection on the overall n field was motivated by the poor agreement among measured n fields and by the oscillating nature of the AFFDL n field. The oscillating values of n taken along radial lines emanating from the assumed noise source location could result from similar oscillations in the center frequency at which the peak level occurs in the one-third octave spectrum. These variations in the peak frequency result from signal interference due to the reflecting ground plane.

The approach used in accounting for the interference effects on the overall SPL measurements and hence the calculated n values is similar to that used in the previous section for the one-third octave band SPL measurements. The overall SPL decay slopes are drawn for the 100 and 50 percent engine settings and the measured SPL's are corrected to the decay slope values for each location. Figures 27 and 28 illustrate this procedure along a radial line. Similar decay slopes and corrections were obtained for other radial lines.

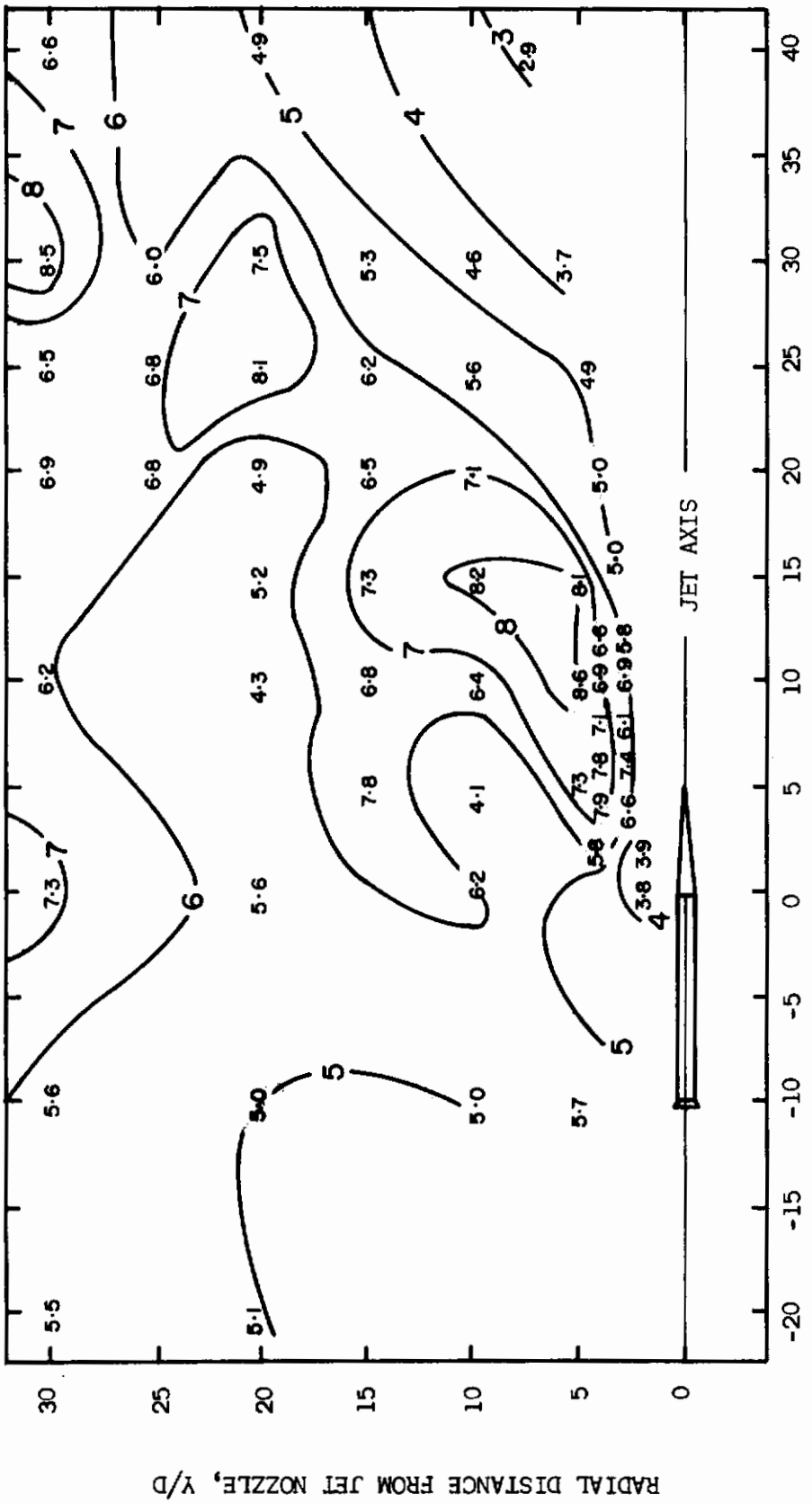


Figure 21. Overall SPL Velocity Exponent Field

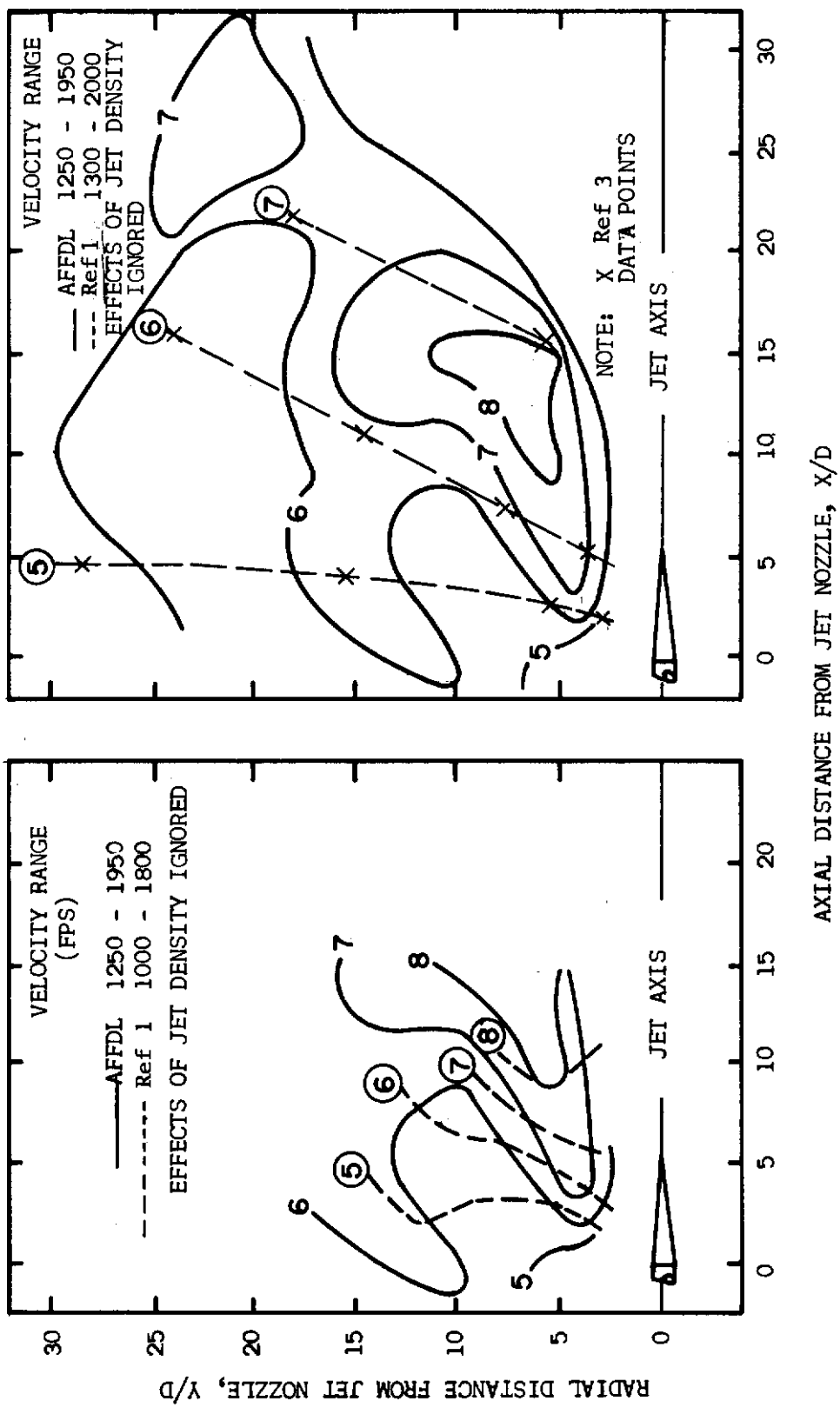


Figure 22. Comparisons of Overall n Contours

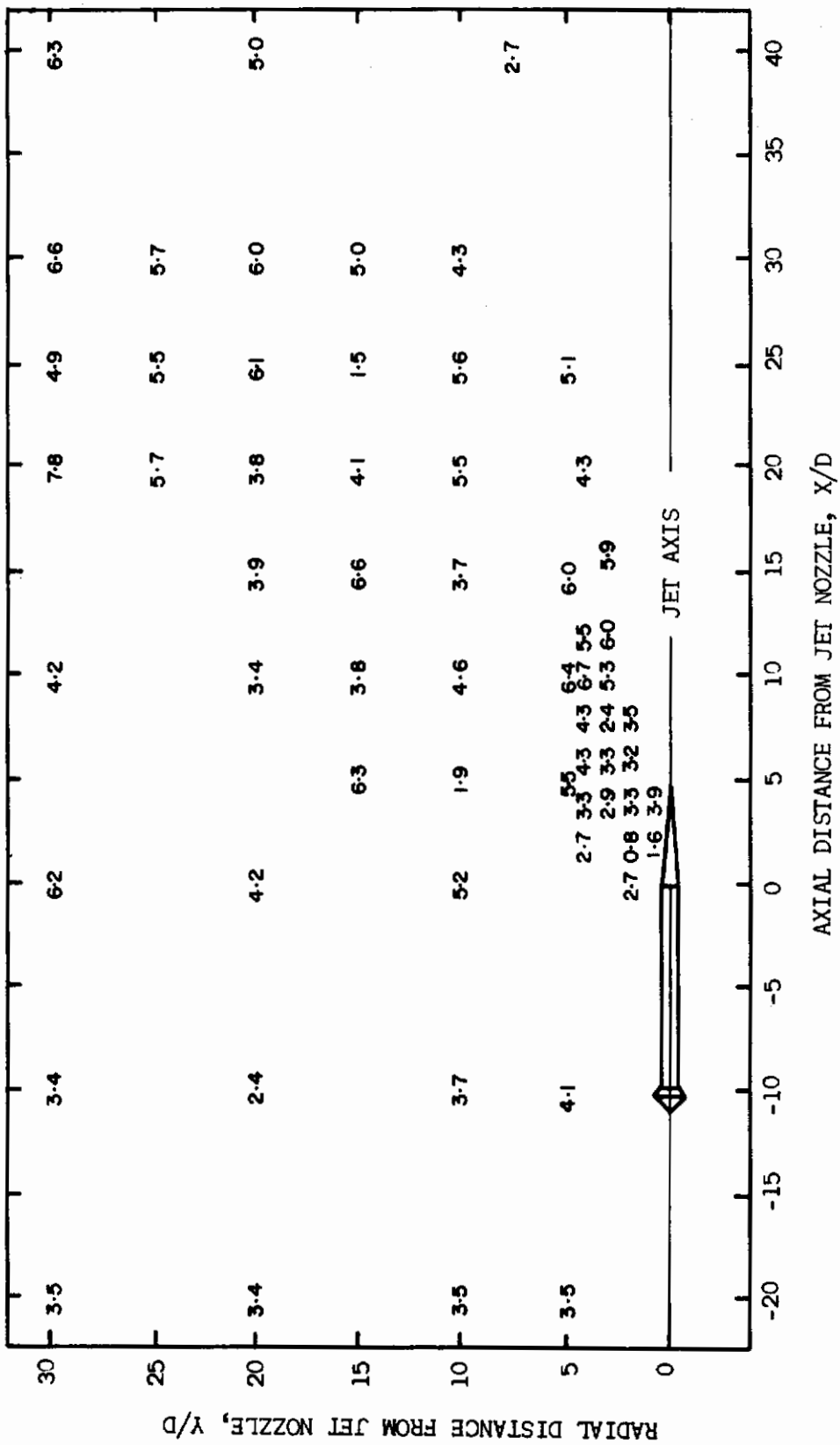


Figure 23. Velocity Indexes for Frequency Band 90-180 CPS

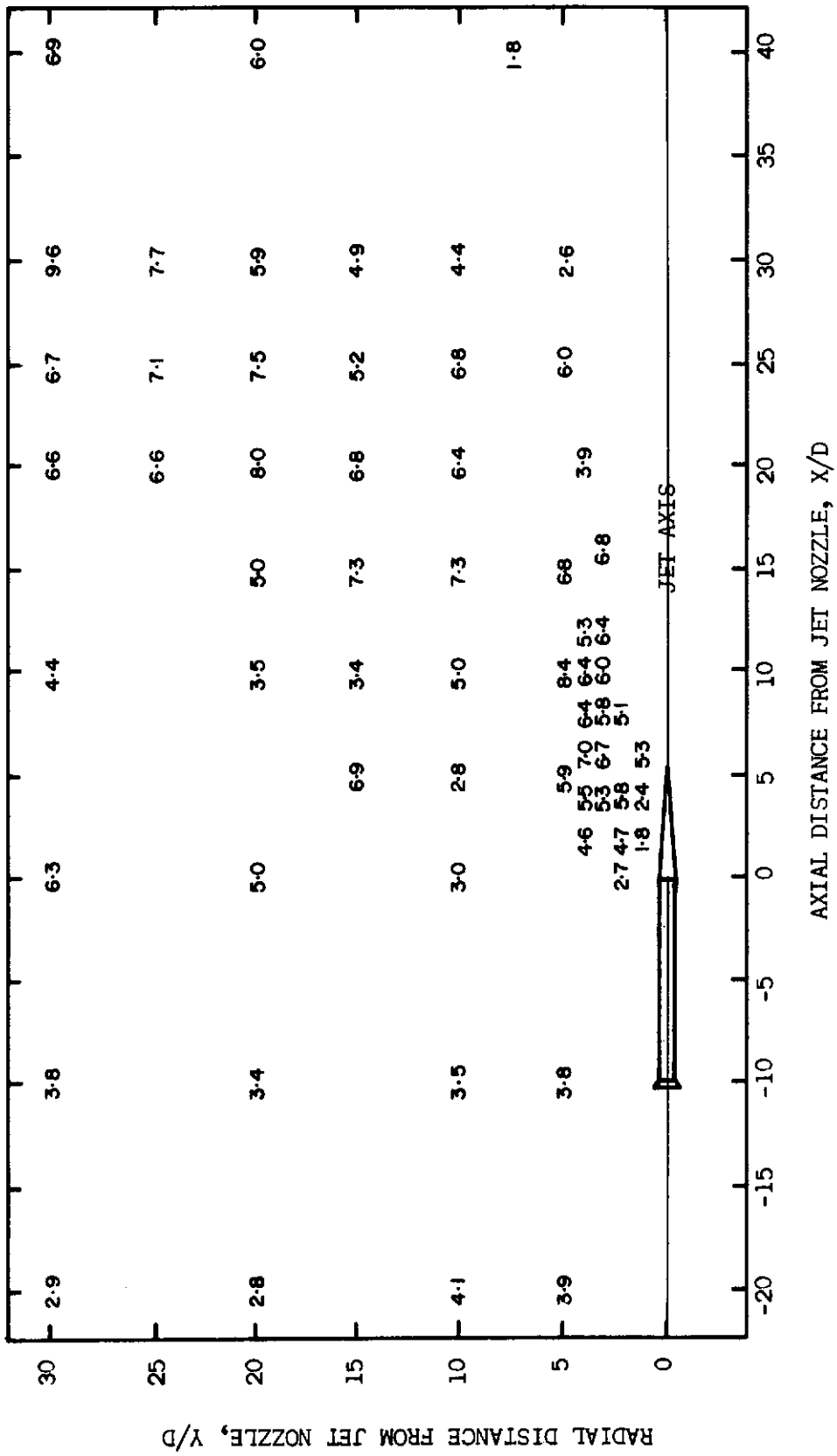


Figure 24. Velocity Indexes for Frequency Band 180-360 CPS

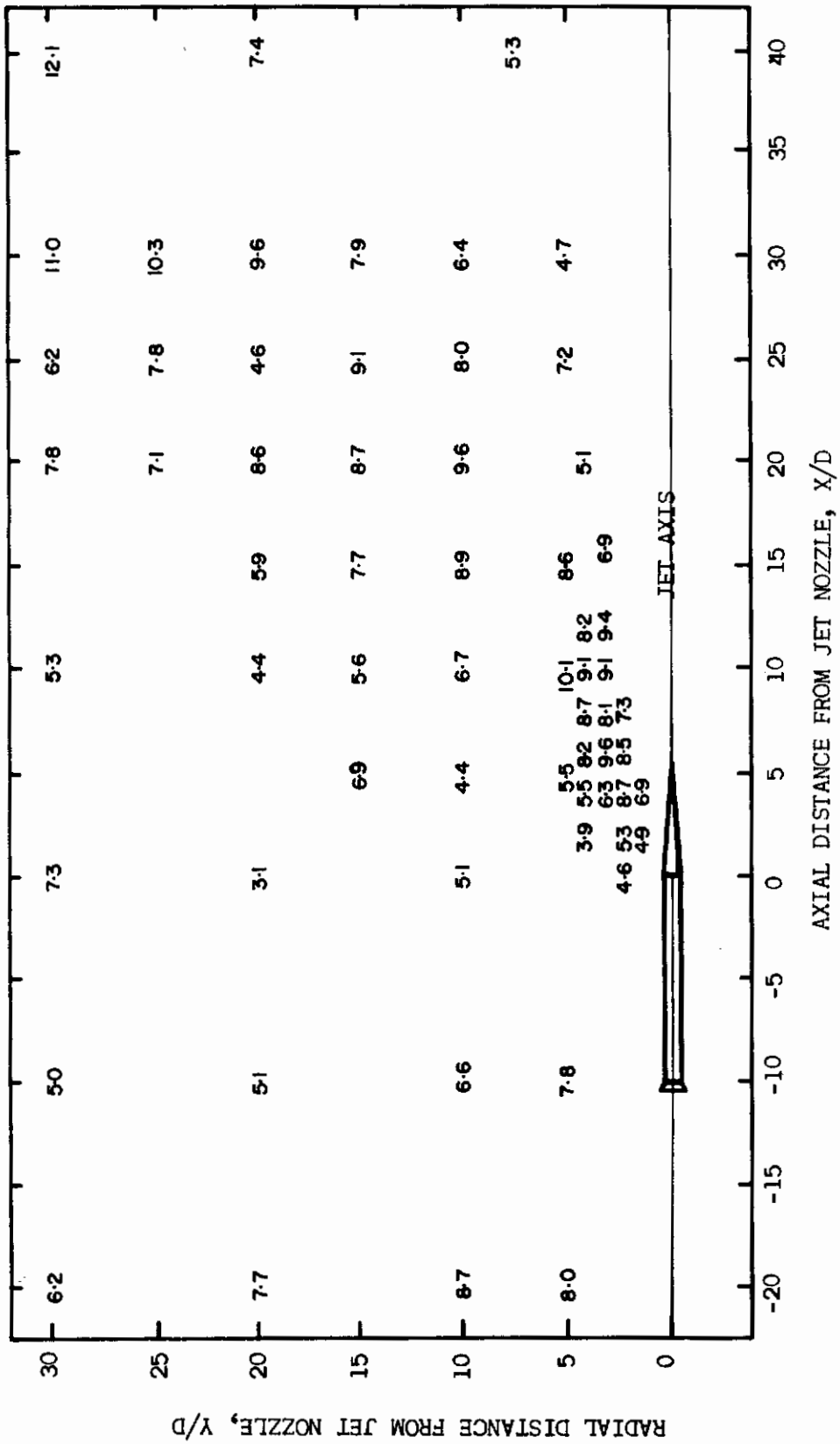


Figure 25. Velocity Indexes for Frequency Band 360-720 CPS

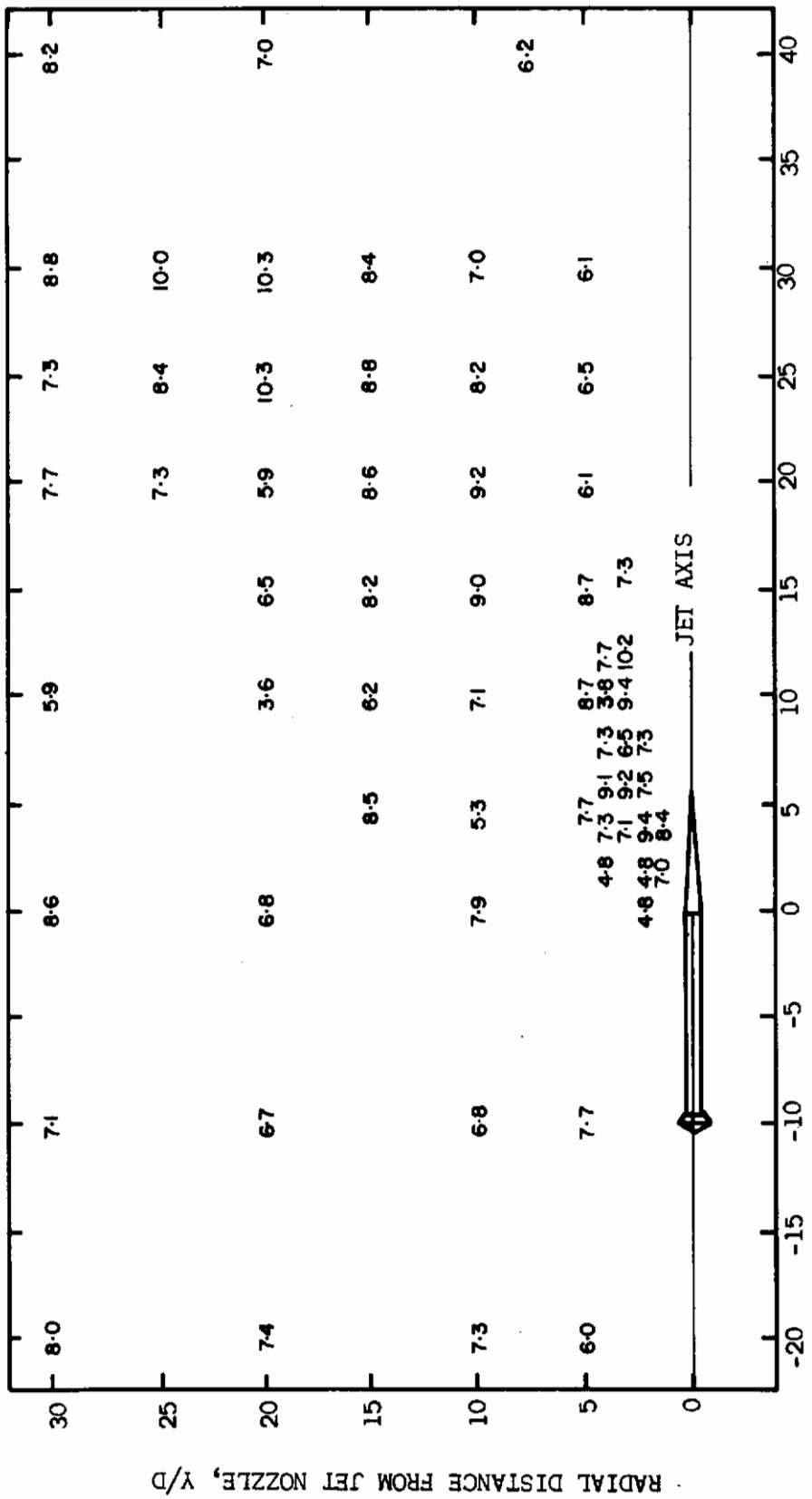


Figure 26. Velocity Indexes for Frequency Band 720-1440 CPS

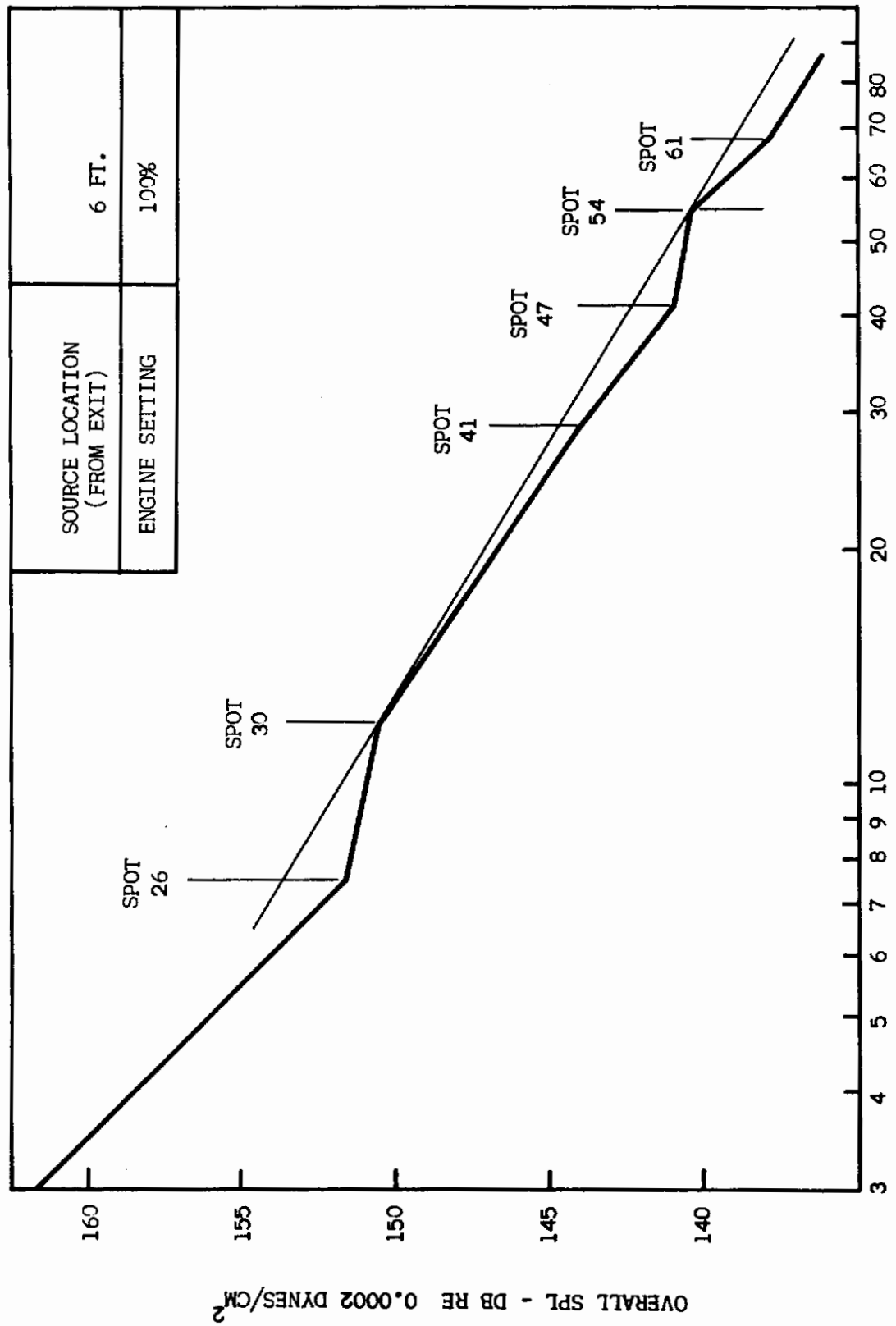


Figure 27. Overall SPL Decay Slope Thru Spot 54

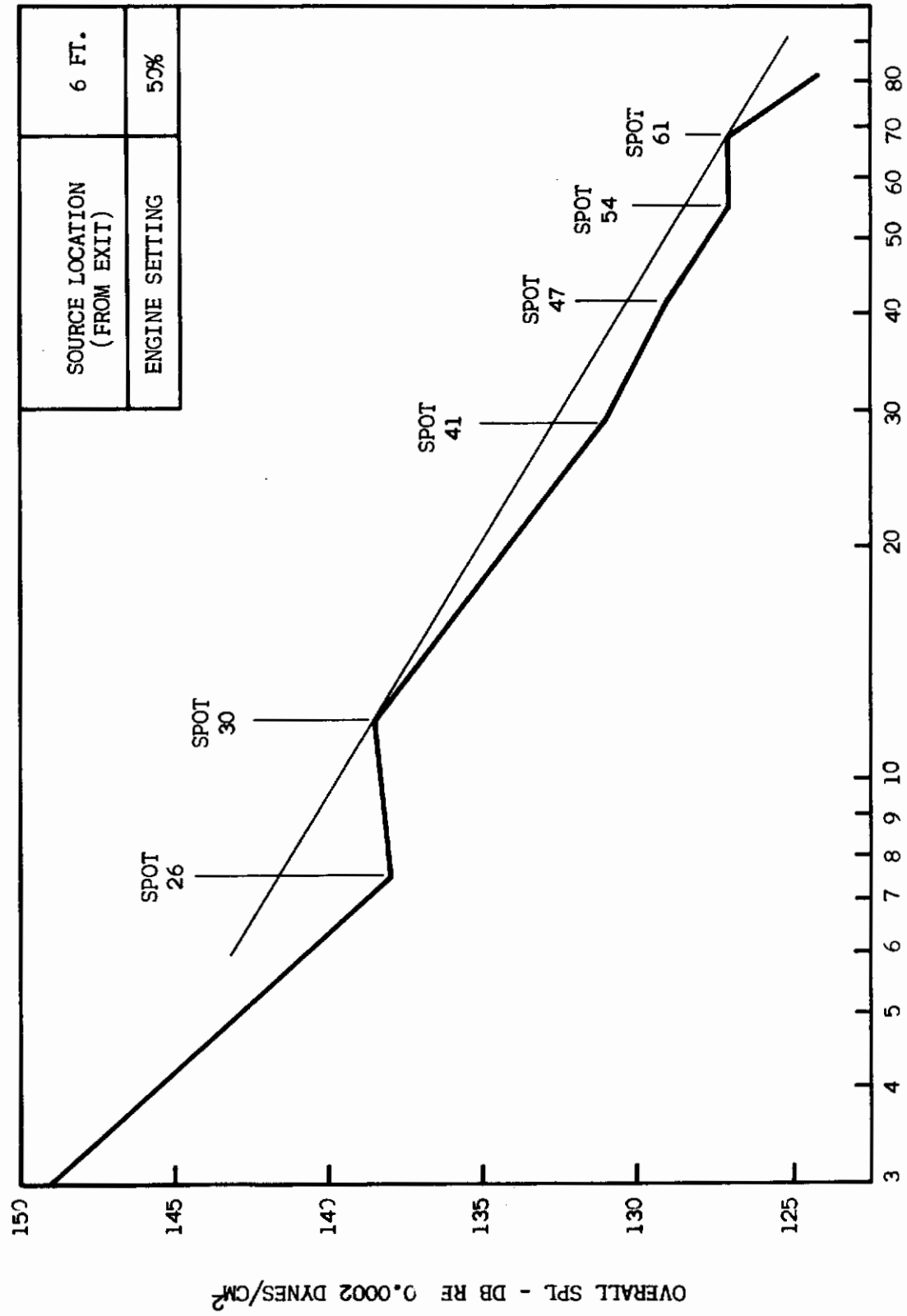


Figure 28. Overall SPL Decay Slope Thru Spot 54

The n values were then calculated from Equation 8 using the decay slope values in place of the measured SPL's. These n values are equivalent to those obtained under free-field conditions since a constant difference exists for all engine settings between the free-field SPL's and those associated with the conditions of maximum reinforcement. The n field corrected for ground reflection effects is shown in Figure 29.

The effects of reflection on the calculated n field may be numerically illustrated by comparing the data from Spot 54. The n value calculated from the measured SPL's is 8.1. In Figures 17 and 18 of Section IV, corrected overall SPL's were obtained from the summation of corrected one-third octave band levels for both 50 and 100 percent engine settings. The n value determined from these levels is 7.1. The n value obtained from the corrected SPL's from the overall decay slopes of Figures 27 and 28 is 6.9. The good agreement in the last two values indicates that the direct application of overall decay slopes will account for reflection effects.

A noticeable trend in the n values is that they follow an angular pattern from the jet axis reaching a maximum value between 40-50 degrees and decreasing in value on both sides of this angular region. This trend suggests that the n values are affected by the changes in the directional properties of the noise field with varying jet velocity.

## 3. EFFECTS OF VARYING DIRECTIONAL PROPERTIES WITH JET VELOCITY

The previous calculations of the velocity index included the assumption that the mean square pressure at each location in the noise field is proportional to the TAP which in turn is proportional to $\rho_j^2 V^n$. This assumption does not account for changes in the directional properties of the noise field with jet velocity. A more realistic assumption, neglecting the effects of jet density, would be:

$$TAP \propto \overline{P_{SA}^2} \propto V^n \tag{11}$$

where $\overline{P_{SA}^2}$ is the space average mean square sound pressure.

From Ribner (Reference 12), the directional properties of the noise field of a turbojet engine as a function of jet velocity are given as:

$$\overline{P_{SA}^2} = \frac{\overline{P_\theta^2}}{K^{-5}\,(1+\cos^4\theta)} \tag{12}$$

where

$$K^{-5} = \left[\left(1-\frac{V_j}{2c_o}\cos\theta\right)^2 + .3\left(\frac{V_j}{2c_o}\right)^2\right]^{-5/2}$$

and $\theta$ is the angel from the jet axis

$V_j$ is the jet exit velocity

$c_o$ is the ambient speed of sound

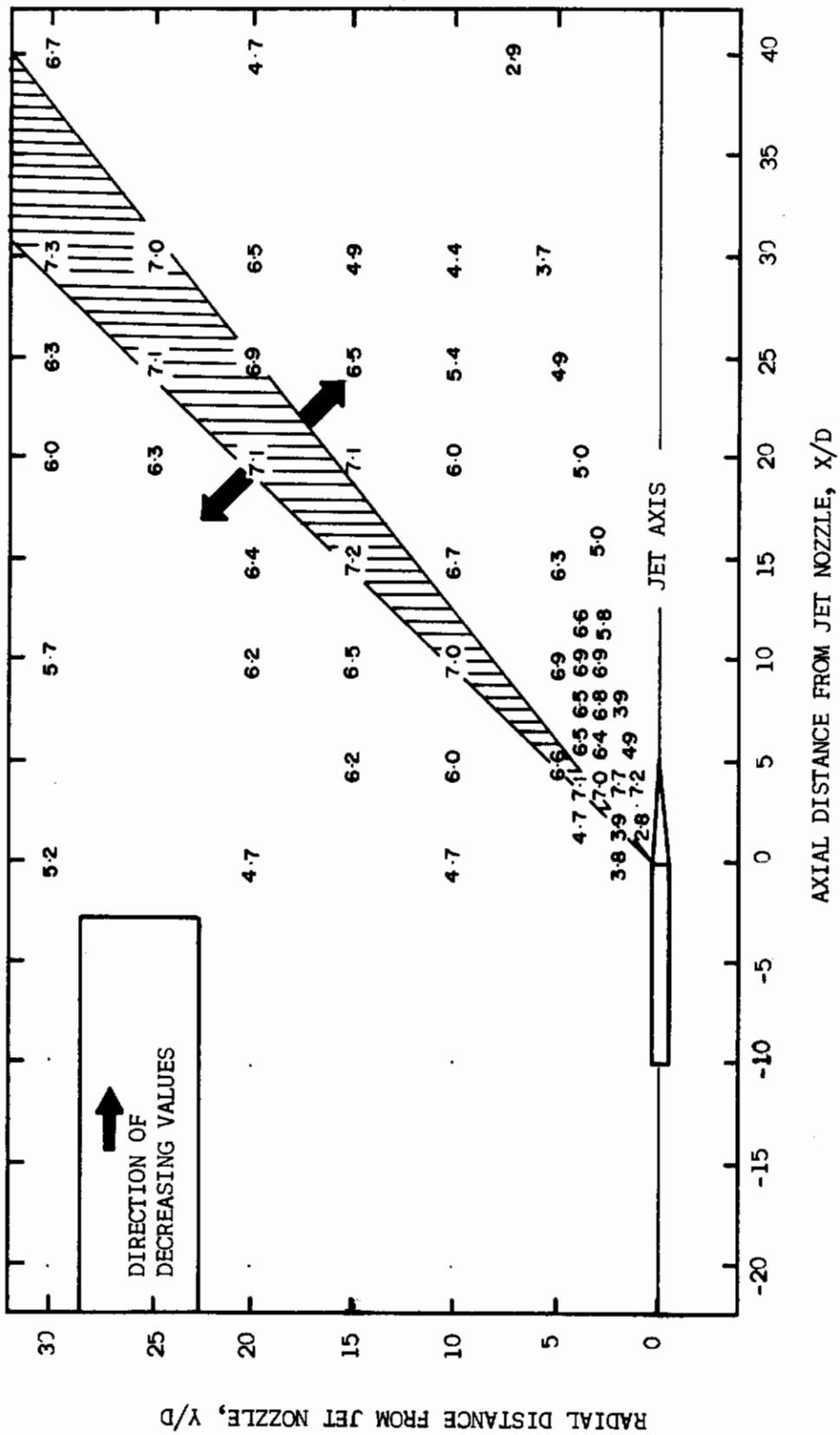


Figure 29. Overall SPL Velocity Exponent Field Corrected for Ground Reflection Effects

Substituting Equation 12 into Equation 11 results in the following equation when a ratio of two conditions is taken:

$$n = \frac{SPL_1 - SPL_2 + 25 \log \left[ \frac{\left(1 - \frac{V_1}{2c_0} \cos\theta\right)^2 + .3\left(\frac{V_1}{2c_0}\right)^2}{\left(1 - \frac{V_2}{2c_0} \cos\theta\right)^2 + .3\left(\frac{V_2}{2c_0}\right)^2} \right]}{10 \left[ \log V_1 - \log V_2 \right]} \qquad (13)$$

where the subscripts 1 and 2, for the present measurements, refer to the 100 percent and 50 percent engine power settings, respectively.

Equation 13 is limited to the angular region from 30 to 90 degrees from the jet axis. The 0-30 degree nonapplicability is due to the disagreement found between Equation 12 and measured data below 30 degrees. The other limitation results from compressor noise effects on sound pressures measured at locations above 90 degrees.

The overall SPL's, corrected for ground reflection effects, were substituted in Equation 13. The resulting n values along with the corrected SPL's are related to the measurement locations in Table V. These n values are equivalent to those obtained from a nondirectional source under free-field conditions. Eighty percent of these values range from 5.0 to 6.0. The median of all the values is 5.5. These values are presented in Figure 30. In the 10 to 30 degree angular region, the directional correction was not made. In this region, the values of n are those given in Figure 21.

Including the effects of jet density would result in an n value increase from 5.5 to 6.5. The latter value should be used in future applications of Equation 13.

The essentially constant value of n agrees with the fully developed theory of jet noise presented in Reference 11. This agreement justifies the transformation of a referenced noise field to a desired noise field of a similar jet engine with different operating conditions by accounting for interference and directional effects. The transformation techniques to account for a change in the overall SPL are presented in this and the previous sections and are believed to be applicable to jet engines with exit Mach number up to 2. Additional information on directional characteristics is required to develop a similar technique for one-third octave band levels.

TABLE V

PARAMETERS AFFECTING THE NONDIRECTIONAL FREE-FIELD n

| SPOT | $SPL_1$ (Maximum reinforcement) | $SPL_2$ | θ | 25 log ( * ) | 10 log $(\frac{V_1}{V_2})$ | n |
|---|---|---|---|---|---|---|
| 10 | 139 | 131.5 | 90 | +1.3 | 1.97 | 4.5 |
| 11 | 130.5 | 121.5 | 90 | +1.3 | 1.93 | 5.4 |
| 12 | 125.5 | 116.5 | 90 | +1.3 | 1.93 | 5.3 |
| 13 | 124 | 114 | 90 | +1.3 | 1.93 | 5.8 |
| 15 | 141.5 | 134 | 45 | -2.3 | 1.91 | 2.7 |
| 16 | 138 | 129 | 65 | -0.9 | 1.90 | 4.3 |
| 20 | 147.5 | 134 | 38 | -2.4 | 1.92 | 5.8 |
| 21 | 145.5 | 132 | 45 | -2.3 | 1.90 | 5.9 |
| 22 | 143.5 | 131 | 45 | -2.3 | 1.90 | 5.4 |
| 23 | 137 | 125.5 | 65 | -.8 | 1.93 | 5.5 |
| 24 | 134 | 122 | 72 | -.2 | 1.93 | 6.1 |
| 27 | 148 | 136 | 35 | -2.4 | 1.85 | 5.2 |
| 34 | 141.5 | 129 | 45 | -2.2 | 1.78 | 5.8 |
| 35 | 136.5 | 125 | 57 | -1.4 | 1.78 | 5.7 |
| 36 | 133.5 | 122.5 | 65 | -.8 | 1.78 | 5.7 |
| 37 | 129.5 | 118.5 | 72 | -.2 | 1.93 | 5.7 |
| 41 | 144.5 | 132.5 | 35 | -2.4 | 1.78 | 5.4 |
| 42 | 140.5 | 127.5 | 45 | -2.2 | 1.80 | 6.0 |
| 43 | 135 | 124 | 54 | -1.6 | 1.75 | 5.4 |
| 47 | 142.5 | 130 | 38 | -2.4 | 1.75 | 5.8 |
| 48 | 138.5 | 126 | 45 | -2.2 | 1.75 | 5.9 |
| 49 | 134.5 | 123.5 | 51 | -1.9 | 1.75 | 5.1 |
| 50 | 131.5 | 121 | 57 | -1.4 | 1.75 | 5.2 |
| 53 | 141.5 | 129.5 | 31 | -2.4 | 1.85 | 5.2 |
| 54 | 140.5 | 128.5 | 39 | -2.3 | 1.75 | 5.5 |
| 55 | 137 | 124.5 | 45 | -2.2 | 1.76 | 5.8 |
| 56 | 133 | 122 | 51 | -1.8 | 1.76 | 5.1 |
| 60 | 139.5 | 128 | 34 | -2.4 | 1.76 | 5.1 |
| 61 | 139 | 127 | 40 | -2.3 | 1.71 | 5.6 |
| 62 | 136 | 123.5 | 45 | -2.0 | 1.71 | 6.1 |
| 65 | 137.5 | 126 | 38 | -2.2 | 1.71 | 5.4 |

$$* \left[ \frac{(1 - \frac{V_1}{2c_0}\cos\theta)^2 + .3(\frac{V_1}{2c_0})^2}{(1 - \frac{V_2}{2c_0}\cos\theta)^2 + .3(\frac{V_2}{2c_0})^2} \right]$$

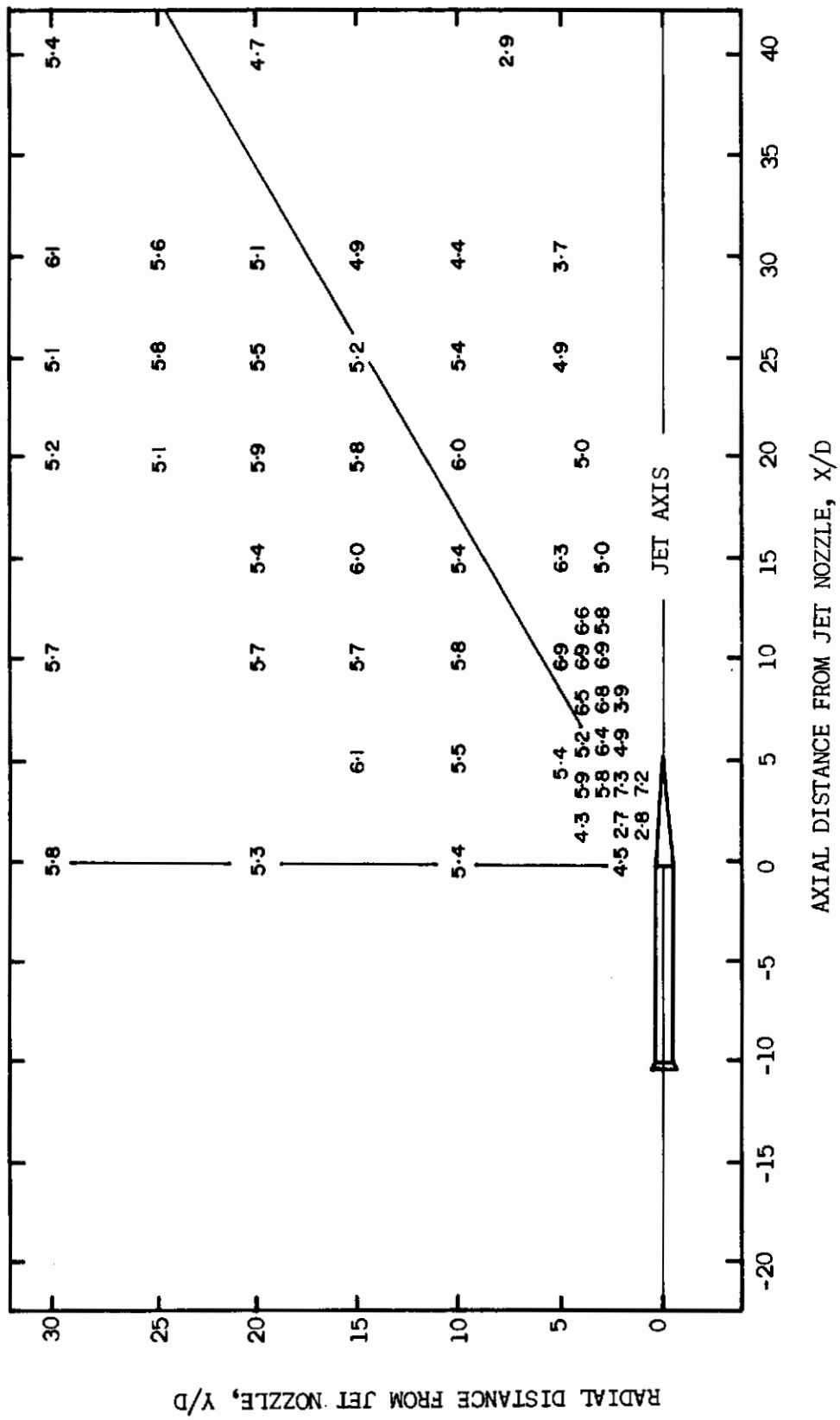


Figure 30. Overall SPL Velocity Exponent Field Corrected to Nondirectional and Free-Field Conditions

# SECTION VI

# CONCLUSIONS

The following conclusions are made on the basis of the present investigation:

1. Noise levels obtained at the same nondimensional locations from different but similar jet engines differ up to 15 db in one-third octave bands and 7.5 db in the overall band.

2. The major differences in the measured levels are caused by interference effects resulting from the presence of a ground plane.

3. The application of a theoretical model to overall and one-third octave band noise levels indicates that interference effects can be reasonably predicted.

4. Major differences result in the value of the velocity exponent when the interference and directional effects on the noise field are not considered.

5. A nearly constant velocity exponent of 6.5 results between 30 and 90 degrees from the jet axis when the interference and directional effects on the noise field are considered.

6. The corrected n field equation is considered to be the basis of a noise prediction method which should be accurate for jet flows with exit Mach numbers ranging from 0.5 to 2.0.

## REFERENCES


1. D. Middleton, Comprehensive Near Field Noise Test on an Avon RA. 26 Engine fitted with Conical Nozzle, Rolls-Royce Report TAS/Spn. 10/MB, Rolls-Royce LTD, Aero Engine Division, April 1959.

2. Walton L. Howes, et al., Near Noise Field of a Jet Engine Exhaust, NACA Report 1338, Lewis Flight Propulsion Laboratory, Cleveland, Ohio, 1957.

3. M. O. W. Wolfe, Near Field Jet Noise, Royal Aircraft Establishment Report 228, AGARD Report 112 DDC-No. AD 154857, Royal Aircraft Establishment, Farnborough England, September 1957.

4. D. L. Smith, The Effect of Operational Data on Sonic Fatigue Estimates, AFIT Thesis GA-63, Air Force Institute of Technology, Wright-Patterson Air Force Base, Ohio, August 1963.

5. B. L. Clarkson, Structural Aspects of Acoustic Loads, AGARDograph 65, DDC Number AD 294146, September 1960.

6. Peter A. Franken, et al., Methods of Flight Vehicle Noise Prediction, WADC-TR-53-343, DDC No. AD 205776, Wright Air Development Center, Wright-Patterson AFB, Ohio, November 1958.

7. C. E. Thomas, Mobile Dynamics Data Acquisition and Analysis Facility, AFFDL-TR-64-182, Research and Technology Division, Wright-Patterson AFB, Ohio, June 1965.

8. G. A. Plzak, et al., 156 Inch Solid Fuel Motor Firing - Acoustic and Vibration Spectra, FDD-TM-64-62, Research and Technology Division, Wright-Patterson AFB, Ohio, July 1964.

9. Pratt & Whitney Aircraft, J57-P21 Engine Specification, No. A-1685-D, January 1956.

10. Walton L. Howes, Ground Reflection of Jet Noise, NASA TR R-35, Lewis Research Center, Cleveland, Ohio, 1959.

11. M. J. Lighthill, "On Sound Generated Aerodynamically: I General Theory," Proceedings of the Royal Society, 211:564-587, 1952.

12. H. S. Ribner, "The Generation of Sound by Turbulent Jets," Advances in Applied Mechanics, 8: 104-178, Academic Press, New York and London, 1964.

# APPENDIX I

# ENVIRONMENTAL AND ENGINE TEST DATA

TABLE VI

EXIT VELOCITY VERSUS SETUP

| Setup | Exit Velocity (fps) | | | |
|---|---|---|---|---|
| | A/B | 100% | 70% | 50% |
| 1 | 2530 | 1950 | 1557 | 1255 |
| 2 | 2520 | 1925 | 1542 | 1239 |
| 3 | 2540 | 1950 | 1557 | 1255 |
| 4 | 2580 | 1960 | 1571 | 1264 |
| 5 | 2530 | 1960 | 1568 | 1258 |
| 6 | 2550 | 1990 | 1568 | 1264 |
| 7 | 2400 | 1920 | | |
| 8 | 2280 | 1875 | | |
| 9 | 2310 | 1875 | | |
| 10 | 2310 | 1920 | | |
| 11 | 2380 | 1895 | | |

TABLE VII

STATIC THRUST VERSUS SETUP

| Setup | Static Thrust (lb ) | | | |
|---|---|---|---|---|
| | A/B | 100% | 70% | 50% |
| 1 | 16,300 | 10,400 | 7,280 | 5,200 |
| 2 | 16,000 | 10,200 | 7,140 | 5,100 |
| 3 | 16,000 | 10,360 | 7,240 | 5,180 |
| 4 | 16,400 | 10,500 | 7,360 | 5,240 |
| 5 | 16,100 | 10,400 | 7,280 | 5,200 |
| 6 | 16,300 | 10,500 | 7,360 | 5,240 |
| 7 | 15,400 | 9,850 | | |
| 8 | 14,800 | 9,700 | | |
| 9 | 15,000 | 9,700 | | |
| 10 | 15,000 | 9,600 | | |
| 11 | 14,900 | 9,600 | | |

TABLE VIII

TURBINE EXHAUST TOTAL PRESSURE VERSUS SETUP

| Setup | Turbine Exhaust Total Pressure ($P_{t7}$ - In.Hg) | | | |
|---|---|---|---|---|
| | A/B | 100% | 70% | 50% |
| 1 | 70.3 | 67.7 | 55.1 | 47.7 |
| 2 | 69.1 | 66.3 | 54.2 | 46.8 |
| 3 | 69.2 | 66.4 | 54.3 | 47.2 |
| 4 | 70.4 | 67.5 | 55.0 | 47.9 |
| 5 | 69.6 | 67.2 | 54.5 | 47.5 |
| 6 | 70.1 | 67.6 | 58.1 | 49.4 |
| 7 | 67.6 | 64.8 | | |
| 8 | 65.9 | 64.1 | | |
| 9 | 66.1 | 63.5 | | |
| 10 | 66.3 | 63.1 | | |
| 11 | 66.6 | 64.1 | | |

TABLE IX

EXHAUST GAS TEMPERATURE VERSUS SETUP

| Setup | Exhaust Gas Temperature (°F) | | | |
|---|---|---|---|---|
| | A/B | 100% | 70% | 50% |
| 1 | 1155 | 1140 | 890 | 780 |
| 2 | 1116 | 1120 | 850 | 725 |
| 3 | 1160 | 1135 | 890 | 760 |
| 4 | 1135 | 1120 | 855 | 735 |
| 5 | 1155 | 1140 | 915 | 790 |
| 6 | 1160 | 1150 | 970 | 832 |
| 7 | 1125 | 1130 | | |
| 8 | 1145 | 1130 | | |
| 9 | 1140 | 1130 | | |
| 10 | 1145 | 1140 | | |
| 11 | 1152 | 1125 | | |

TABLE X

HIGH PRESSURE ROTOR SPEED VERSUS SETUP

| Setup | High Pressure Rotor Speed ($N_2$ - rpm) | | | |
|---|---|---|---|---|
| | A/B | 100% | 70% | 50% |
| 1 | 9400 | 9480 | 8800 | 8440 |
| 2 | 9400 | 9430 | 8820 | --- |
| 3 | 9400 | 9420 | 8830 | 8480 |
| 4 | 9390 | 9400 | 8810 | 8460 |
| 5 | 9400 | 9420 | 8820 | 8470 |
| 6 | 9410 | 9410 | 8930 | 8540 |
| 7 | 9460 | 9470 | | |
| 8 | 9440 | 9460 | | |
| 9 | 9430 | 9460 | | |
| 10 | 9450 | 9460 | | |
| 11 | 9420 | 9460 | | |

TABLE XI

LOW PRESSURE ROTOR SPEED VERSUS SETUP

| Setup | Low Pressure Rotor Speed ($N_1$ - rpm) | | | |
|---|---|---|---|---|
| | A/B | 100% | 70% | 50% |
| 1 | 5800 | 5940 | 5280 | 4800 |
| 2 | 5840 | 5930 | 5380 | 4800 |
| 3 | 5820 | 5830 | 5290 | 4810 |
| 4 | 5820 | 5940 | 5280 | 4820 |
| 5 | 5800 | 5830 | 5280 | 4810 |
| 6 | 5820 | 5940 | 5440 | 4920 |
| 7 | 5820 | 5930 | | |
| 8 | 5790 | 5830 | | |
| 9 | 5800 | 5820 | | |
| 10 | 5810 | 5820 | | |
| 11 | 5800 | 5920 | | |

TABLE XII

ATMOSPHERIC CONDITIONS VERSUS SETUP

| Setup | Wind | | Barometric Pressure (In. Hg) | Ambient Temperature (°F) |
|---|---|---|---|---|
| | Speed (Knots) | Direction[1] | | |
| 1 | 4 | 310 | 30.14 | 36 |
| 2 | 10 | 250 | 30.09 | 47 |
| 3 | 10 | 290 | 30.06 | 49 |
| 4 | 2 | — | 30.20 | 39 |
| 5 | 2 | — | 30.23 | 45 |
| 6 | 8 | 360 | 30.41 | 46 |
| 7 | 2 | — | 30.26 | 58 |
| 8 | 10 | 150 | 30.23 | 70 |
| 9 | 6 | 160 | 30.24 | 70 |
| 10 | 6 | 200 | 30.21 | 72 |
| 11 | 10 | 220 | 30.23 | 67 |

1 The jet engine inlet is facing north, i.e., zero degrees

# APPENDIX II

## ONE-THIRD OCTAVE BAND SPECTRA AND OVERALL SPL's

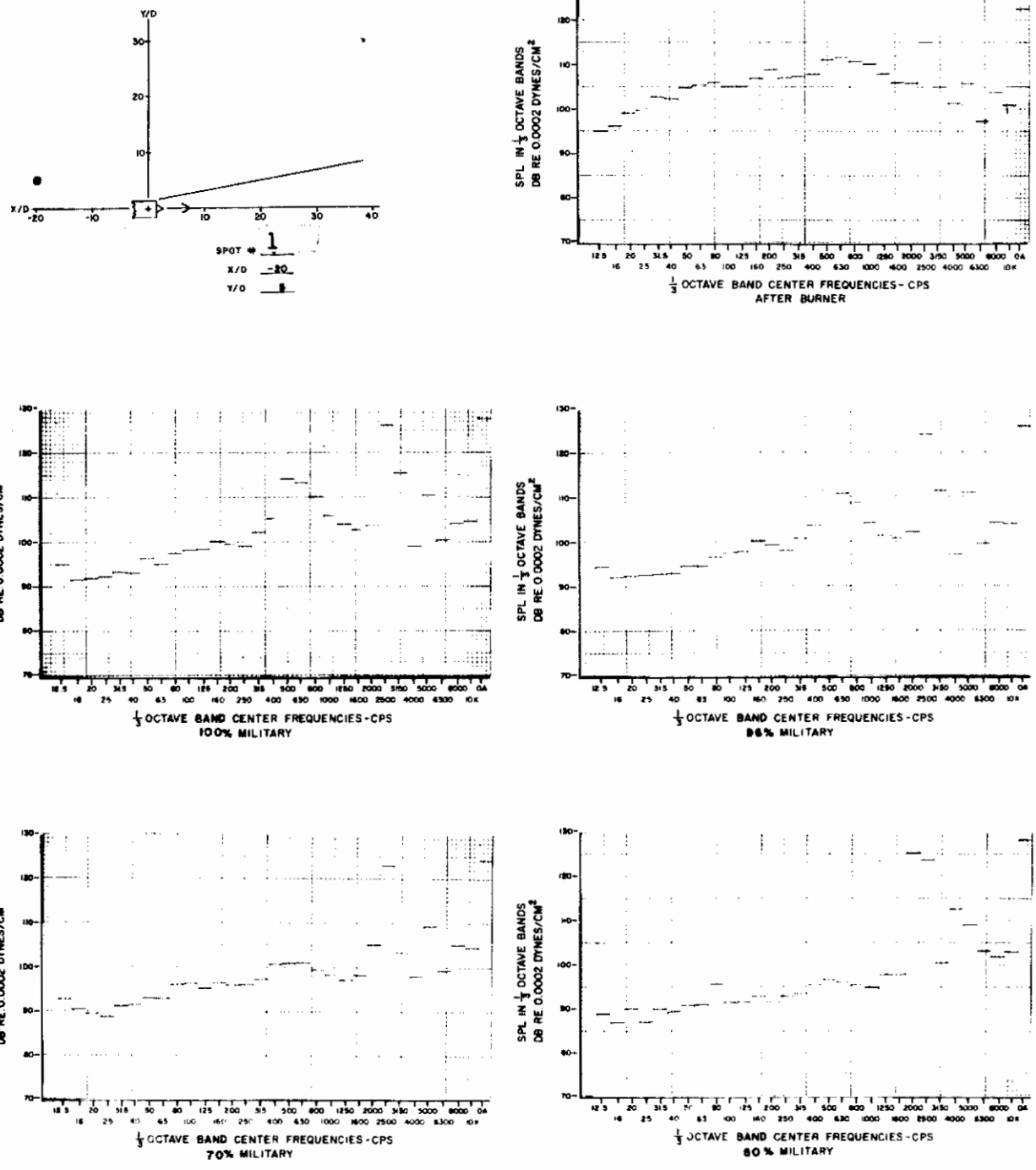


Figure 31. One-Third Octave Band Spectra and Overall SPL for Spot 1

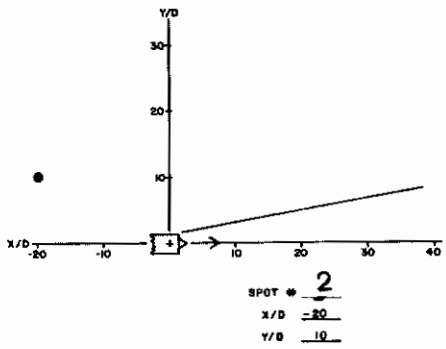


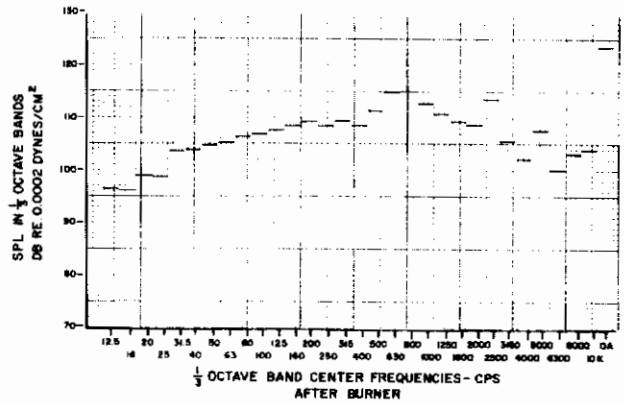


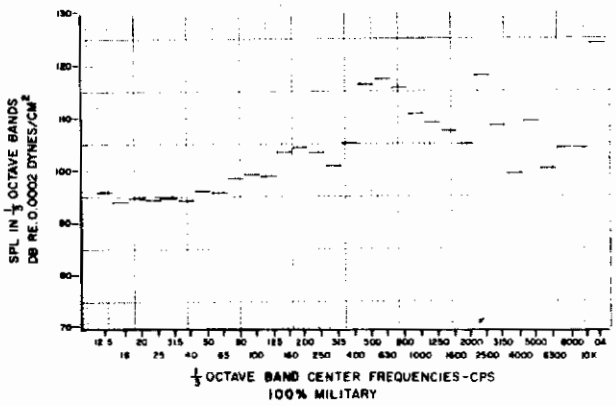


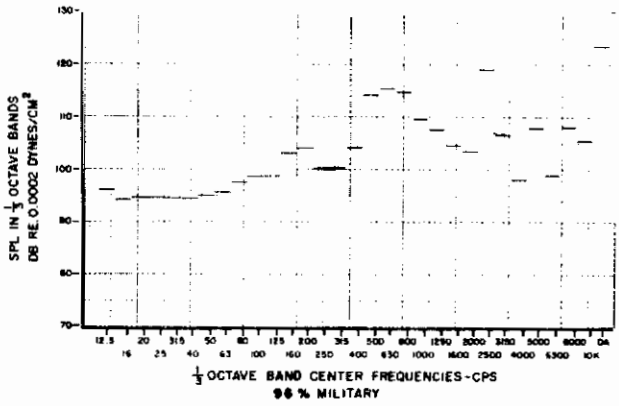


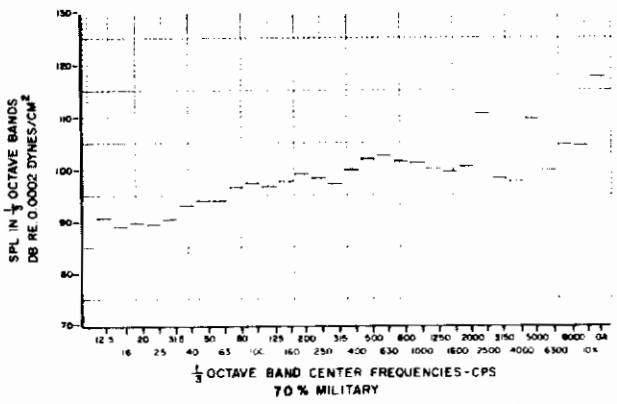


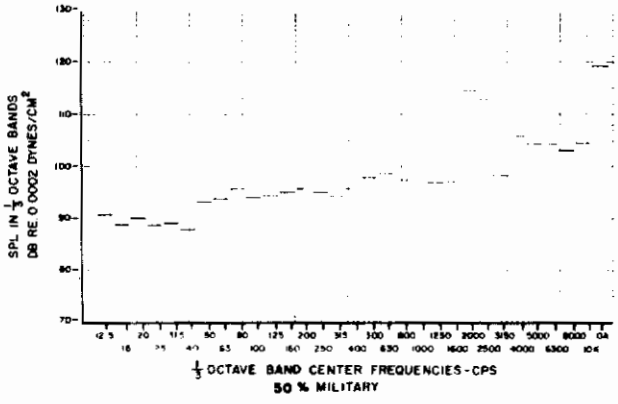


Figure 32. One-Third Octave Band Spectra and Overall SPL for Spot 2

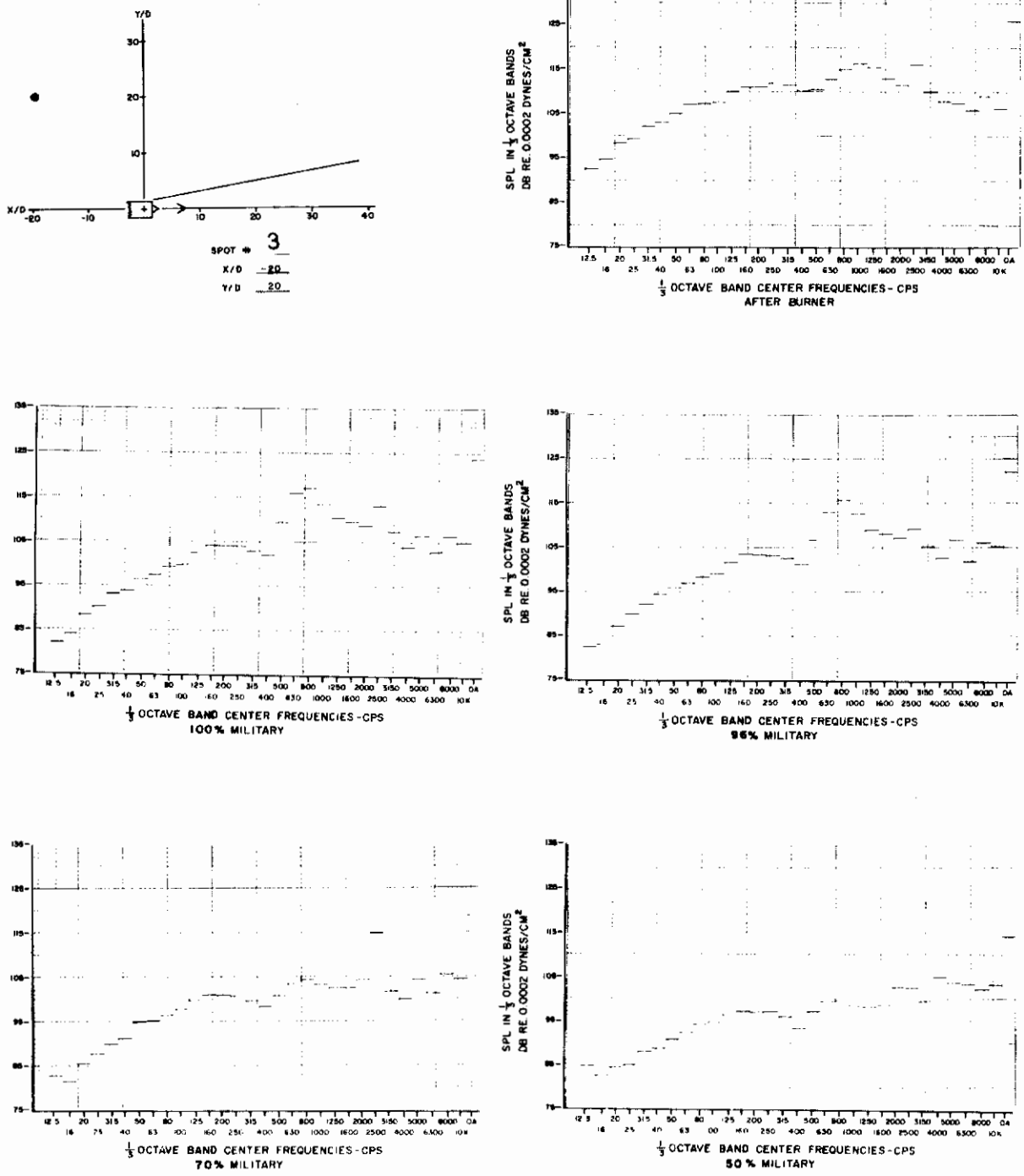


Figure 33. One-Third Octave Band Spectra and Overall SPL for Spot 3

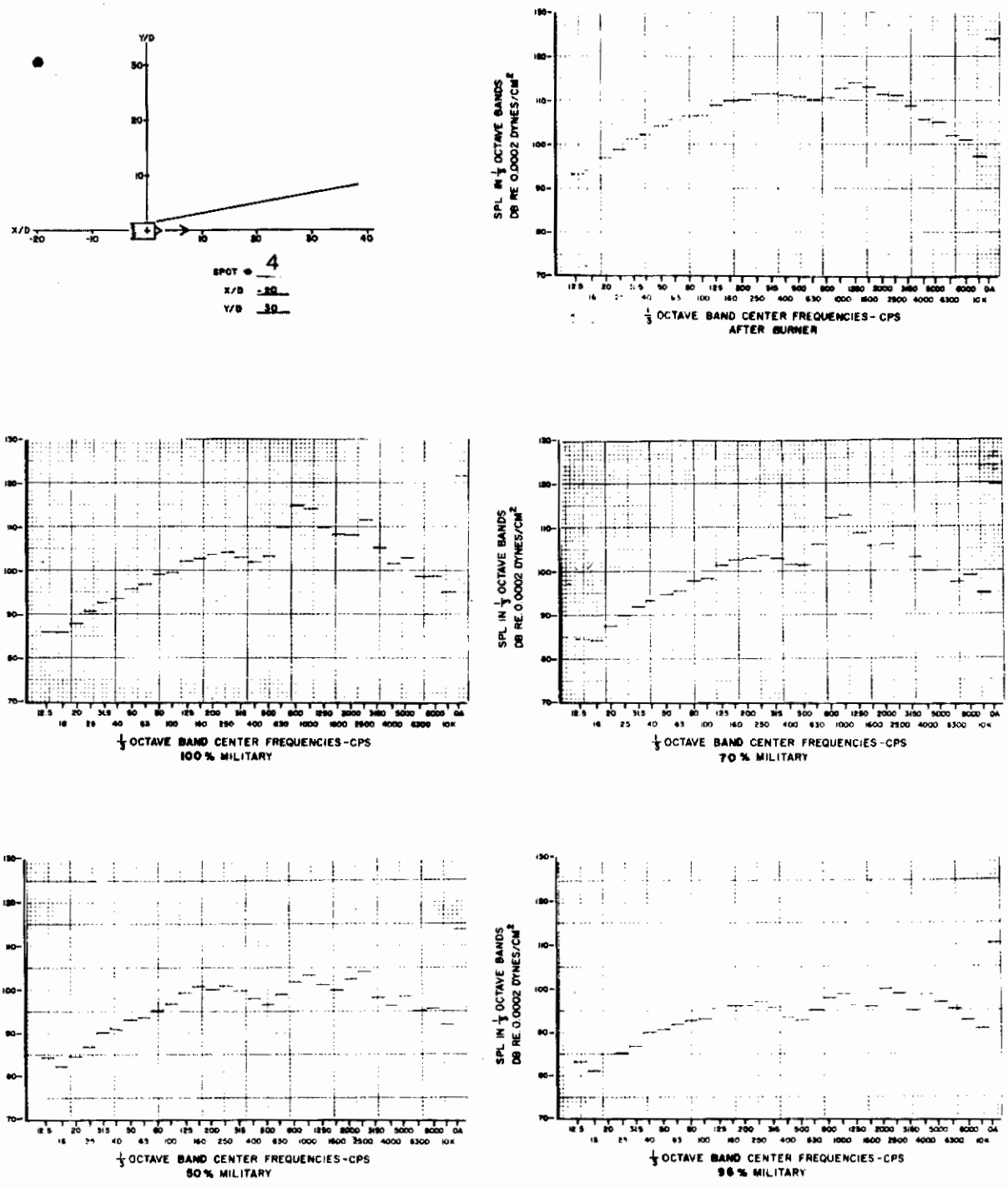


Figure 34. One-Third Octave Band Spectra and Overall SPL for Spot 4

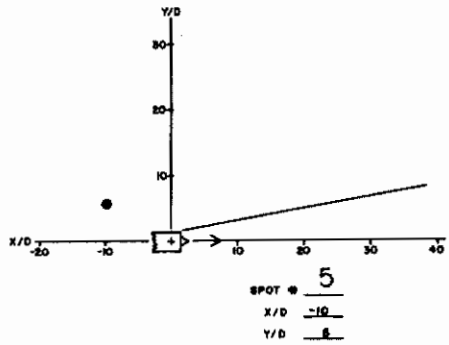


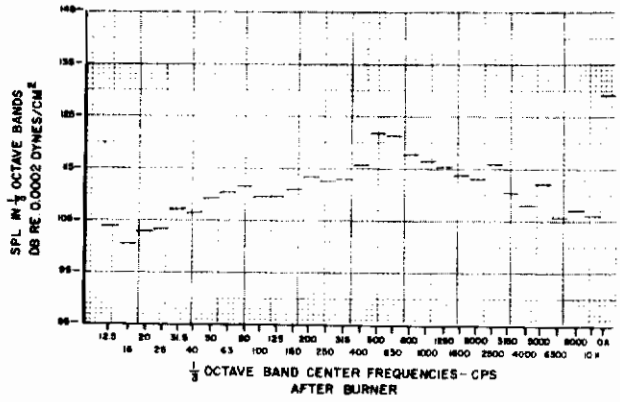


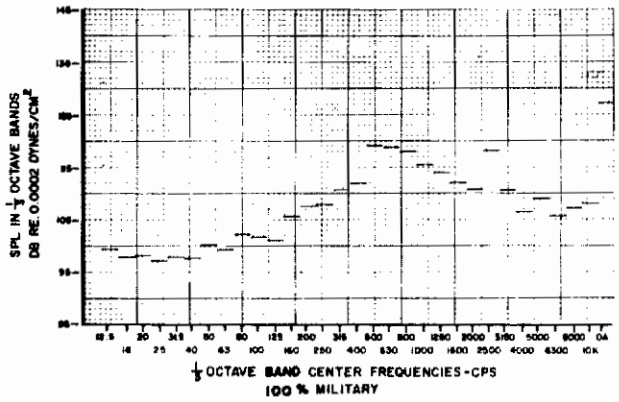


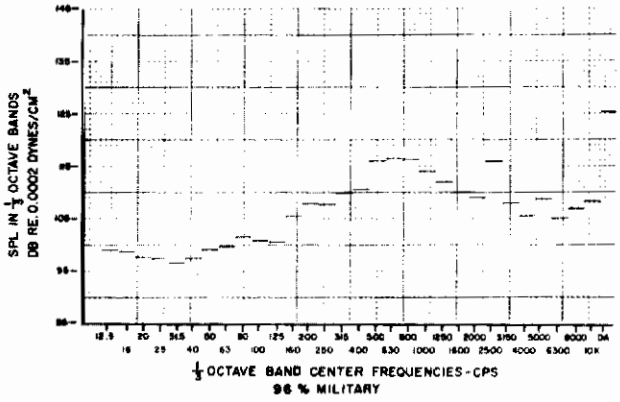


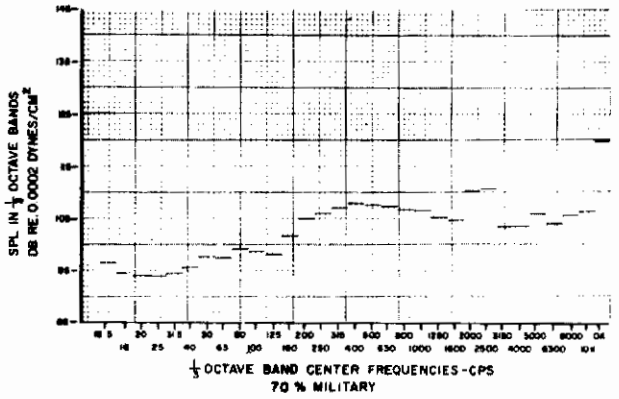


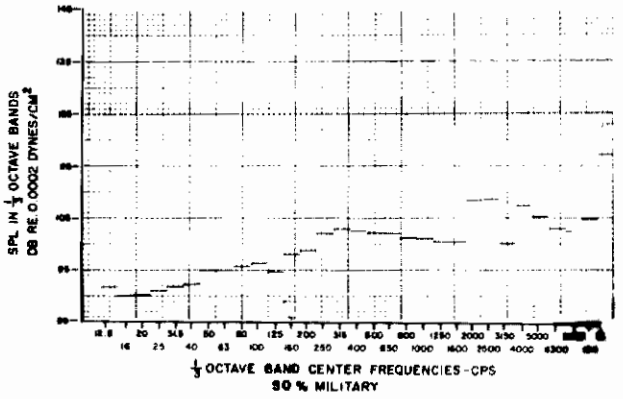


Figure 35. One-Third Octave Band Spectra and Overall SPL for Spot 5

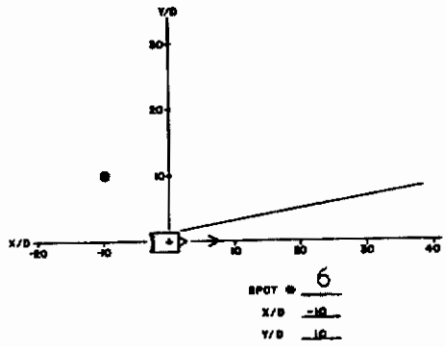


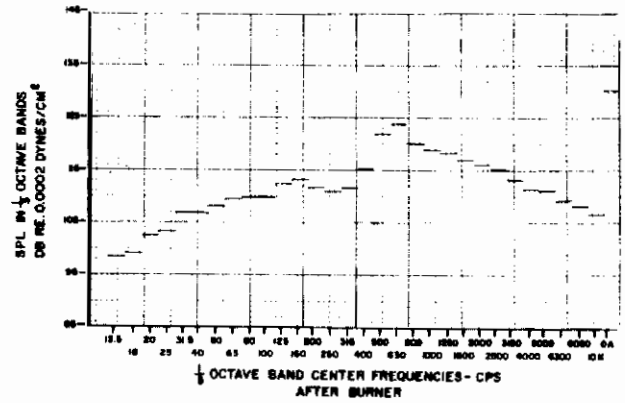


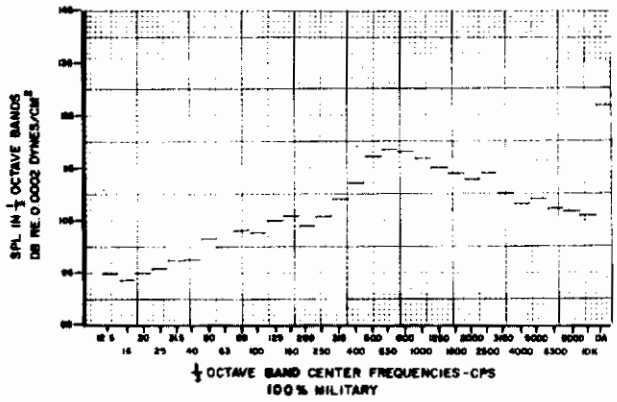


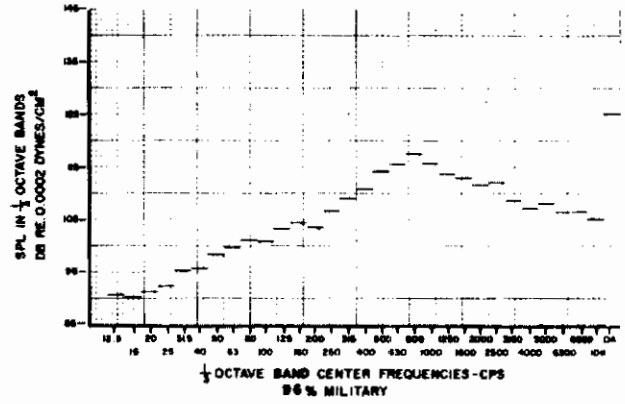


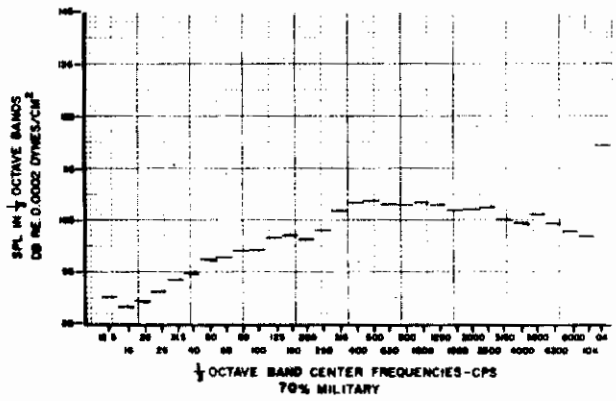


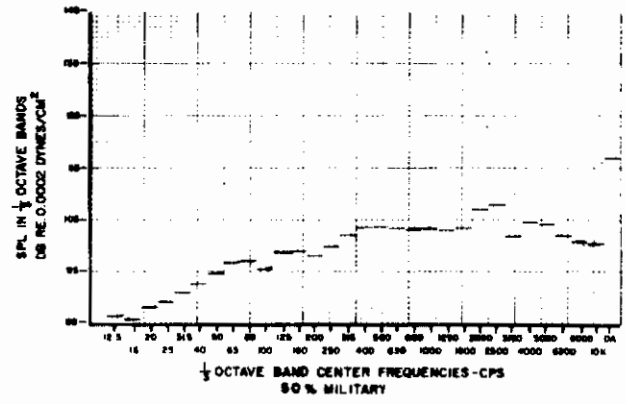


Figure 36. One-Third Octave Band Spectra and Overall SPL for Spot 6

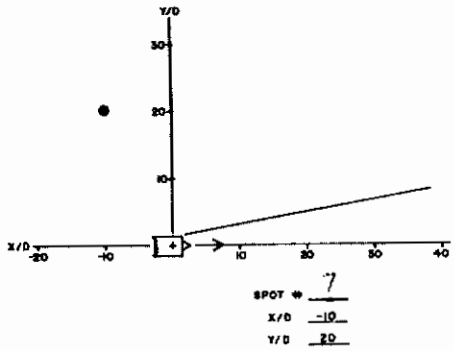


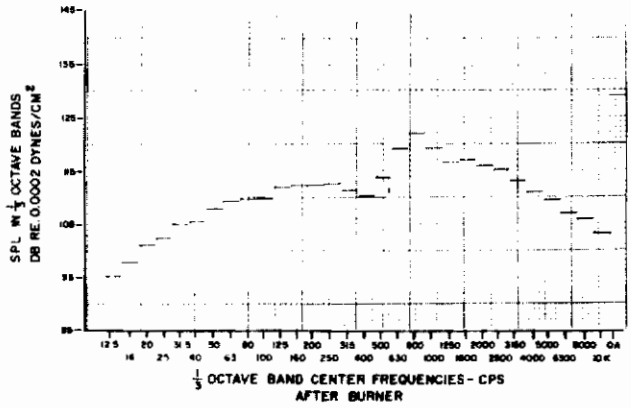


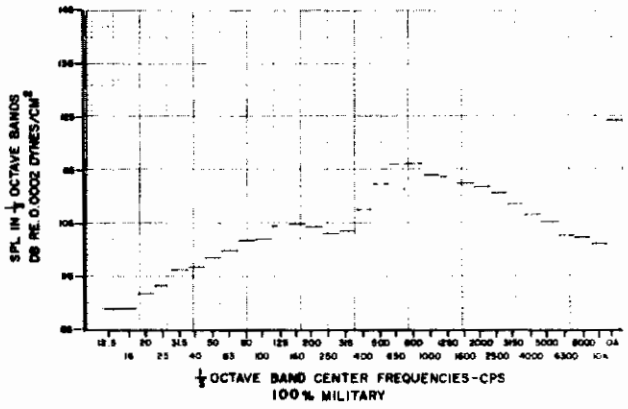


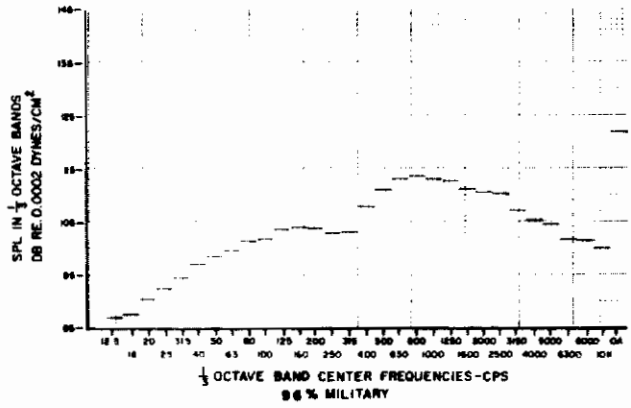


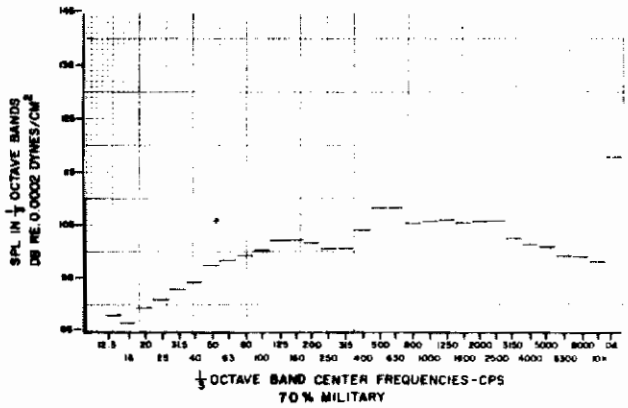


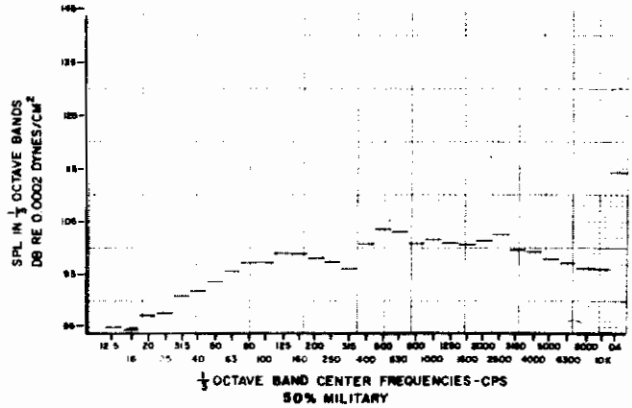


Figure 37. One-Third Octave Band Spectra and Overall SPL for Spot 7

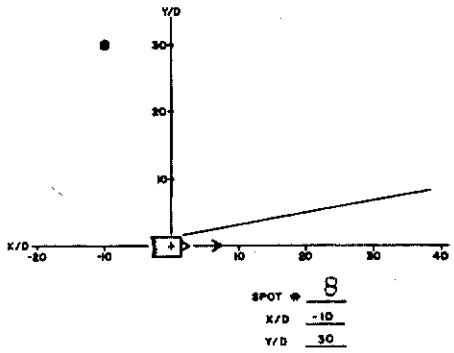


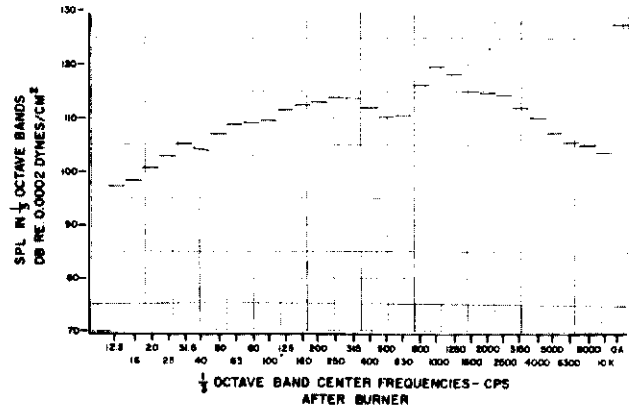


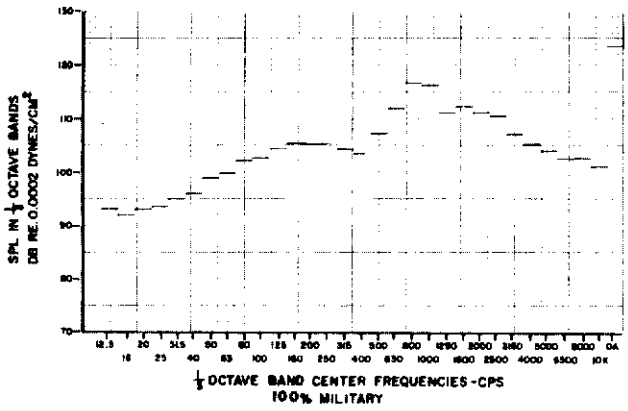


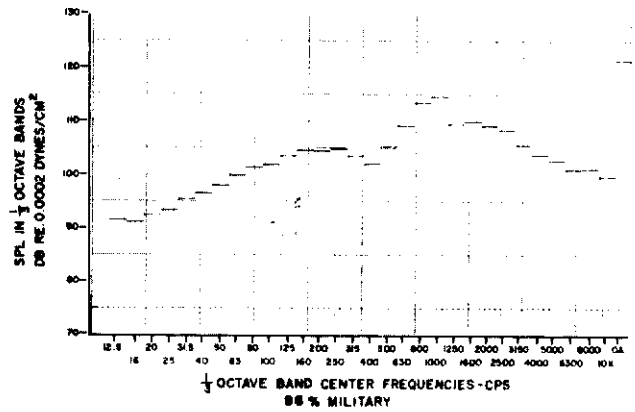


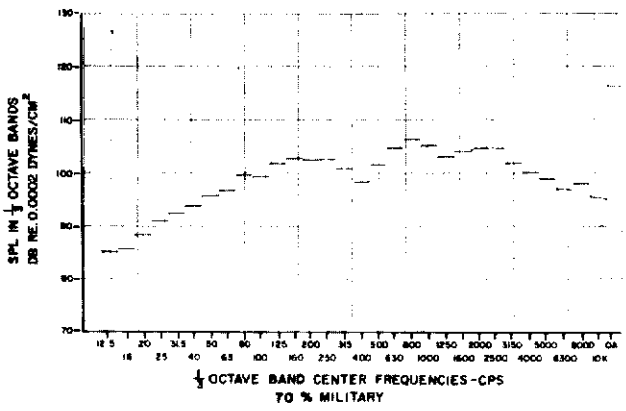


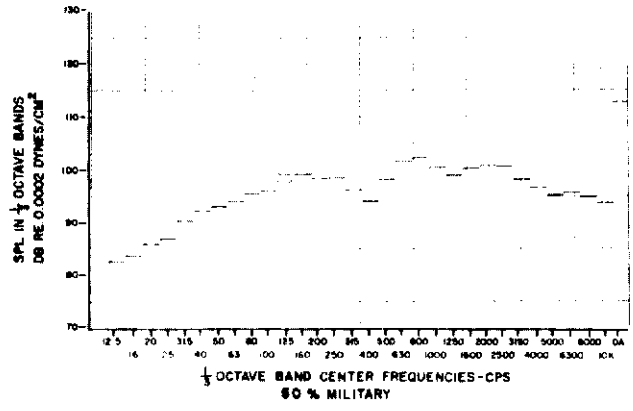


Figure 38. One-Third Octave Band Spectra and Overall SPL for Spot 8

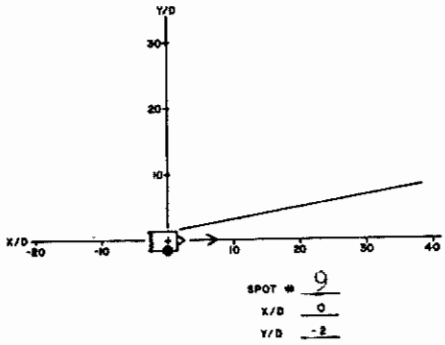


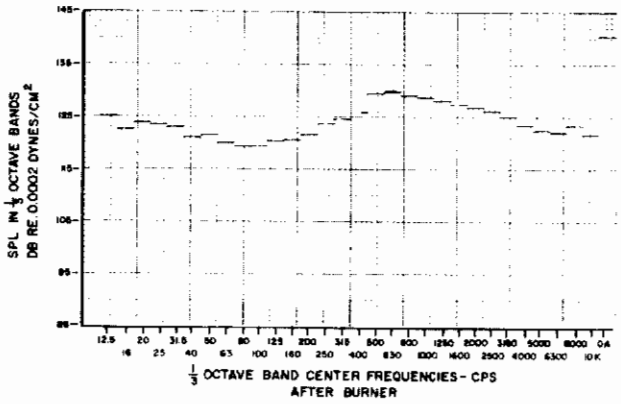


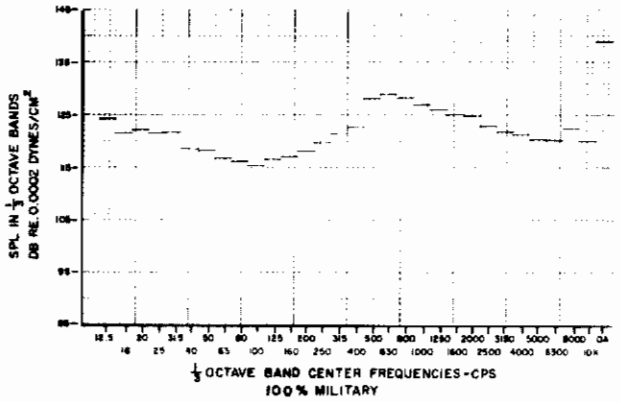


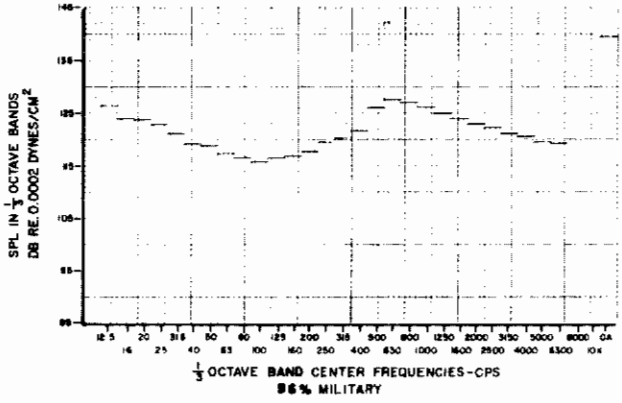


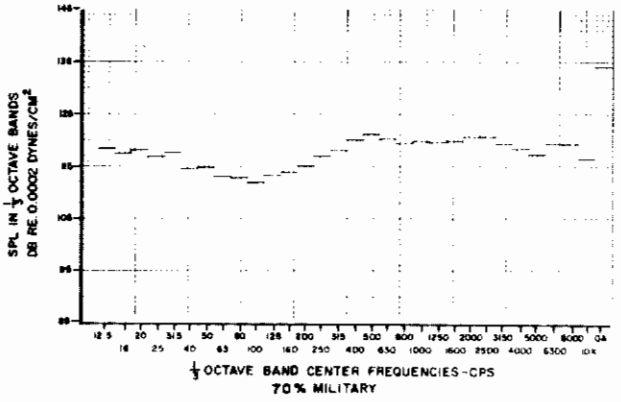


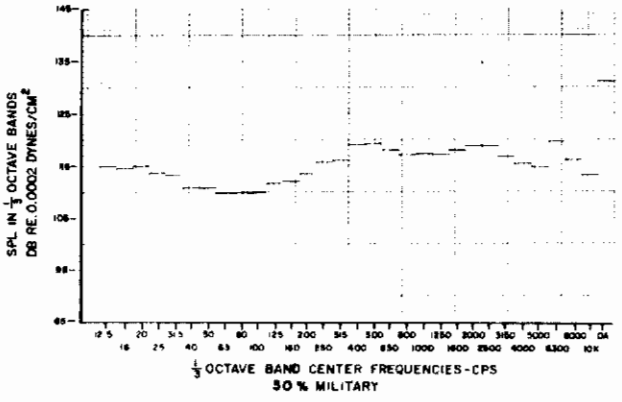


Figure 39. One-Third Octave Band Spectra and Overall SPL for Spot 9

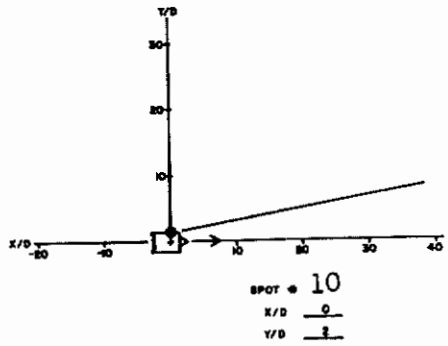


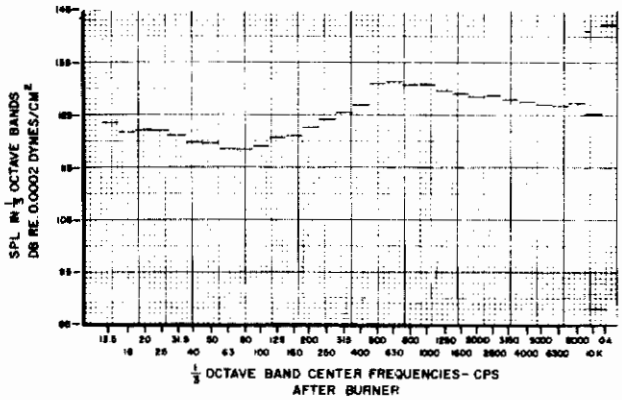


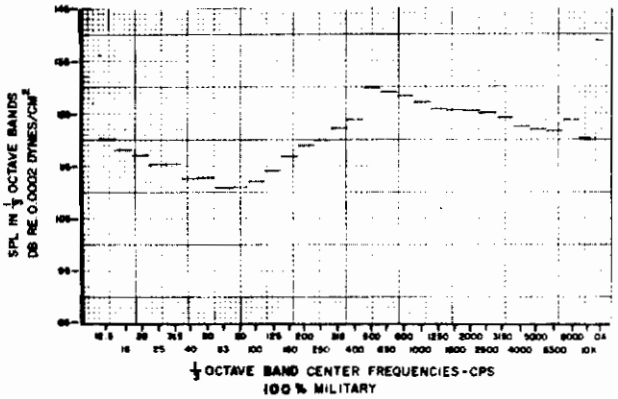


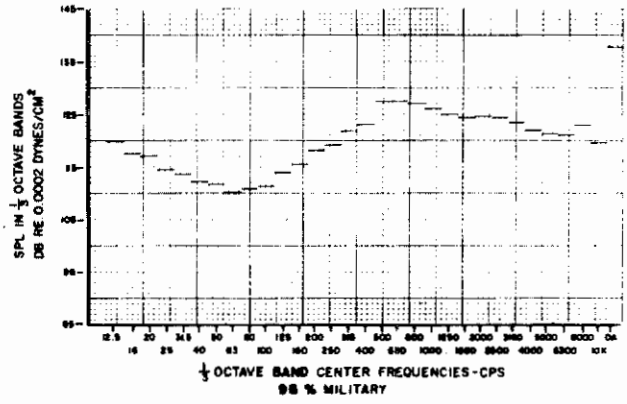


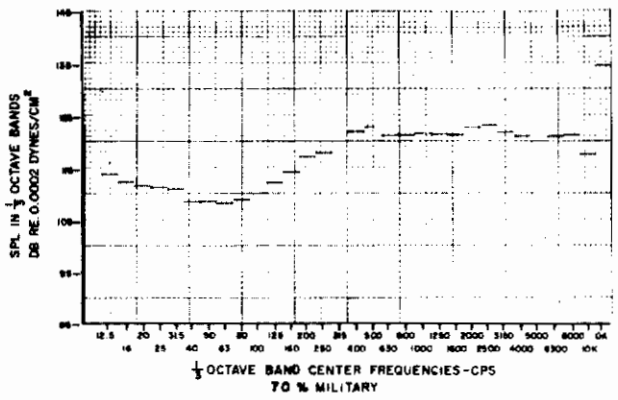


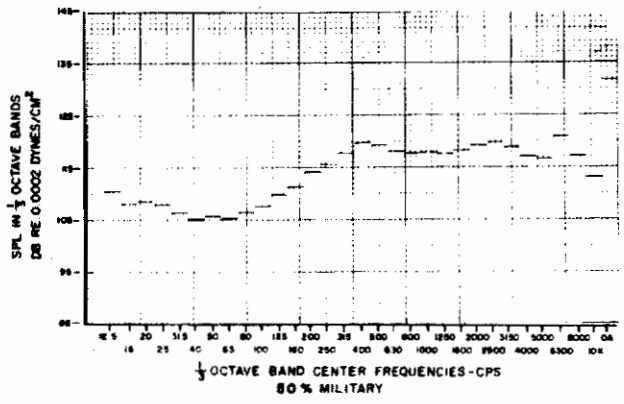


Figure 40. One-Third Octave Band Spectra and Overall SPL for Spot 10

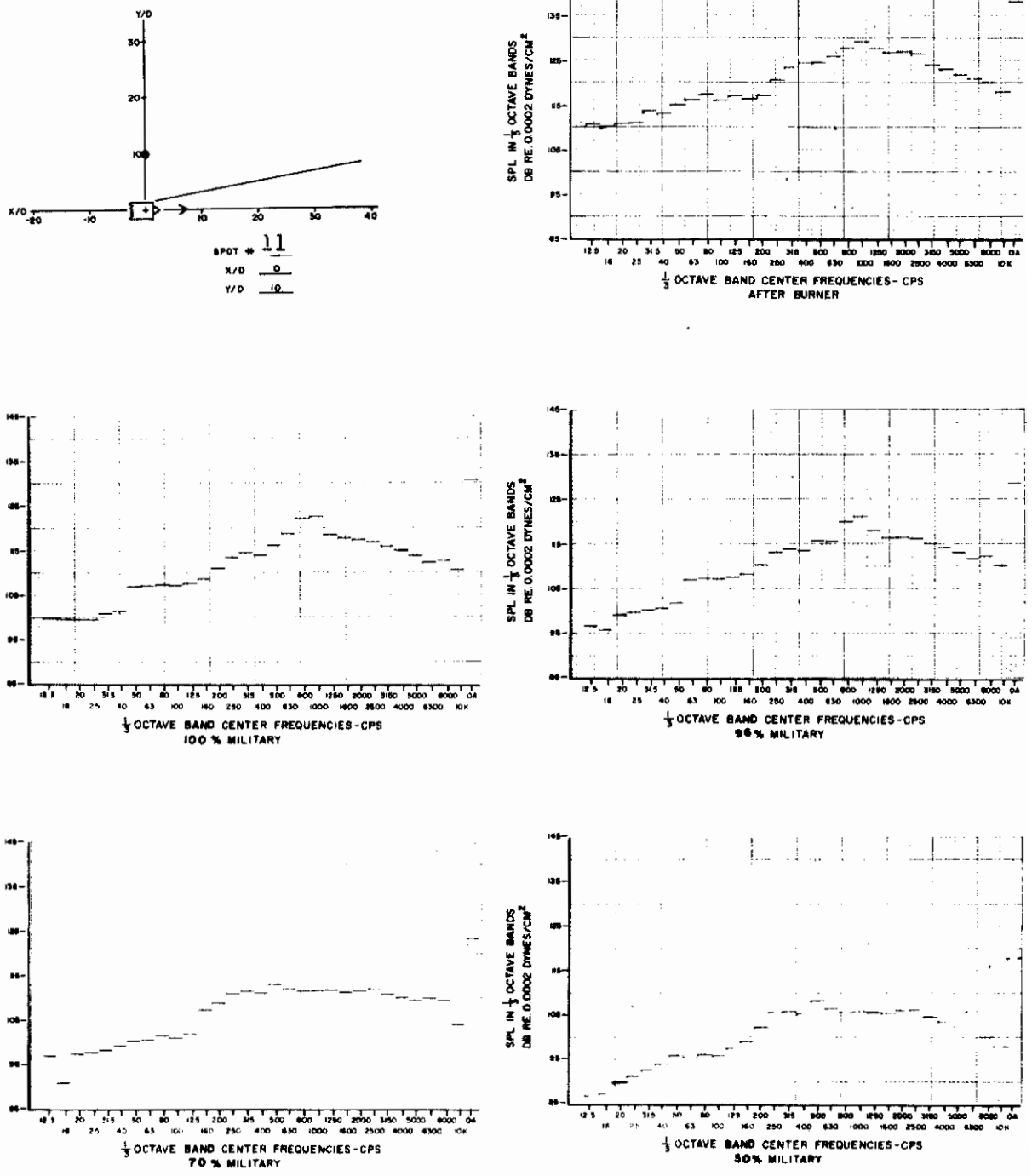


Figure 41. One-Third Octave Band Spectra and Overall SPL for Spot 11

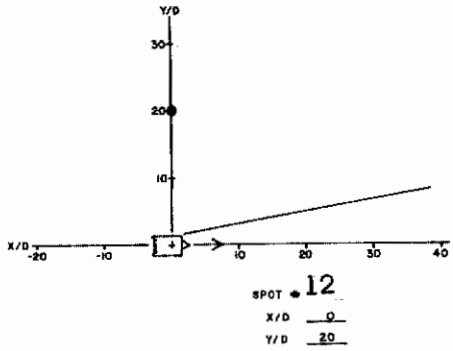


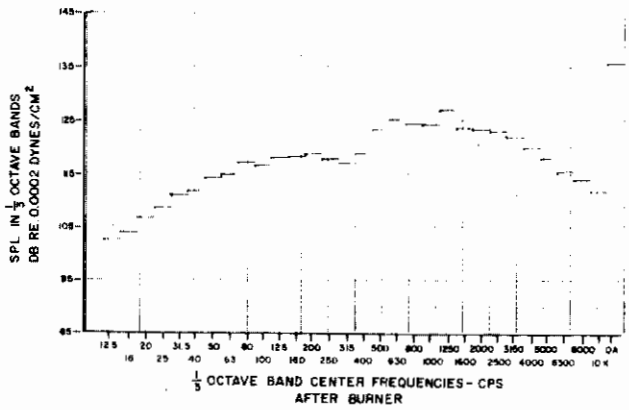


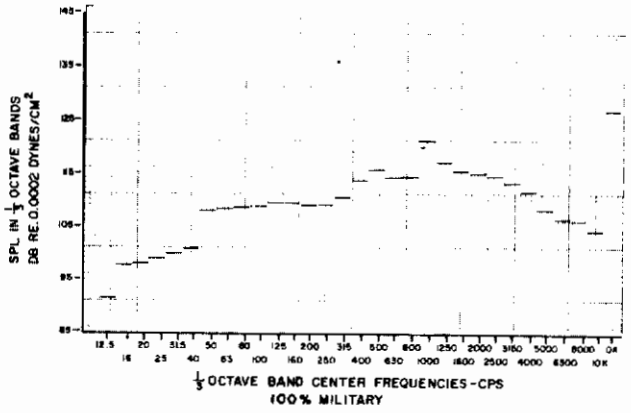


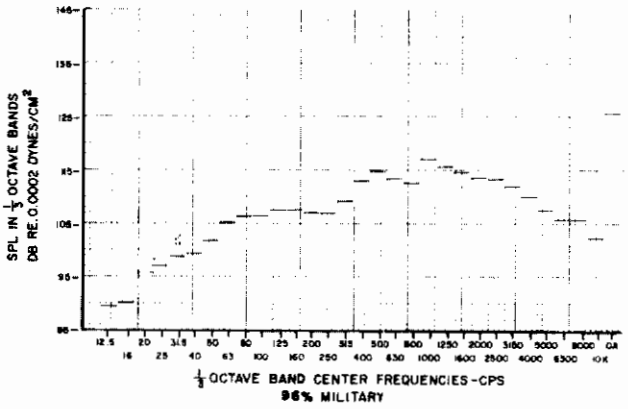


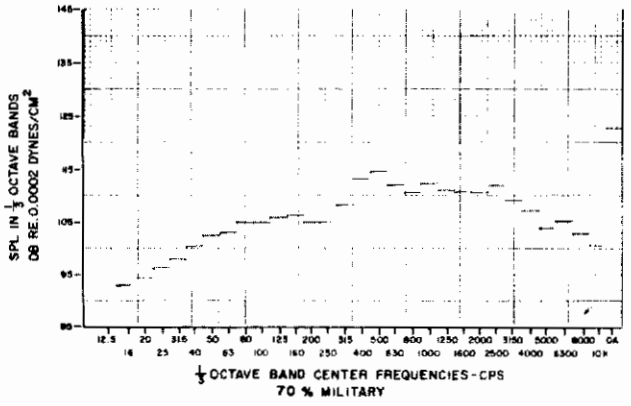


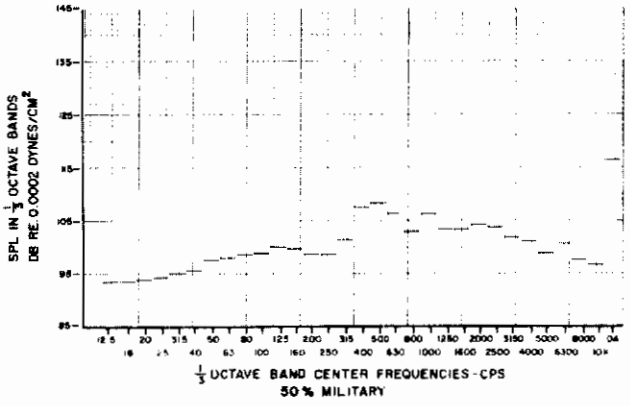


Figure 42. One-Third Octave Band Spectra and Overall SPL for Spot 12

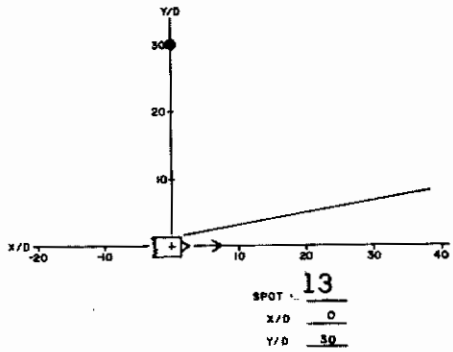


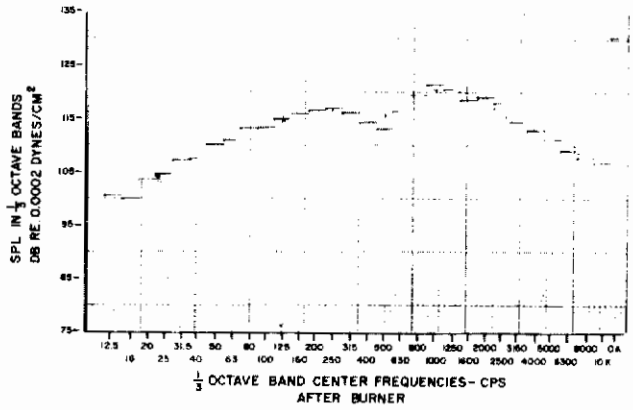


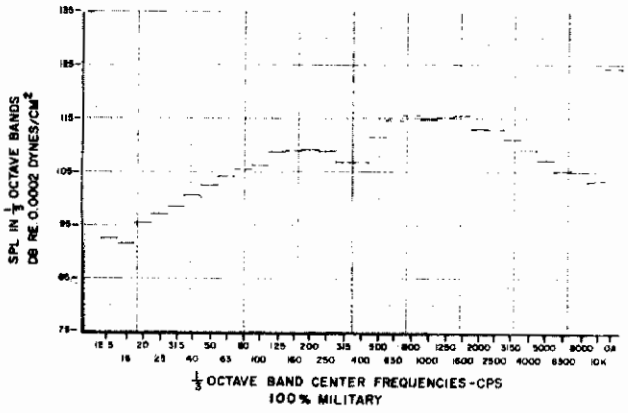


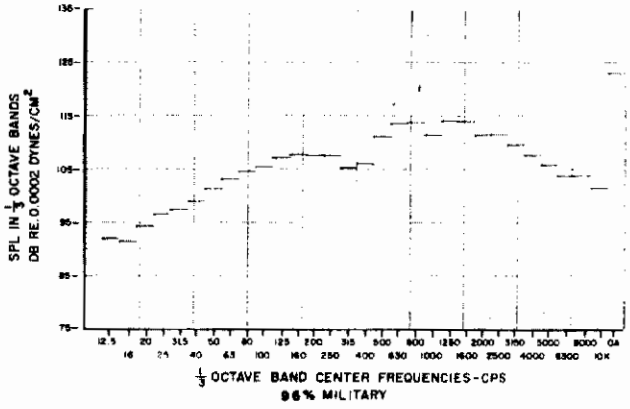


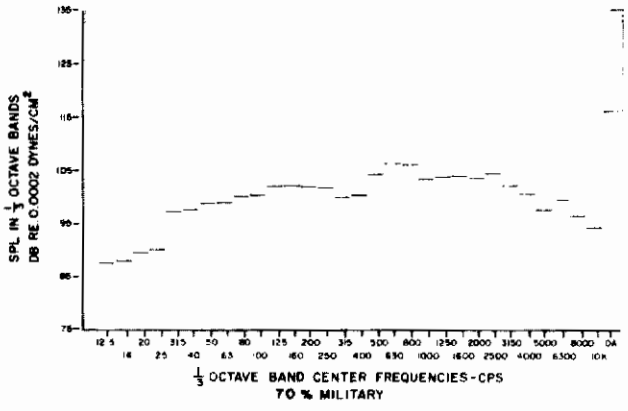


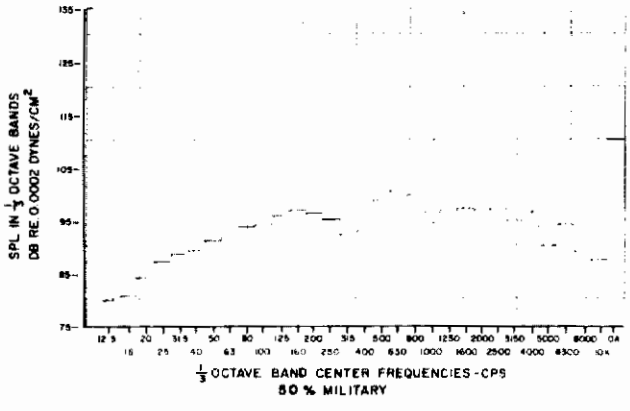


Figure 43. One-Third Octave Band Spectra and Overall SPL for Spot 13

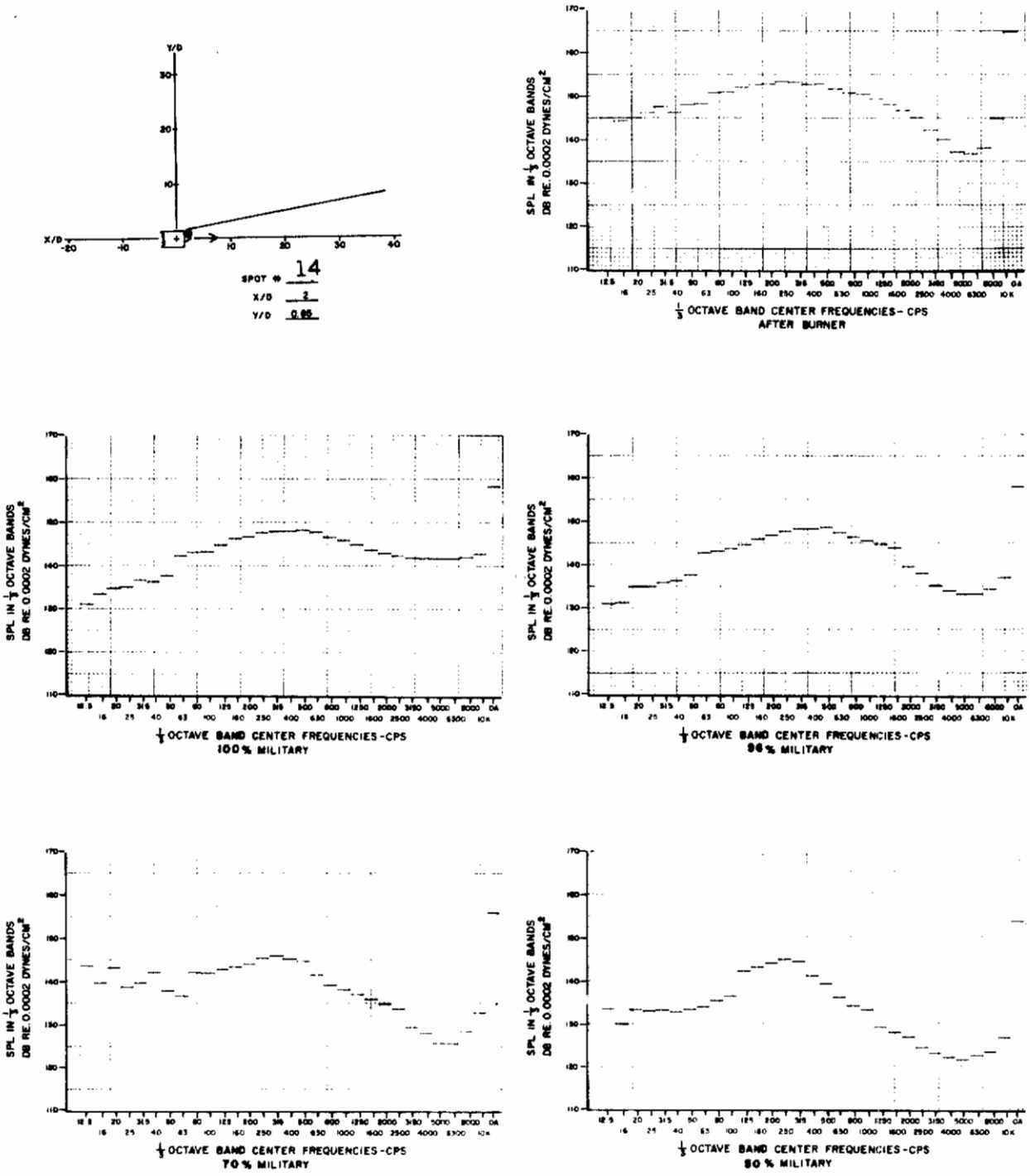


Figure 44. One-Third Octave Band Spectra and Overall SPL for Spot 14

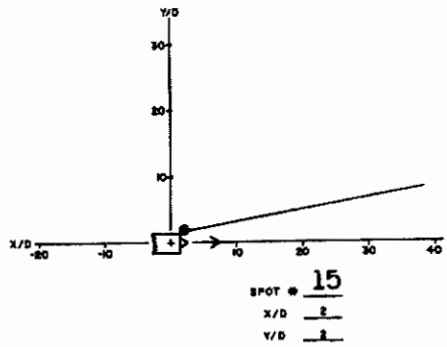


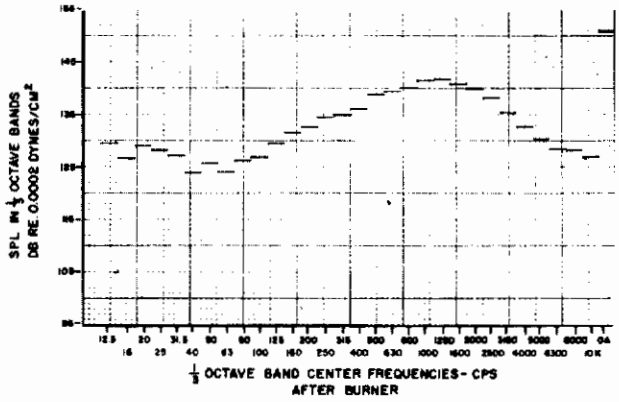


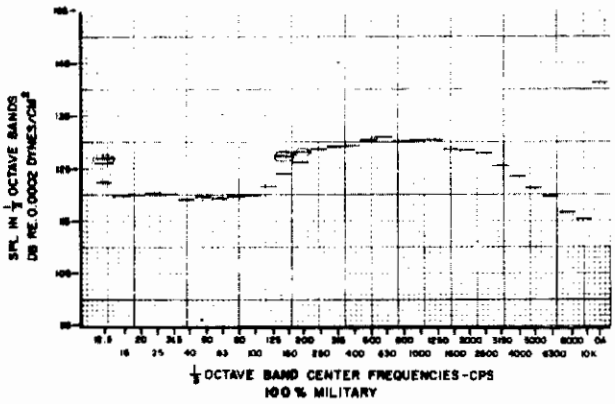


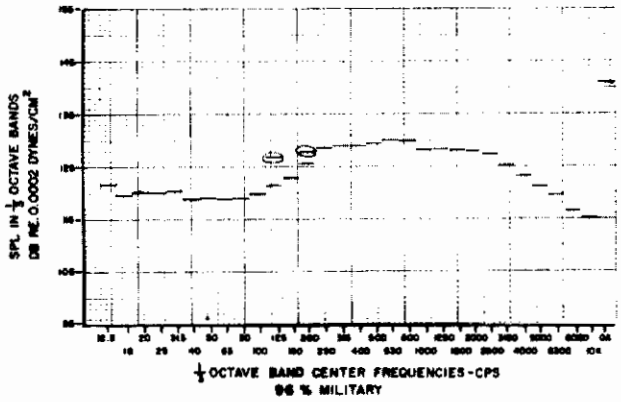


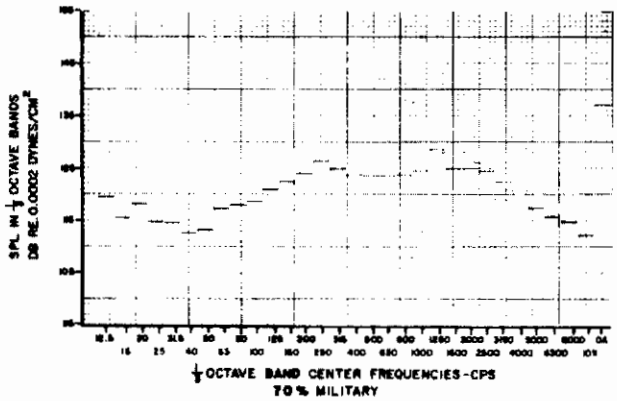


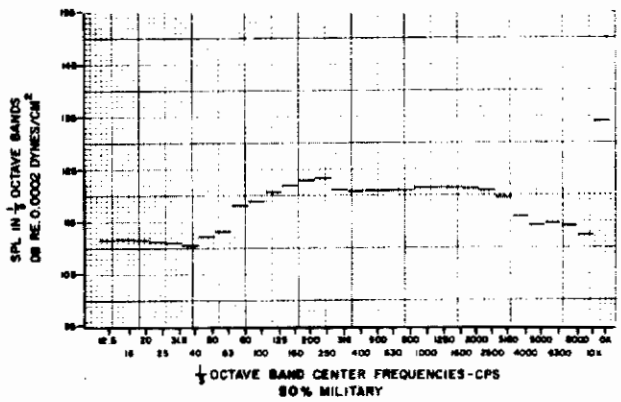


Figure 45. One-Third Octave Band Spectra and Overall SPL for Spot 15

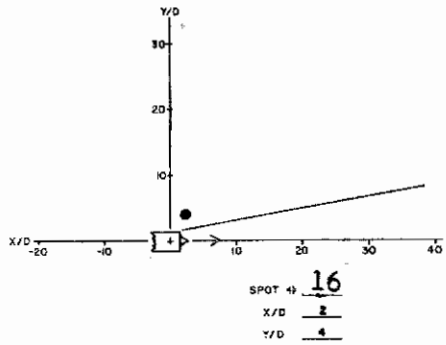


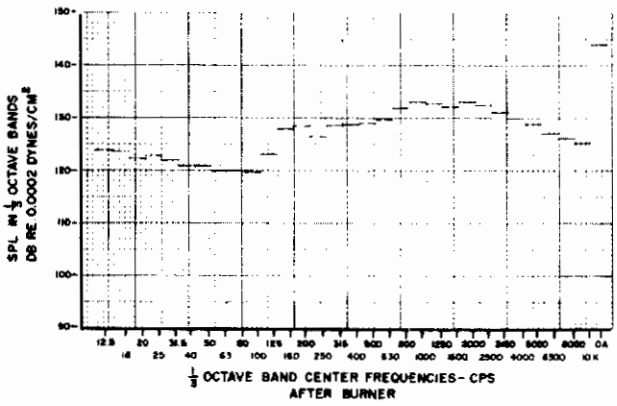


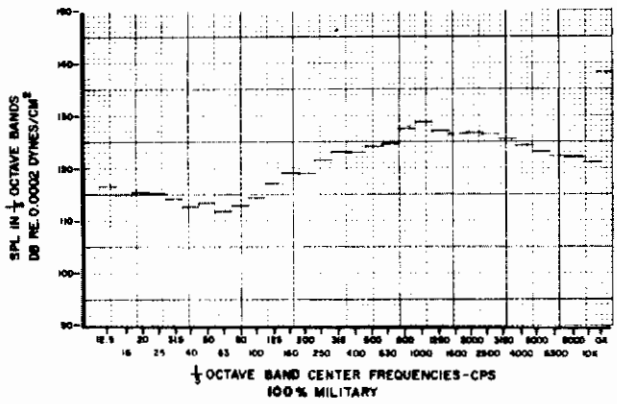


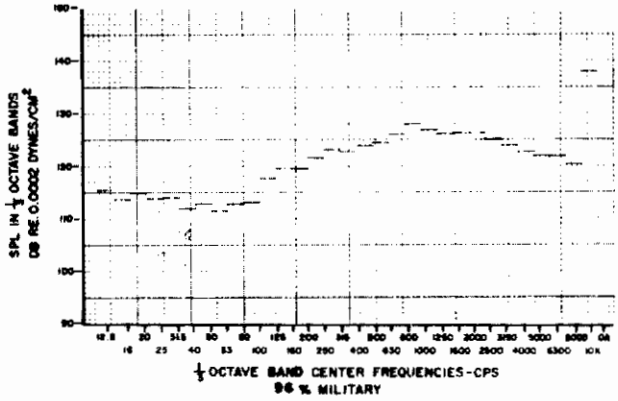


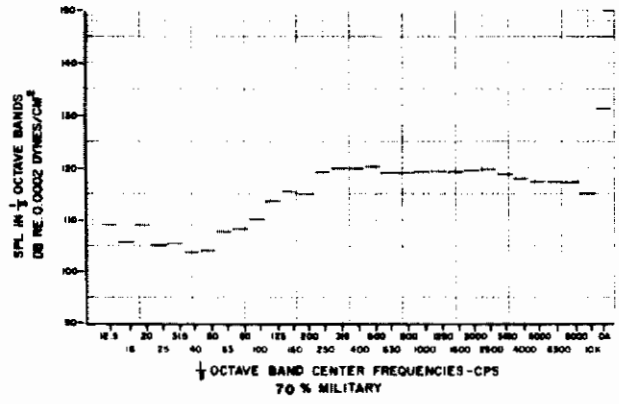


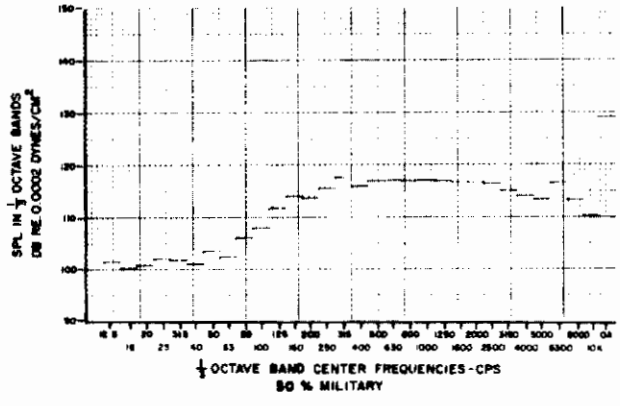


Figure 46. One-Third Octave Band Spectra and Overall SPL for Spot 16

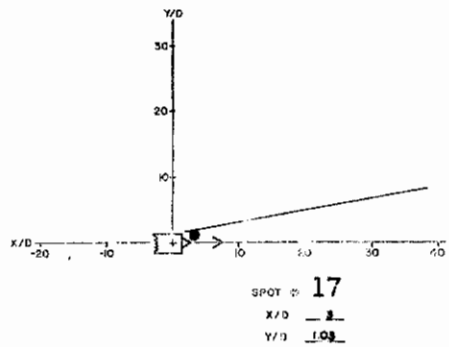


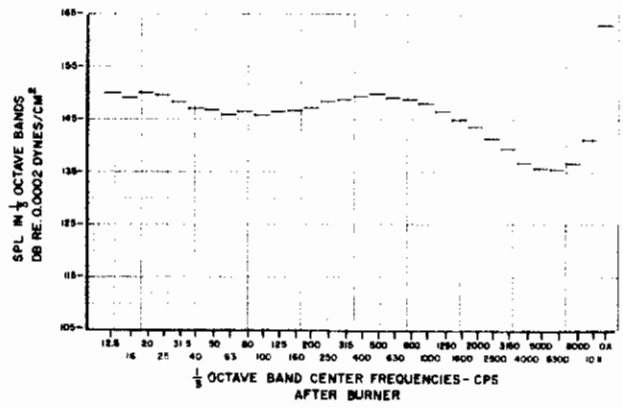


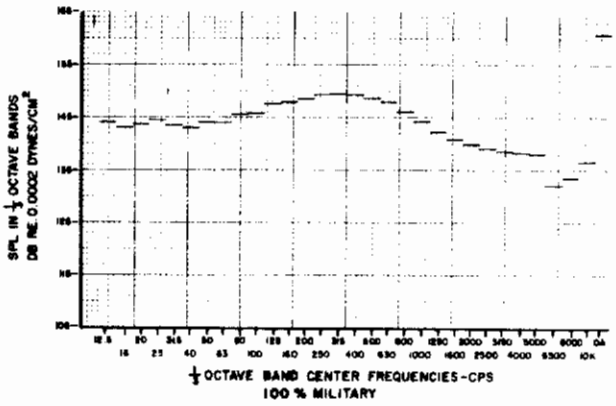


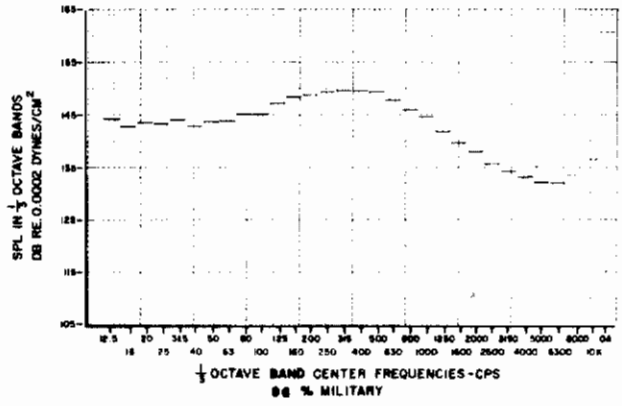


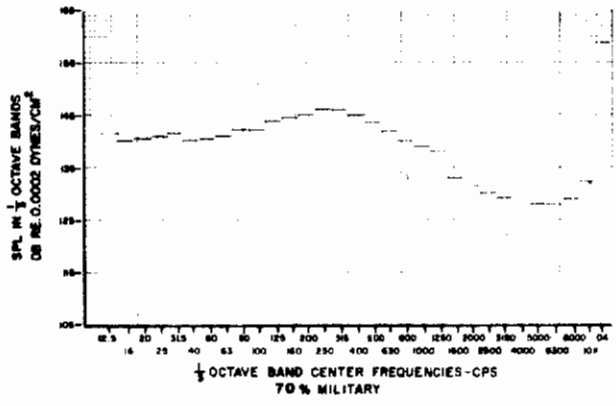


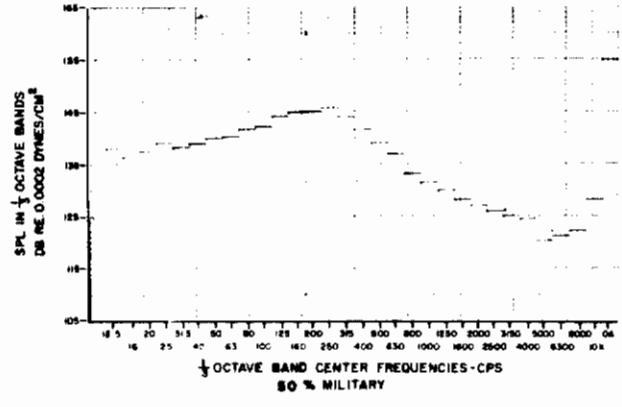


Figure 47. One-Third Octave Band Spectra and Overall SPL for Spot 17

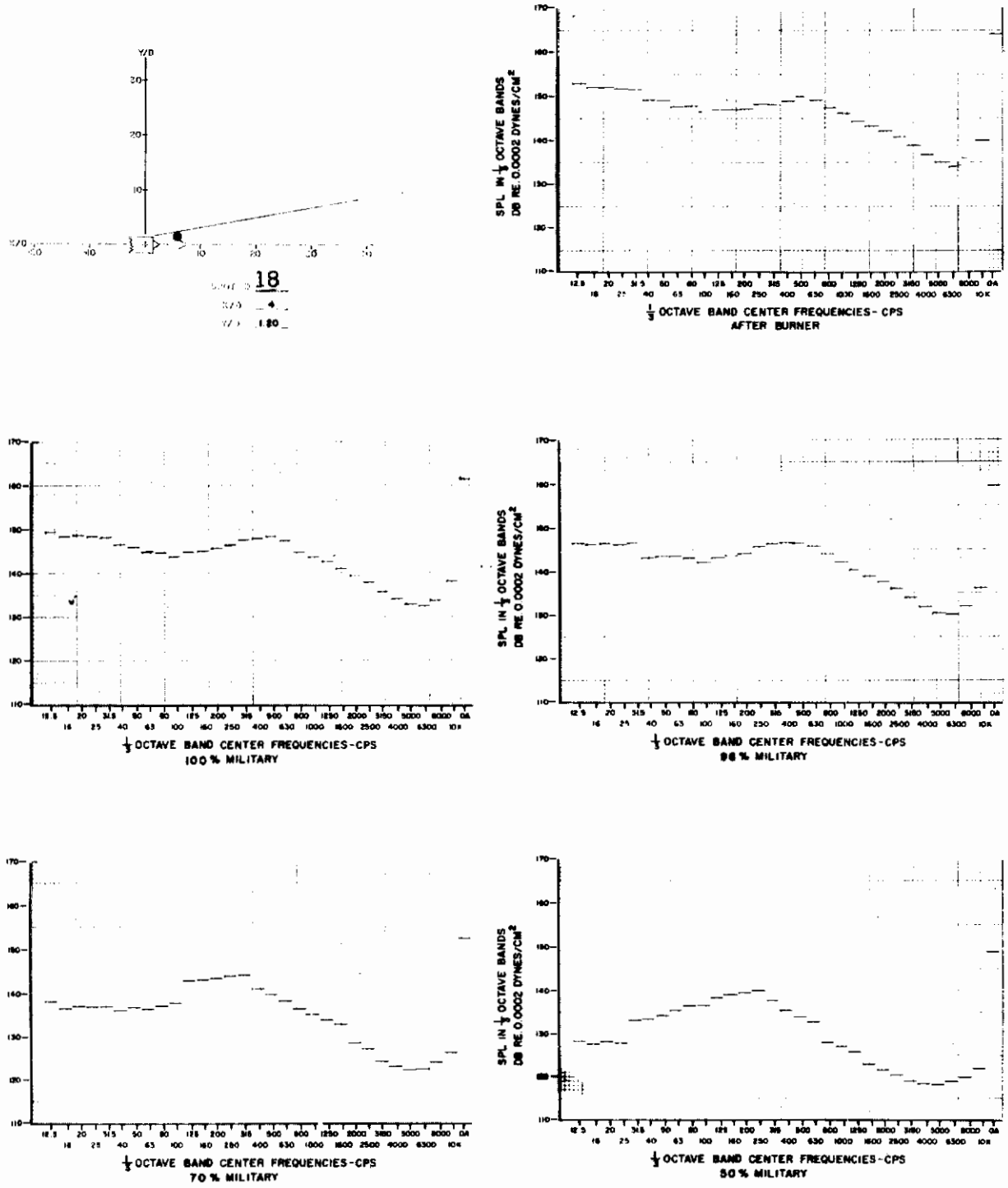


Figure 48. One-Third Octave Band Spectra and Overall SPL for Spot 18

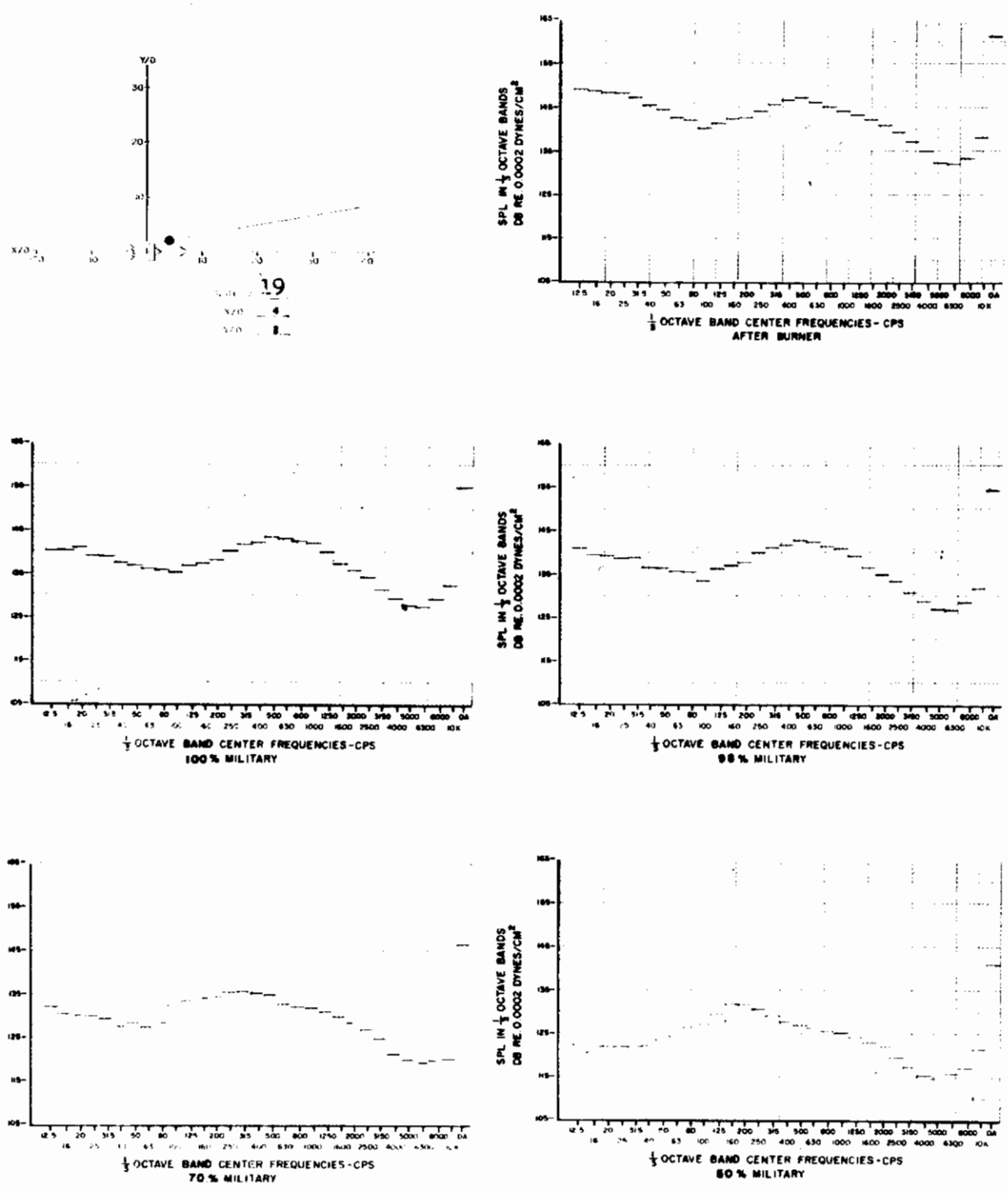


Figure 49. One-Third Octave Band Spectra and Overall SPL for Spot 19

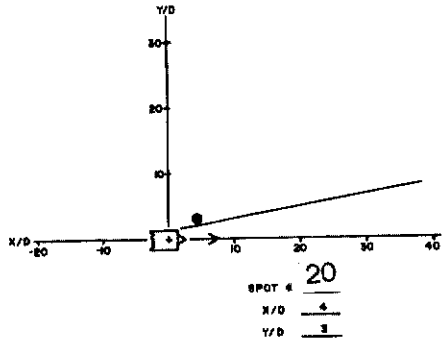


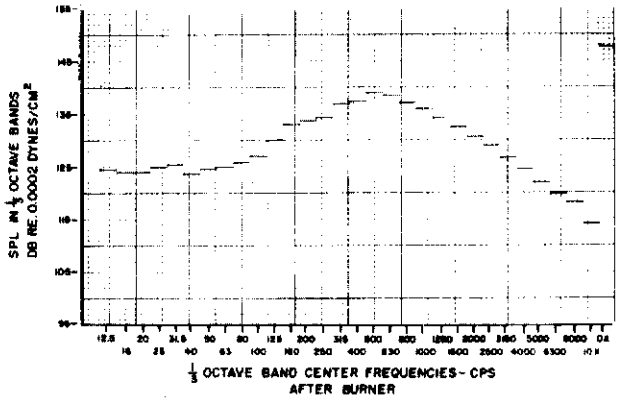


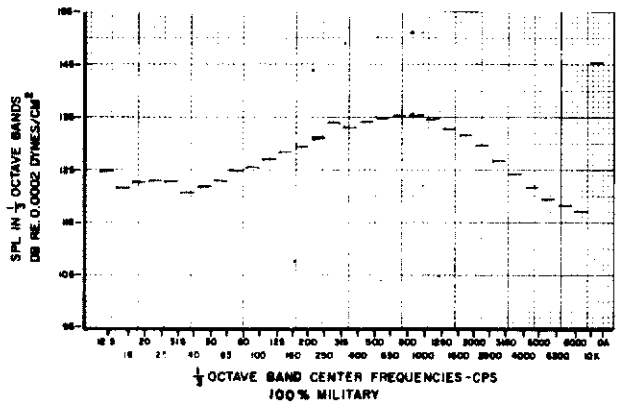


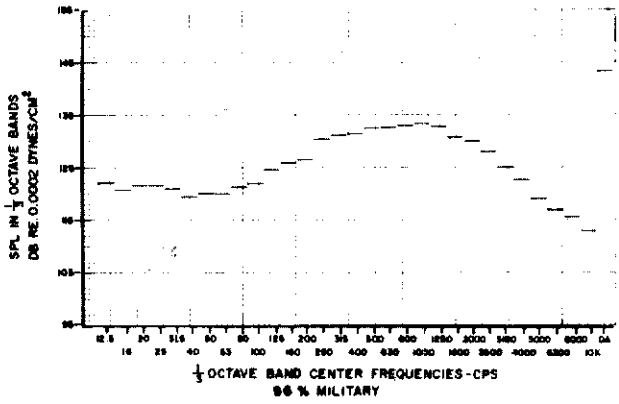


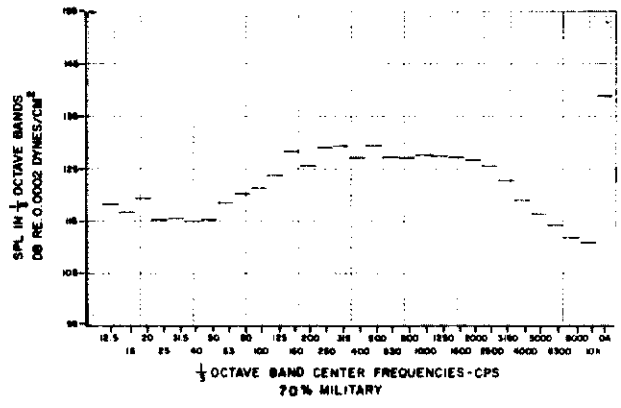


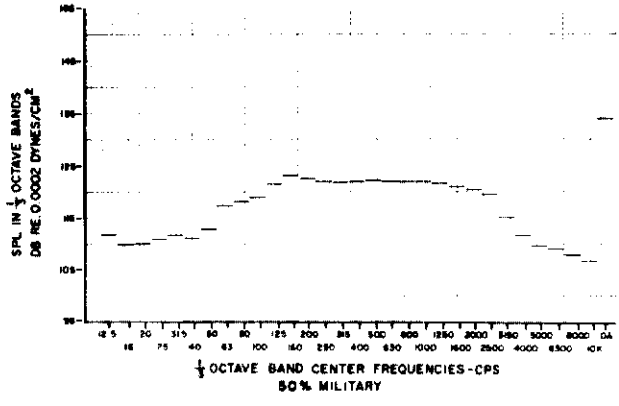


Figure 50. One-Third Octave Band Spectra and Overall SPL for Spot 20

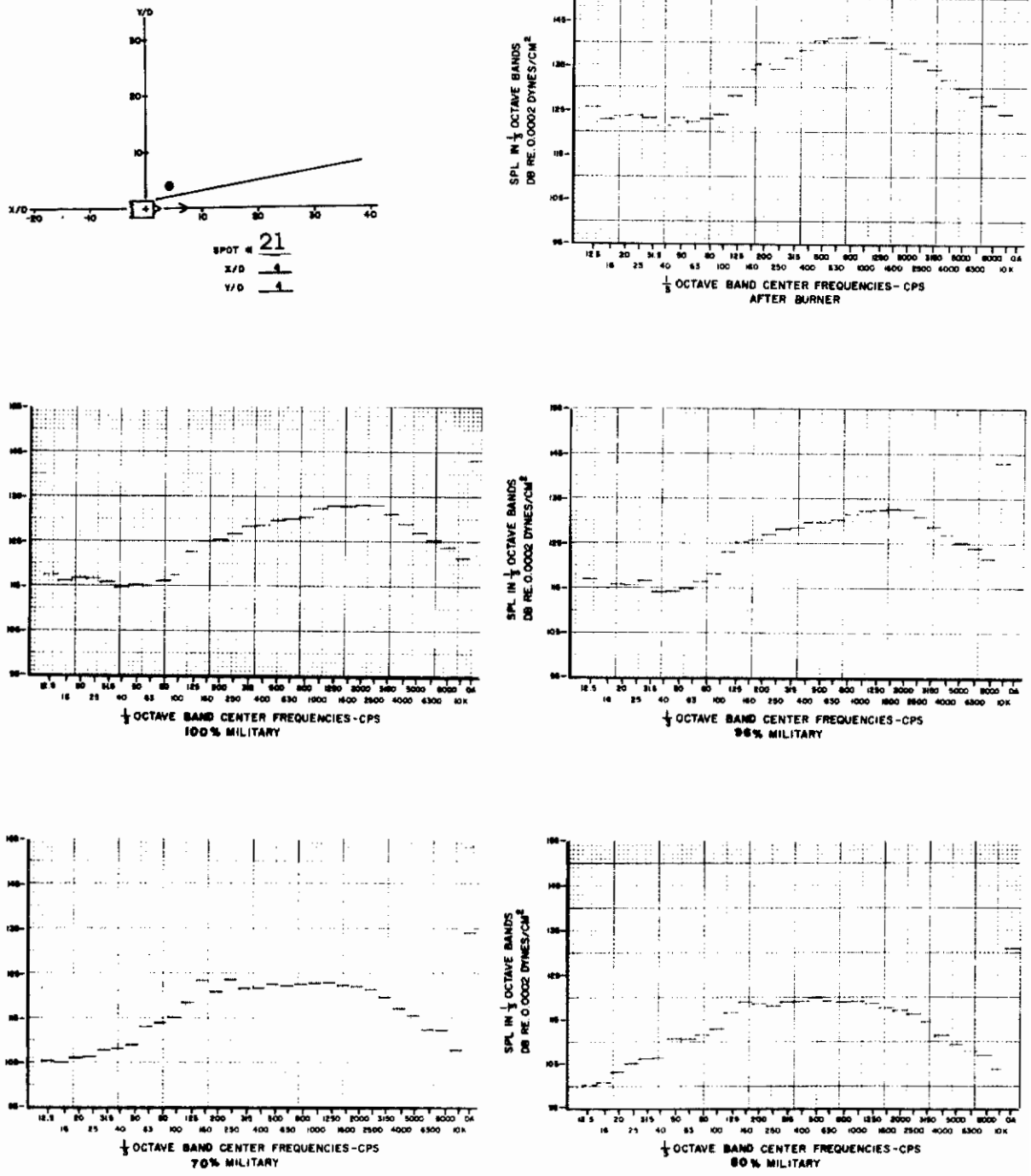


Figure 51. One-Third Octave Band Spectra and Overall SPL for Spot 21

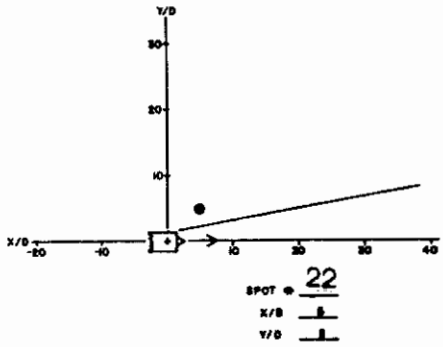


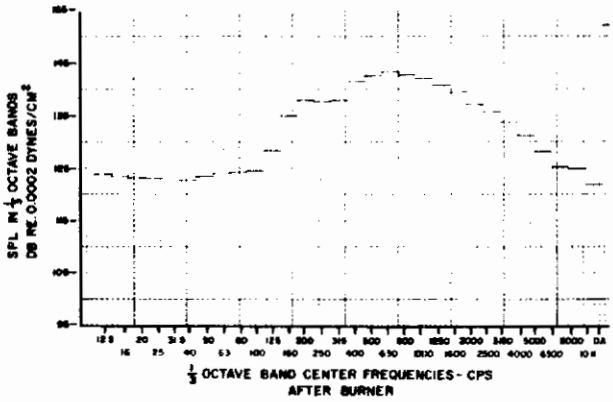


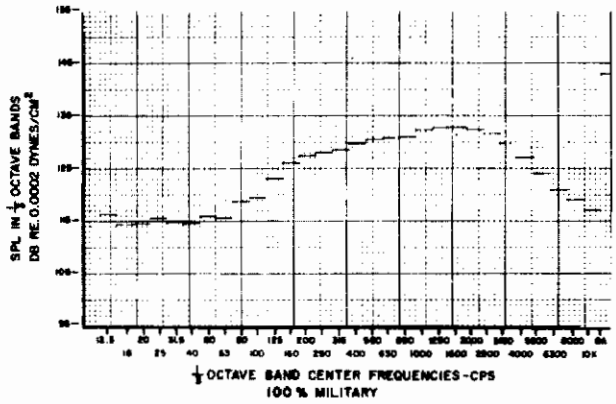


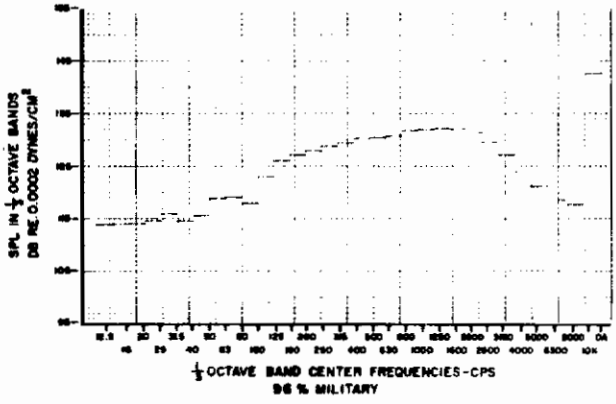


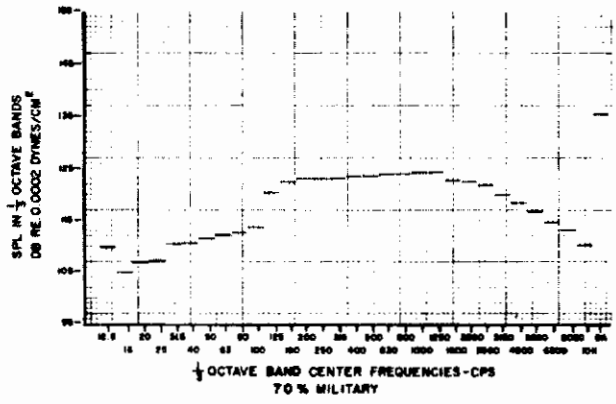


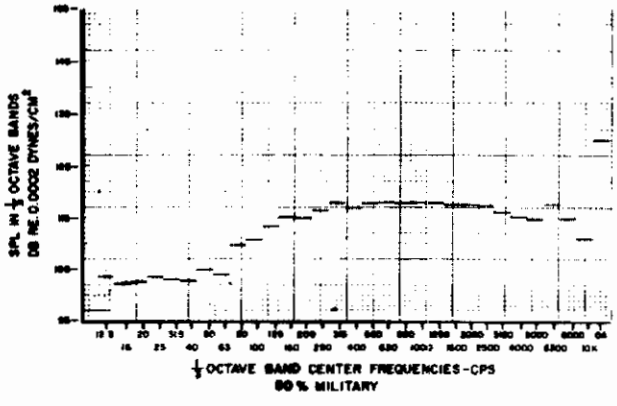


Figure 52. One-Third Octave Band Spectra and Overall SPL for Spot 22

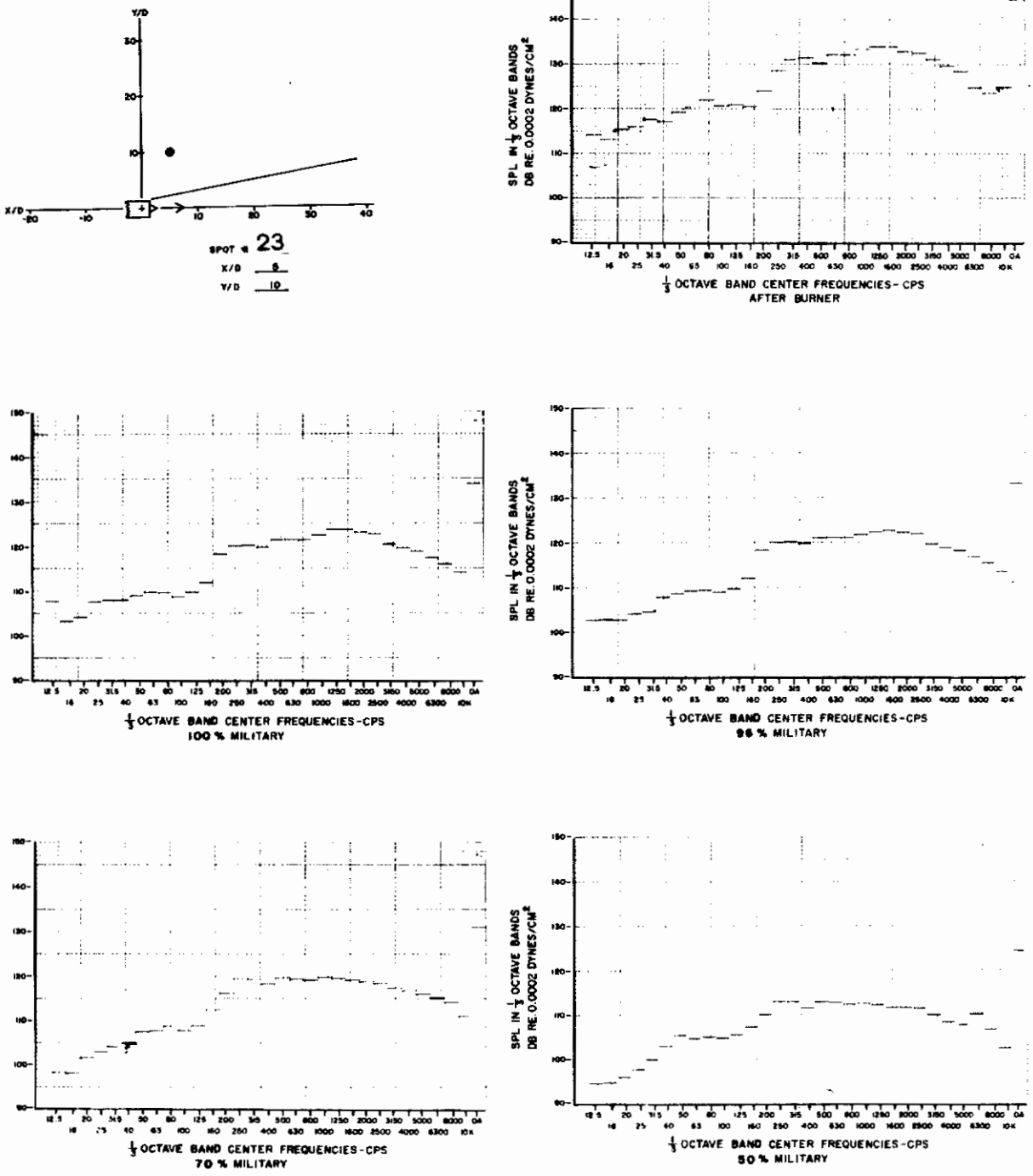


Figure 53. One-Third Octave Band Spectra and Overall SPL for Spot 23

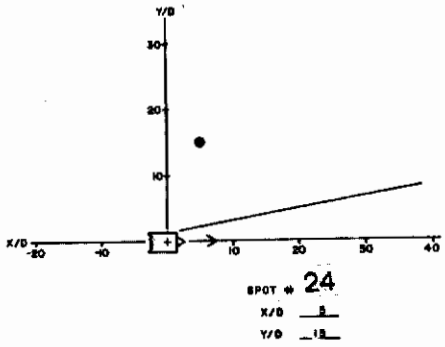


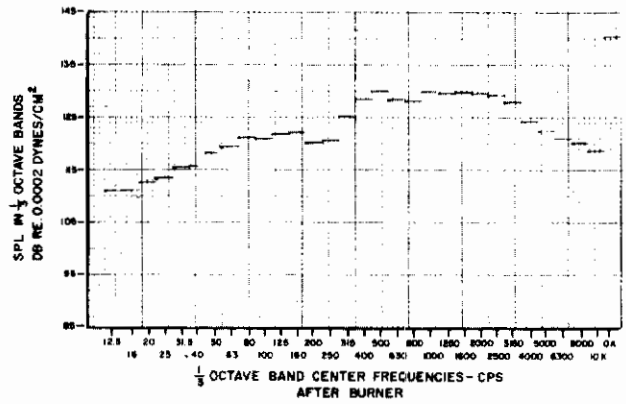


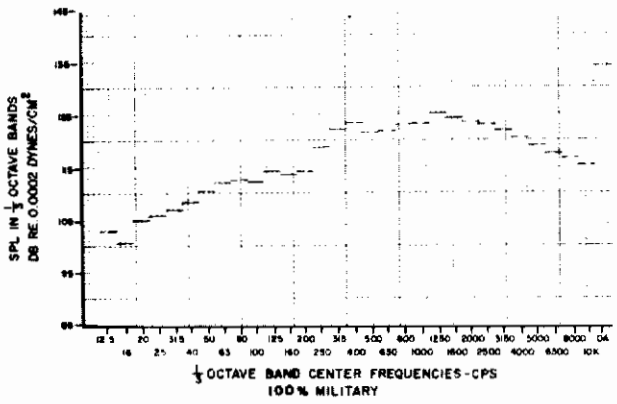


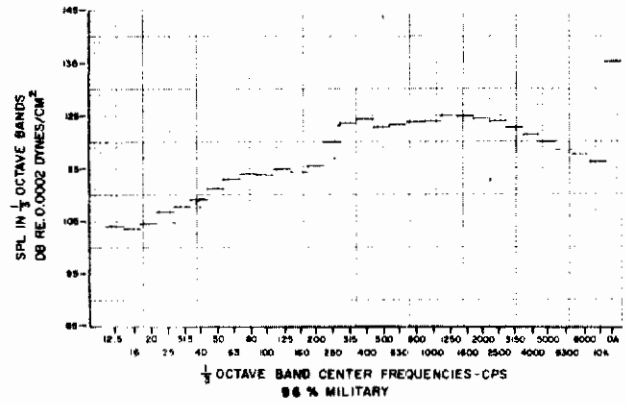


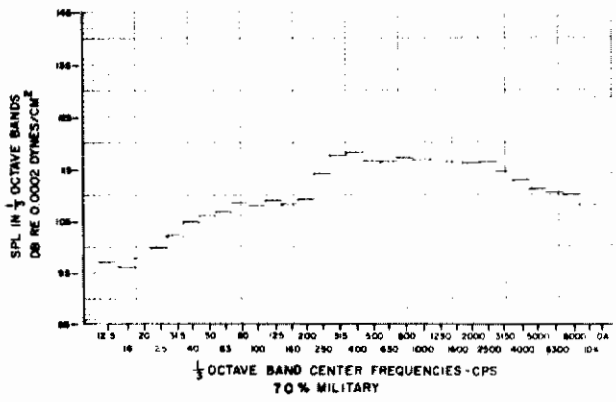


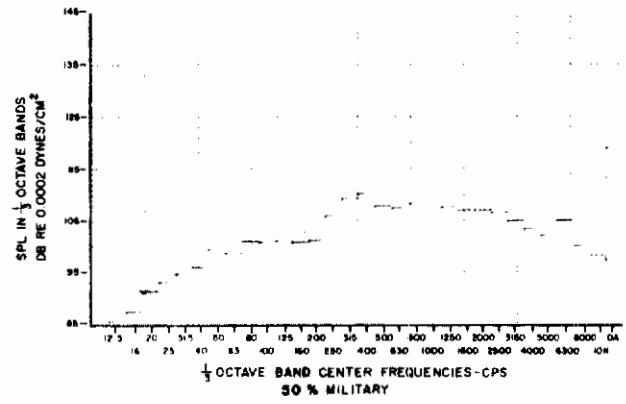


Figure 54. One-Third Octave Band Spectra and Overall SPL for Spot 24

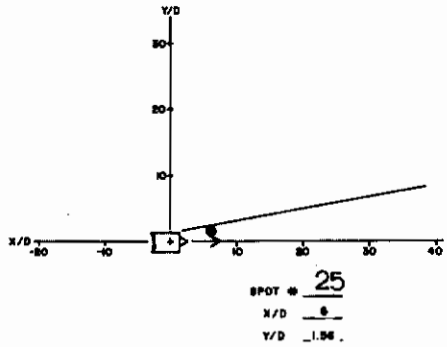


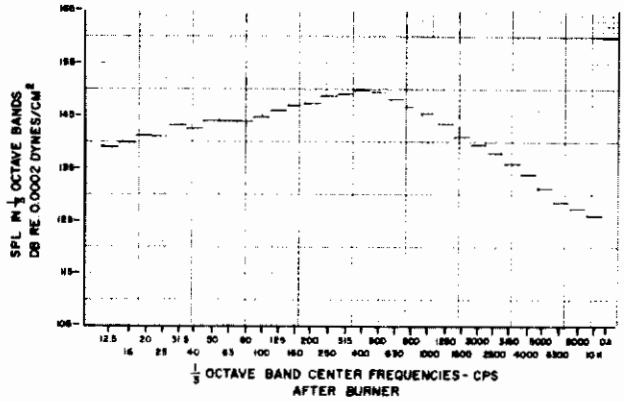


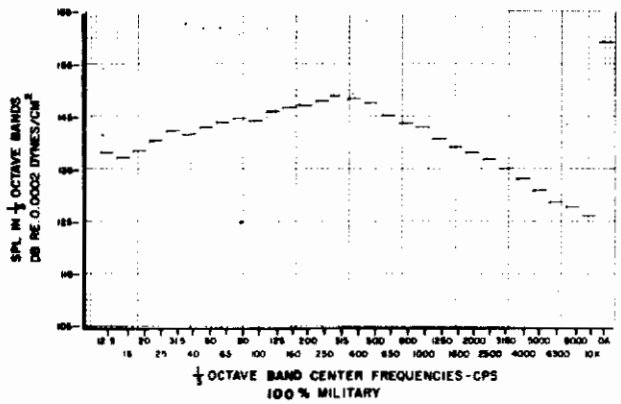


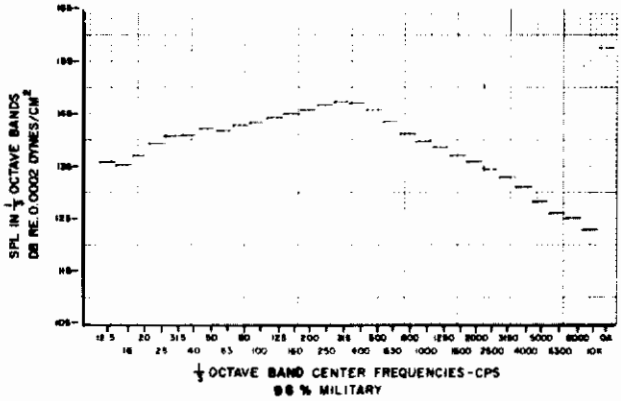


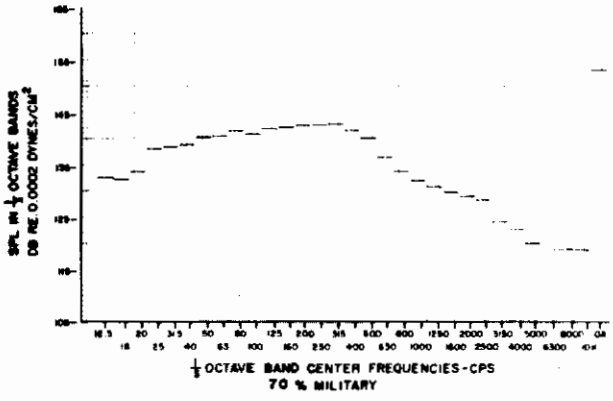


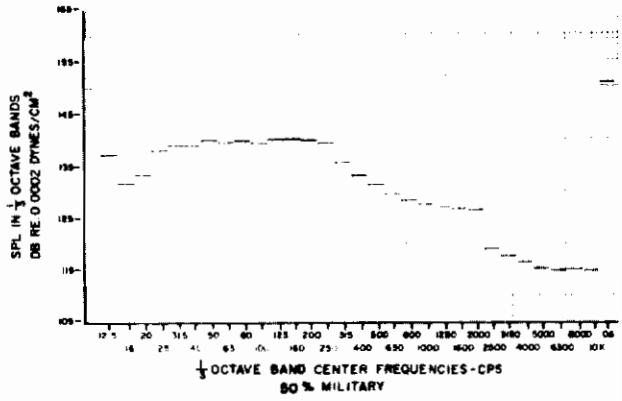


Figure 55. One-Third Octave Band Spectra and Overall SPL for Spot 25

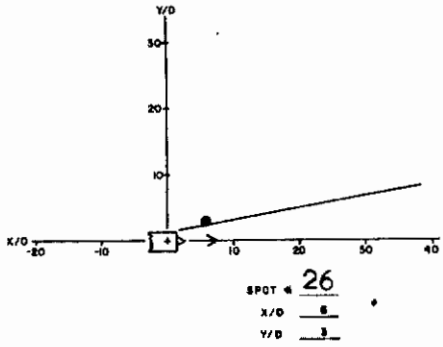


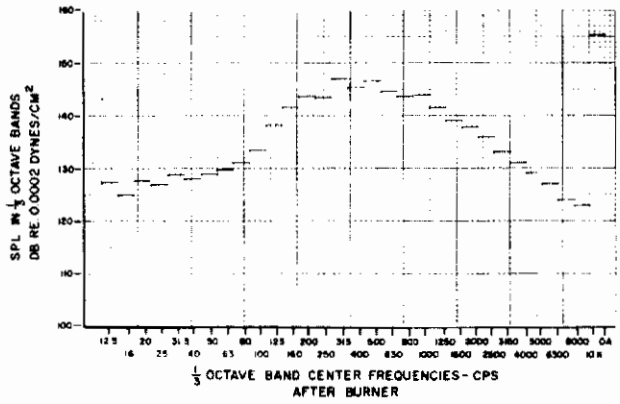


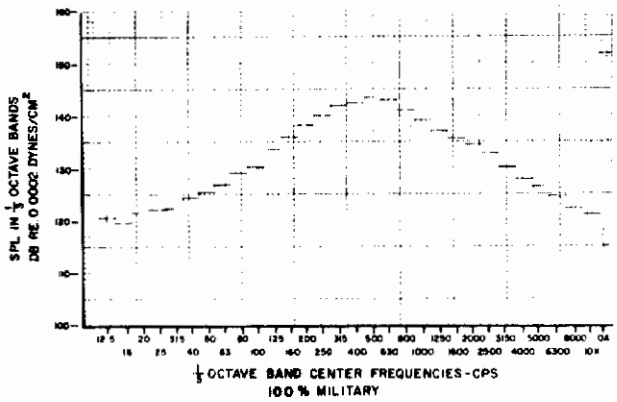


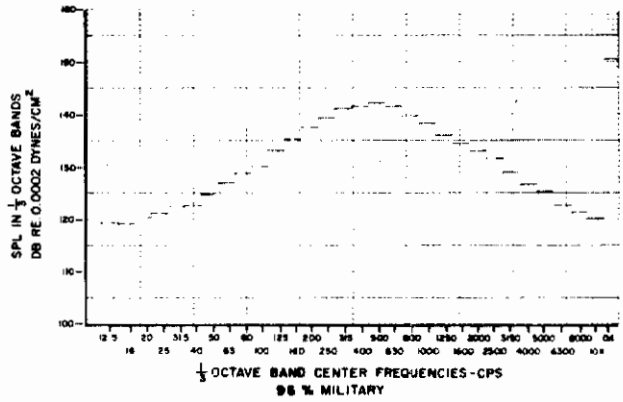


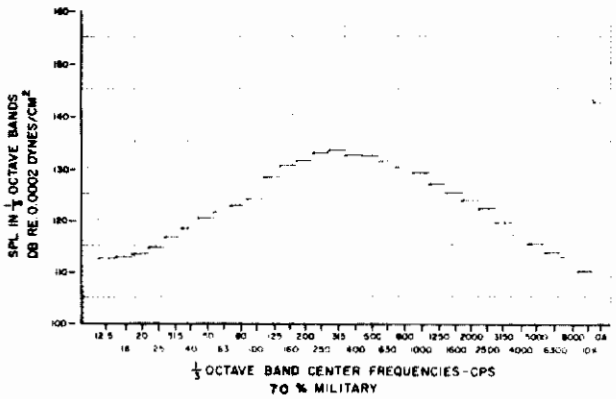


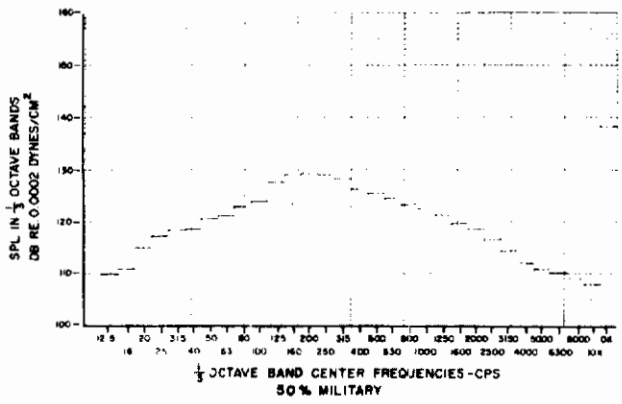


Figure 56. One-Third Octave Band Spectra and Overall SPL for Spot 26

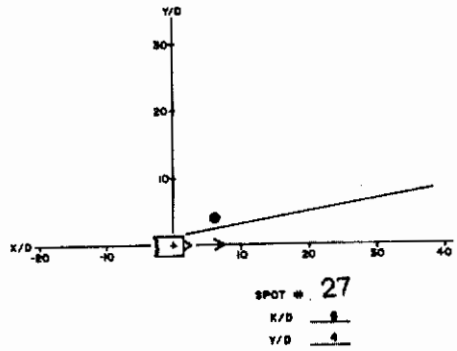


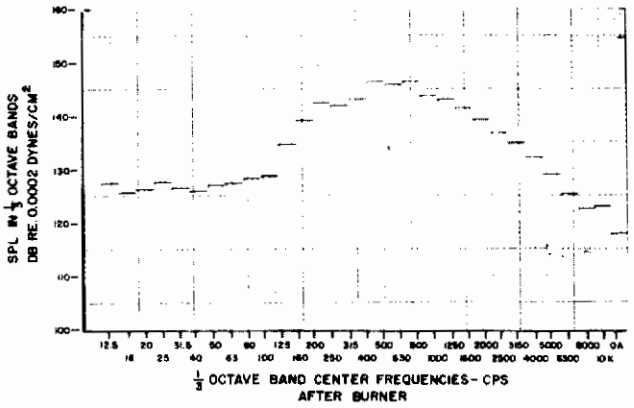


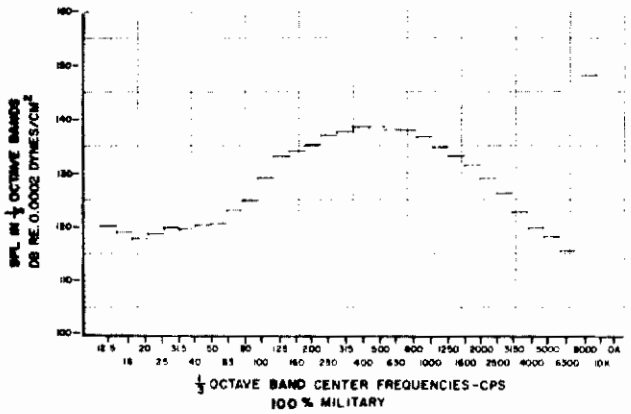


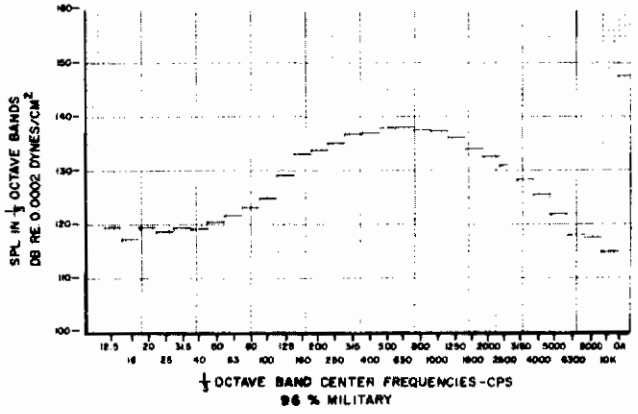


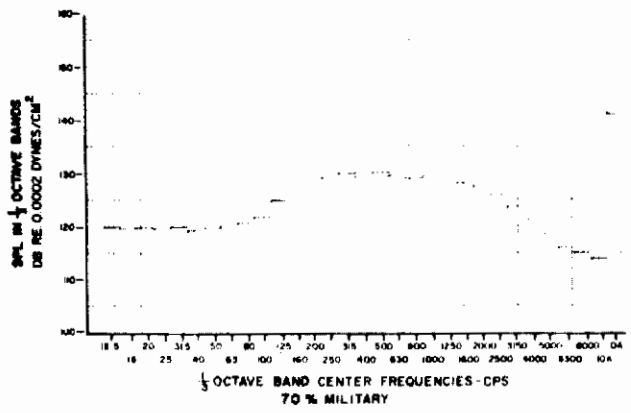


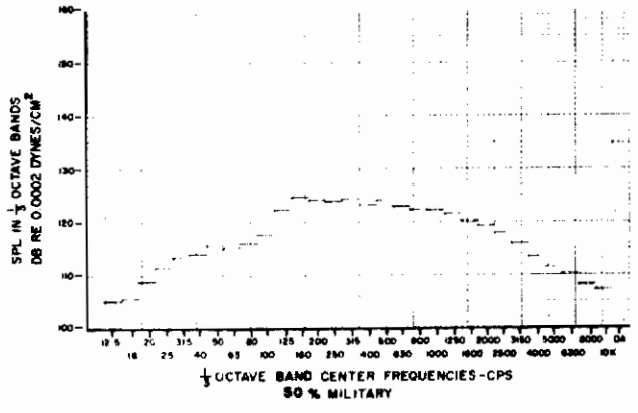


Figure 57. One-Third Octave Band Spectra and Overall SPL for Spot 27

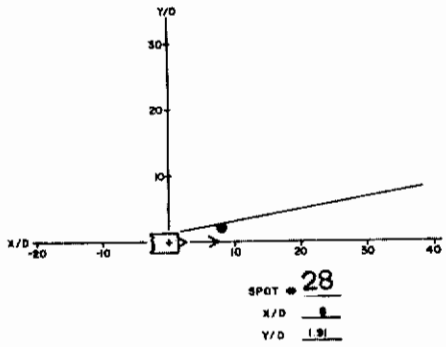


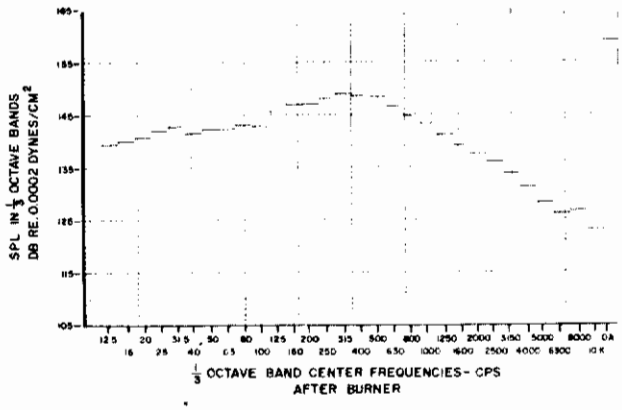


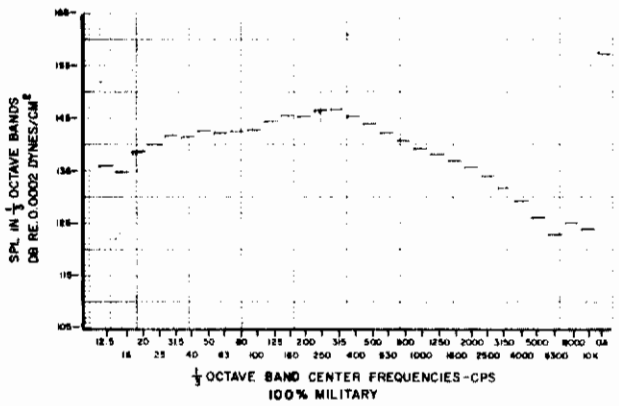


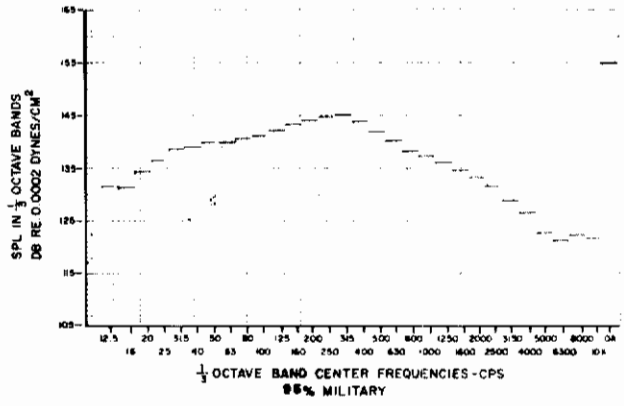


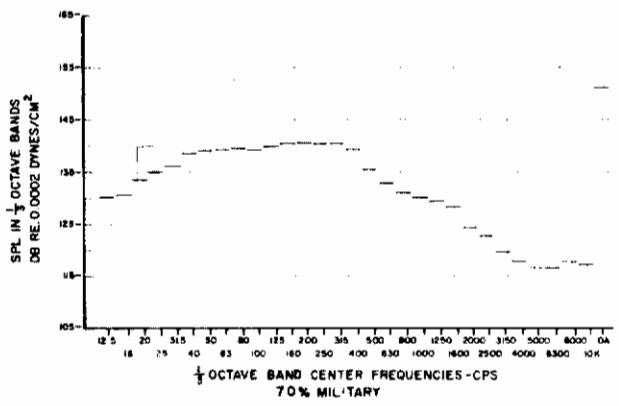


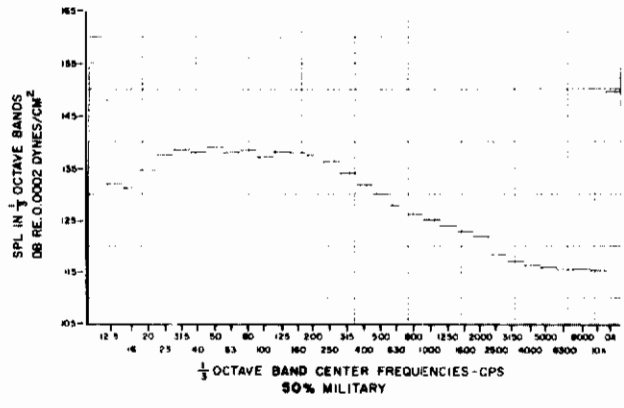


Figure 58. One-Third Octave Band Spectra and Overall SPL for Spot 28

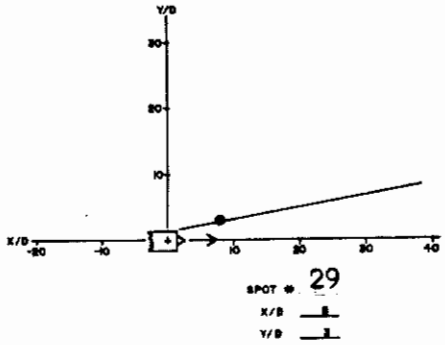


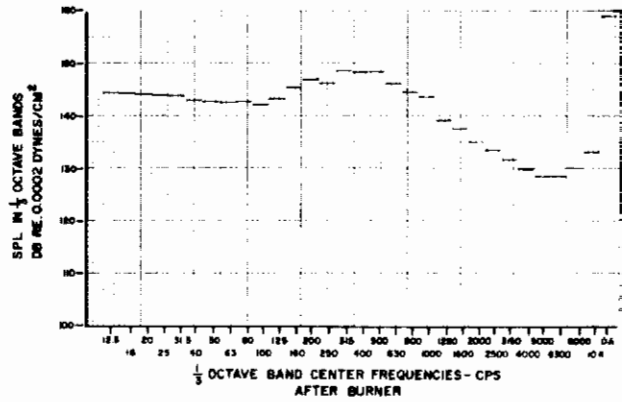


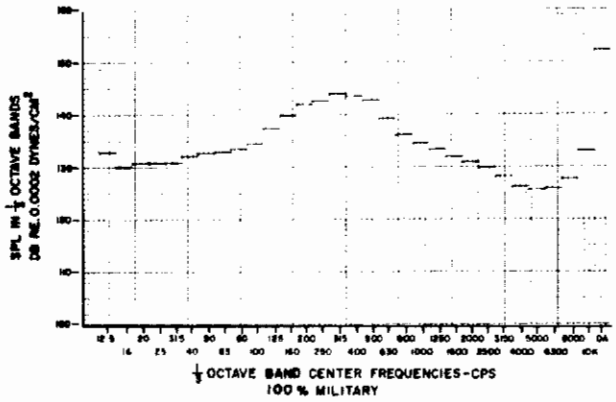


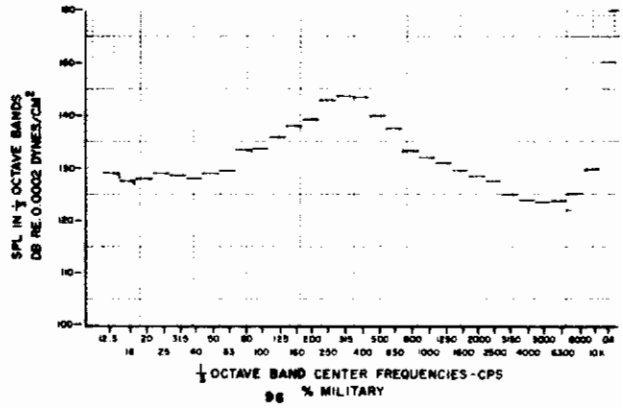


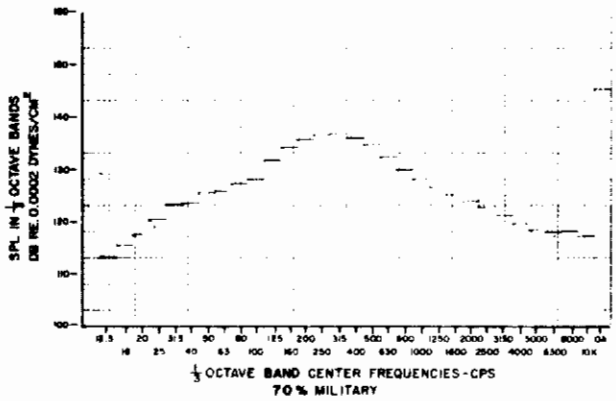


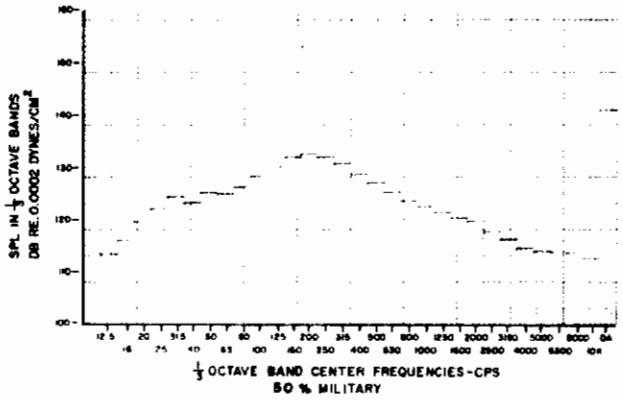


Figure 59. One-Third Octave Band Spectra and Overall SPL for Spot 29

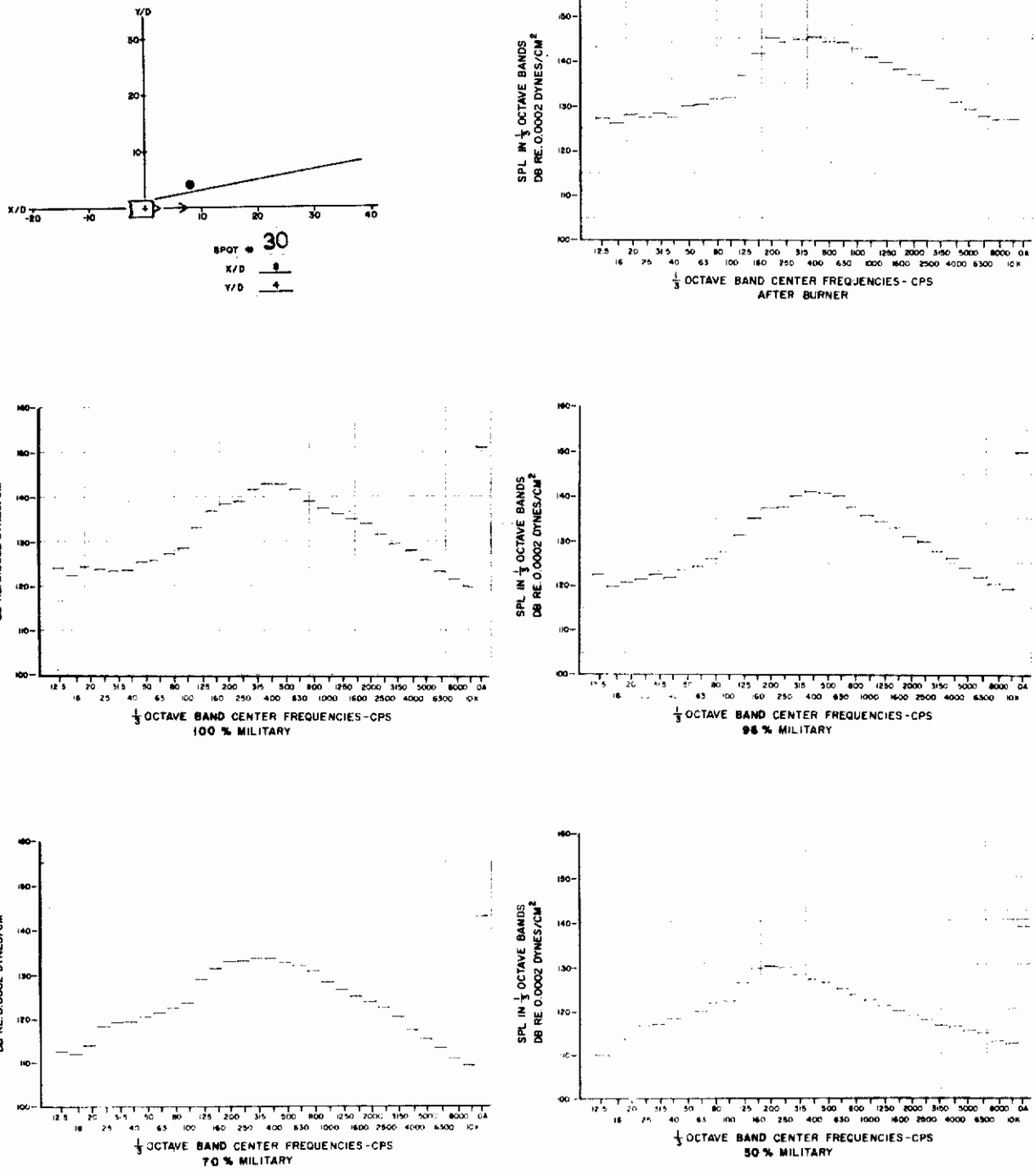


Figure 60. One-Third Octave Band Spectra and Overall SPL for Spot 30

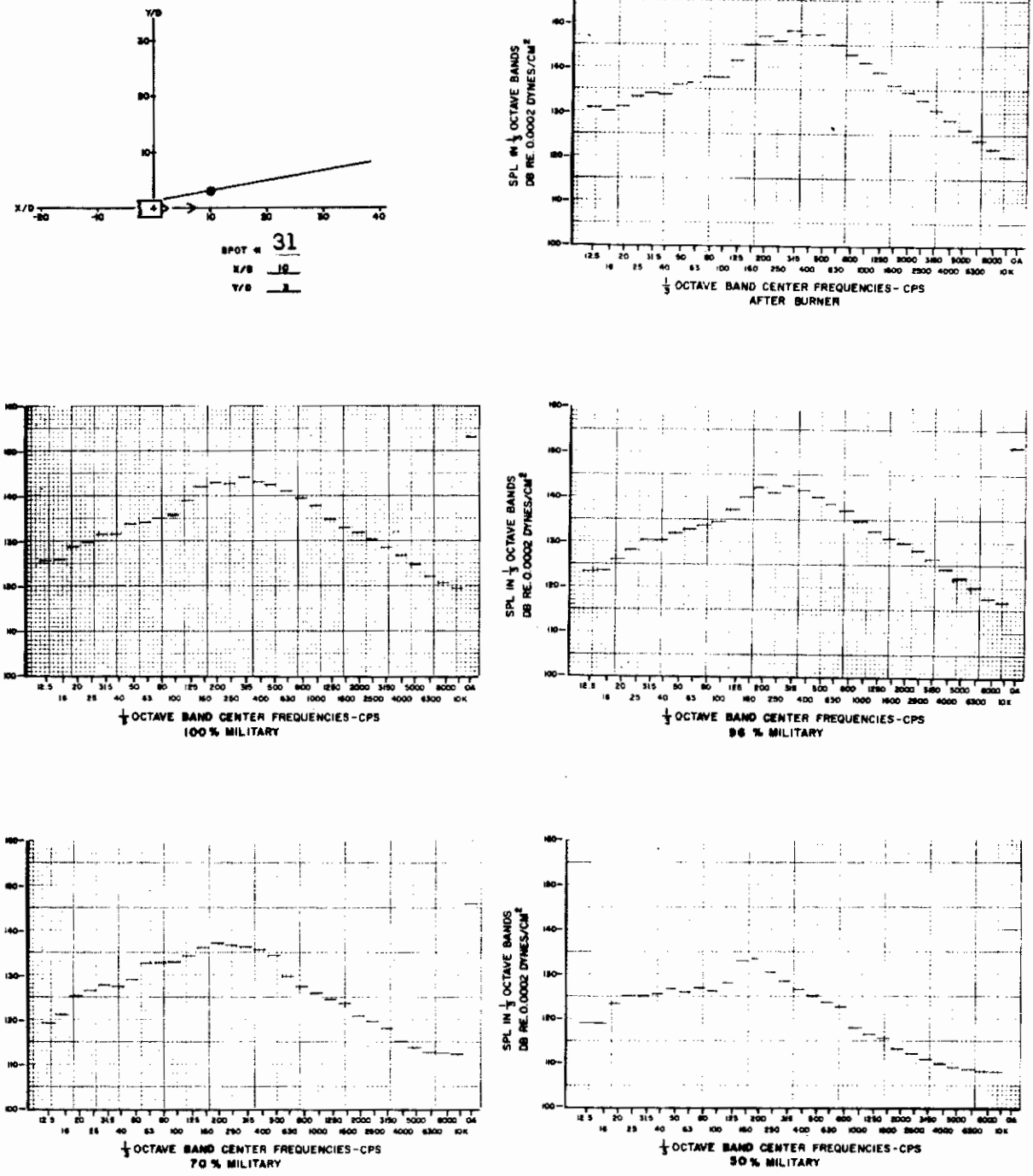


Figure 61. One-Third Octave Band Spectra and Overall SPL for Spot 31

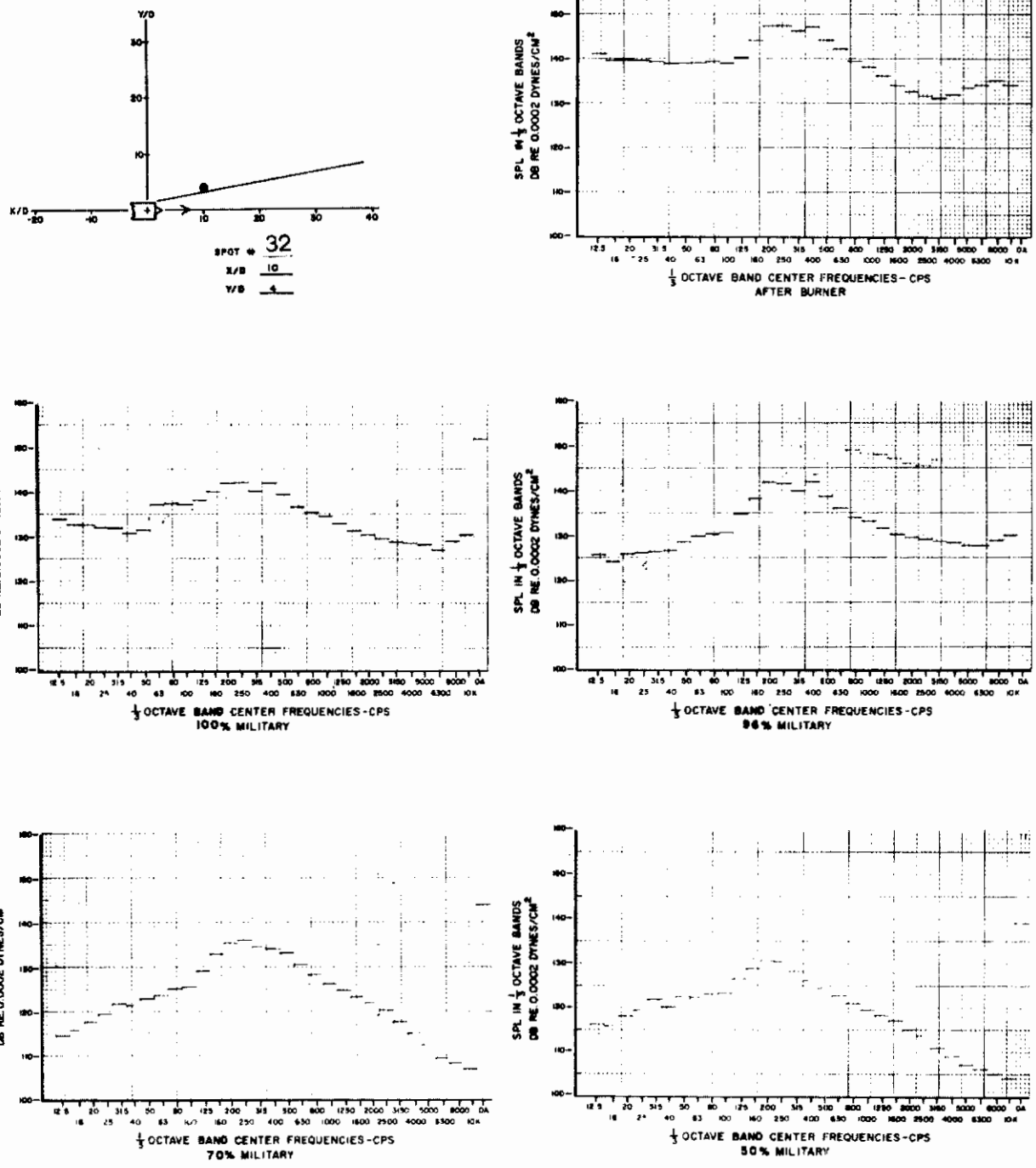


Figure 62. One-Third Octave Band Spectra and Overall SPL for Spot 32

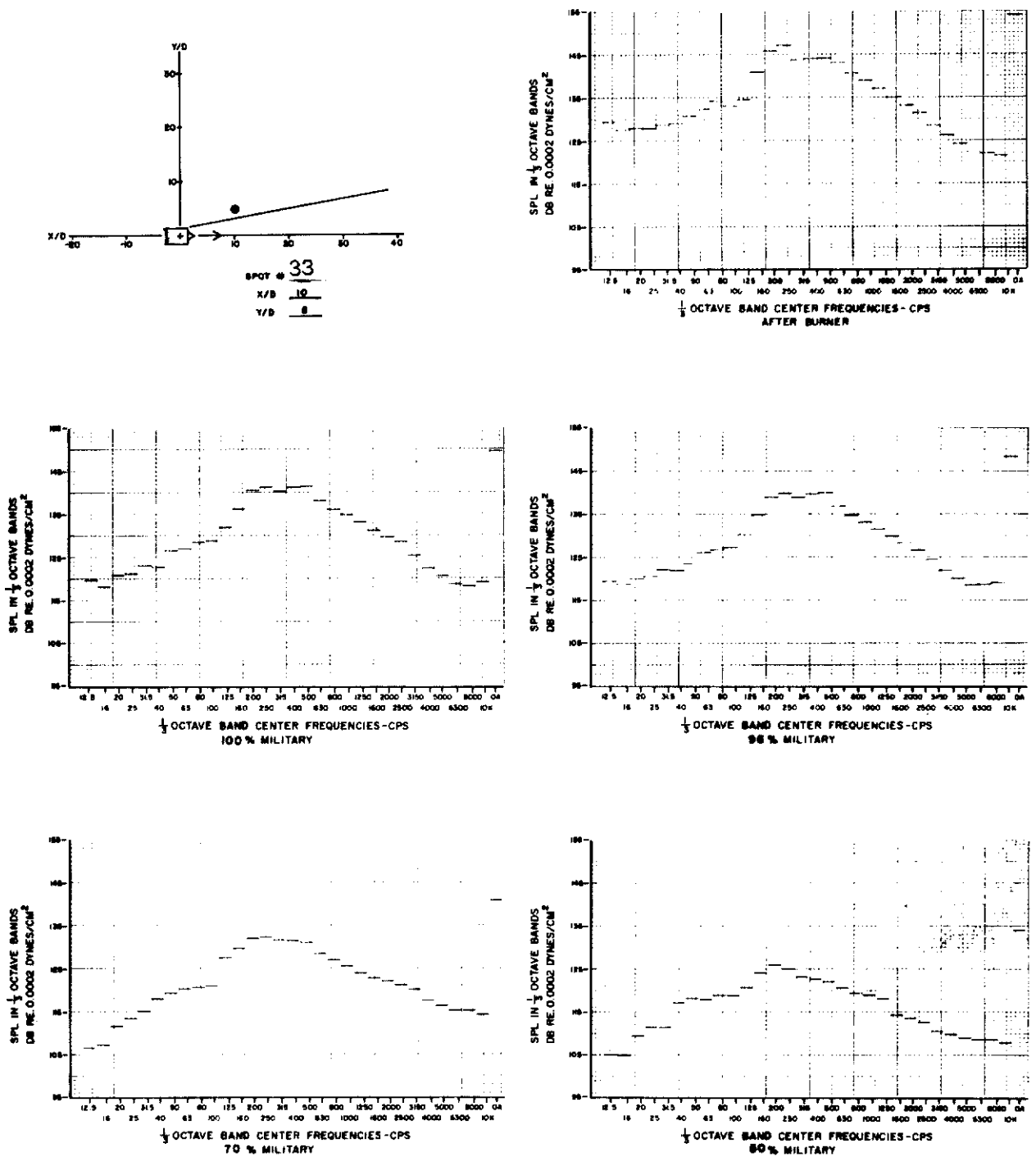


Figure 63. One-Third Octave Band Spectra and Overall SPL for Spot 33

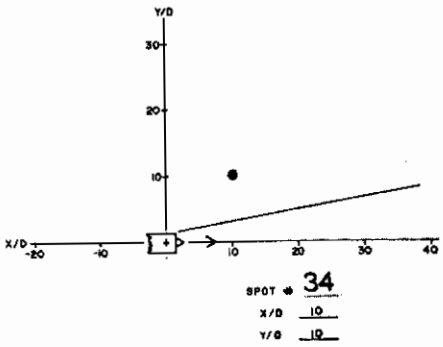


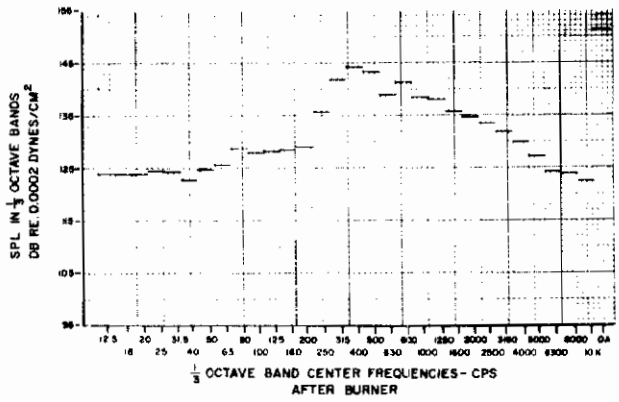


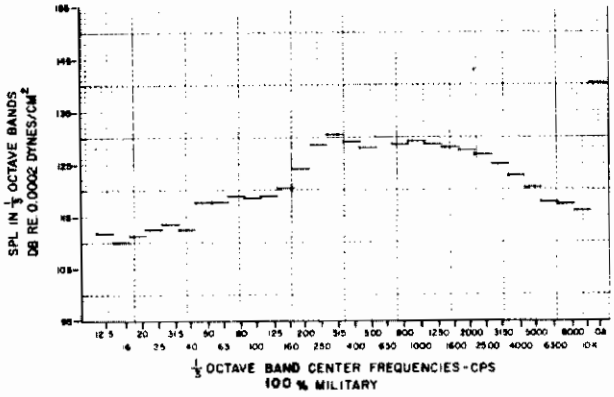


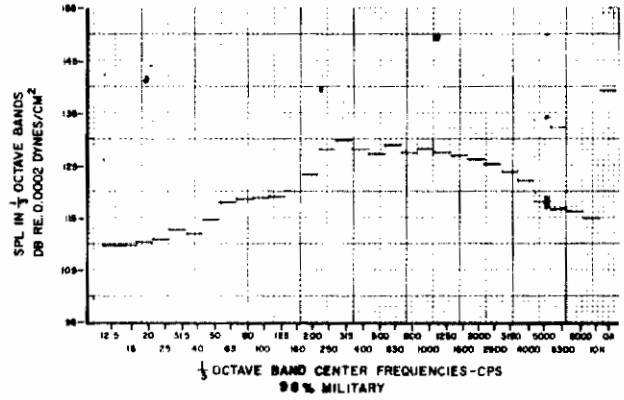


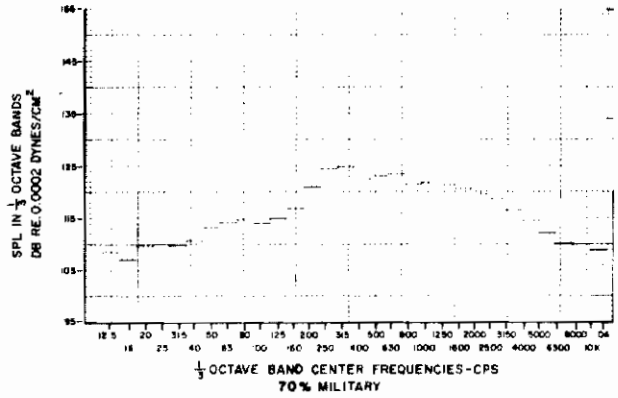


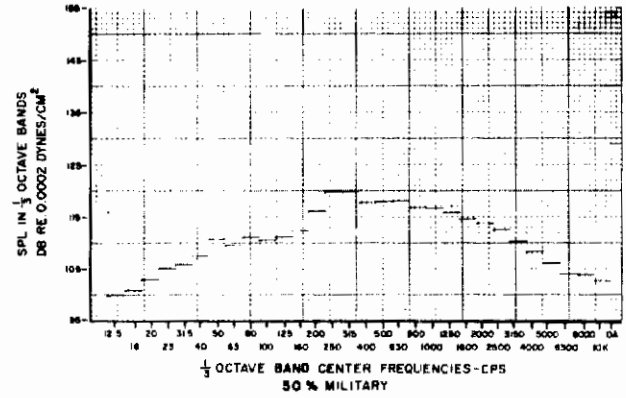


Figure 64. One-Third Octave Band Spectra and Overall SPL for Spot 34

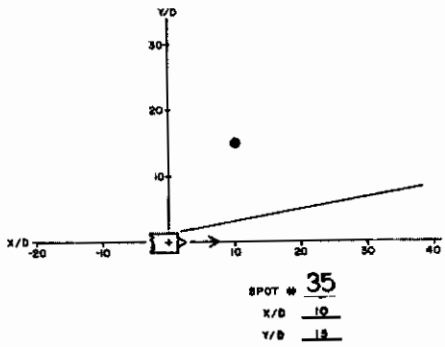


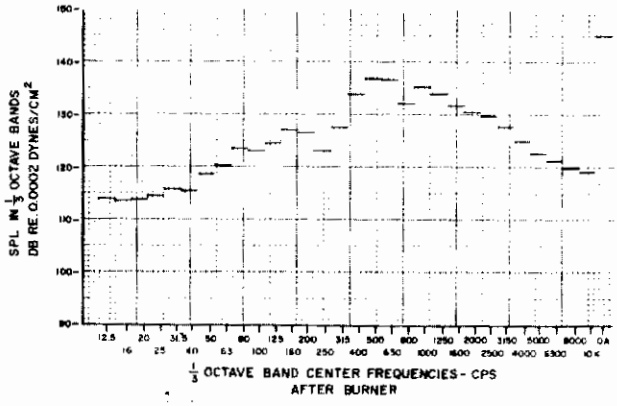


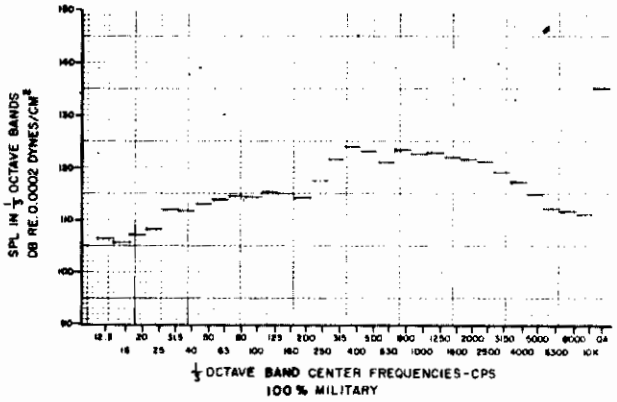


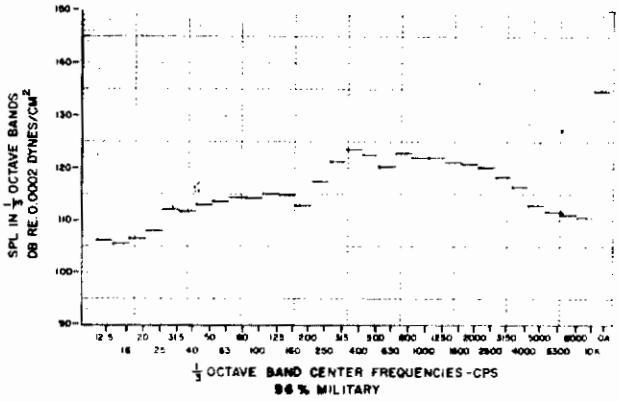


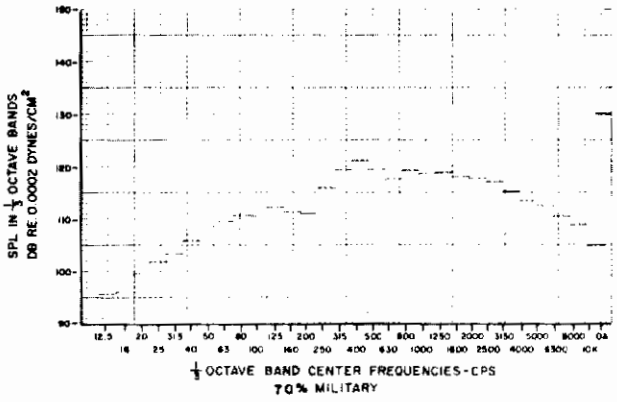


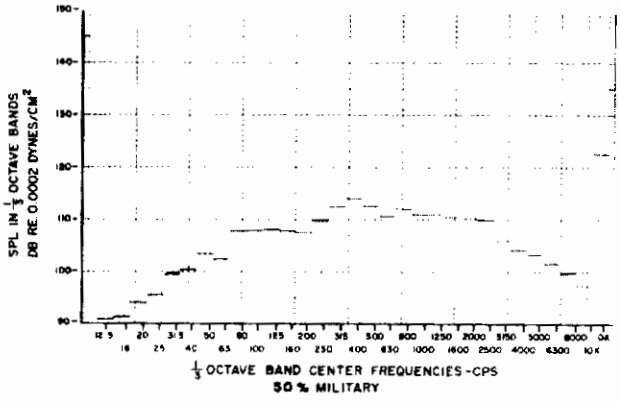


Figure 65. One-Third Octave Band Spectra and Overall SPL for Spot 35

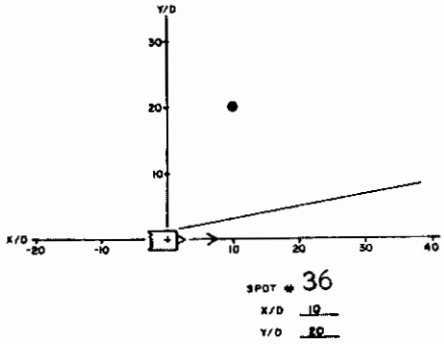


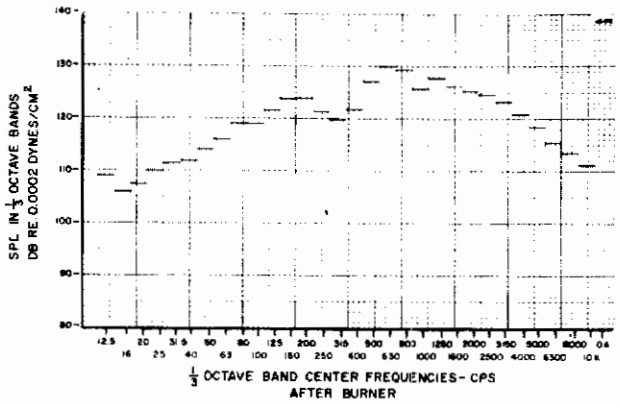


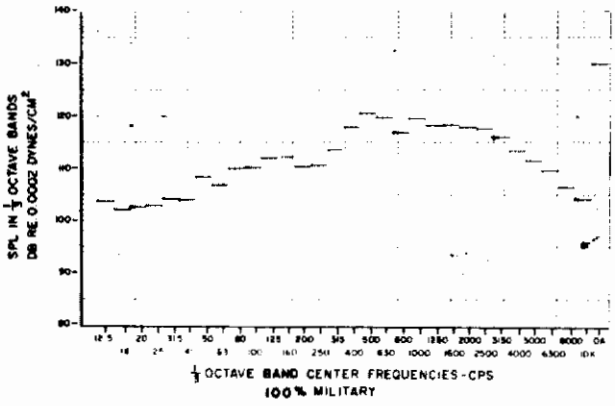


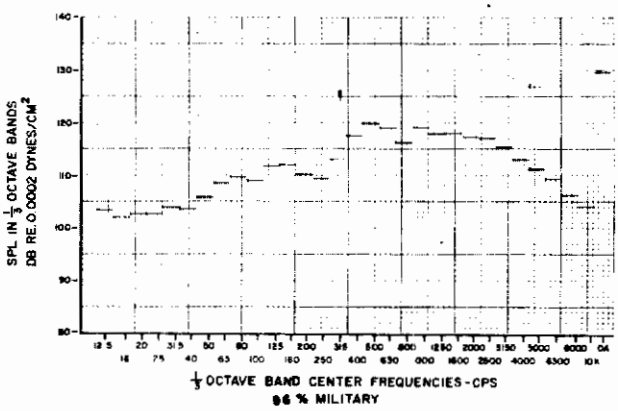


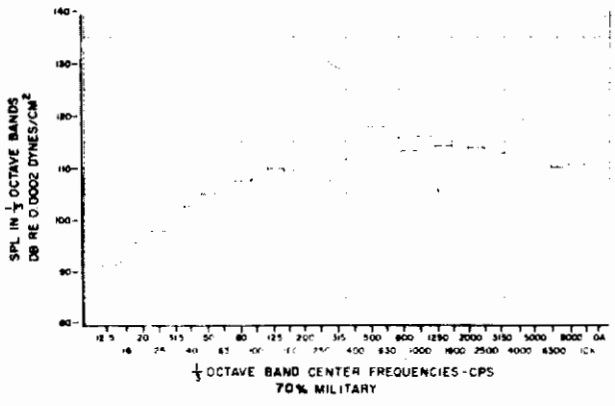


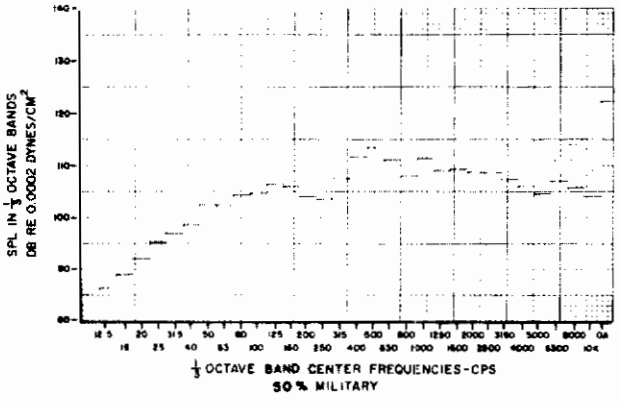


Figure 66. One-Third Octave Band Spectra and Overall SPL for Spot 36

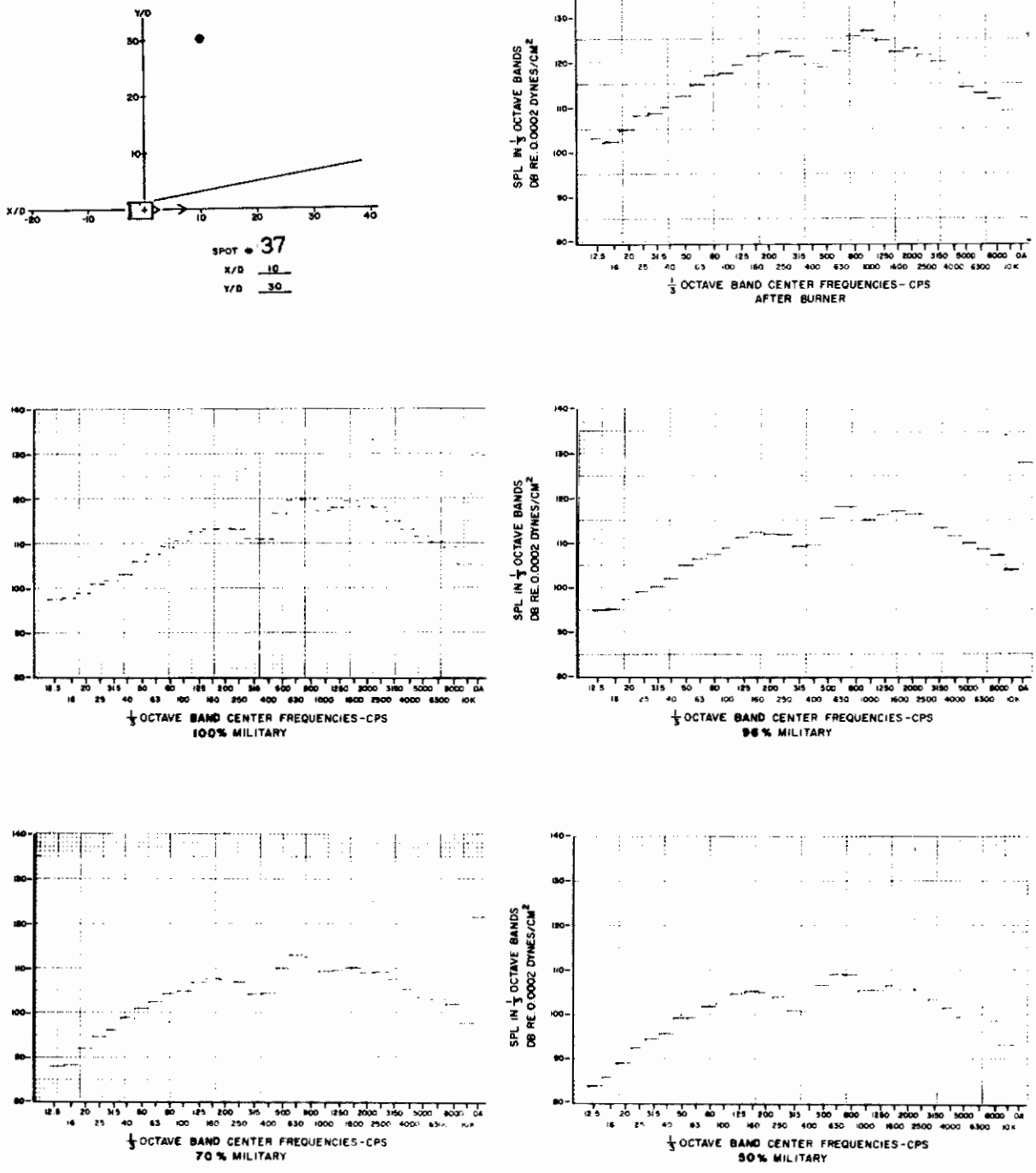


Figure 67. One-Third Octave Band Spectra and Overall SPL for Spot 37

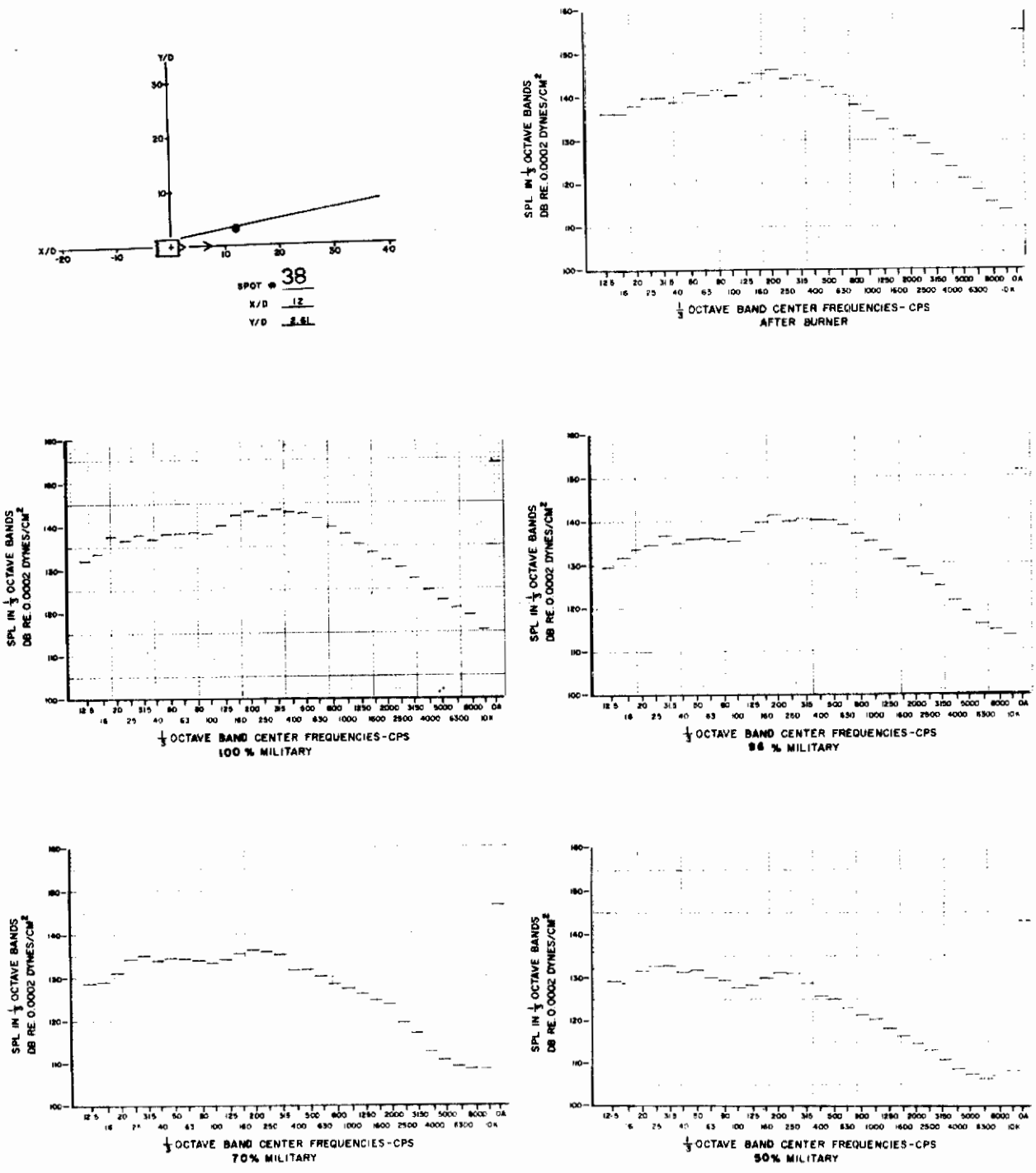


Figure 68. One-Third Octave Band Spectra and Overall SPL for Spot 38

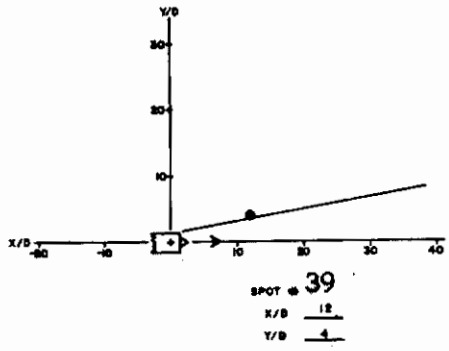


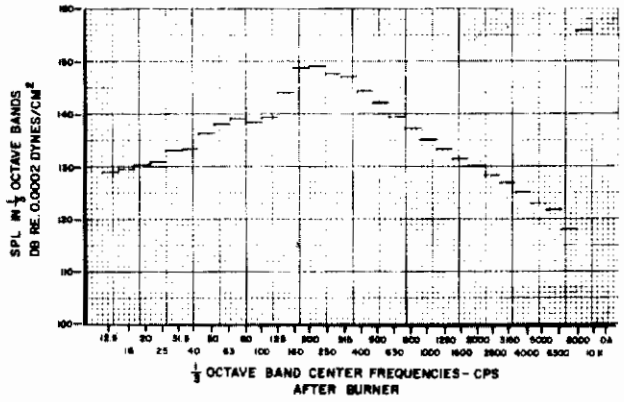


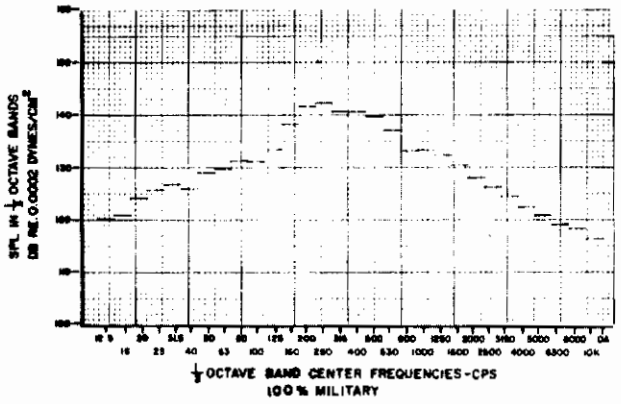


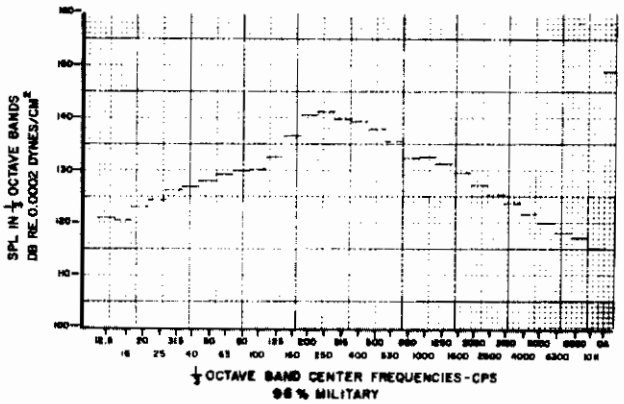


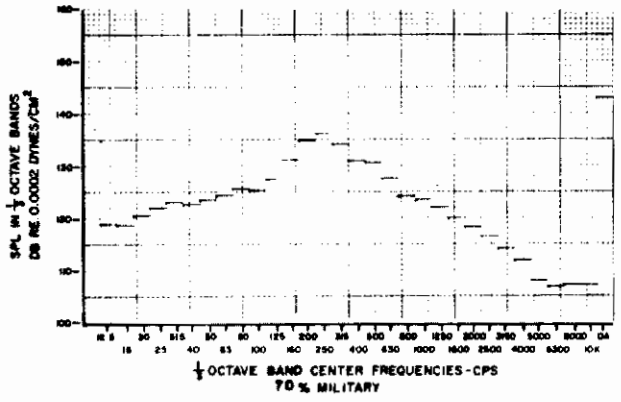


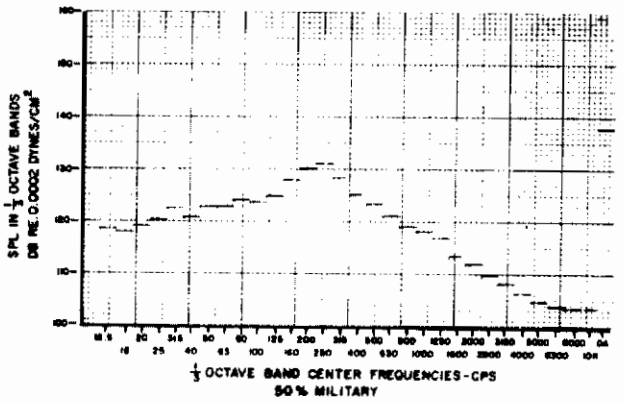


Figure 69. One-Third Octave Band Spectra and Overall SPL for Spot 39

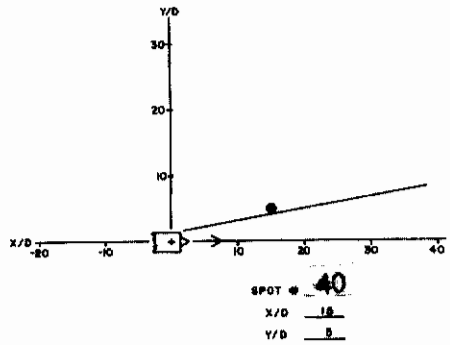


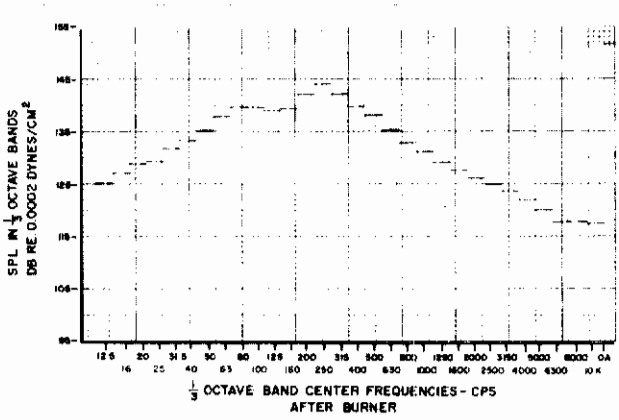


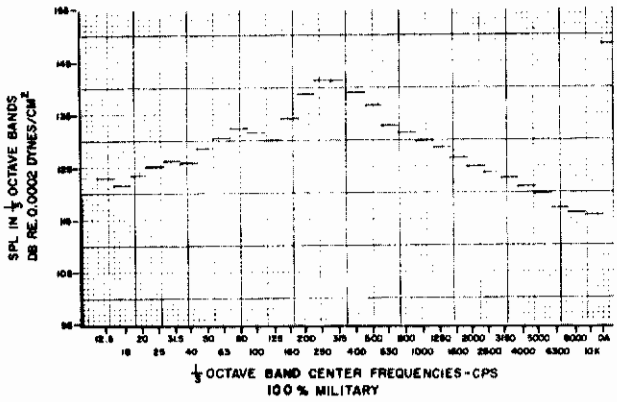


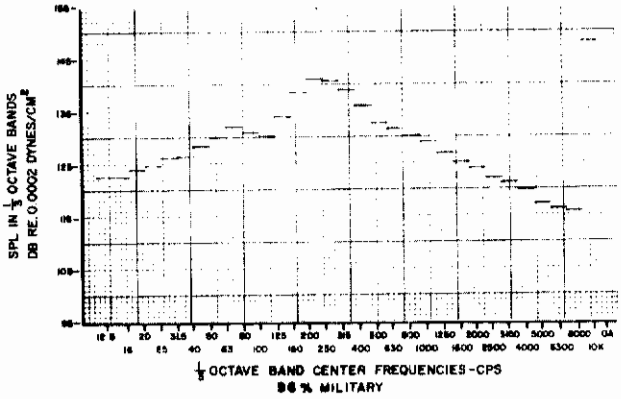


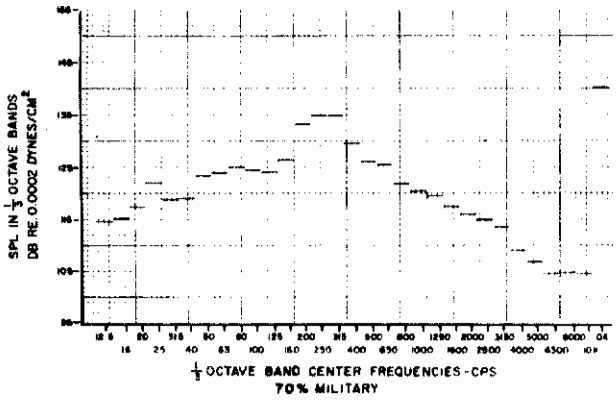


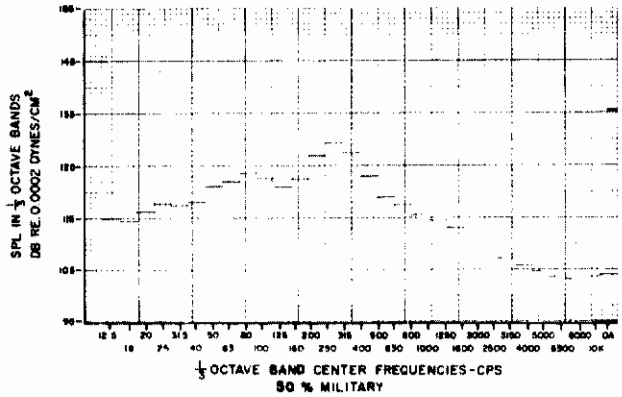


Figure 70. One-Third Octave Band Spectra and Overall SPL for Spot 40

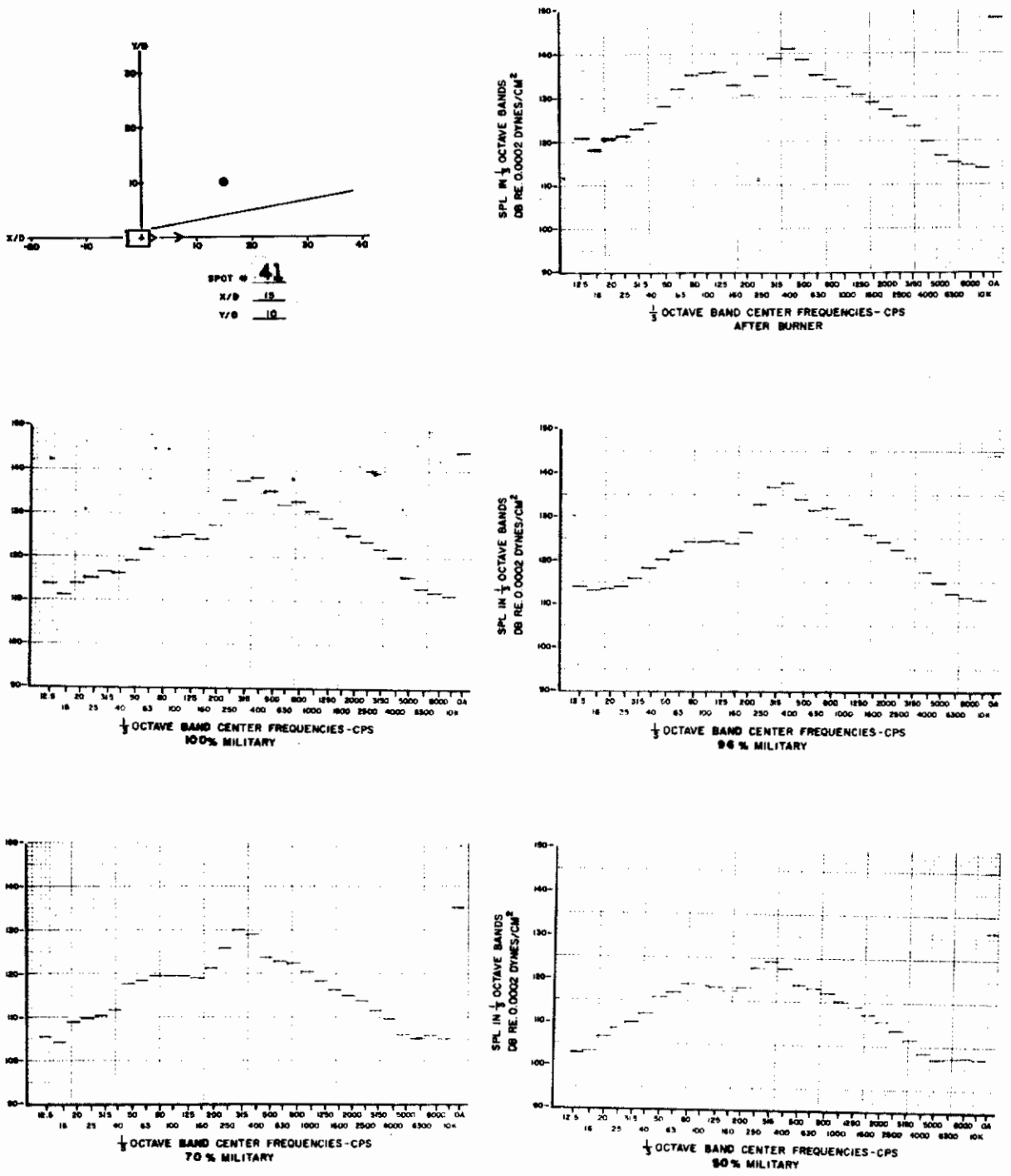


Figure 71. One-Third Octave Band Spectra and Overall SPL for Spot 41

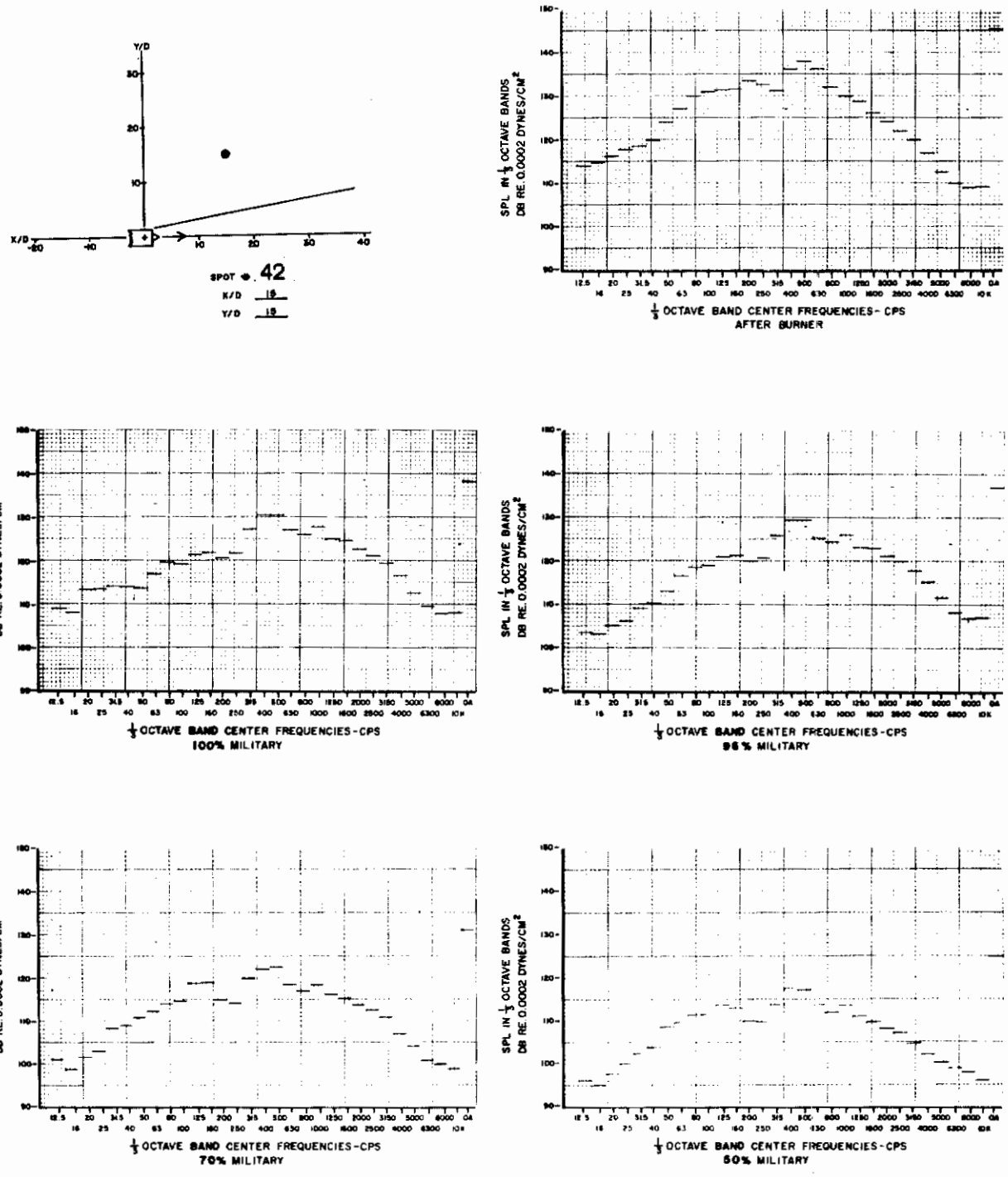


Figure 72. One-Third Octave Band Spectra and Overall SPL for Spot 42

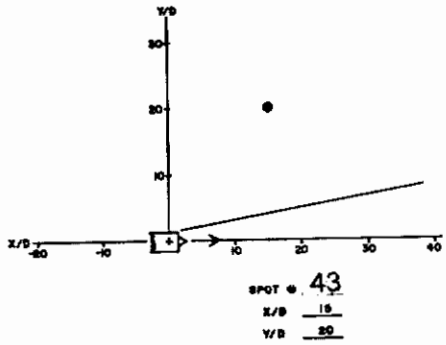


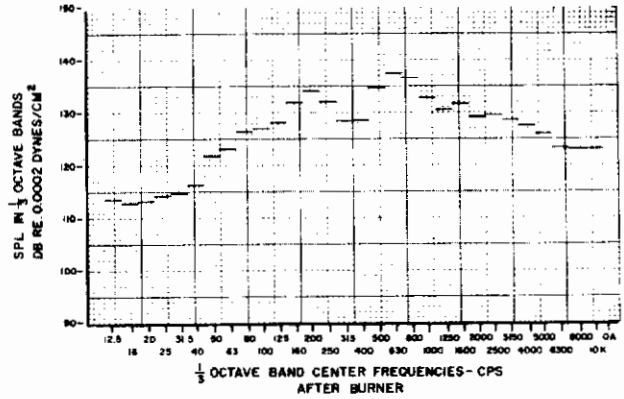


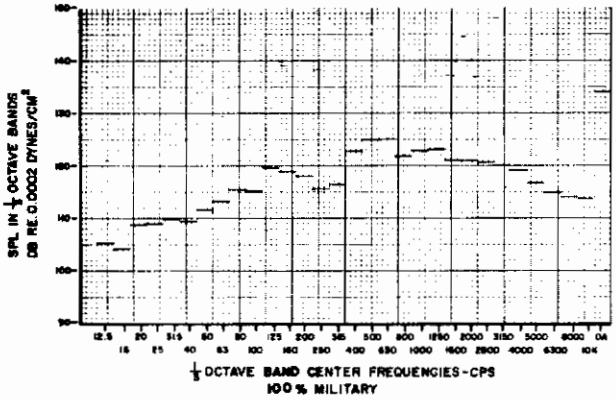


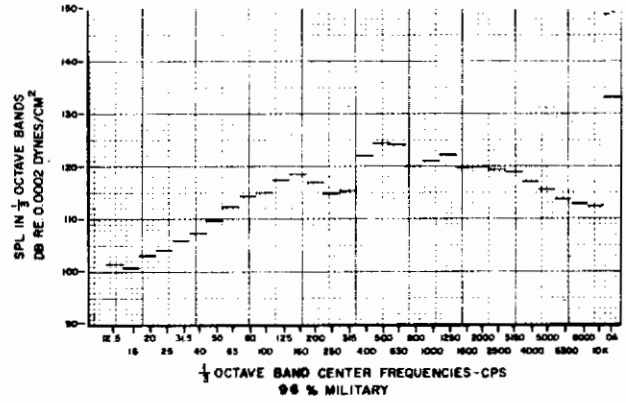


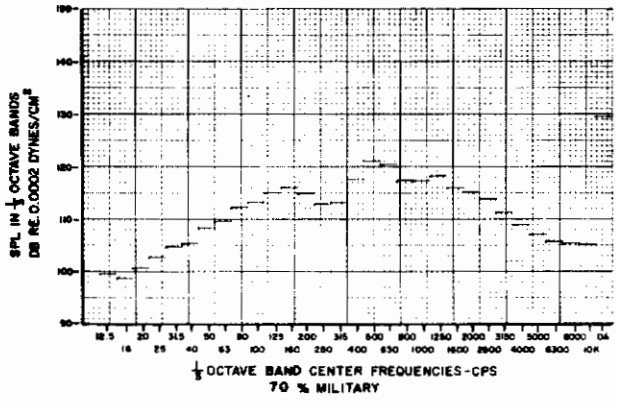


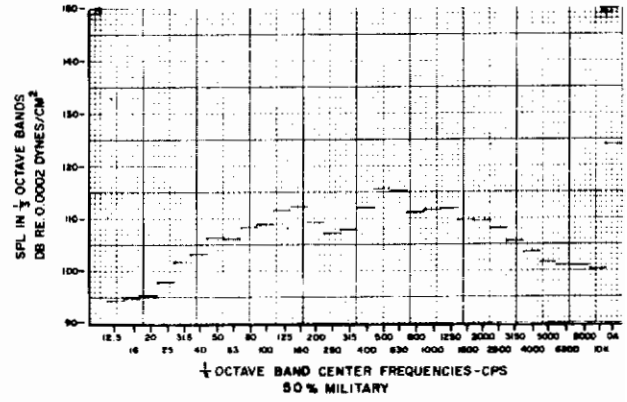


Figure 73. One-Third Octave Band Spectra and Overall SPL for Spot 43

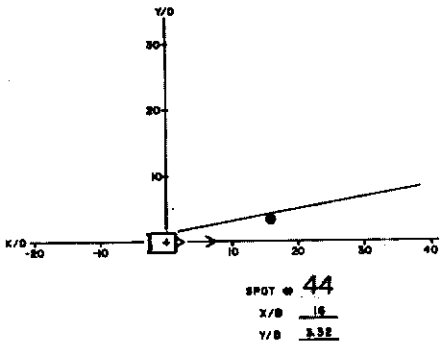


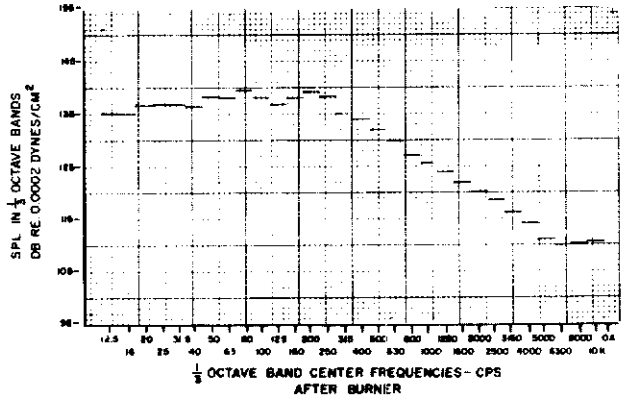


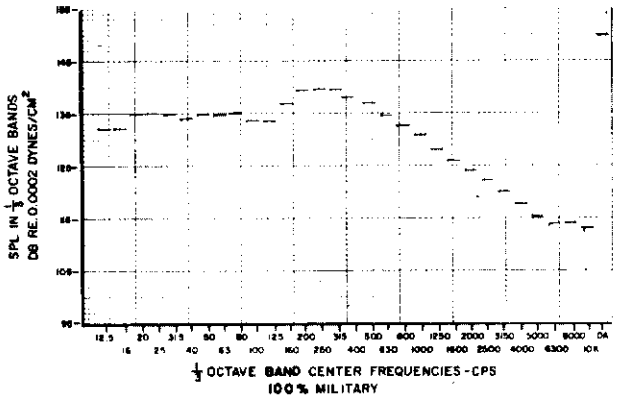


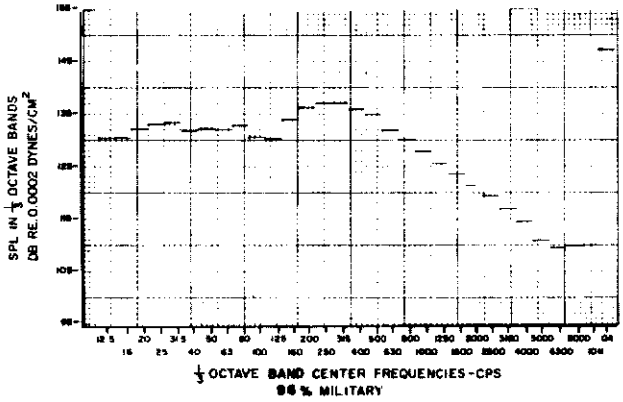


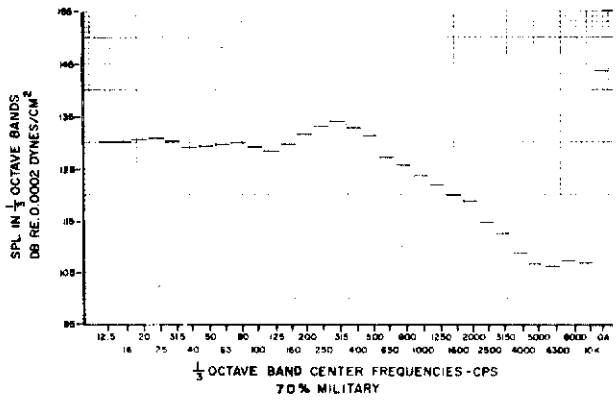


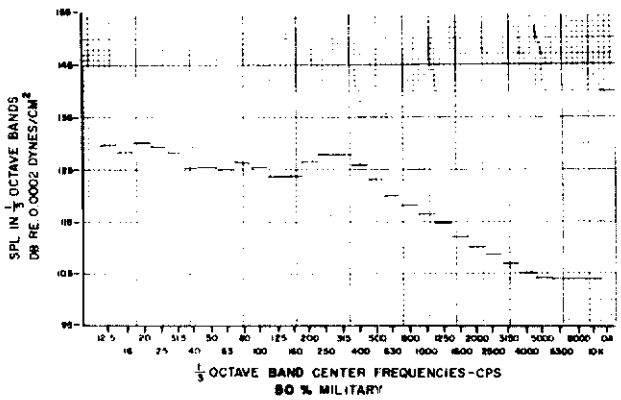


Figure 74. One-Third Octave Band Spectra and Overall SPL for Spot 44

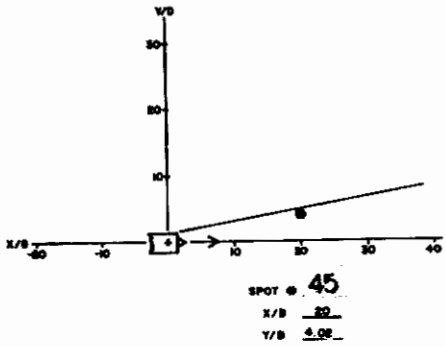


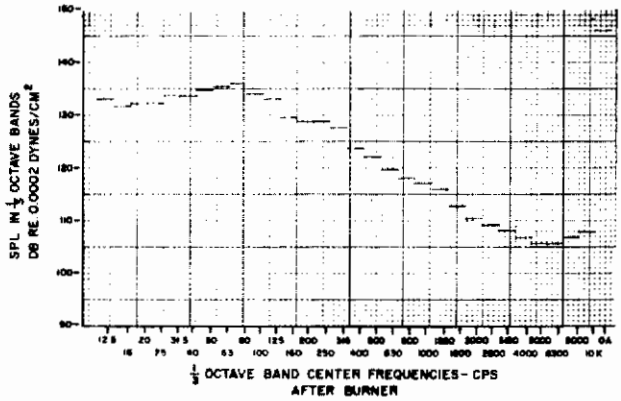


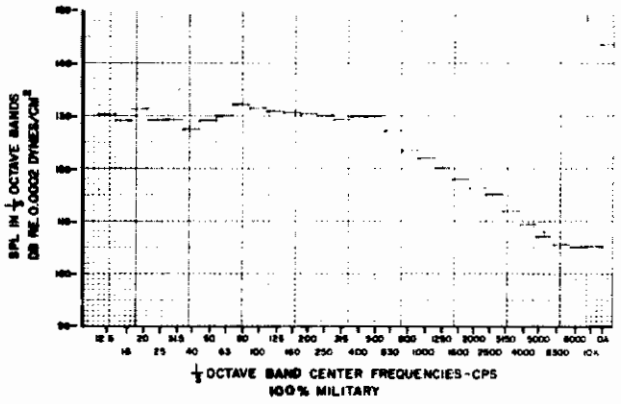


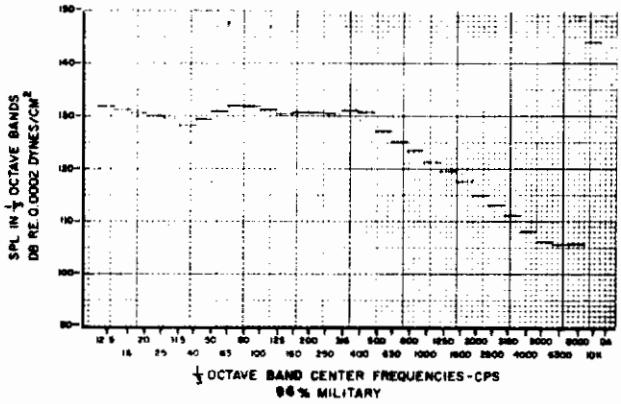


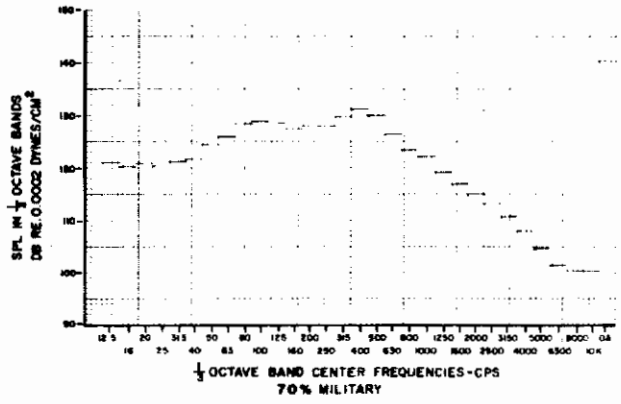


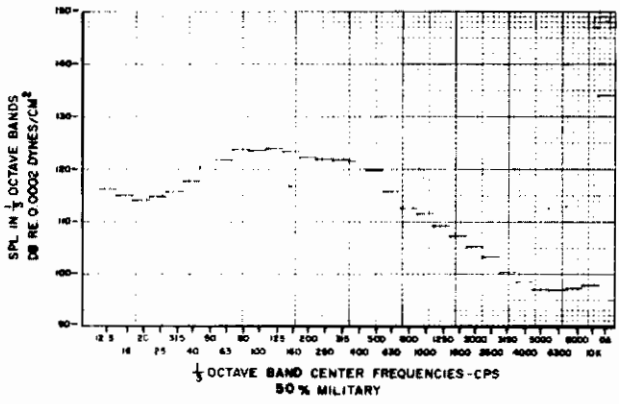


Figure 75. One-Third Octave Band Spectra and Overall SPL for Spot 45

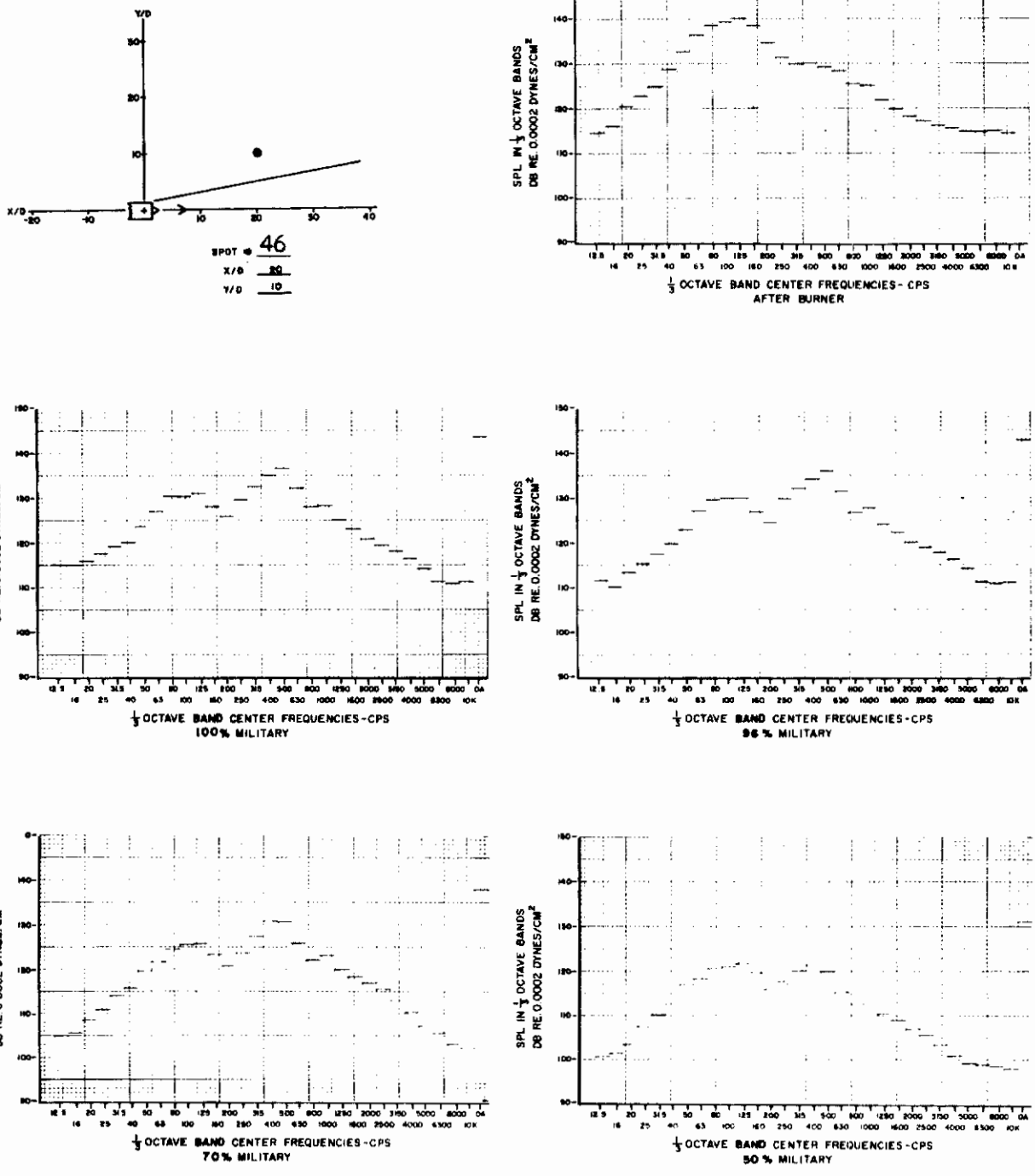


Figure 76. One-Third Octave Band Spectra and Overall SPL for Spot 46

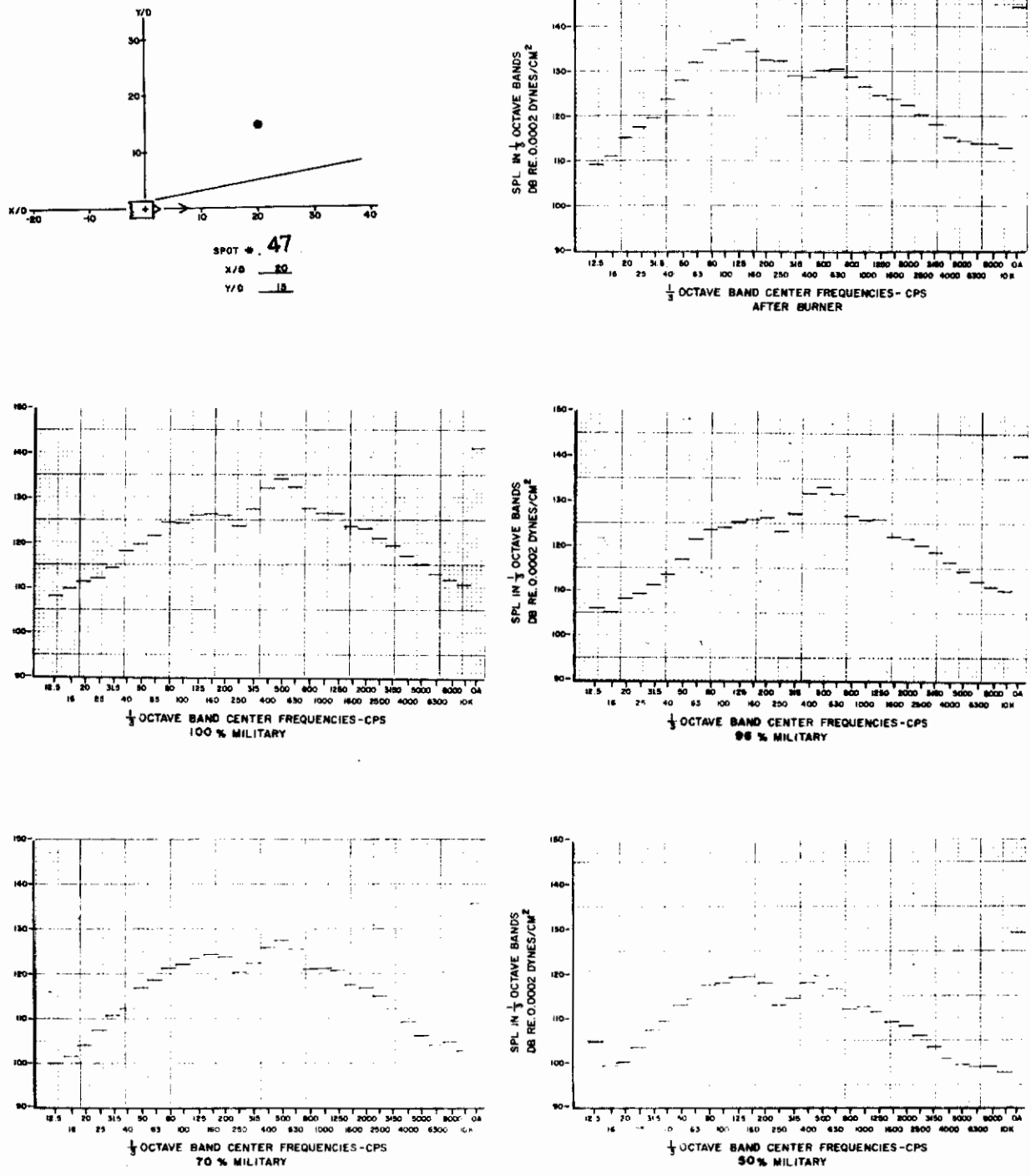


Figure 77. One-Third Octave Band Spectra and Overall SPL for Spot 47

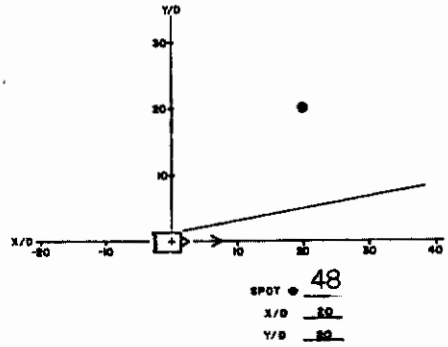


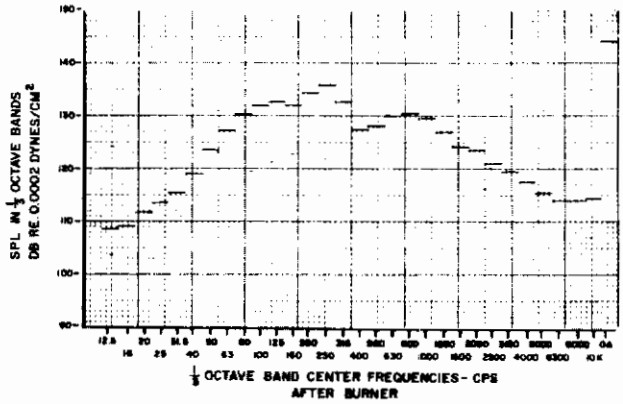


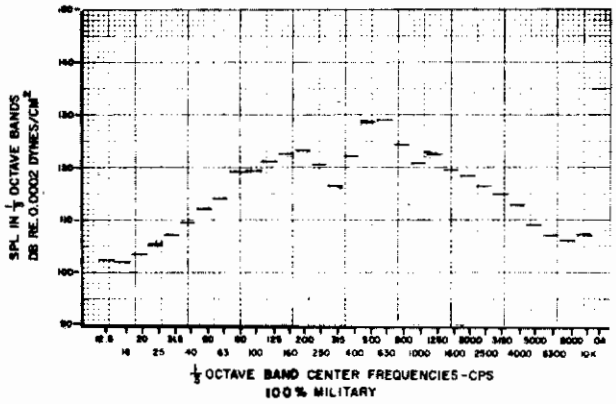


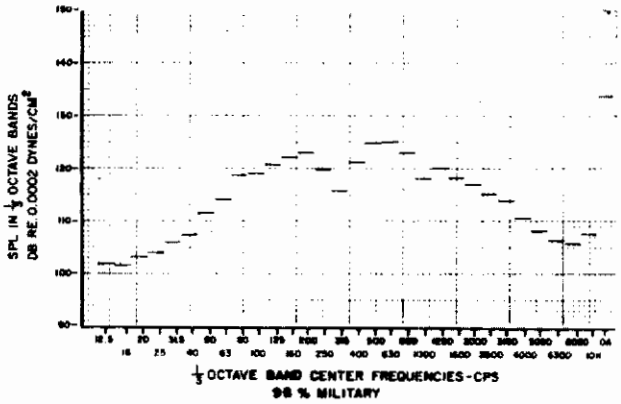


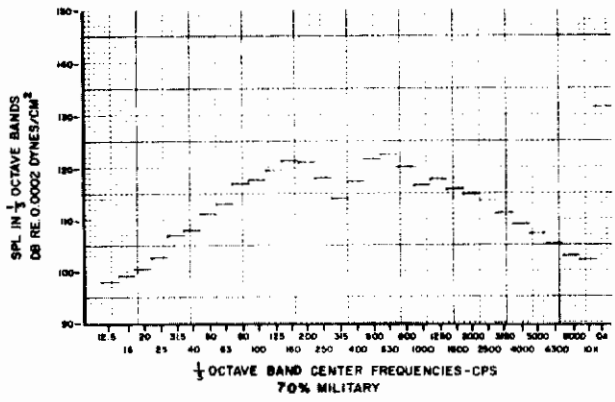


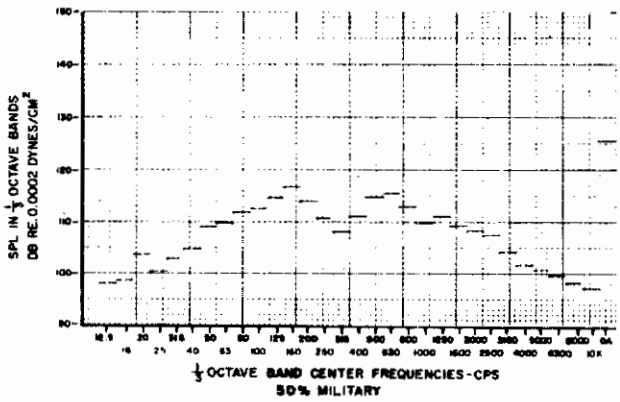


Figure 78. One-Third Octave Band Spectra and Overall SPL for Spot 48

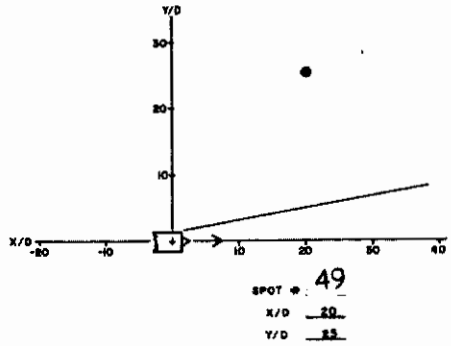


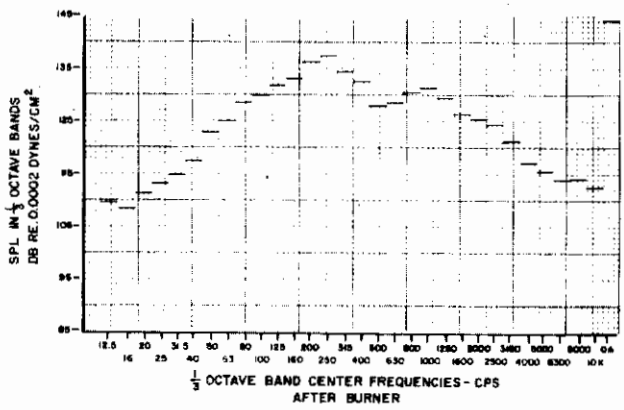


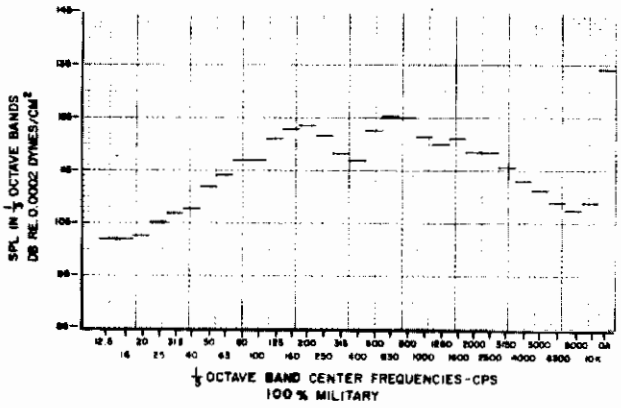


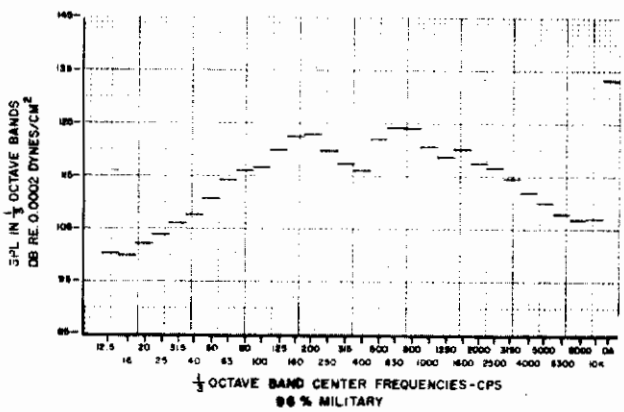


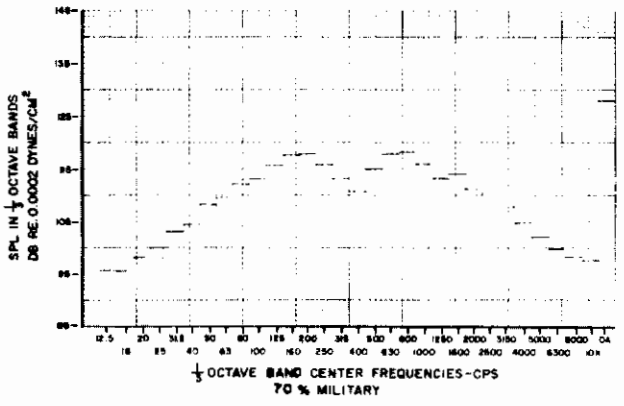


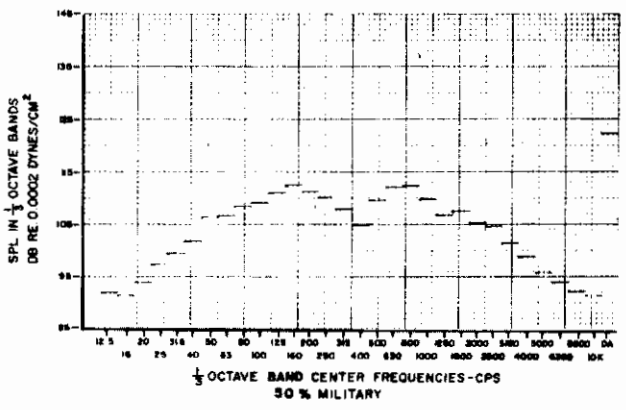


Figure 79. One-Third Octave Band Spectra and Overall SPL for Spot 49

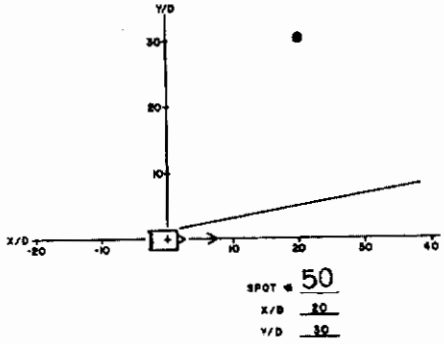


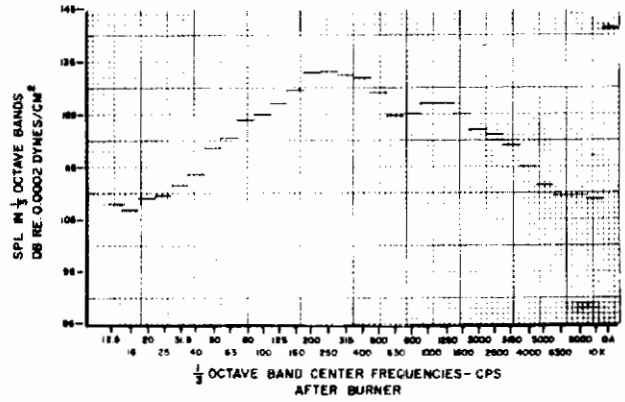


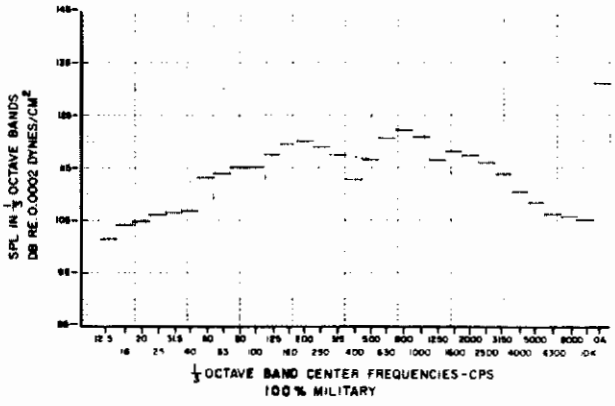


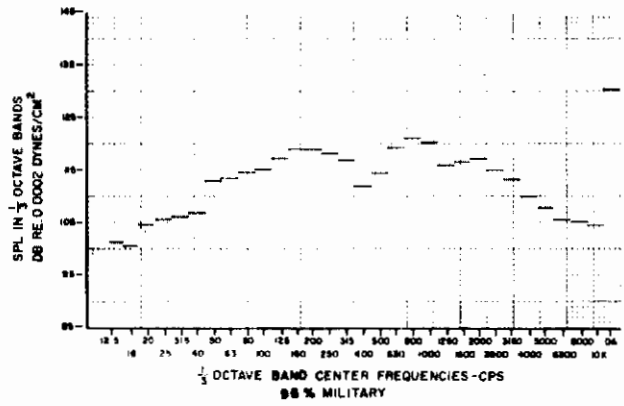


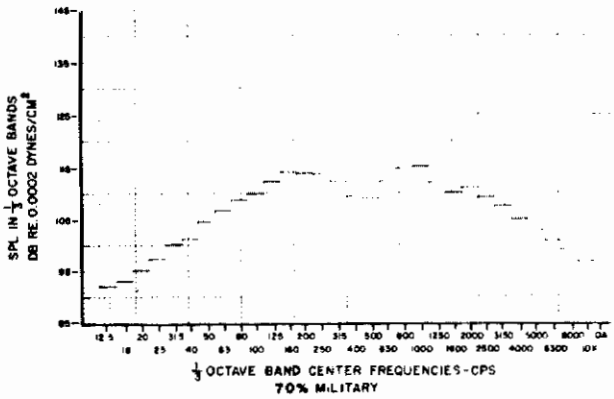


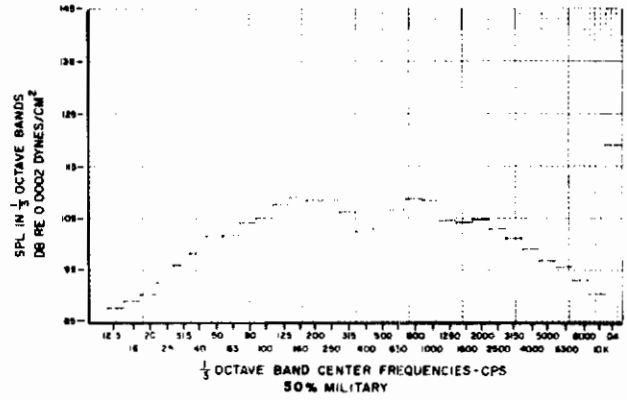


Figure 80. One-Third Octave Band Spectra and Overall SPL for Spot 50

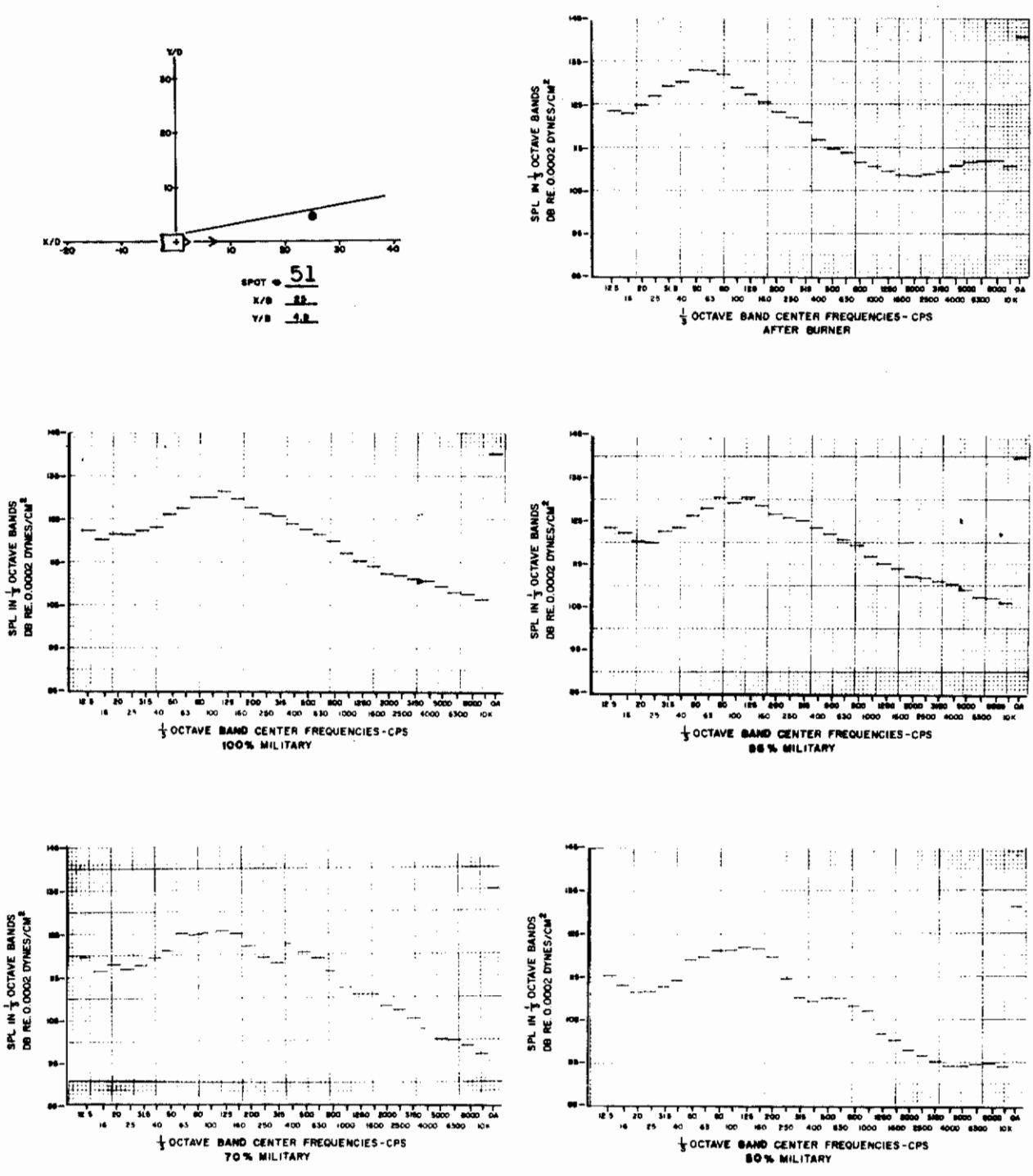


Figure 81. One-Third Octave Band Spectra and Overall SPL for Spot 51

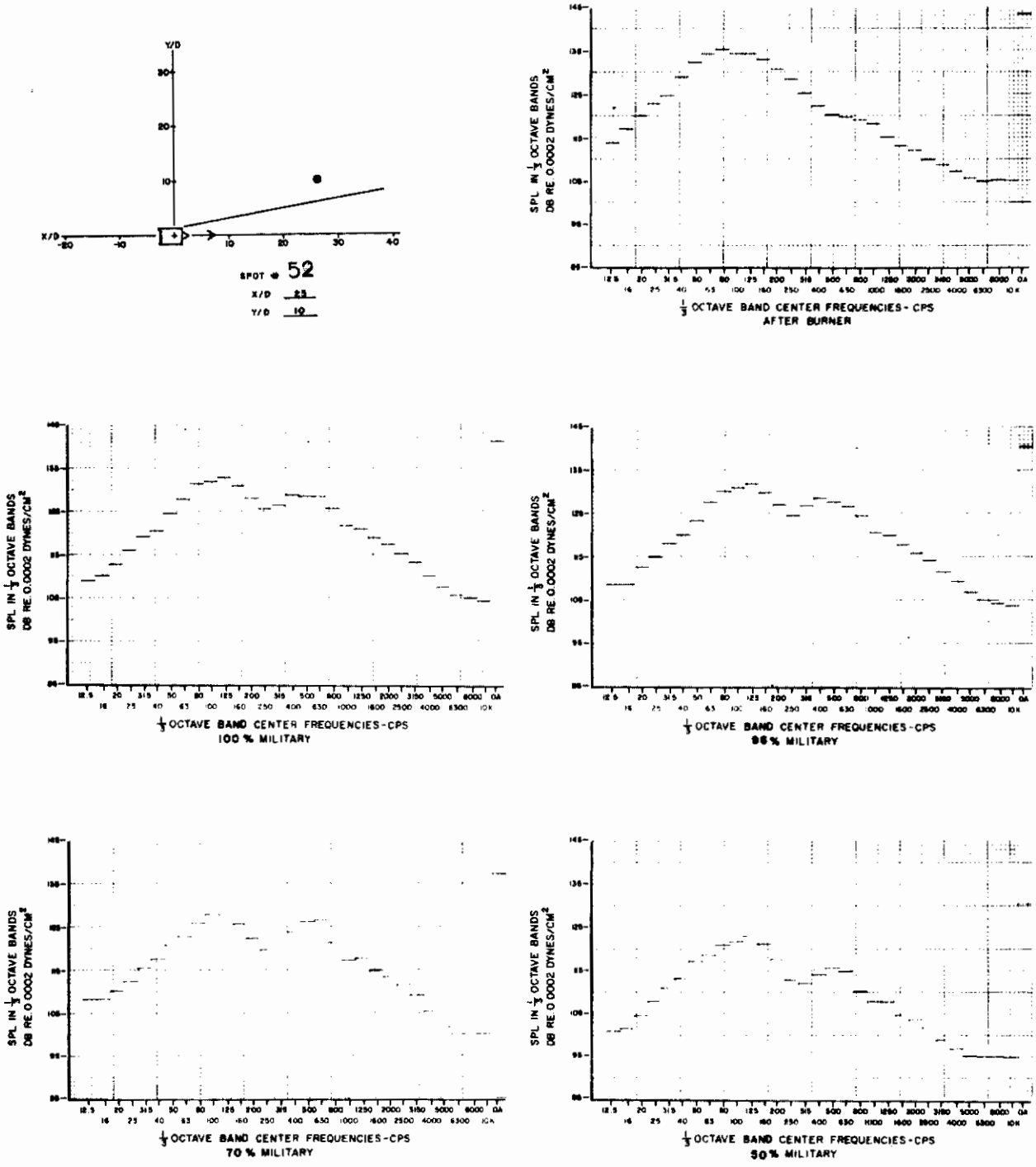


Figure 82. One-Third Octave Band Spectra and Overall SPL for Spot 52

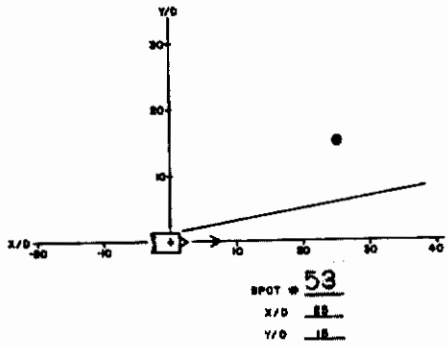


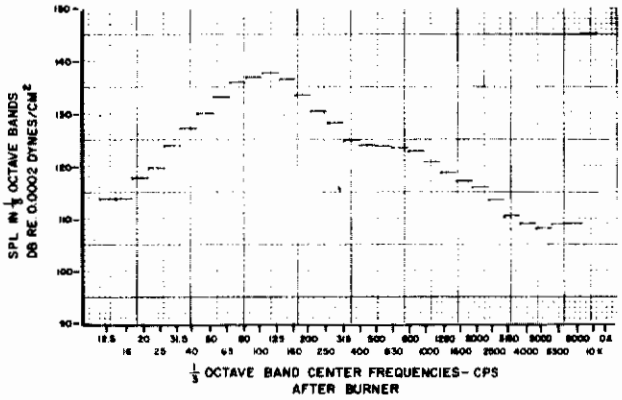


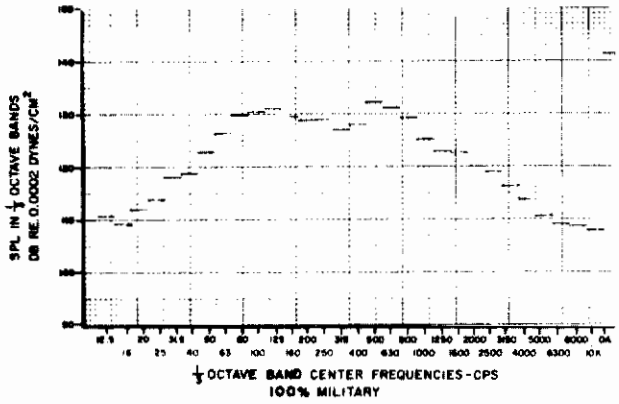


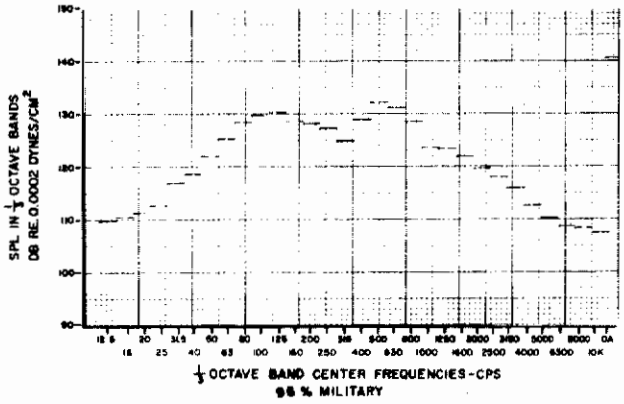


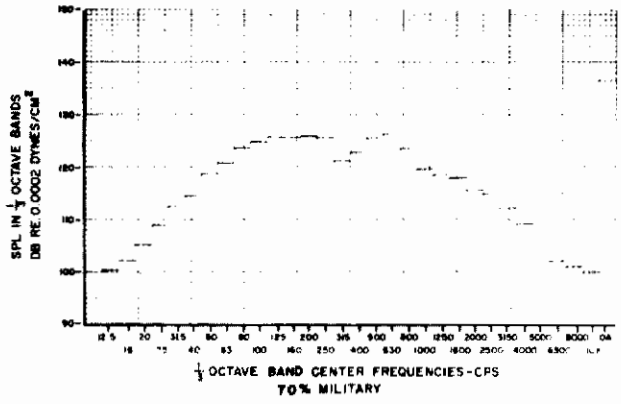


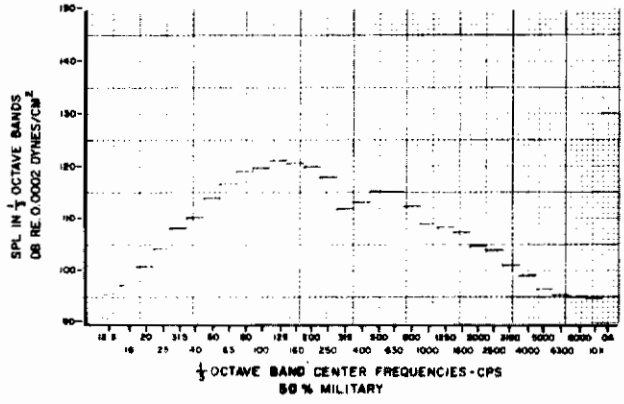


Figure 83. One-Third Octave Band Spectra and Overall SPL for Spot 53

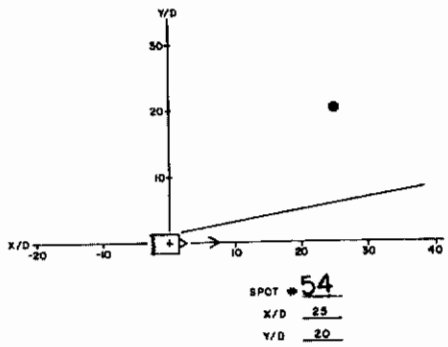


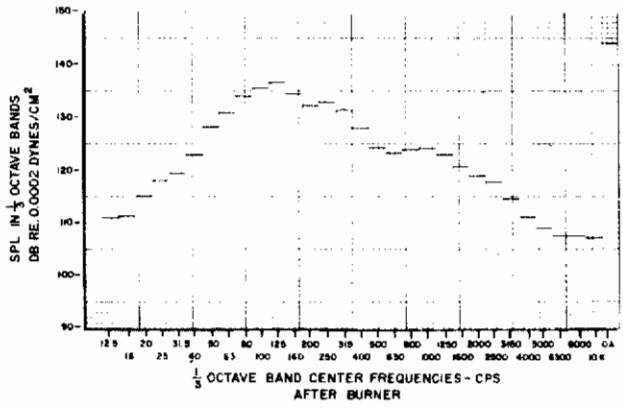


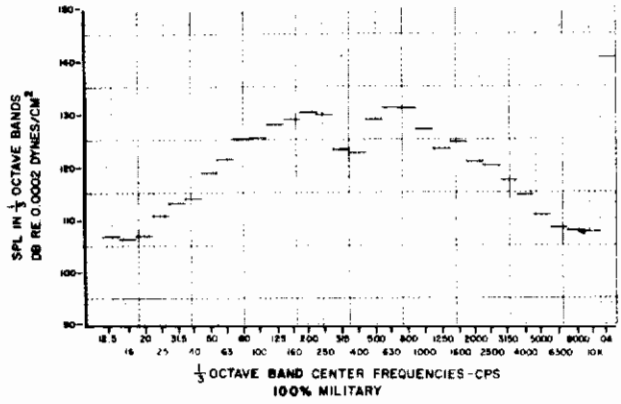


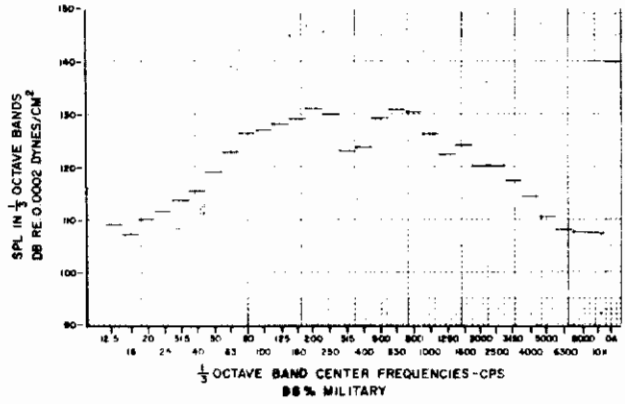


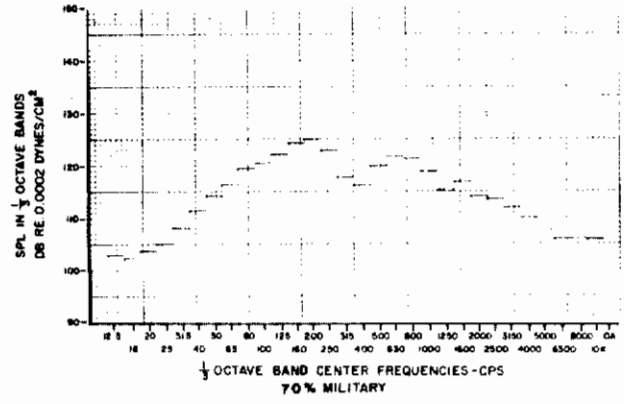


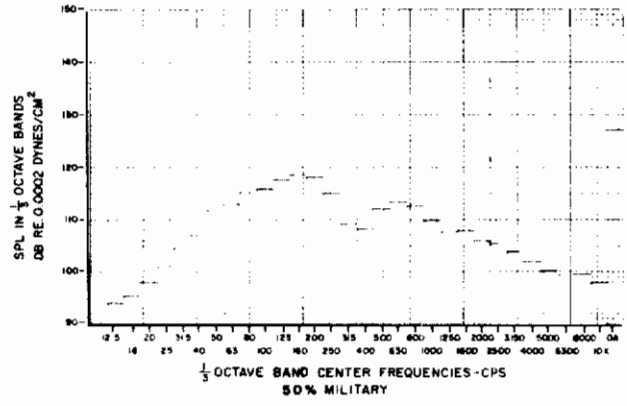


Figure 84. One-Third Octave Band Spectra and Overall SPL for Spot 54

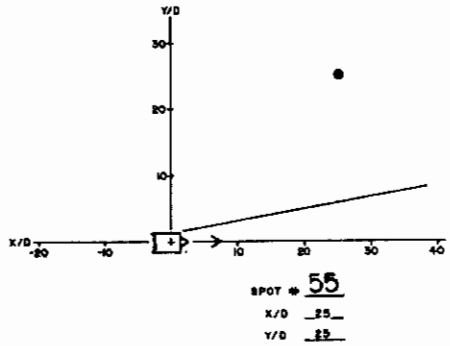


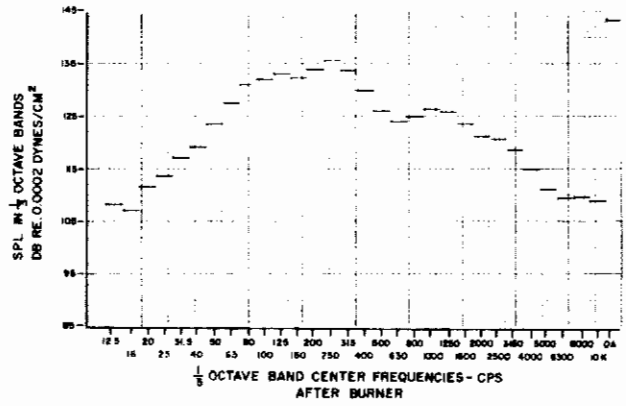


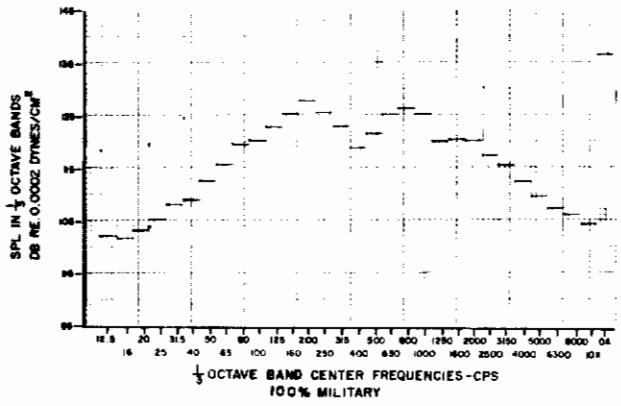


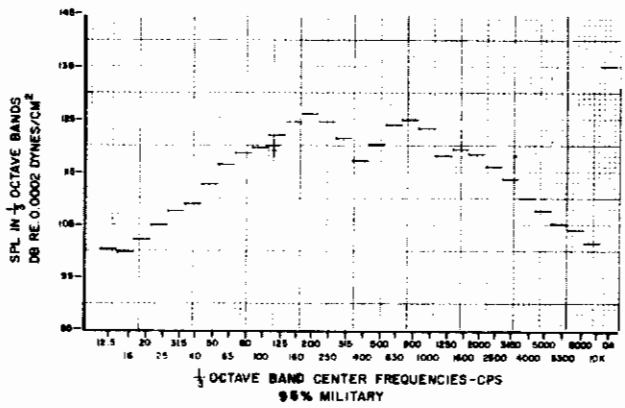


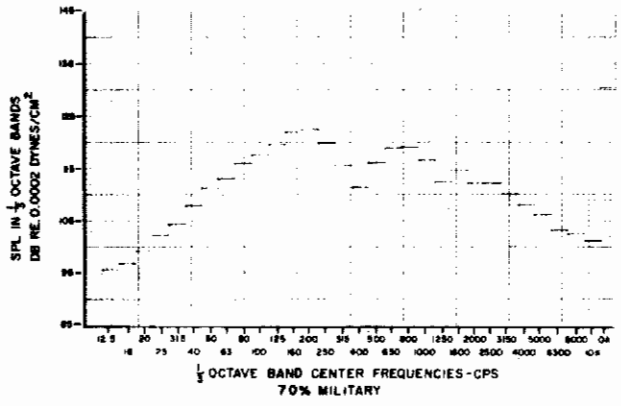


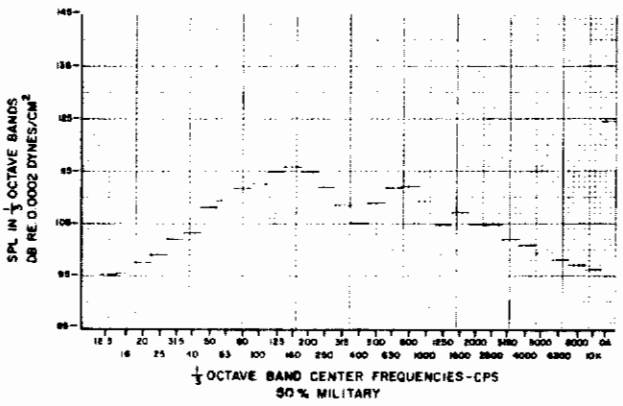


Figure 85. One-Third Octave Band Spectra and Overall SPL for Spot 55

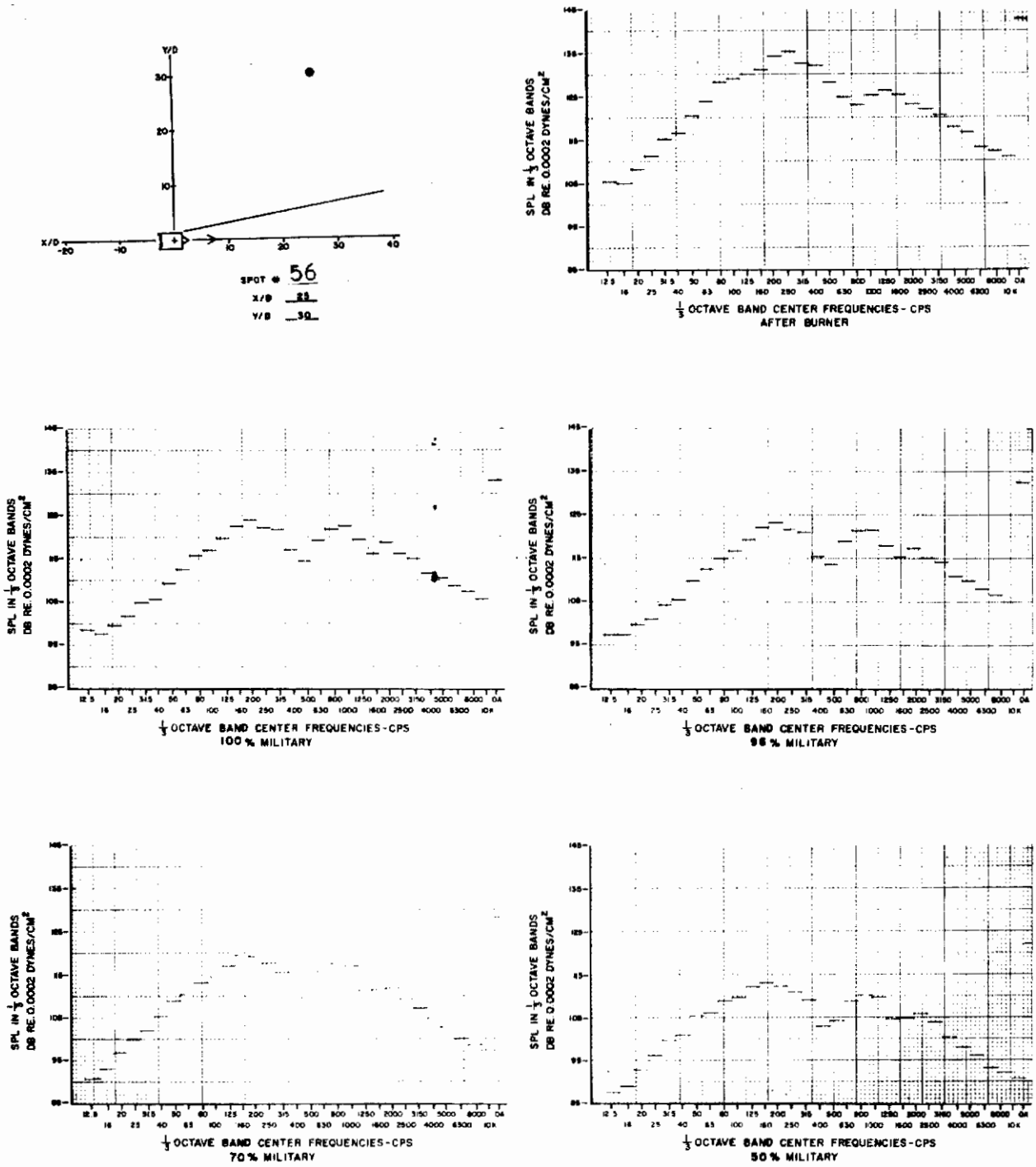


Figure 86. One-Third Octave Band Spectra and Overall SPL for Spot 56

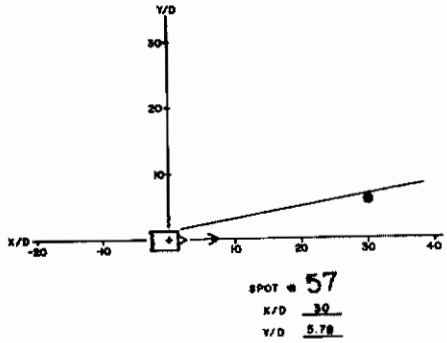


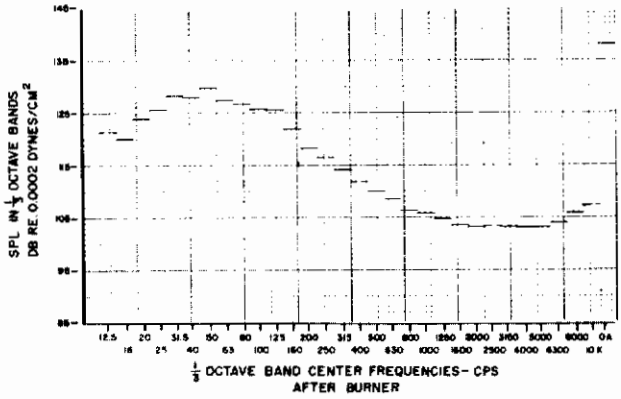


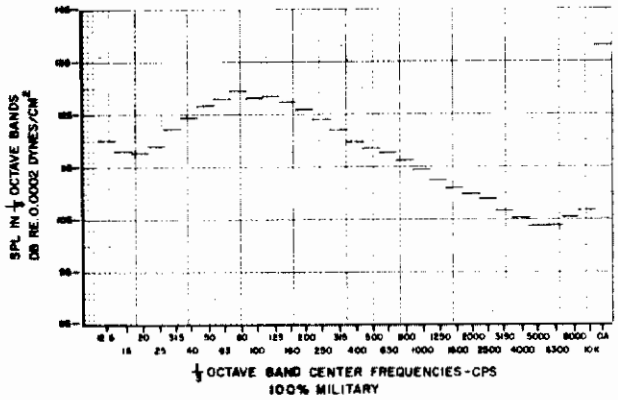


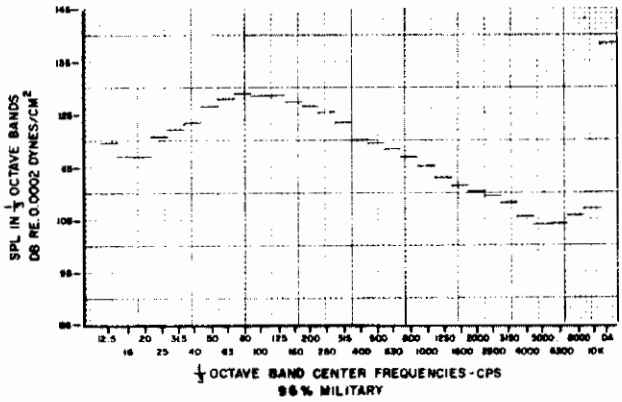


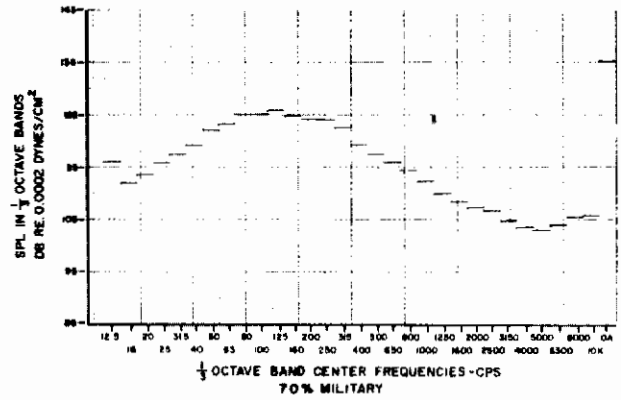


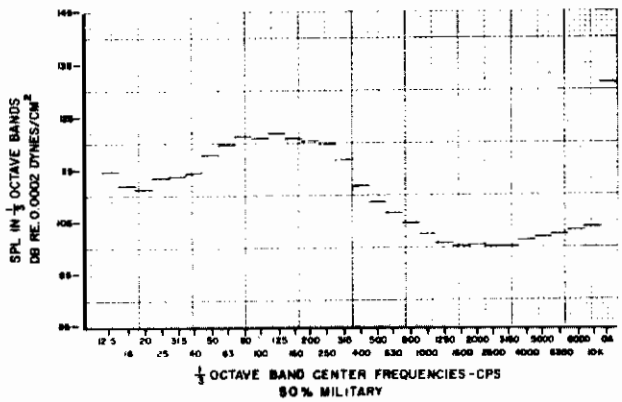


Figure 87. One-Third Octave Band Spectra and Overall SPL for Spot 57

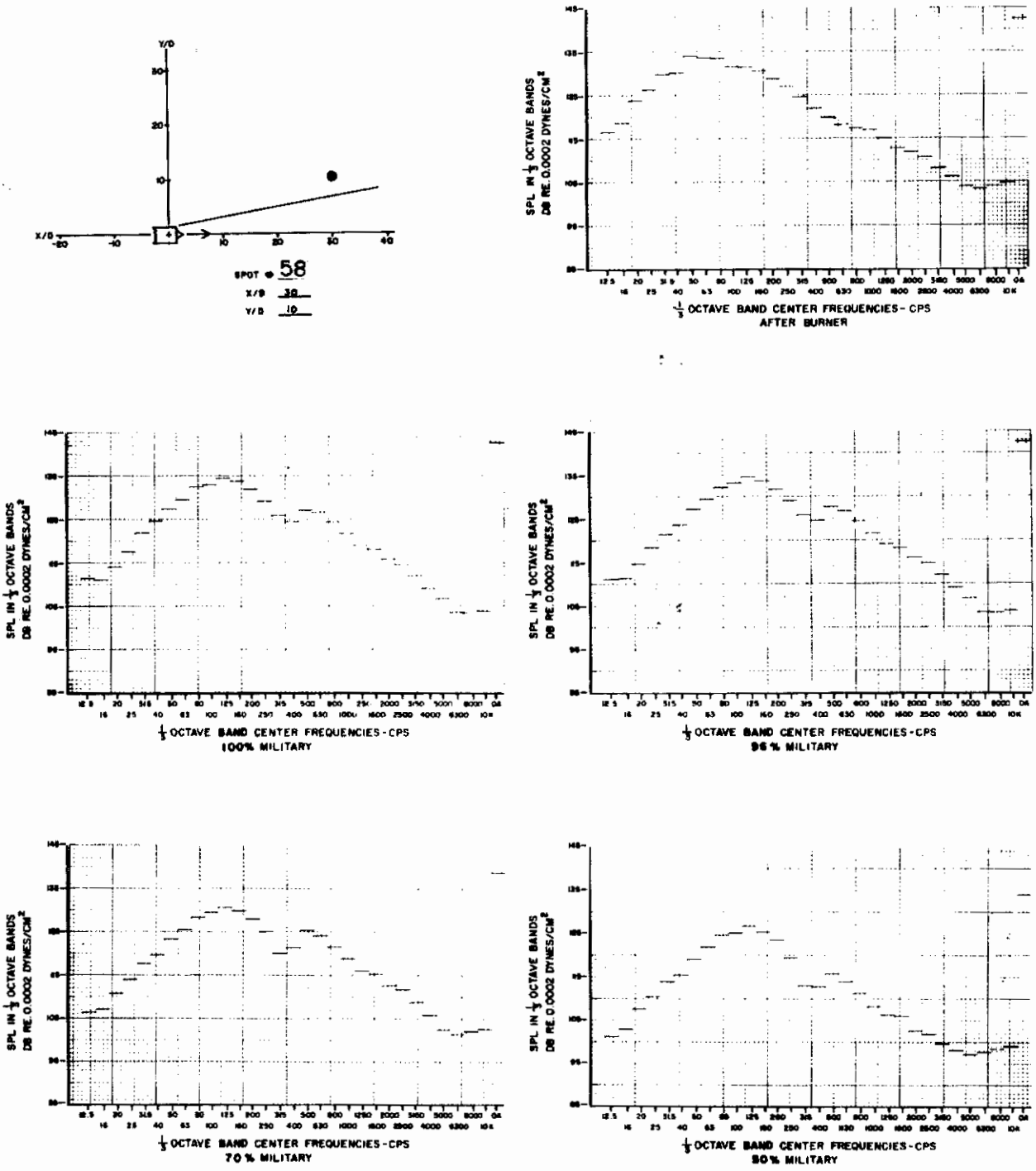


Figure 88. One-Third Octave Band Spectra and Overall SPL for Spot 58

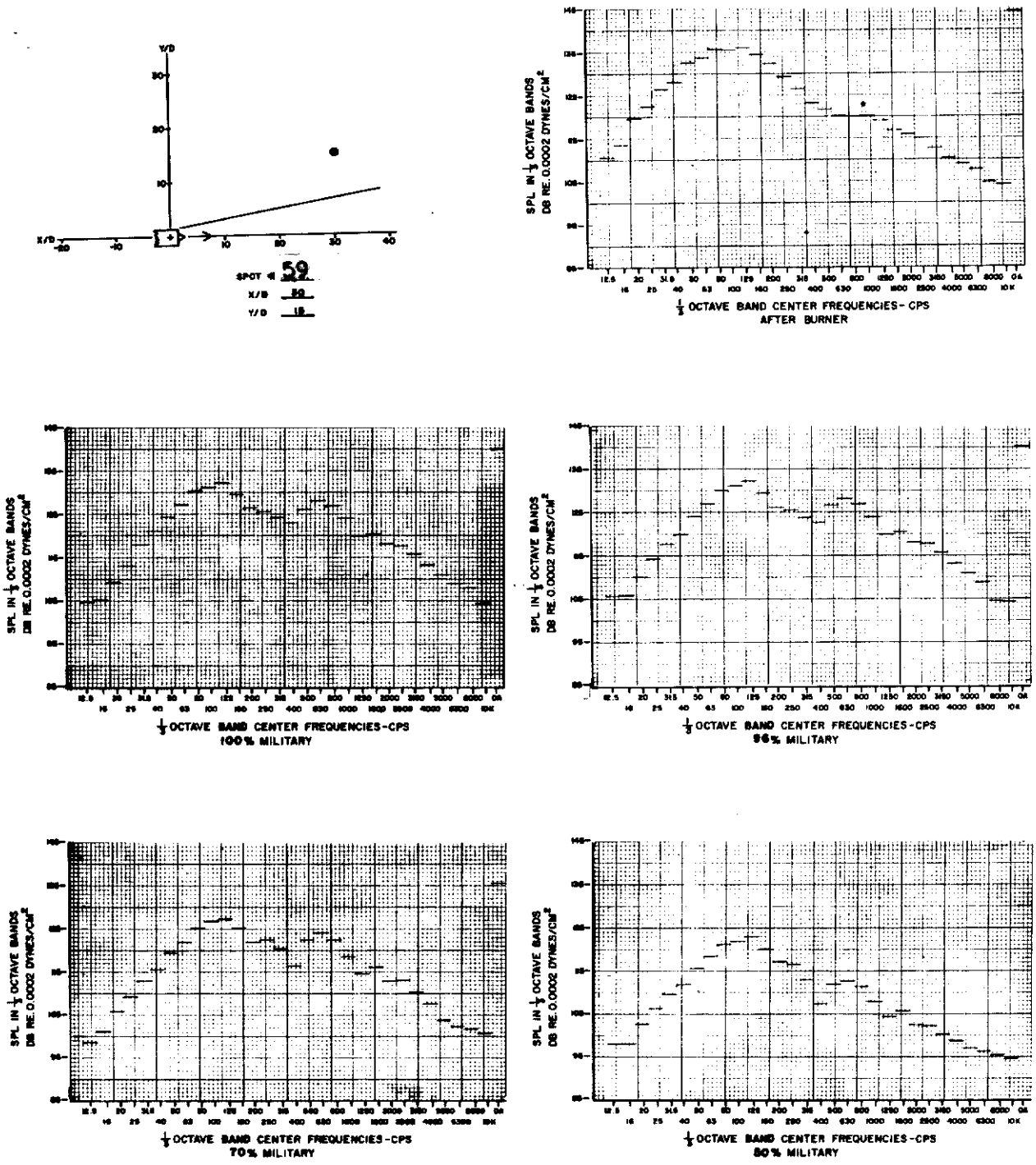


Figure 89. One-Third Octave Band Spectra and Overall SPL for Spot 59

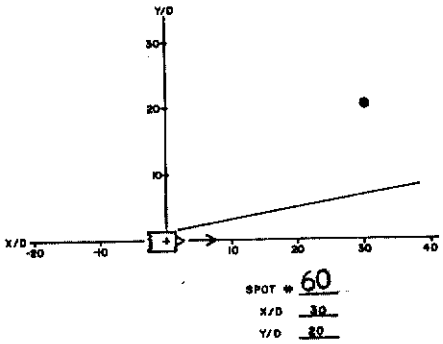


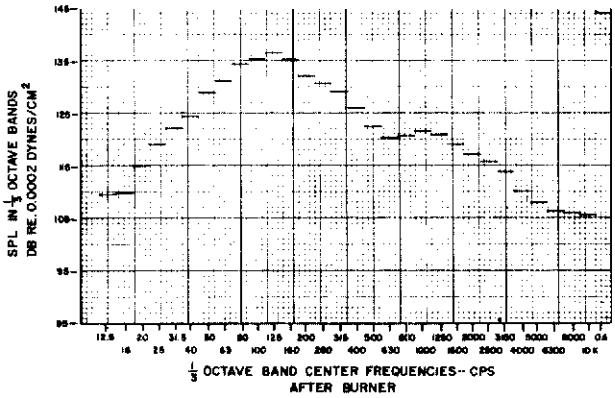


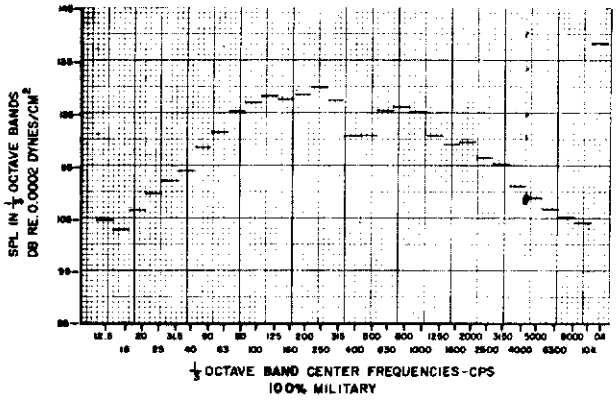


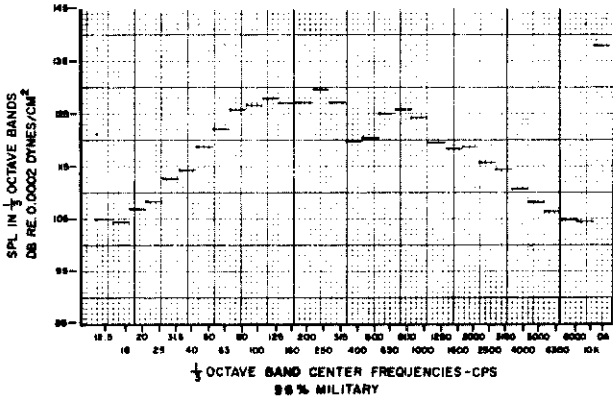


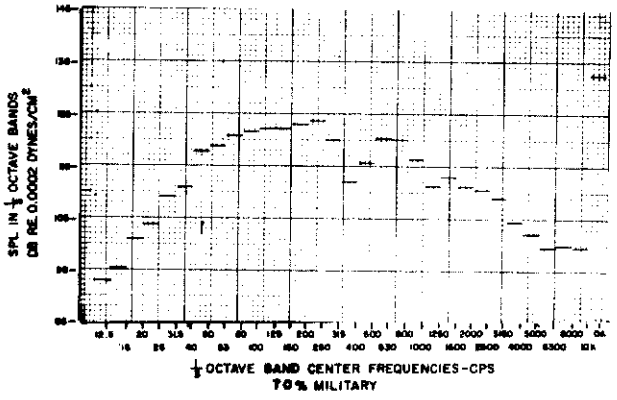


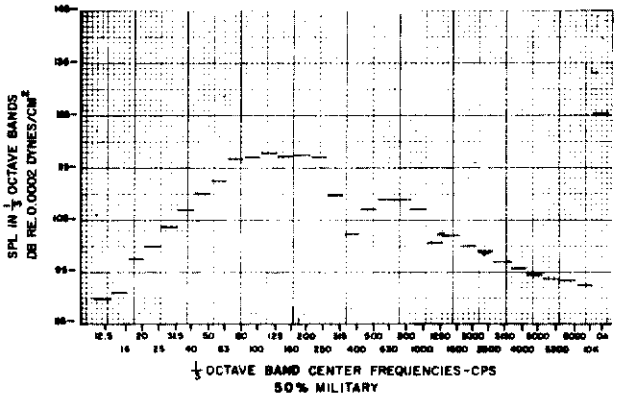


Figure 90. One-Third Octave Band Spectra and Overall SPL for Spot 60

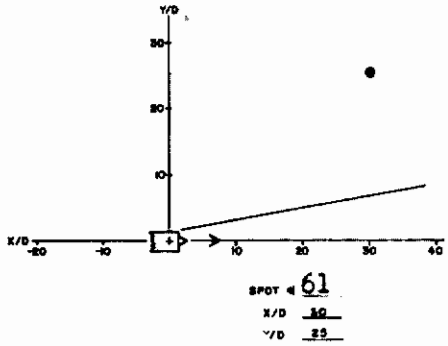


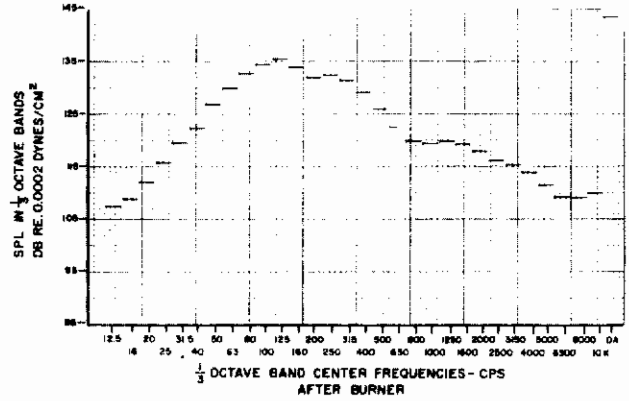


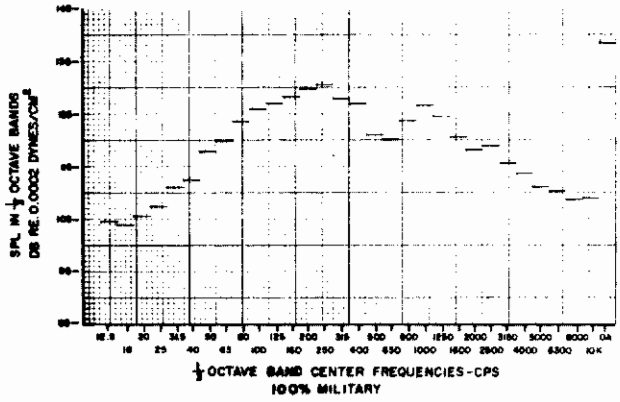


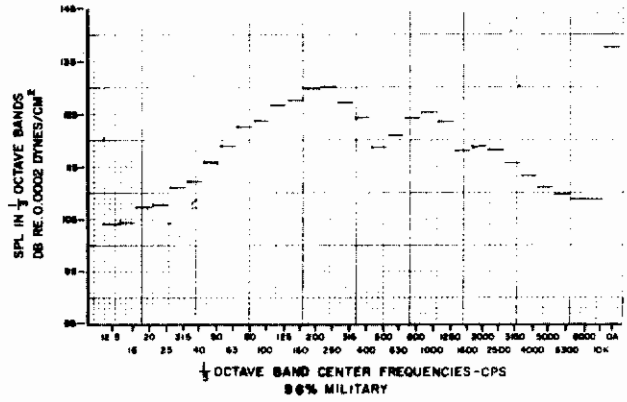


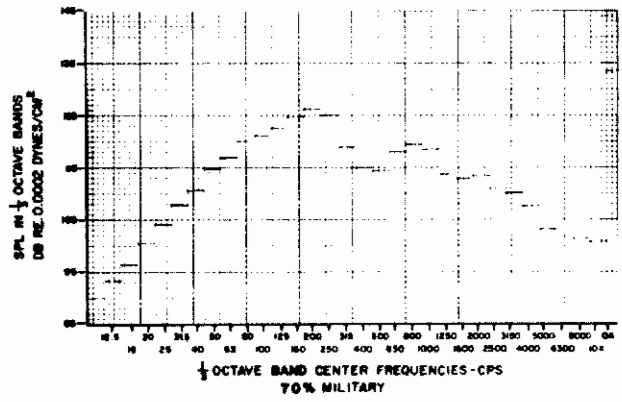


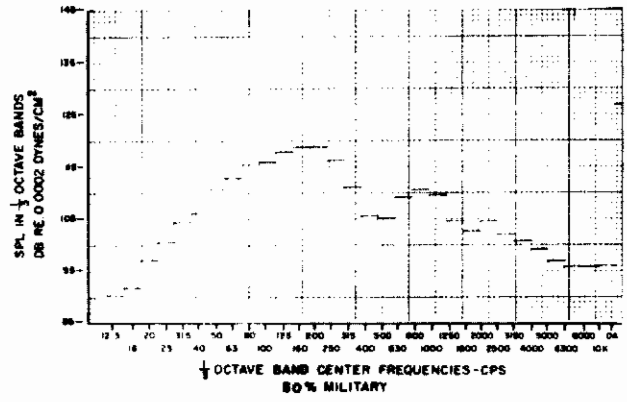


Figure 91. One-Third Octave Band Spectra and Overall SPL for Spot 61

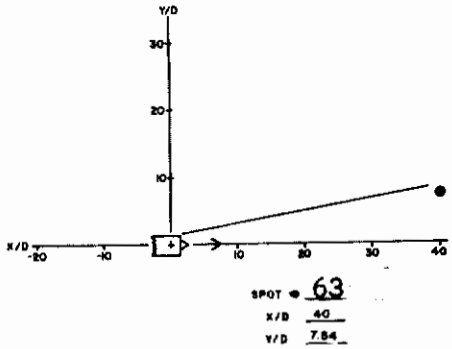


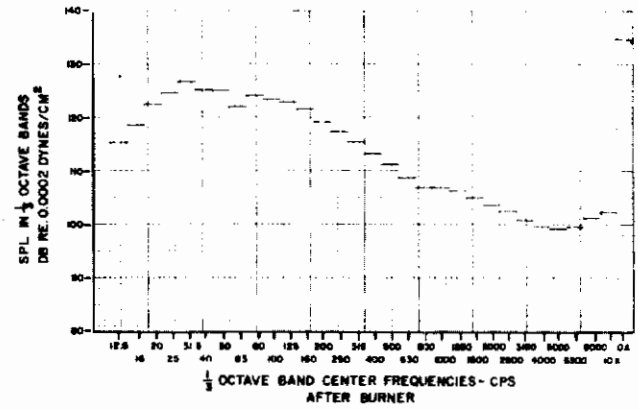


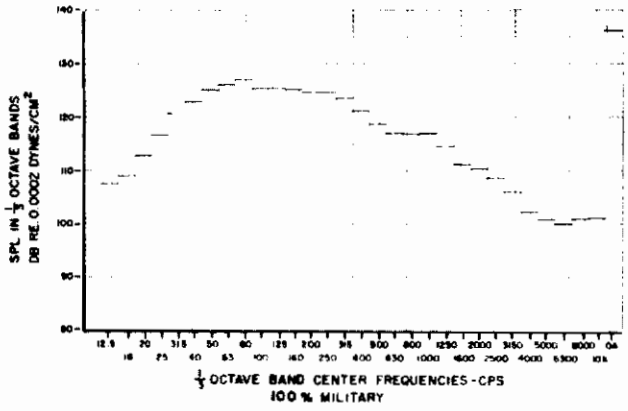


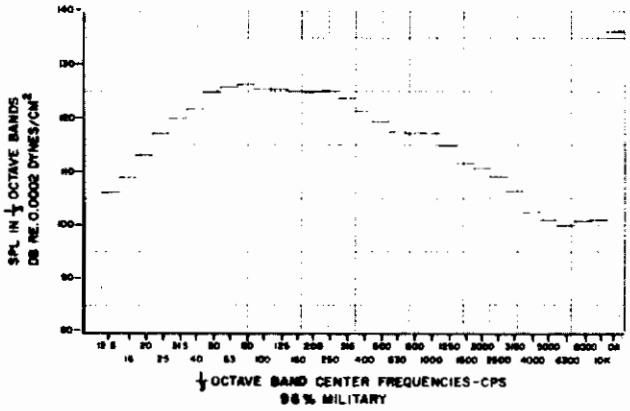


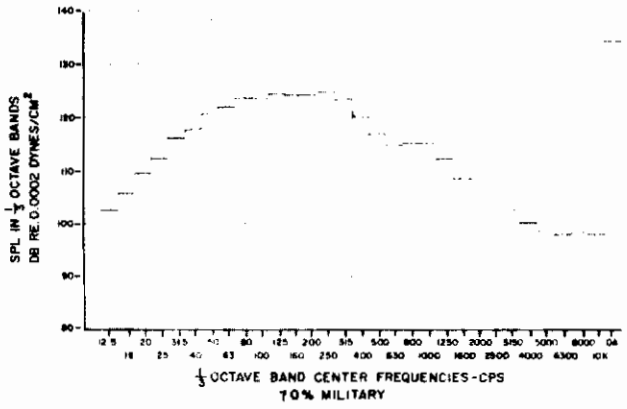


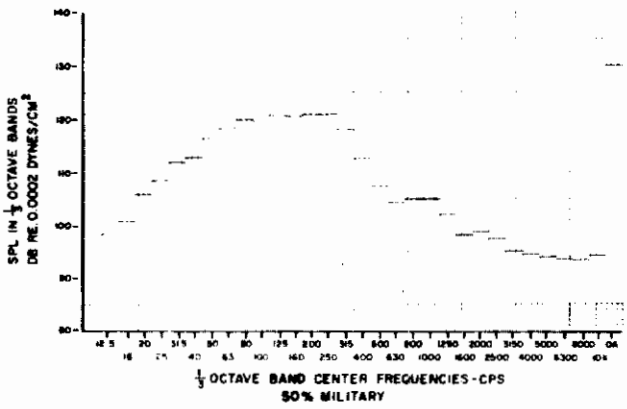


Figure 93. One-Third Octave Band Spectra and Overall SPL for Spot 63

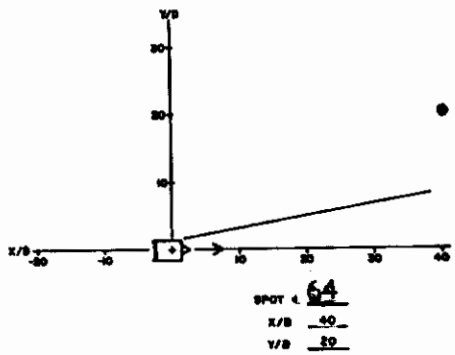


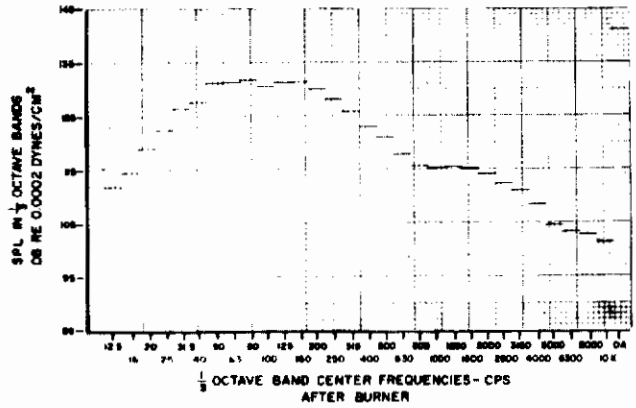


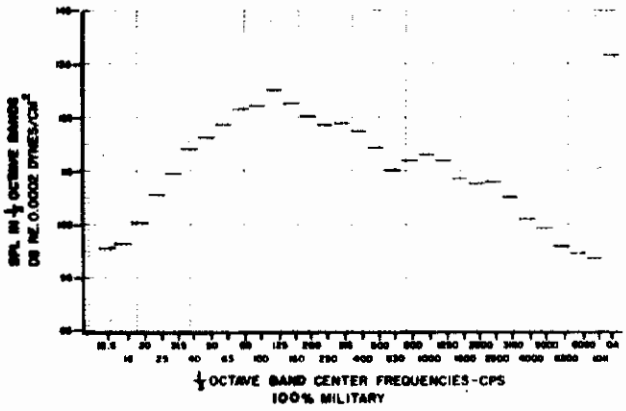


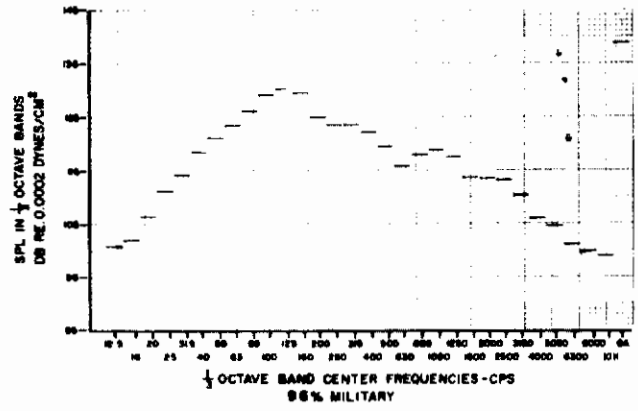


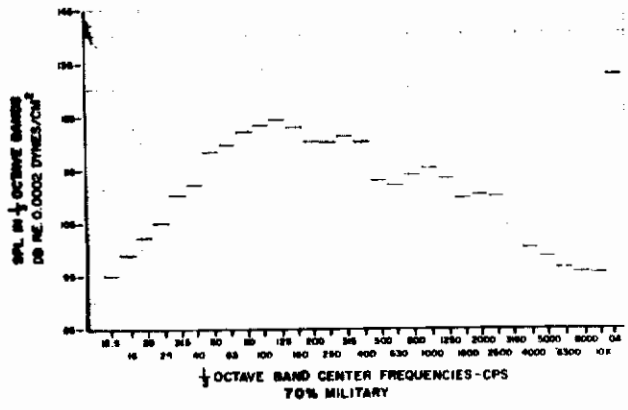


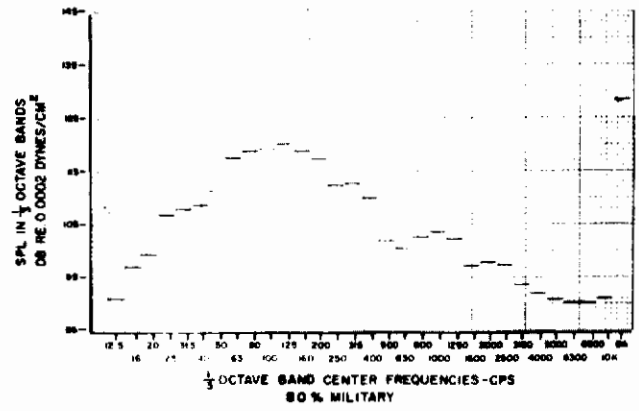


Figure 94. One-Third Octave Band Spectra and Overall SPL for Spot 64

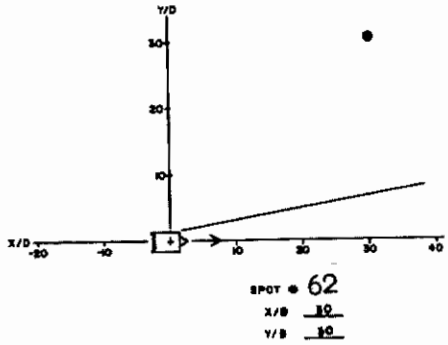


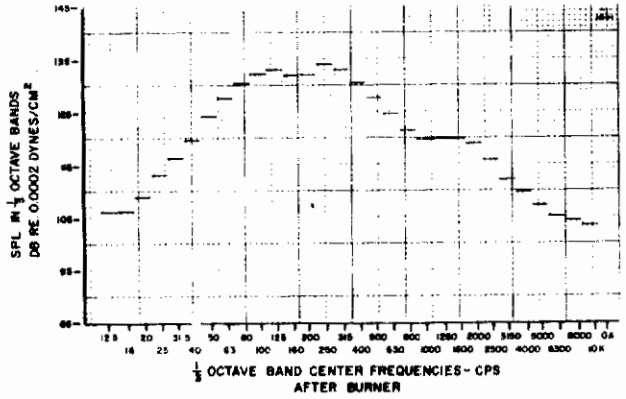


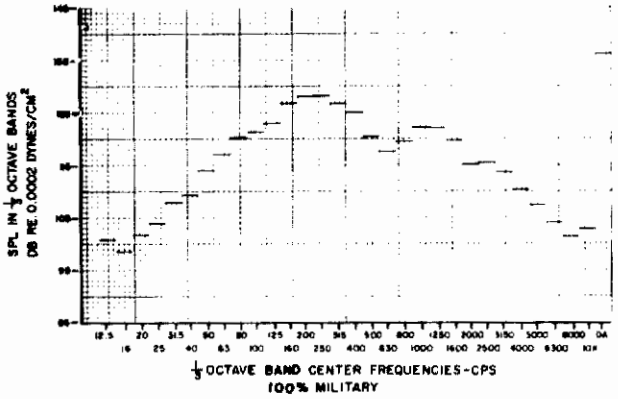


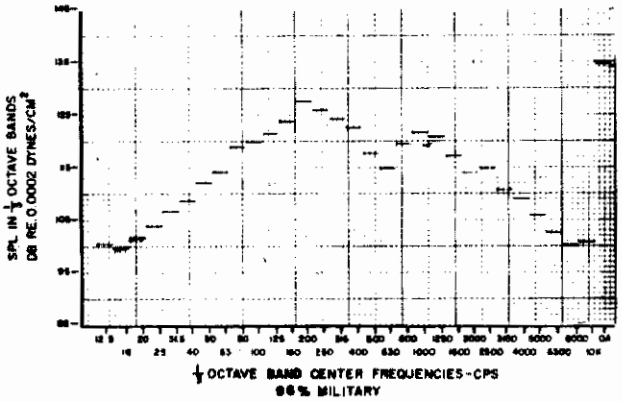


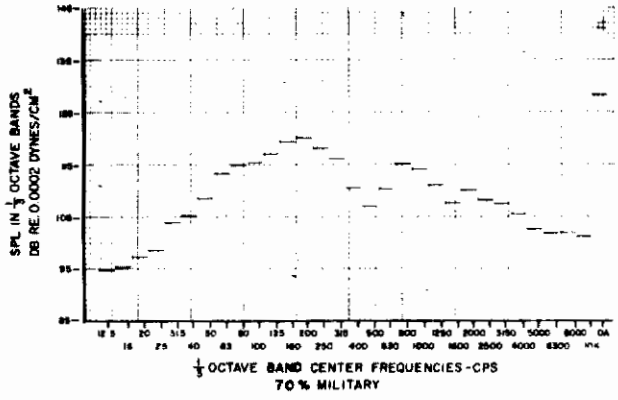


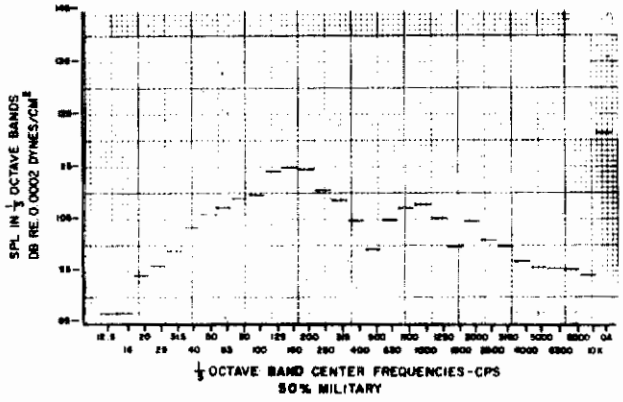


Figure 92. One-Third Octave Band Spectra and Overall SPL for Spot 62

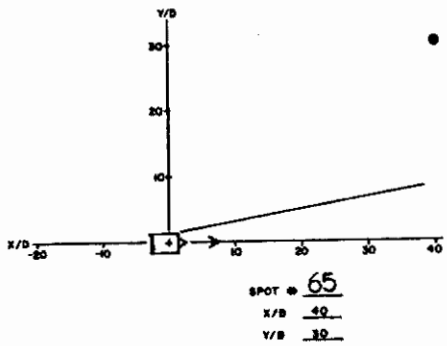


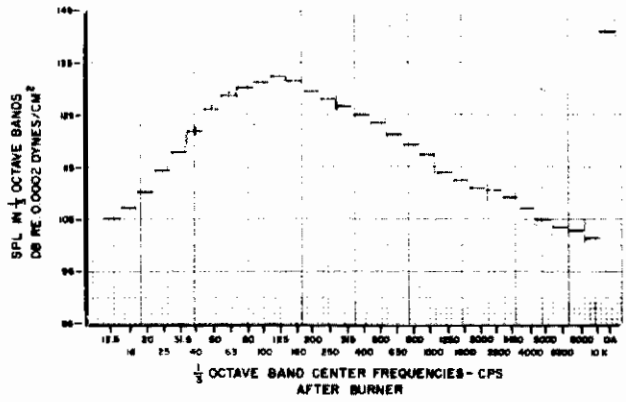


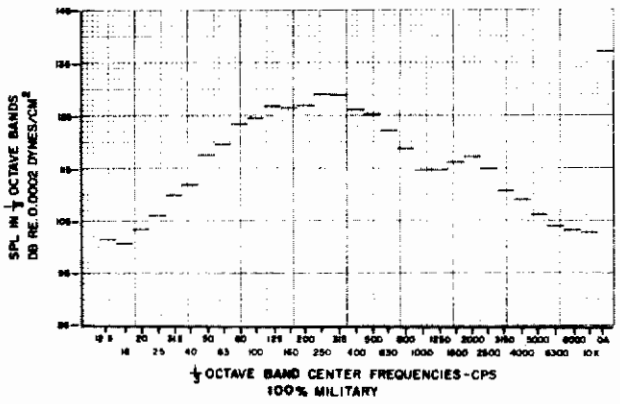


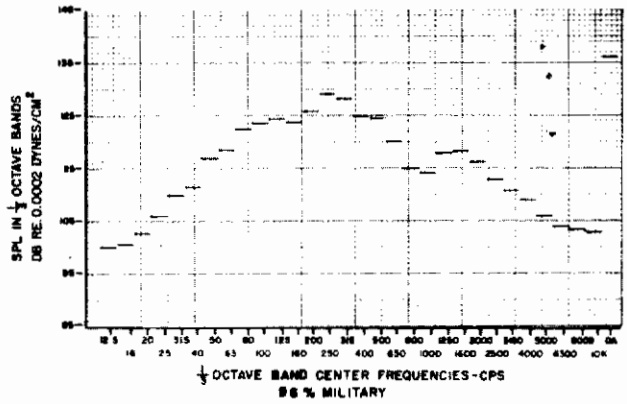


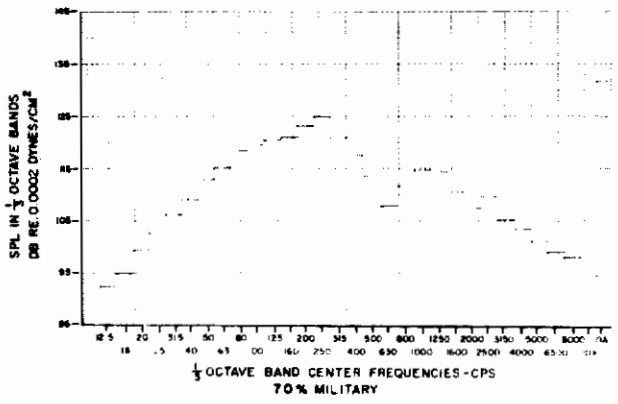


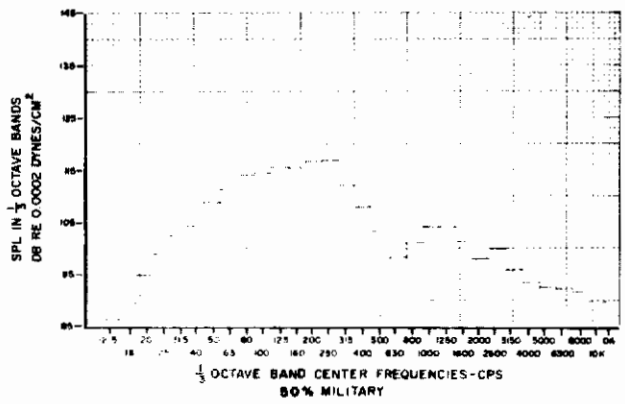


Figure 95. One-Third Octave Band Spectra and Overall SPL for Spot 65

Unclassified
Security Classification

**DOCUMENT CONTROL DATA - R&D**
*(Security classification of title, body of abstract and indexing annotation must be entered when the overall report is classified)*

| | |
|---|---|
| 1. ORIGINATING ACTIVITY (Corporate author)<br>Air Force Flight Dynamics Laboratory<br>Wright-Patterson AFB, Ohio | 2a. REPORT SECURITY CLASSIFICATION<br>Unclassified<br>2b. GROUP |

3. REPORT TITLE

Measurement and Analyses of the J57-P21 Noise Field

4. DESCRIPTIVE NOTES (Type of report and inclusive dates)
November 1964 to August 1966

5. AUTHOR(S) (Last name, first name, initial)
Hermes, P. H.
Smith, D. L.

| 6. REPORT DATE | 7a. TOTAL NO. OF PAGES | 7b. NO. OF REFS |
|---|---|---|
| October 1966 | 133 | 12 |

| 8a. CONTRACT OR GRANT NO. | 9a. ORIGINATOR'S REPORT NUMBER(S) |
|---|---|
| b. PROJECT NO. 1471 | AFFDL-TR-66-147 |
| c. Task No. 147102 | 9b. OTHER REPORT NO(S) (Any other numbers that may be assigned this report) |
| d. | |

10. AVAILABILITY/LIMITATION NOTICES
Distribution of this document is unlimited.

| 11. SUPPLEMENTARY NOTES | 12. SPONSORING MILITARY ACTIVITY |
|---|---|
| | Air Force Flight Dynamics Laboratory, Research and Technology Division, Air Force Systems Command, Wright-Patterson AFB, Ohio |

13. ABSTRACT A noise survey of a J57-P21 turbojet engine was conducted to provide a basis for the development of a refined empirical noise prediction technique. The measurements were obtained at 65 locations for 5 engine power settings. The 1/3 octave and overall sound pressure levels (SPL's) for each location and engine power setting are presented. SPL contours are presented for overall and selected 1/3 octave bandwidths. Ground reflection effects on the 1/3 octave band SPL's are evaluated. Comparisons are made with other existing data. Differences of up to 15 decibels (db) are found when comparing the 1/3 octave band levels. Velocity exponents (n), based on the Lighthill parameter, are presented for each location and compared with existing data. Poor agreement is found among the measurement programs. The effect of ground reflection on the n values is investigated and an n field is presented in which interference effects are eliminated. The effect of varying noise directional properties with jet velocity on the n values is evaluated. An n field, corrected for both ground reflection and varying noise directional properties, is presented. The corrected n values range from 5.0 to 6.0 for 80% of the measurement locations between 30 and 90° from the jet axis when jet density effects are neglected. The median value of 5.5 increases to 6.5 with the effects of jet density included. This essentially constant n field clearly indicates the heavy dependence of the n values on noise directional changes with jet velocity. The corrected n field equation is considered the basis of a noise prediction method which appears to be accurate for jet flows with exit Mach numbers ranging from 0.5 to 2.0.

DD FORM 1 JAN 64 1473

Unclassified
Security Classification

Unclassified
Security Classification

| 14. KEY WORDS | LINK A | | LINK B | | LINK C | |
|---|---|---|---|---|---|---|
| | ROLE | WT | ROLE | WT | ROLE | WT |
| Jet Noise<br>Prediction Techniques<br>Noise Measurements | | | | | | |

## INSTRUCTIONS

1. ORIGINATING ACTIVITY: Enter the name and address of the contractor, subcontractor, grantee, Department of Defense activity or other organization *(corporate author)* issuing the report.

2a. REPORT SECURITY CLASSIFICATION: Enter the overall security classification of the report. Indicate whether "Restricted Data" is included. Marking is to be in accordance with appropriate security regulations.

2b. GROUP: Automatic downgrading is specified in DoD Directive 5200.10 and Armed Forces Industrial Manual. Enter the group number. Also, when applicable, show that optional markings have been used for Group 3 and Group 4 as authorized.

3. REPORT TITLE: Enter the complete report title in all capital letters. Titles in all cases should be unclassified. If a meaningful title cannot be selected without classification, show title classification in all capitals in parenthesis immediately following the title.

4. DESCRIPTIVE NOTES: If appropriate, enter the type of report, e.g., interim, progress, summary, annual, or final. Give the inclusive dates when a specific reporting period is covered.

5. AUTHOR(S): Enter the name(s) of author(s) as shown on or in the report. Enter last name, first name, middle initial. If military, show rank and branch of service. The name of the principal author is an absolute minimum requirement.

6. REPORT DATE: Enter the date of the report as day, month, year, or month, year. If more than one date appears on the report, use date of publication.

7a. TOTAL NUMBER OF PAGES: The total page count should follow normal pagination procedures, i.e., enter the number of pages containing information.

7b. NUMBER OF REFERENCES: Enter the total number of references cited in the report.

8a. CONTRACT OR GRANT NUMBER: If appropriate, enter the applicable number of the contract or grant under which the report was written.

8b, 8c, & 8d. PROJECT NUMBER: Enter the appropriate military department identification, such as project number, subproject number, system numbers, task number, etc.

9a. ORIGINATOR'S REPORT NUMBER(S): Enter the official report number by which the document will be identified and controlled by the originating activity. This number must be unique to this report.

9b. OTHER REPORT NUMBER(S): If the report has been assigned any other report numbers *(either by the originator or by the sponsor)*, also enter this number(s).

10. AVAILABILITY/LIMITATION NOTICES: Enter any limitations on further dissemination of the report, other than those imposed by security classification, using standard statements such as:

(1) "Qualified requesters may obtain copies of this report from DDC."

(2) "Foreign announcement and dissemination of this report by DDC is not authorized."

(3) "U. S. Government agencies may obtain copies of this report directly from DDC. Other qualified DDC users shall request through _____."

(4) "U. S. military agencies may obtain copies of this report directly from DDC. Other qualified users shall request through _____."

(5) "All distribution of this report is controlled. Qualified DDC users shall request through _____."

If the report has been furnished to the Office of Technical Services, Department of Commerce, for sale to the public, indicate this fact and enter the price, if known.

11. SUPPLEMENTARY NOTES: Use for additional explanatory notes.

12. SPONSORING MILITARY ACTIVITY: Enter the name of the departmental project office or laboratory sponsoring *(paying for)* the research and development. Include address.

13. ABSTRACT: Enter an abstract giving a brief and factual summary of the document indicative of the report, even though it may also appear elsewhere in the body of the technical report. If additional space is required, a continuation sheet shall be attached.

It is highly desirable that the abstract of classified reports be unclassified. Each paragraph of the abstract shall end with an indication of the military security classification of the information in the paragraph, represented as *(TS), (S), (C), or (U)*.

There is no limitation on the length of the abstract. However, the suggested length is from 150 to 225 words.

14. KEY WORDS: Key words are technically meaningful terms or short phrases that characterize a report and may be used as index entries for cataloging the report. Key words must be selected so that no security classification is required. Identifiers, such as equipment model designation, trade name, military project code name, geographic location, may be used as key words but will be followed by an indication of technical context. The assignment of links, rules, and weights is optional.

Unclassified
Security Classification